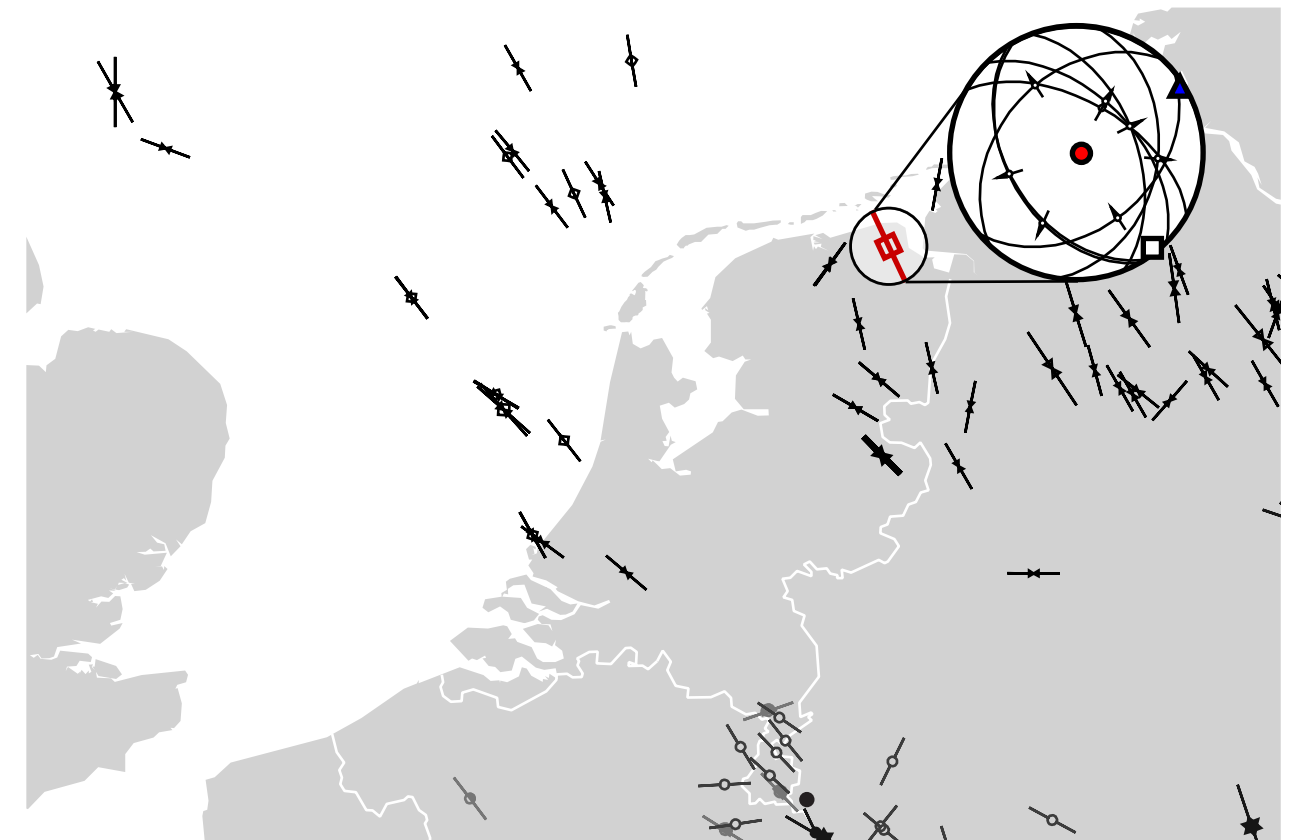


Heijn van Gent

Dissertation

Stress and strain from reflection seismic data





Part of the SPP 1135 research program “Dynamics of sedimentary systems under varying stress regimes: The example of the Central European Basin”, funded by the German Ministry of Education and Research (BMBF) and the German Research Foundation (DFG): Grant UR 64/7-1.



Data was provided by the Nederlandse Aardolie Maatschappij (NAM); a Shell operated 50:50 joint-venture between Shell and ExxonMobil.

The image on the front of this thesis is an adoption of Figure 8 of Chapter 1. The map and stress data was taken from the World Stress Map Project website (dc-app3-14.gfz-potsdam.de). The design of the cover has benefited considerably from the advise of David Schulze.

“Stress and strain from reflection seismic data”

Von der Fakultät für Georessourcen und Materialtechnik der
Rheinisch -Westfälischen Technischen Hochschule Aachen

zur Erlangung des akademischen Grades eines
Doktor der Naturwissenschaften

genehmigte Dissertation
vorgelegt von **M.Sc. Geology**

Heijnderik Willem van Gent

aus 's-Hertogenbosch, die Niederlande

Berichter: Univ.-Prof. Dr. Janos Urai
Univ.-Prof. Peter Kukla, Ph.D.

Tag der mündlichen Prüfung: 23. Dezember 2009

Diese Dissertation ist auf den Internetseiten der Hochschulbibliothek online verfügbar

"A dissertation is meant to be written, not to be read"

- *Miquel Bulnes – Lab (Translated from Dutch)*

Table of Contents

Introduction	11
<hr/>	
Aims and overview	12
Slickensides and fault undulation – the topography of fractures and faults	12
The geometrical determination of slip – connecting the dots...	14
Stress from ductile salt?	15
Parts of this thesis which have been published	16
References	17
Chapter 1: Paleostresses of the Groningen area, the Netherlands – results of a seismic based structural reconstruction	23
<hr/>	
Abstract	23
Introduction	23
Methods	27
Fault interpretation results	34
Retro-deformation and paleostress results	36
Discussion	38
Conclusions	44
Acknowledgements	45
References	45
Chapter 2: Small-scale faulting in the Upper Cretaceous of the Groningen Block (The Netherlands): 3D seismic interpretation, fault plane analysis and regional paleostress	51
<hr/>	
Abstract	51
Introduction	52
Geological setting	56
Methods	58
Results	61
Discussion	70
Conclusions and outlook	74
Acknowledgement	74
References	74
Chapter 3: The internal geometry of salt structures - a first look using 3D seismic data from the Zechstein of the Netherlands	83
<hr/>	
Abstract	83
Introduction	83

The stratigraphy of the Zechstein	86
Study areas and methodology	88
Stringer geometry	92
Discussion	101
Conclusions:	109
Acknowledgements	109
References	110
Concluding remarks	119
<hr/>	
Faults in outcrop vs. seismic faults	119
Multiple kinematic indicators on a single movement plane	120
The integration of salt structure knowledge	122
Conclusions	123
<i>Outlook: Is seismic paleostress determination worth the effort?</i>	123
<hr/>	
References	124
Appendix 1: Excel applets	129
<hr/>	
Acknowledgements:	129
References	129
„Stereogram_v2.2.xls“	130
„StressTensor_v2.4.xls“	137
Appendix 2: Monte Carlo analysis of seismic based paleostress results of NW Groningen.	147
<hr/>	
Introduction	147
The datasets	147
Method	148
Results	150
Discussion	151
Conclusions	152
References:	152
The results	155
Appendix 3: Bootstrapping the data	165
<hr/>	
References:	166
The Results	167
Appendix 4: Synthetic data Paleostress sensitivity test	171
<hr/>	
References:	171

Appendix 5: Differences between NDA with different Θ angles	181
<hr/>	
References:	181
Appendix 6: The stratigraphy of the Dutch Zechstein	185
<hr/>	
The Zechstein carbonates facies	185
Zechstein stratigraphy	186
References	187
Summary	189
Zusammenfassung	191
Acknowledgements	195
<hr/>	

Introduction

"Nobody said it was easy, no one ever said it would be this hard."

- *Coldplay - The scientist*

In-situ borehole measurements allow the determination of the present-day stress field in many sedimentary basins. These measurements include the determination of the orientation of tensile or (artificial) hydro fractures (e.g., but not exclusively: Frikken, 1999; Stephenson et al., 2007), borehole breakouts (e.g. Reinecker et al., 2003) or focal mechanisms (e.g.: Hinzen, 2003; Ilic and Neubauer, 2005; Plenefisch and Klinge, 2007). Several reflection 3-D seismic attributes are also employed to estimate paleostress. These methods are mainly based on anisotropy of seismic ray velocity, and can be used to predict the orientation of fractures in the subsurface. Thus the orientation of the present-day principle stress axes are constrained (e.g.: Neves et al., 2003). These methods however are also influenced by sedimentological and/or diagenetic processes.

Pre-drilling knowledge of the present-day stress field can be used to optimize both drilling and production, as borehole stability, fluid flow properties and the orientation and sealing-properties of both natural and induced fractures are directly dependant on the present-day stress field (Henk, 2005). Whether from pre-drilling or in-situ measurements, present-day stress measurements not only are important for hydrocarbon production and exploration, geothermal or brine wells, they also provide a valuable insight into the evolution of the Earth's crust from a scientific point of view, and help risking for example earthquakes.

However, just as important as the present-day stress, is the paleostress; as many of the present-day structures are not newly formed, but inherited structures, with movement adjusted to the present-day stress field. There are several methods that allow the determination of paleostress, and these can be separated in those that constrain paleostress directions (not magnitude) solely based on the orientation and structural style of large scale fault or fold patterns, and those that calculate the reduced stress tensor. These include both directions and (relative) magnitude of the principle stresses.

The first type of paleostress methods depends on the Andersonian Theory of Faulting and uses the large scale orientation and structural style of fault patterns (Anderson, 1942; Michon et al., 2003). The orientation of dykes and elongated calderas are also used (although these are not common in sedimentary basins, e.g.: Muller and Pollard, 1977; Angelier et al., 1997; Paulsen and Wilson, 2007). Paleostress calculation methods, such as the Direct Stress Inversion (Angelier, 1990) or the Numeric Dynamic Analysis (Turner, 1953; Spang, 1972; Sperner et al., 1993), and many related or similar methods (including: Will and Powell, 1991; Yamaji, 2000; Fry, 2001; Yamaji et al., 2006; Zalohar and Vrabec, 2007; Sippel et al., 2009) use direct outcrop measurements of the fault orientation and slip direction to calculate the reduced stress tensor at the moment of fault slip. The reduced stress tensor consists of the orientation of the principle stress axes and their relative size. Since fault measurements are required for these methods, direct access to the fault in outcrop is a requirement.

Different types of (sub-)grain piezometry (Carter et al., 1993; Franssen, 1993; Schleder and Urai, 2005), dislocation density and other crystal based stress gauges, can be used as paleostress

estimators. These include methods such as such as calcite twinning (e.g.: Turner, 1953; Spang, 1972; Larroque and Laurant, 1988; Rocher et al., 2004), and most of them only provided the differential stress ($\sigma_1 - \sigma_3$). These crystal-based methods will not be discussed here.

Aims and overview

The requirement of direct outcrop access for paleostress calculation methods makes the determination of paleostress in subsurface settings a challenge. In some on-shore settings, the study of outcrops can give indication to the paleostress conditions at depth. However, much of the earth's crust is covered by younger sedimentary basins.

In this work, a workflow to determine paleostress from brittle deformation structures, solely using 3D reflection-seismic data is developed and tested. Therefore a reliable method of extracting paleo-slip information from 3D reflection seismic data is required. In the first two chapters, two main methods are introduced, the geometrical determination of paleo-slip, and fault plane analysis. The third chapter represents an initial attempt to develop a similar method of paleostress determination (based on brittle deformation of rocks) for the basically ductile deformation in the Upper Permian Zechstein evaporites (Geluk, 2007; Geluk et al., 2007). Interesting insights in the complex, 3D geometries that develop as a result of the coeval deformation of brittle deposits contained in ductile evaporites are presented (Bornemann, 1991; Zulauf and Zulauf, 2005; Chemia et al., 2008; Zulauf et al., 2009). This initial understanding of the strain inside deforming evaporites can be developed into a full method of determining paleostress from deforming ductile materials that contain brittle markers.

In the concluding remarks the strengths and weaknesses of the seismic based paleostress determination methods will be discussed. First however, slickensides and larger scale fault undulations will be discussed in general terms.

Two Excel applets (available on www.ged.rwth-aachen.de) are discussed in Appendix 1 that are designed to visualize stress tensors and help understand the effect of stress tensors on arbitrary planes. In Appendices 2 to 5, several of the general assumptions of paleostress calculations are investigated, and several real and artificial datasets are tested for the robustness of the different paleostress methods. In Appendix 6, the stratigraphy of the Zechstein deposits of the Dutch subsurface are discussed in a bit more detail than in Chapter 3.

Slickensides and fault undulation – the topography of fractures and faults

Shear movement on faults and fractures can leave a slickenside on the fault surface. This is a polished fault surface that might contain parallel sets of ridges and grooves, streaks or linear mineral fibers (so-called slickenfibres or slickensides) which represent movement striae (Fig. 1 and e.g.: Means, 1987; Ramsay and Huber, 1987; Twiss and Moores, 1992). It is noted that many authors also call these striae slickensides, although that actually only applies to the polished fault surface. These striations form by scratching, gauging or smearing on fault surfaces (Means, 1987), and generally are smaller than 1 mm. These structures are also called kinematic indicators (Doblas, 1998).

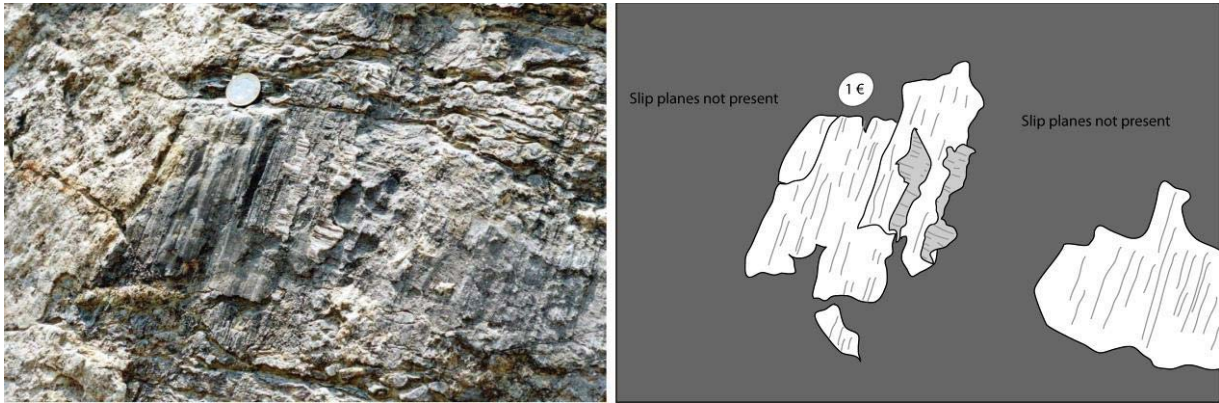


Fig. 1: Kinematic indicators on a normal fault in a quarry in the Leine Graben near Hillerse, north of Göttingen, Germany. The patches of kinematic indicator show two orthogonal movement striae orientations (shown in white and light grey shades). These sets of overlapping movement striae can be used to establish a paleostress stratigraphy (the evolution of the paleostress tensor with time, Kleinspehn et al., 1989), as this fault has two kinematic indicators. Image shows the same fault plane as in Fig. 2.

Most existing paleostress analyses require a combination of fault orientation and direction of the slip on the fault as input. Outcrop measurements of these slickensides have been used as slip direction indicators and in some cases also slip-sense indicators “for generations” (Means, 1987), and are also used in paleostress analyses (e.g.: Angelier, 1979; Angelier, 1989; Wojtal and Pershing, 1991; Vandycke, 2002; Sippel, 2008; Sippel et al., 2009, and references therein). These movement striae, which are often clearly visible in outcrop (Fig. 1), are too small to be recognized in 3D reflection seismic datasets, which have a resolution of about 15-25 m at best.

Fault plane topography is however not limited to the scale of slickensides. Field observations, laboratory experiments and laser measurements (LiDAR; Light Detection And Ranging) of natural fault surfaces (Fig. 2 and e.g.: Brown and Scholz, 1985; Power et al., 1987; Power et al., 1988; Power and Tullis, 1991; Lee and Bruhn, 1996; Power and Durham, 1997; Develi and Babadagli, 1998; Van der Zee, 2001; Kokkalas et al., 2007; Sagy et al., 2007a; Sagy et al., 2007b; Candela et al., in press) have shown fault undulations on many different scales. These undulations are shown to be self-similar and thus follow a fractal scaling law (e.g.: Power et al., 1988; Power and Tullis, 1991; Lee and Bruhn, 1996; Power and Durham, 1997; Renard et al., 2006; Candela et al., in press). It must be noted that the fault undulations meant here are something different than variations in fault shape and orientation as a result of the coalesce of different faults (segmentation of faults, e.g.: Childs et al., 1996; Schöpfer et al., 2007; Lohr et al., 2008). The latter is caused by linkage of previously independent and individual faults with slightly different orientations, and the related curving of faults when they grow towards each other. The former is usually interpreted to be the result of inherent random roughness in the initial failure of single fault planes, which is then selectively preserved or even amplified in the direction of

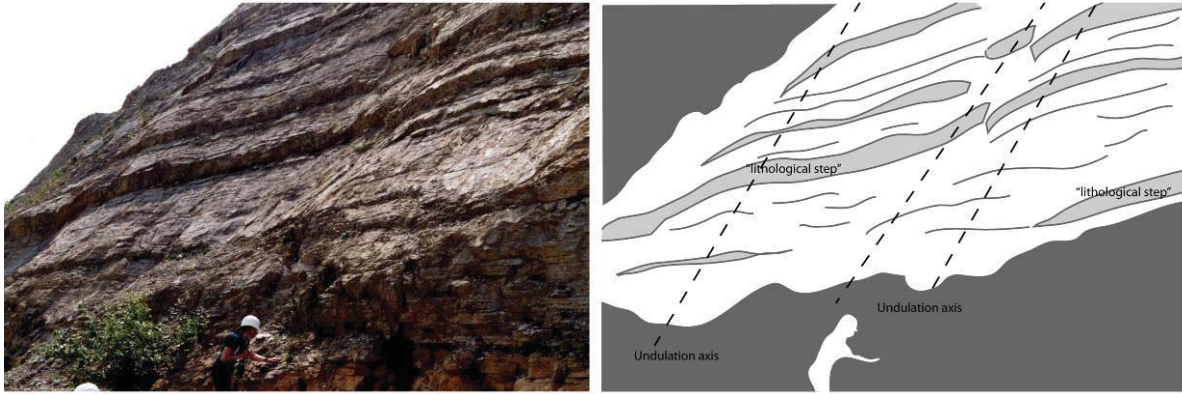


Fig. 2: Oblique view of a normal fault surface, in a quarry in the Leine Graben near Hillerse, north of Göttingen, Germany. The fault plane (white in interpretation) shows two types of fault plane topography. The first type is represented by a number of “lithological steps”, down dip steps, running roughly horizontal and parallel to the bedding. These steps formed most likely due to vertical segmentation (*sensu*: Childs et al., 1996; Schöpfer et al., 2007), local differences in material properties (e.g.: Ferrill and Morris, 2003), weathering, or a combination of the above. The second type of topography is a low amplitude wave (undulation) of the fault plane along strike. It is this type of undulation we are interested in here. Stippled lines are used to indicate the approximate locations of the axis of undulation.

the most recent slip (Lee and Bruhn, 1996; Renard et al., 2006; Kokkalas et al., 2007; Sagy et al., 2007a; Candela et al., in press). Several studies have shown that fault undulations have their axis parallel to the main slip direction (Lee and Bruhn, 1996; Renard et al., 2006; Sagy et al., 2007a; Candela et al., in press). Thus, a detailed determination of the fault surface undulations in (neoformed, non-reactivated) faults in 3D reflection seismic data will give information regarding the slip direction (see Chapter 2, and e.g. Needham et al., 1996; Marchal et al., 2003). This information can then be used for paleostress determination.

The geometrical determination of slip – connecting the dots...

Although fault undulations provide an elegant way to constrain movement directions on non-reactivated faults, there is a simpler way to determine how two fault blocks have moved relative to each other, even when the fault was reactivated. Comparing the positions of two points before and after deformation will determine the movement vector between these points, in a “connect the dots-fashion”. In 3D seismic data from sedimentary basins, one plausible candidate is to use faulted linear features, such as channels. Back et al. (2006) for example, have shown how maps of the seismic coherency signature from a delta setting can be used to connect a set of horizons on two sides of a fault on the basis of the presence of the a faulted channel in both fault blocks. Alternatively, connecting the channel from both sides of the fault gives the movement vector of the channel. This vector represents the fault slip vector and thus allows the determination of the paleostress tensor. This approach also allows the calculation of a paleostress stratigraphy (Kleinspehn et al., 1989). The fault plane analysis only works in neo-formed, non reactivated faults, as newer movement in a different direction will destroy the undulation. A number of channels intersecting a synsedimentary fault at

different stratigraphic levels in a setting with changing stress directions will show the change of movement direction with time. A similar approach was followed in Chapter 1, where fault slip vectors were (amongst other methods) constrained by comparing the shape of detailed horizon interpretations. No faulted channels were located in the seismic data, and as a result, minor, elongated irregularities in the horizon on both sides of the fault were used. The three-dimensional expression of these irregularities on the horizon around the fault plane was used, rather than the simple, essentially two-dimensional expression on the Allan map (Allan, 1989).

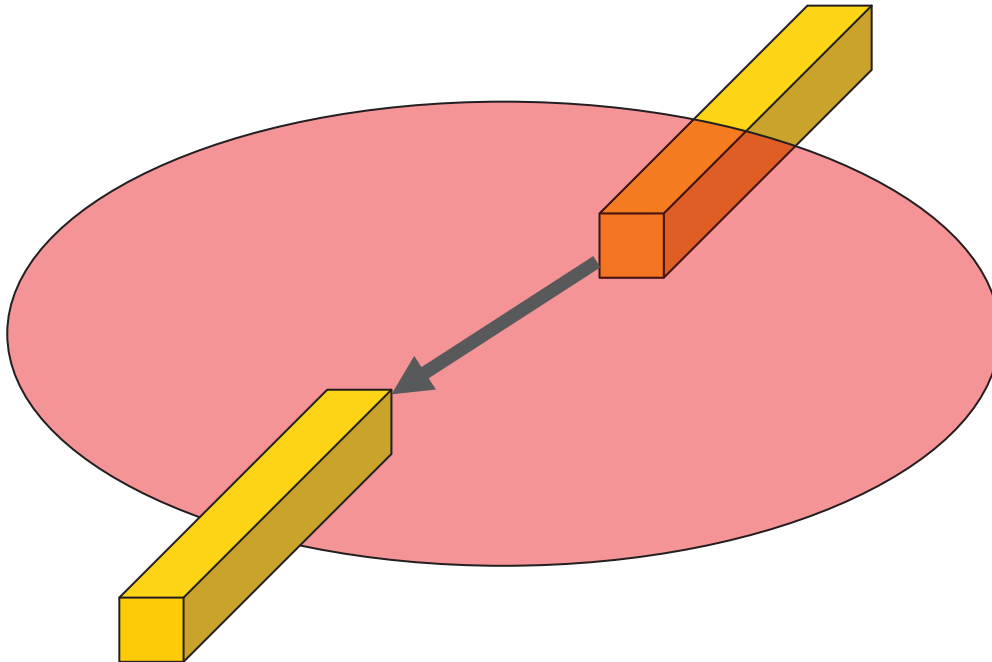


Fig 3: Connecting the two ends of a faulted beam is a quick way to determine the slip on the fault.

Stress from ductile salt?

Using for example subgrain piezometry (Carter et al., 1993; Franssen, 1993; Schleder and Urai, 2005), it is possible to determine the maximum differential stress in halite. The orientations of the stress axes however can not be determined. The ductility of salt in the subsurface prevents the use of the “conventional” paleostress methods, as they are developed for brittle failure. In fact, to-date, studying the deformation and flow of salt in nature was only discussed in detailed, but very local studies in mines or wells (e.g.: Borchert and Muir, 1964; Woods, 1979; Bornemann, 1991; Geluk, 1995; Burliga, 1996; Smith, 1996; Schléder et al., 2008), in analogue or numerical models (e.g.: Koyi, 1996; Koyi, 2001; Callot et al., 2006; Chemia et al., 2008), or by studying the overburden (e.g.: Mohr et al., 2005). Here we describe in detail the large scale geometry of a brittle layer in the ductile Zechstein salts. This layer consists of clay, anhydrite and carbonate/dolomite and is part of the Z3 cycle of the Zechstein deposition. This layer has been shown to contain large scale folds already (Geluk, 1995), but here we describe a large scale, detailed geometrical analysis of this layer in two study areas. It will be shown that the early diagenetic history of this layer has a strong effect on the further development of salt structures in the Central European Basin System.

This work will further show that the development of strain in flowing natural salt deposits is extremely complex. Since the description and determination of deformation or strain is the first step in understanding the relevant stress(-evolution), this study is an important step in constraining paleostress evolution from brittle enclosures in a ductile matrix. The study of this layer is further of relevance since the Z3 brittle layer poses a problem while drilling sub-salt targets and since the European Zechstein deposits are considered as repositories for radioactive waste and gas and are the sites for potasch salt dissolution (Bornemann, 1991; Williamson et al., 1997; van Eijs and Breunse, 2003; Evans and Chadwick, 2009).

Parts of this thesis which have been published

- ◇ van Gent, H. W., Urai, J., Kukla, P., Back, S., Terken, J., de Keijzer, M. (2006) Paleostress inversion using seismic data for the North West Groningen gas field (the Netherlands). SPP1135 Erdingerfeld Tagung 2006, Erdingerfeld, Germany, 15-17-11-2006.
- ◇ van Gent, H., Back, S., Urai, J., Kukla, P. A., Reicherter, K. (2007a) The estimation of paleostress through the palinspastic reconstruction of 3D seismic data from the Groningen gas field, the Netherlands. DRT 2007 -16th conference on Deformation mechanics, Rheology and Tectonics, Milano, Italy, 27-29 September, Rendiconti della Società Geologica Italiana - Nuova Serie, Società Geologica Italiana - Roma, V, pp. 96.
- ◇ van Gent, H. W., Back, S., Urai, J. L., Kukla, P. A. (2007b) Paleostress analysis of the Groningen gas field, the Netherlands, based on high-resolution 3D seismic data. Published Abstract. European Geosciences Union General Assembly, Geophysical Research Abstracts, 9.
- ◇ van Gent, H. W., Urai, J. L., Back, S., Kukla, P. (2007c) Paleostress estimation from 3D seismic data, Groningen gas field, the Netherlands. 67. Jahrestagung der Deutschen Geophysikalen Gesellschaft, Aachen, 26-29 March 2007, Abstracts der 67. Jahrestagung der Deutschen Geophysikalischen Gesellschaft, pp. 239.
- ◇ Kley, J., Franzke, H.-J., Jähne, F., Krawczyk, C., Lohr, T., Reicherter, K., Scheck-Wenderoth, M., Sippel, J., Tanner, D., van Gent, H. W. (2008) Strain and Stress. In: Littke, R., Bayer, U., Gajewski, D. & Nelskamp, S. (Eds.), Dynamics of complex intracontinental basins: The Central European Basin System. Springer-Verlag, Berlin Heidelberg, pp. 98-124.
- ◇ van Gent, H., Back, S., Urai, J. L., Kukla, P. A., Reicherter, K. (2008a) Stress states based on 3D seismic data from the Dutch subsurface. 3rd World Stress Map Conference, Potsdam, Germany, 15.-17. October, pp. 97.
- ◇ van Gent, H. W., Back, S., Urai, J. L., Kukla, P. A., Reicherter, K. (2008b) Paleostress based on seismic data - examples from the NW Groningen and Dutch offshore gas fields. Tectonics Studies Group Annual Meeting, La Roche-en-Ardenne, Belgium, 8th-11th January, 2008, pp. 68-70.
- ◇ van Gent, H. W., Back, S., Urai, J. L., Reicherter, K., Kukla, P. A. (2008c) Paleostress from an internal fault system in the Upper Cretaceous Chalk of the Northern Netherlands. Geo 2008; International Conference and 106th annual meeting of the Deutsche Gesellschaft für Geowissenschaften e. V. (DGG) and 98th annual meeting of the Geologische Vereinigung e.V. (GV), Aachen, Germany, September 29 - October 2, 2008, Schriftenreihe der Deutschen

Gesellschaft für Geowissenschaften, Deutschen Gesellschaft für Geowissenschaften e.V. (DGG), 60, pp. 270.

- ◇ van Gent, H. W., Urai, J. L., Kukla, P. A. (2008d) The 3D Geometry of the Zechstein Z3 Carbonate/Anhydrite Member: Implications for Salt Dynamics and Hydrocarbon Production. AAPG International Conference & Exhibition, Cape Town, South Africa, October 26-29, 2008.
- ◇ Li, S., Abe, S., Urai, J. L., van Gent, H. W. (2009) Sinking of carbonate and anhydrite stringers in rock salt: insights from numerical simulations. EGU General Assembly 2009, Vienna, Austria, 19 – 24 April 2009, Geophysical Research Abstracts, 11.
- ◇ van Gent, H. W., Back, S., Urai, J. L., Kukla, P. A., Reicherter, K. (2009) Paleostresses of the Groningen area, the Netherlands – results of a seismic based structural reconstruction. *Tectonophysics - Progress in understanding sedimentary basins* 470(1-2), 147-161.
- ◇ van Gent, H. W., Back, S., Urai, J. & Kukla, P. A. 2010. Small-scale faulting in the Upper Cretaceous of the Groningen Block (The Netherlands): 3D seismic interpretation, fault plane analysis and paleostress. *Journal of Structural Geology* 32(4), 537-553.
- ◇ van Gent, H. W., Urai, J. & De Keijzer, M. in press. The internal geometry of salt structures - a first look using 3D seismic data from the Zechstein of the Netherlands. *Journal of Structural Geology*. Doi: 10.1016/j.jsg.2010.07.005.

References

- ◇ Allan, U. S., 1989. Model for Hydrocarbon Migration and Entrapment Within Faulted Structures. *AAPG Bulletin* 73(7), 803-811.
- ◇ Anderson, E. M., 1942. *The Dynamics of Faulting*. Oliver&Boyd, Edinburgh, First edition, pp. 206.
- ◇ Angelier, J., 1979. Determination of the mean principal directions of stresses for a given fault population. *Tectonophysics* 56(3-4), T17.
- ◇ Angelier, J., 1989. From orientation to magnitudes in paleostress determinations using fault slip data. *Journal of Structural Geology* 11(1/2), 37-50.
- ◇ Angelier, J., 1990. Inversion of field data in fault tectonics to obtain the regional stress-III. A new rapid direct inversion method by analytical means. *Geophysics Journal International* 103, 363-376.
- ◇ Angelier, J., Bergerat, F., Dauteuil, O., Villemin, T., 1997. Effective tension-shear relationships in extensional fissure swarms, axial rift zone of northeastern Iceland. *Journal of Structural Geology* 19, 673-678.
- ◇ Back, S., Höcker, C., Brundiers, M. B., Kukla, P. A., 2006. Three-dimensional-seismic coherency signature of Niger Delta growth faults: integrating sedimentology and tectonics. *Basin Research* 18, 323-337.
- ◇ Borchert, H., Muir, R. O., 1964. *Salt Deposits. The Origin, Metamorphism and Deformation of Evaporites*. D. van Nostrand Company, Ltd., London, New York, Toronto, pp. 338.
- ◇ Bornemann, O., 1991. Zur Geologie des Salzstocks Gorleben nach den Bohrerergebnissen. *BfS-Schriften* 4, 1-67.
- ◇ Brown, S. R., Scholz, C. H., 1985. Broad Bandwidth Study of the Topography of Natural Rock Surfaces. *Journal of Geophysical Research* 90(B14), 12575-12582.

- ◇ Burliga, S., 1996. Kinematics within the Klodawa salt diapir, central Poland. In: Alsop, G. I., Blundell, D. J. & Davison, I. (Eds.), Salt tectonics. Geological Society Special Publication 100. Geological Society, London, 11-21.
- ◇ Callot, J.-P., Rondon, D., Rigollet, C., Letouzey, J., Pillot, D., Mengus, J.-M., 2006. Stringers and evolution of salt diapirs, insight from analogue models. 2006 AAPG International Conference and Exhibition, Perth, Australia.
- ◇ Candela, T., Renard, F., Bouchon, M., Marsan, D., Schmittbuhl, J., Voisin, C., in press. Characterization of Fault Roughness at Various Scales: Implications of Three-Dimensional High Resolution Topography Measurements. HAL: hal-00326981, version 1, available online at: <http://hal.archives-ouvertes.fr/hal-00326981/en/>.
- ◇ Carter, N. L., Handin, J., Russell, J. E., Horseman, S. T. (1993) Rheology of rocksalt. *Journal of Structural Geology* 15(9/10), 1257-1271.
- ◇ Chemia, Z., Koyi, H., Schmeling, H., 2008. Numerical modelling of rise and fall of a dense layer in salt diapirs. *Geophysical Journal International* 172, 798–816.
- ◇ Childs, C., Nicol, A., Walsh, J. J., Watterson, J., 1996. Growth of vertically segmented normal faults. *Journal of Structural Geology* 18(12), 1389-1397.
- ◇ Develi, K., Babadagli, T., 1998. Quantification of Natural Fracture Surfaces Using Fractal Geometry. *Mathematical Geology* 30(8), 971.
- ◇ Doblas, M., 1998. Slickenside kinematic indicators. *Tectonophysics* 295(1-2), 187.
- ◇ Evans, D. J., Chadwick, R. A. (Editors), 2009. *Underground Gas Storage: Worldwide Experiences and Future Development in the UK and Europe*. Geological Society, London, Special Publications, 313.
- ◇ Ferrill, D. A., Morris, A. P., 2003. Dilational normal faults. *Journal of Structural Geology* 25(2), 183-196.
- ◇ Franssen, R. C. M. W. (1993a) Rheology of Synthetic Rocksalt with Emphasis on the Influence of Deformation History and Geometry on the Flow Behaviour. Universiteit Utrecht, Utrecht, 113, 221.
- ◇ Frikken, H. W., 1999. Reservoir-geological aspects of productivity and connectivity of gasfields in the Netherlands. PhD thesis, Technical University Delft.
- ◇ Fry, N., 2001. Stress space: striated faults, deformation twins, and their constraints on paleostress. *Journal of Structural Geology* 23, 1–9.
- ◇ Geluk, M. C., 1995. Stratigraphische Gliederung der Z2-(Staßfurt-) Salzfolge in den Niederlanden: Beschreibung und Anwendung bei der Interpretation von halokinetisch gestörten Sequenzen. *Zeitschrift der deutschen Gesellschaft für Geowissenschaften* 146, 458-465.
- ◇ Geluk, M. C., 2007. Permian. In: Wong, T. E., Batjes, D. A. J. & De Jager, J. (Eds.), *Geology of the Netherlands*. Royal Netherlands Academy of Arts and Sciences, Amsterdam, 63 - 84.
- ◇ Geluk, M. C., Paar, W. A., Fokker, P. A., 2007. Salt. In: Wong, T. E., Batjes, D. A. J. & De Jager, J. (Eds.), *Geology of the Netherlands*. Royal Netherlands Academy of Arts and Sciences, Amsterdam, 283 - 294.
- ◇ Henk, A., 2005. Pre-drilling prediction of the tectonic stress field with geomechanical models. *First Break* 23, 53-57.

- ◇ Hinzen, K.-G., 2003. Stress field in the Northern Rhine area, Central Europe, from earthquake fault plane solutions. *Tectonophysics* 377, 325-356.
- ◇ Ilic, A., Neubauer, F., 2005. Tertiary to recent oblique convergence and wrenching of the Central Dinarides: Constraints from a palaeostress study. *Tectonophysics* 410, 465-484.
- ◇ Kleinspehn, K. L., Pershing, J., Teyssier, C., 1989. Paleostress stratigraphy: A new technique for analyzing tectonic control on sedimentary-basin subsidence. *Geology* 17, 253-256.
- ◇ Kokkalas, S., Jones, R. R., McCaffrey, K. J. W., Clegg, P., 2007. Quantitative fault analysis at Arkitsa, Central Greece, using terrestrial Laser-Scanning ("LiDAR"). *Bulletin of the Geological Society of Greece XXXVII (Proceedings of the 11th International Congress, Athens, May, 2007)*, 1-14.
- ◇ Koyi, H., 1996. Salt flow by aggrading and prograding overburdens. *Geological Society Special Publications* 100, 243-258.
- ◇ Koyi, H., 2001. Modeling the influence of sinking anhydrite blocks on salt diapirs targeted for hazardous waste disposal. *Geology* 29(5), 387-390.
- ◇ Larroque, J. M., Laurant, P., 1988. Evolution of the stress field pattern in the south of the Rhine Graben from the Eocene to the present. *Tectonophysics* 148, 41-58.
- ◇ Lee, J.-J., Bruhn, R. L., 1996. Structural anisotropy of normal faults. *Journal of Structural Geology* 18(8), 1043-1059.
- ◇ Lohr, T., Krawczyk, C. M., Oncken, O., Tanner, D. C., 2008. Evolution of a fault surface from 3D attribute analysis and displacement measurements. *Journal of Structural Geology* 30(6), 690-700.
- ◇ Marchal, D., Guiraud, M., Rives, T., 2003. Geometric and morphologic evolution of normal fault planes and traces from 2D and 4D data. *Journal of Structural Geology* 25, 135-158.
- ◇ Means, W. D., 1987. A newly recognized type of slickenside striation. *Journal of Structural Geology* 9(5-6), 585.
- ◇ Michon, L., van Balen, R. T., Merle, O., Pagnier, H., 2003. The Cenozoic evolution of the Roer Valley Rift System integrated at a European scale. *Tectonophysics* 367, 101-126.
- ◇ Mohr, M., Kukla, P. A., Urai, J. L., Bresser, G., 2005. Multiphase salt tectonic evolution in NW Germany: seismic interpretation and retro-deformation. *International Journal of Earth Sciences (Geologische Rundschau)* 94, 914-940.
- ◇ Muller, O.H., Pollard, D.D., 1977. The Stress State Near Spanish Peaks, Colorado Determined From a Dike Pattern. *Pure and Applied Geophysics*, 115, 69-86.
- ◇ Needham, D. T., Yielding, G., Freeman, B., 1996. Analysis of fault geometry and displacement patterns. In: Buchanan, P. G. & Nieuwland, D. A. (Eds.), *Modern Developments in Structural Interpretation, Validation and Modelling*. Geological Society Special Publication 99, 189-199.
- ◇ Neves, F. A., Al-Marzoug, A., Kim, J. J., Nebrija, A. L., 2003. Fracture characterization of deep tight gas sands using azimuthal velocity and AVO seismic data in Saudi Arabia. *The Leading Edge*, 469-475.
- ◇ Paulsen, T. S., Wilson, T. J., 2007. Elongate summit calderas as Neogene paleostress indicators in Antarctica. A Keystone in a Changing World – Online Proceedings of the 10th ISAES, USGS Open-File Report 2007-1047, Short Research Paper 072, 6 p.; doi:10.3133/of2007-1047.srp072.

- ◇ Plenefisch, T., Klinge, K., 2007. Spatiotemporal changes of the stress field in the Sunda Arc subduction zone after the 26 December 2004 Northern Sumatra earthquake inferred from inversions of earthquake focal mechanisms. 67. Jahrestagung der Deutschen Geophysikalen Gesellschaft, Aachen, 26-29 March 2007, Abstracts der 67. Jahrestagung der Deutschen Geophysikalischen Gesellschaft.
- ◇ Power, W. L., Durham, W. B., 1997. Topography of Natural and Artificial Fractures in Granitic Rocks: Implications for Studies of Rock. *International Journal of Rock Mechanics and Mining Sciences* 34(6), 979-989.
- ◇ Power, W. L., Tullis, T. E., 1991. Euclidean and Fractal Models for the Description of Rock Surface Roughness. *Journal of Geophysical Research* 96(B1), 415-424.
- ◇ Power, W. L., Tullis, T. E., Brown, S. R., Boitnott, G. N., Scholz, C. H., 1987. Roughness of natural fault surfaces. *Geophysical Research Letters* 14(1), 29-32.
- ◇ Power, W. L., Tullis, T. E., Weeks, J. D., 1988. Roughness and Wear During Brittle Faulting. *Journal of Geophysical Research* 93(B12), 15268-15278.
- ◇ Ramsay, J. G., Huber, M. I., 1987. *The Techniques of modern structural Geology. Volume 2: Folds and Fractures.* Academic Press, London Orlando San Diego New York Austin Boston Sydney Tokyo Toronto, pp. 391.
- ◇ Reinecker, J., Tingay, M., Müller, B., 2003. Borehole breakout analysis from four-arm caliper logs (guideline available online at www.world-stress-map.org).
- ◇ Renard, F., Voisin, C., Marsan, D., Schmittbuhl, J., 2006. High resolution 3D laser scanner measurements of a strike-slip fault quantify its morphological anisotropy at all scales. *Geophysical Research Letters* 33, L04305.
- ◇ Rocher, M., Cushing, M., Lemeille, F., Lozac'h, Y., Angelier, J., 2004. Intraplate paleostresses reconstructed with calcite twinning and faulting: improved method and application to the eastern Paris Basin (Lorraine, France). *Tectonophysics* 387, 1-21.
- ◇ Sagy, A., Brodsky, E. E., Axen, G. J., 2007a. Evolution of fault-surface roughness with slip. *Geology* 35(3), 283-286.
- ◇ Sagy, A., Brodsky, E. E., van der Elst, N., Di Toro, G., Collettini, C., 2007b. Geometrical and Structural Asperities on Fault Surfaces. AGU 2007 Fall Meeting, San Fransisco, Eos Transtricpts, 88 (53).
- ◇ Schleder, Z., Urai, J. L. (2005) Microstructural evolution of deformation- modified primary Halite from Hengelo, the Netherlands. *International Journal of Earth Sciences* 94(5-6), 941-956.
- ◇ Schléder, Z., Urai, J. L., Nollet, S., Hilgers, C., 2008. Solution-precipitation creep and fluid flow in halite: a case study of Zechstein (Z1) rocksalt from Neuhof salt mine (Germany). *International Journal of Earth Sciences* 97(5), 1045-1056.
- ◇ Schöpfer, M. P. J., Childs, C., Walsh, J. J., Manzocchi, T., Koyi, H., 2007. Geometrical analysis of the refraction and segmentation of normal faults in periodically layered sequences. *Journal of Structural Geology* 29, 318-335.
- ◇ Sippel, J., 2008. *The Paleostress History of the Central European Basin System.* Dr. rer. nat. thesis, Freien Universität.

- ◇ Sippel, J., Scheck-Wenderoth, M., Reicherter, K., Mazur, S., 2009. Paleostress states at the south-western margin of the Central European Basin System - Application of fault-slip analysis to unravel a polyphase deformation pattern. *Tectonophysics - Progress in understanding sedimentary basins* 470(1-2), 129-146.
- ◇ Smith, D. B., 1996. Deformation in the Late Permian Boulby Halite (EZ3Na) in Teesside, NE England. *Geological Society Special Publications* 100, 77-88.
- ◇ Spang, J. H., 1972. Numerical method for dynamic analysis of calcite twin lamellae. *Geological Society of America Bulletin* 83(1), 467-472.
- ◇ Sperner, B., Ratschbacher, L., Ott, R., 1993. Fault-striae analysis: a Turbo pascal program for graphical presentation and reduced stress tensor calculation. *Computers & Geosciences* 19(9), 1361-1388.
- ◇ Stephenson, B. J., Koopman, A., Hillgartner, H., McQuillan, H., Bourne, S., Noad, J. J., Rawnsley, K., 2007. Structural and stratigraphic controls on fold-related fracturing in the Zagros Mountains, Iran: implications for reservoir development. *Geological Society, London, Special Publications* 270(1), 1-21.
- ◇ Turner, F. J., 1953. Nature and dynamic interpretation of deformation lamellae in Calcite of three marbles. *American Journal of Science* 251, 276-298.
- ◇ Twiss, R. J., Moores, E. M., 1992. *Structural Geology*. W.H. Freeman and Company, New York, pp. 532.
- ◇ Van der Zee, W., 2001. Dynamics of fault gouge development in layered sand-clay sequences. Shaker Verlag, Aachen, PhD thesis
- ◇ van Eijs, R., Breunse, J., 2003. Evidence for two different creep mechanisms in rocksalt - Solution mining in the Barradeel concession. *TNO-NITG – INFORMATION*, 5-9.
- ◇ Vandycke, S., 2002. Paleostress records in Cretaceous formations in NW Europe: extensional and strike-slip events in relationships with Cretaceous-Tertiary inversion tectonics. *Tectonophysics* 357, 119-136.
- ◇ Will, T. M., Powell, R., 1991. A robust approach to the calculation of paleostress fields from fault plane. *Journal of Structural Geology* 13(7), 813-821.
- ◇ Williamson, M. A., Murray, S. J., Hamilton, T. A., Copland, M. A., 1997. A review of Zechstein drilling issues. *SPE Drilling & Completion* 13(3), 174-181.
- ◇ Wojtal, S., Pershing, J., 1991. Paleostresses associated with faults of large offset. *Journal of Structural Geology* 13(1), 49-62.
- ◇ Woods, P. J. E., 1979. The Geology of Boulby Mine. *Economic Geology* 74, 409-418.
- ◇ Yamaji, A., 2000. The multiple inverse method: a new technique to separate stresses from heterogeneous fault-slip data. *Journal of Structural Geology* 22, 441-452.
- ◇ Yamaji, A., Otsubo, M., Sato, K., 2006. Paleostress analysis using the Hough transform for separating stresses from heterogeneous fault-slip data. *Journal of Structural Geology* 28, 980-990.
- ◇ Zolohar, J., Vrabec, M., 2007. Paleostress analysis of heterogeneous fault-slip data: the Gauss method. *Journal of Structural Geology* 29(11), 1798-1810.

- ◇ Zulauf, G., Zulauf, J., Bornemann, O., Kihm, N., Peinl, M., Zanella, F., 2009. Experimental deformation of a single-layer anhydrite in halite matrix under bulk constriction. Part 1: Geometric and kinematic aspects. *Journal of Structural Geology* 31(4), 460.
- ◇ Zulauf, J., Zulauf, G., 2005. Coeval folding and boudinage in four dimensions. *Journal of Structural Geology* 27, 1061-1068.

Chapter 1: Paleostresses of the Groningen area, the Netherlands – results of a seismic based structural reconstruction¹

Abstract

We describe a novel workflow to reconstruct paleostress in the subsurface where the traditional outcrop-based method that uses fault-slip measurements is not possible. We use 3D seismic data and structural restoration to determine fault surfaces and slip vectors. These data are then used as input for paleostress-reconstruction algorithms.

The study area of ca. 750 km² is situated in the Groningen High, the Netherlands. Excellent quality 3D seismic data were used to interpret 11 horizons and approximately 80 faults between the Tertiary and the Top Rotliegend. Indicators of fault slip direction are fault undulations, sedimentary structures offset by faults, fault branch lines and shapes of horizon cut-outs. These indicators were used as a basis of 3D restoration of the interpreted horizons. A stepwise restoration approach was chosen that removed younger deformation to obtain slip vectors for older deformation events. In a following work step, Numeric Dynamic Analysis (NDA) was used to calculate paleostress tensors for the Middle and Lower Tertiary, Upper Cretaceous and Upper Rotliegend sequences.

The results presented in this paper are consistent with existing paleostress interpretations for NW Europe; however, in contrast to previous studies they are derived from a subsurface volume where paleostress information was lacking until now. Issues that need further study include the effect of the size of the study area on the assumptions of a homogenous stress field, and an analysis of the ambiguity of the interpretation of fault-slip indicators on 3D seismic data.

Keywords: Groningen High; paleostress; structural restoration; seismic interpretation; Central European Basin System.

Introduction

An understanding of the evolution of the stress field is essential in studies of the tectonic evolution of the crust (e.g. Gruenthal and Stromeyer, 1986). Furthermore, analysis of the paleostress field can help to explain fault reactivation, the timing and patterns of fault leakage and to analyse the migration of geofluids (Du Rouchet, 1981; Gartrell and Lisk, 2005; Henk, 2005).

There are many methods to determine the present-day in-situ stress. Earthquake focal mechanisms (e.g. Hinzen, 2003; Reinecker et al., 2005) provide information on the size and orientation of the stress

¹ Heijn van Gent, Stefan Back, Janos Urai, Peter Kukla, Kleus Reicherter. *Tectonophysics* 470, 2009, 147-161

tensor in seismically active areas. Analysis of borehole deformation and related methods (e.g. Gölke and Brudy, 1996; Reinecker et al., 2003, 2005) are widely used tools to establish the present stress field in the subsurface.

Quantifying stress in the past is much more difficult. Large scale fault patterns (e.g. Anderson, 1942; Michon et al., 2003) provide a first order estimate of the orientation of the principle stresses, without quantifying stress anisotropy. This Andersonian interpretation for example uses the observation of a newly formed North-South oriented graben system to postulate a vertical σ_1 (largest principle stress) and an E-W oriented σ_3 , while generally ignoring the possibility of oblique slip. Furthermore, the relative size of the principle stresses remains unknown. Andersonian interpretation has been used to quantify paleostress and the coefficient of static friction from deep seismic lines (see discussion in McBride, 1989). Field-based paleostress studies can provide information on the evolution of the entire paleostress tensor, as fault orientations and slip direction (as indicated by slickensides) can be measured directly. Slickensides should, according to the Wallace & Bott hypothesis (Wallace, 1951; Bott, 1959; Angelier, 1994), be parallel to the maximum resolved shear stress on the fault surface. This allows inversion of the field data to obtain the stress tensor. A correct separation of different fault populations is however essential (e.g. Bergerat, 1987; Larroque and Laurant, 1988; Hibschi et al, 1995; Vandycke, 2002; Reicherter and Peters, 2005; Caiazza et al., 2006; Sippel et al, in press, this volume). Some methods (like the NDA used in this work) however calculate the orientation and relative size of the principle strains instead of the principle stresses. Assuming coaxial deformation however, these strain axes can be considered to coincide with the stress axes (Sperner et al., 1993; Sperner, 1996; Ilic and Neubauer, 2005).

In the subsurface of sedimentary basins, 3D reflection seismic data can be used to map large numbers of fault surfaces in three dimensions. Provided that the slip vectors of these faults can be reconstructed, the paleostress analyses could be extended to much larger fault populations and rock volumes in the crust. The interception of faults with the surface is no longer required for paleostress studies. Previous analyses using this approach were presented by Gartrell and Lisk (2005) for the Miocene in the Timor Sea, and Lohr (2007) for the Rotliegendes of the Central European Basin.

In this paper we present a paleostress analysis of a structurally complex, subsurface setting in the Central European Basin System, using 3D seismic data. The high quality and quantity of 3D seismic data available for this study, and existing paleostress studies in the neighbouring countries make the Groningen area suitable for this approach. We estimated parts of the paleostress stratigraphy over a period of about 260 Ma and compared the results with published paleostress data from NW Europe. For this we studied the 3D seismic data set (provided by Nederlandse Aardolie Maatschappij, NAM, a Shell operated 50-50 joint-venture with Exxon Mobil) of the NW corner of the Groningen High, the Netherlands (Fig. 1). The workflow developed for this study consists of three steps: (i) a high resolution seismic interpretation that defines horizons and fault surfaces, with sufficient detail to locally support the analysis of the paleo-slip directions on individual fault surfaces, (ii) a stepwise 3D reconstruction to incrementally remove younger deformation and determine the direction of slip of earlier faulting, and (iii) the analysis of fault-slip and fault-orientation data to calculate paleostress tensors. The following

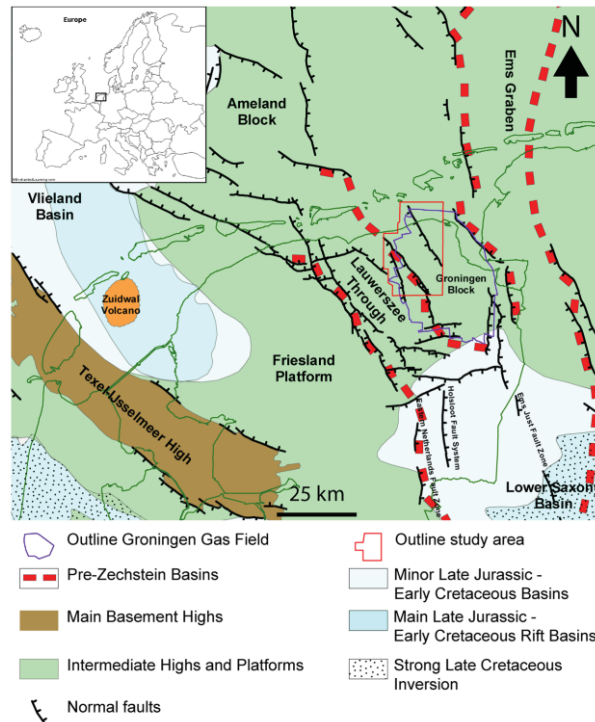


Figure 1: The study area in the NW corner of the Groningen High, a structural high bounded by the Lauwerszee Trough in the west, the Ems Graben in the east and the Lower Saxony Basin in the south (modified from NAM).

paragraphs provide an account of the data analysis and methodology used for this paleostress estimation based on 3D-seismic data, followed by a discussion on the applicability of this approach in settings where fault exposure is lacking and tectonic information is restricted to the subsurface.

Dataset

Our study is based on a high resolution, Pre-Stack Depth Migrated (PSDM) seismic volume of the Groningen High (Fig. 2), comprising 16 individual seismic surveys acquired between 1984 and 1988, and data from approximately 300 wells. For this study, the NW corner (25 by 35 km, Fig. 1) of this giant survey was selected because of its relative structural simplicity, the high quality of data and the relatively thick accumulation of Cenozoic deposits compared to other parts of the Groningen High. This allows for a more quantitative analysis of the Cenozoic stress field in this area than in other parts of the Groningen High.

Geological setting

The Groningen gas field is located on the Groningen High (Fig. 1). The Groningen gas field was discovered in 1959 after drilling of the Slochteren-1 well. This is the largest natural gas accumulation in Western Europe that initiated a revival of hydrocarbon exploration and production in the Netherlands (Breunse and Rispens, 1996). The Groningen High structure is part of the North Netherlands High

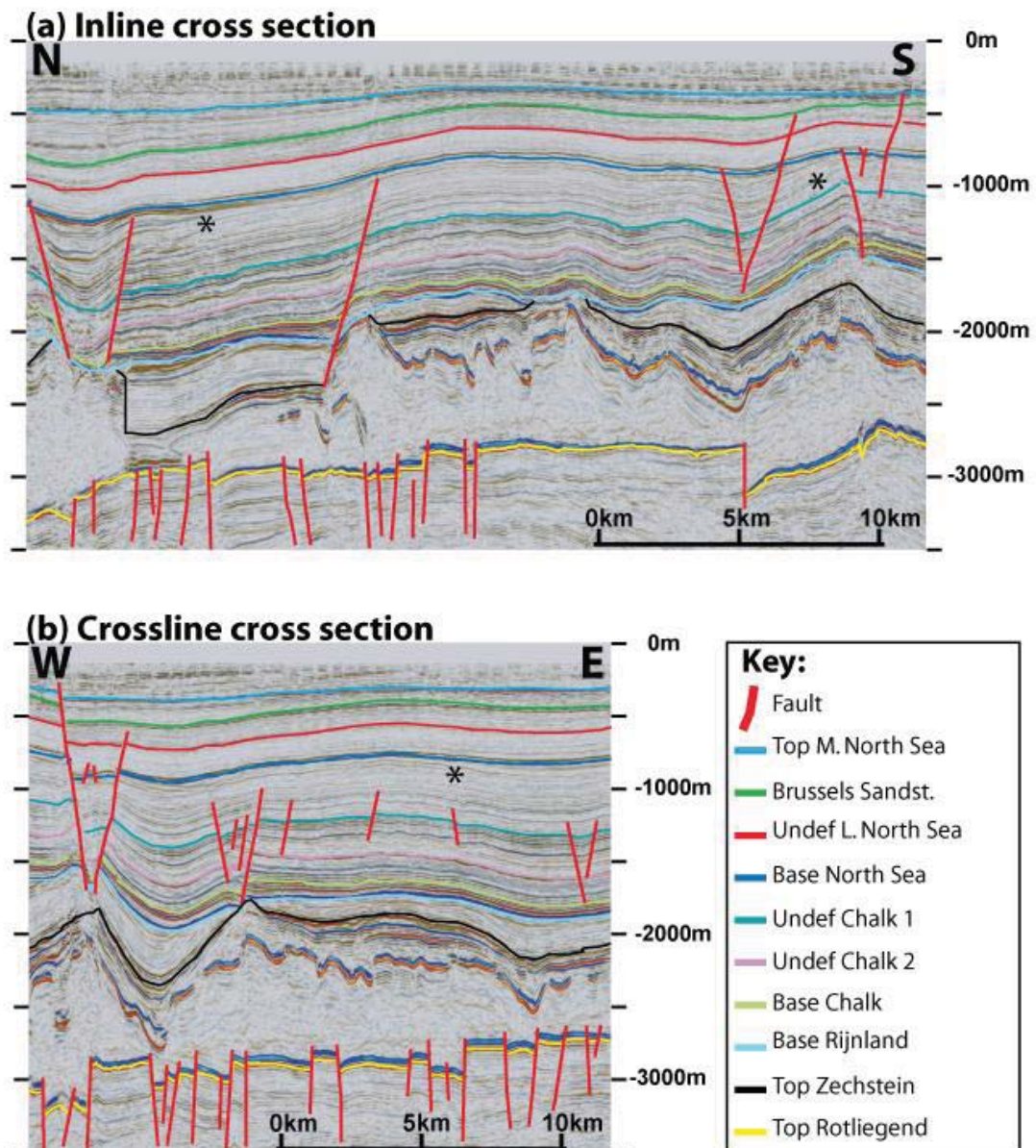


Figure 2: Representative interpreted seismic in- and cross-line from the Groningen area. Position of the sections is shown in Figure 6. Note steep segments of the Top Rotliegend horizon interpreted to represent faults. The stars denote locations of Chalk deposits being truncated by the Base North Sea Super Group. This erosion is not the result of localized fault inversion, but reflecting the uplift of the Groningen High as an internally stable block, sensu Stäuble and Milius (1970).

(TNO-NITG, 2004; Wong et al. 2007). The Groningen High is bounded by the Ems Graben in the east, the Lower Saxony Basin (LSB) in the south, and the Lauwerszee Trough in the West.

The Groningen High has been a relatively stable structure since the latest Jurassic, when the North Netherlands High was formed (Ziegler, 1982; TNO-NITG, 2004; Duin et al., 2006; Wong et al. 2007), and it has probably been a positive structural element since about the Late Carboniferous (Wong et al, 2007). Vitrinite reflectance data and magnetic anomalies have led to the inference of an intrusive body below the Groningen High of at least Kimmerian age, and apatite fission track data indicate an additional heat pulse in pre-Permian times (Kettel, 1983; Wong et al., 2007). The source rocks for the

Groningen gas field are Namurian and Westphalian coals and the reservoir rocks are Rotliegend (Permian) sandstones. The seal is formed by Zechstein evaporites (Van Adrichem-Boogaert and Kouwe, 1993-1997; Wong et al. 2007). The thickness of the Zechstein in this area varies between 500 and 1500 m (TNO-NITG, 2004) due to halokinesis that started in the Early Triassic (Mohr et al., 2005). The Triassic to Lower Cretaceous deposits of the Groningen High are relatively thin (max. 800m) due to erosion and non-deposition (Ziegler, 1982; TNO-NITG, 2004; Wong et al. 2007). The Upper Cretaceous Chalk Group is 400 to 1200m thick (TNO-NITG, 2004) and consists mainly of carbonates and marls. During the (Late Cretaceous) Subhercynian tectonic phase, parts of the chalks were locally eroded. In the surrounding areas the Laramide inversion (Latest Cretaceous) caused intense uplift, associated with truncation, erosion, fault reactivation and inversion. The NW corner of the Groningen High however, remained relatively stable with only minor regional uplift, archived in the erosion of the uppermost Cretaceous deposits, while along the southern fringes of the Groningen High, some minor inversion was documented (Stäuble and Milius, 1970; Ziegler, 1982; Van Wijhe, 1987; Dronkers and Mrozek, 1991; Van Adrichem-Boogaert and Kouwe, 1993-1997; Gras and Geluk, 1999; De Jager, 2003; TNO-NITG, 2004; Worum and Michon, 2005; Duin et al., 2006; Wong et al., 2007). The Cenozoic North Sea Supergroup, deposited from the Early Paleocene onwards is predominantly siliciclastic and between 500 and 1250 m thick (Van Adrichem-Boogaert and Kouwe, 1993-1997; TNO-NITG, 2004).

Methods

Interpretation

The selected seismic PSDM data (Fig. 2) were interpreted with high lateral resolution (25-50 m). Eleven mainly formation bounding horizons were interpreted from laterally continuous high-amplitude reflectors, partly based on interpretations done by NAM (see Table 1). During structural interpretation, particular attention was given to fault shapes, the mapping of en- echelon fault segments as arrays of multiple faults, and exact position and shape of horizons to prepare horizon-fault intersections or juxtaposition maps ("Allan map", see Allan, 1989). We interpreted 55 faults in the Supra-Zechstein and 23 at the Top Rotliegend level (Table 2), focussing on faults with sufficient spatial extent and throw to allow the estimation of the displacement vector. Data from 20 wells with (bio-) stratigraphic age constraints were used for accurate dating of the selected marker horizons. An overview of the interpreted horizons is given in Table 1. For one reflector in the Lower North Sea Group and for two reflectors in the Chalk group no well tops were available; the approximate age of these deposits was constrained by their position in wells (van Ojik, personal communication, 2007). The Lower North Sea reflector is of Middle Eocene age, probably Early Lutetian. The younger of the two undifferentiated Chalk reflectors is of Middle to Late Campanian age and the older Chalk reflector is from Late Santonian to Early Campanian age. In some places, poor seismic reflectivity limited horizon interpretation of the deeper reflectors in the Upper Cretaceous sequences.

Horizon:	Group:	Age:	Max depth (m):	Interpretation by:
Base Upper North Sea	Middle North Sea	Tertiary; Priaboran (19 Ma)	600	Authors
Brussels Sandstone Member	Lower North Sea	Tertiary; Ypresian to Lutetian (52 Ma)	1000	Authors
Undef. Lower North Sea reflector	Lower North Sea	Tertiary; E Lutetian (?), aprox. 45-48 Ma	1050	Authors
Base North Sea	Lower North Sea	Tertiary; Thanetian (60 Ma)	1300	NAM / Authors
Undefined reflector Chalk inside 1	Chalk	L. Cretaceous; M.-U. Campanian (75-80 Ma)	1700	Authors
Undefined reflector Chalk inside 2	Chalk	L. Cretaceous; Lower Campanian (82-84 Ma)	1900	Authors
Base Chalk	Chalk	L. Cretaceous; (E) Cenomanian (97 Ma)	2200	NAM / Authors
Base Rijnland	Rijnland	E. Cretaceous; Latest Ryazanian (140 Ma)	2250	NAM
Top Röt Salt Main Evaporite Member	Upper Germanic Trias	Triassic, E. Anisian (245 Ma)	2800	NAM
Top Zechstein	Zechstein	L. Permian; Thuringian (251 Ma)	2900	NAM
Top Rotliegend	Upper Rotliegendes	E. Permian; Saxonian (258 Ma)	3400	NAM

Table 1: Horizons described in this study, with ages based on seismic-to-well ties and their maximum depth. For three horizons no well ties were available and approximate ages are given based on stratigraphic position of the reflector (van Ojik, Personal communication, 2006).

Fault slip vectors

We carefully examined the data for all possible indicators of fault slip such as fault intersections, fault bifurcations, the shape of the fault surface (Cartwright et al., 1995; Needham et al., 1996; Marshal et al., 2003), displaced linear objects (Back et al., 2006), and similarities of horizon cut-offs in Allan Maps (Allen, 1989). In the Cenozoic section, the best indicators of fault slip were obtained by a combination of fault undulation (Fig. 3), matching structures on horizons on both sides of the fault (Fig. 4), and occasionally from the asymmetric shape the of the horizon cut-offs on Allan Maps (Fig. 5). Slip vectors were only reconstructed from faults which generated a significant horizon offset (>50 m). Faults that penetrated a horizon with offsets <50 m were classified as “not active” during the timeframe under review. The high-resolution 3D interpretation of faults revealed undulations on many fault surfaces.


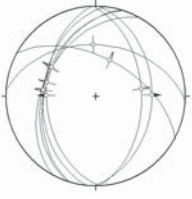
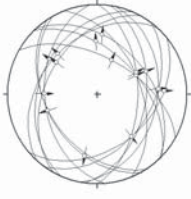
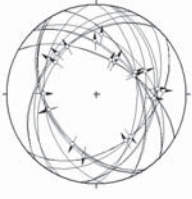


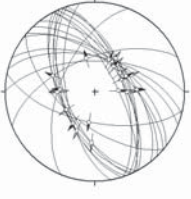
	No significant fault heaves after reconstruction.		Not reconstructed; deposits too thin.
Top Mid North Sea No: of Faults: 8	Base North Sea	Chalk_inside2 No: of Faults: 9	Base Rijnland
		No significant fault heaves after reconstruction.	Not reconstructed; deformation not brittle.
Brussels Sandstone No: of Faults: 15	All North Sea data No: of Faults: 23	Base Chalk	Top Zechstein
No significant fault heaves after reconstruction.			
Undef Lower North Sea	Chalk_inside1 No: of Faults: 18	All Chalk data No: of Faults: 27	Top Rotliegend No: of Faults: 23

Table 2: Orientation of reconstructed faults for each horizon. Arrows on the great circles show the reconstructed slip direction for the corresponding fault. For the reconstructed Tertiary and Cretaceous, an additional plot shows the combined data of the entire time period. All stereonets are lower-hemisphere, equal-area projections with North at the top of the circle.

These undulations are persistent when the interpretation is carried out at different angles to the fault (Fig. 3). The minor overprinting of the undulation by an interpretation-parallel curvature (most clear in Fig. 3c) shows that these features are not strongly influenced by interpretation effects. The fault surface undulations are often described to be parallel to the slip direction (Lee and Bruhn, 1996; Needham et al., 1996; Renard et al., 2006; Lohr, 2007; Kokkalas et al., 2007; Lohr et al., 2008). We interpret the undulations to be parallel to the last direction of fault movement, as only corrugations parallel to the most recent slip direction are likely to be preserved or even amplified, irrespective of their formation mechanism. (Kokkalas et al, 2007). A second method used for fault-slip analysis was matching of minor, elongated irregularities in the horizon on both sides of a fault (e.g. Fig. 4a), although it was not always clear what these features were (small faults or sedimentary features close to the limit of seismic resolution). We studied these features on the 3D horizons surrounding the fault

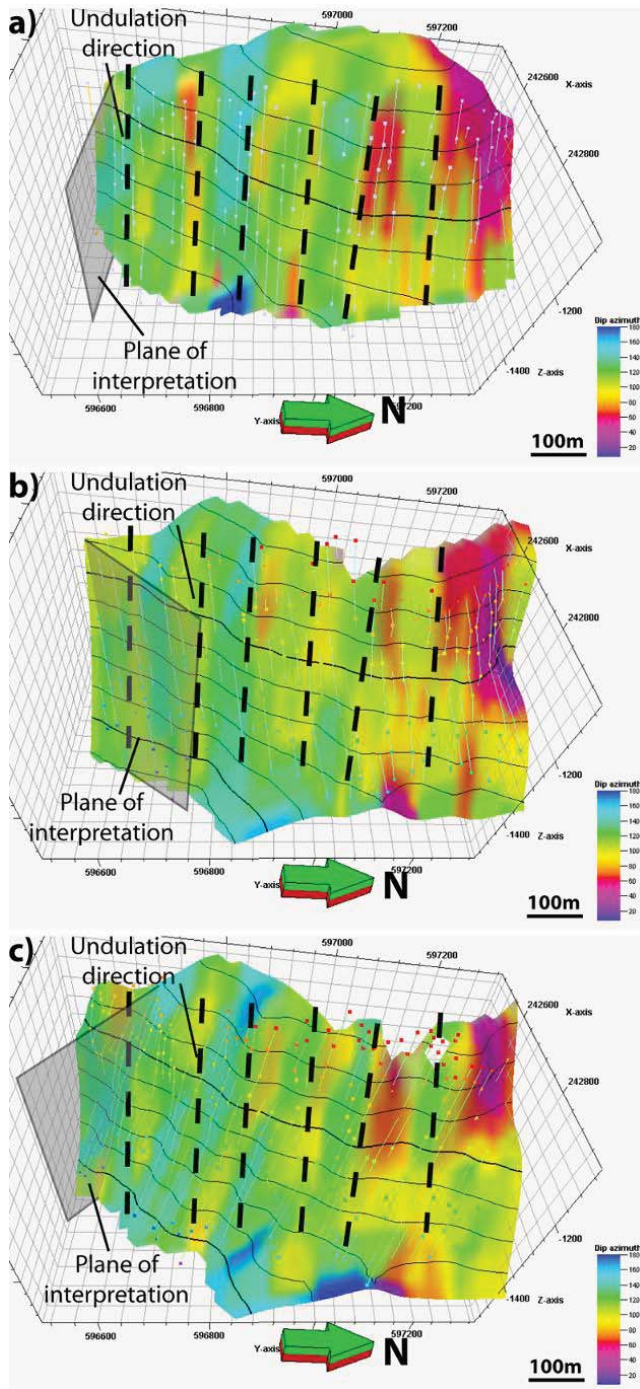


Figure 3: Three different sets of fault interpretation sticks (the 3D representation of the interpreted fault trace in cross section) and resultant interpolated fault surfaces of a single fault in the Upper Cretaceous, interpreted in three different directions. Fault sticks are indicated by the colored points connected by a colored line and a representation of the plane of interpretation is indicated. During interpretation, the plane is moved parallel to its normal about 25 m after the stick is interpreted in order to interpret the next stick. The resultant, interpolated fault surfaces are slightly smoothed and colored for dip direction (azimuth). The exact shape of the fault surface is controlled by the fault sticks, and since these are different in each interpretation, the size and shape of the surface also varies. The black horizontal lines are depth contours. Several systematic changes in the dip direction of the fault (indicated by dashed black lines) are present in all three interpretation directions, documenting that these trend lines are consistent and independent of interpretation direction. Note that in c), the undulations are still present but slightly overprinted by undulations in the interpretation direction, documenting the sensitivity of this type of analysis with respect to the individual interpretation input. In all interpretations, the undulation wavelength is larger than interpretation distance (25m.)

(see Fig 4a), rather than on the projection of the horizon on the fault surface (the pure Allan map), as the lateral continuity and 3D shape of the features often indicated whether these

features were real or interpretation artefacts.

Thirdly, we analyzed the shape of the horizon-fault intersections in plan view for indicators of the slip direction. In Figure 4b, the matching of convex and concave shapes on both sides of the fault surface strongly indicates the opening direction of this fault. Similar to the analysis of fault undulations, the geometry matching of fault footwall and hangingwall was very sensitive to the quality of the preceding fault and horizon interpretation. The fourth method used the shape of the Allan map between the two

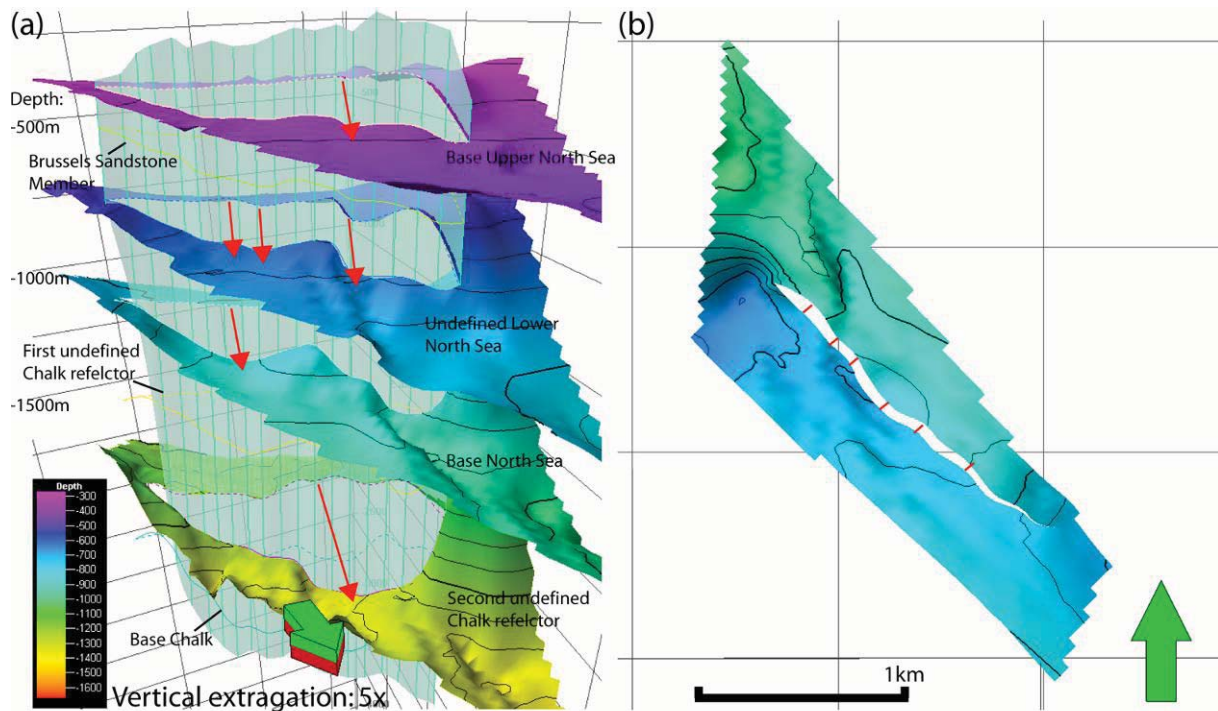


Figure 4: (a) A fault with Allan lines (horizon cutoffs) of a Cenozoic fault from this study illustrating the footwall and hangingwall horizon cutoffs projected on the fault surface. The solid lines represent the hangingwall cutoffs, and the dashed lines are the fault-footwall intersections. For four horizons, parts of the associated 3D surface are shown (shaded for depth). These show the 3D continuation of the corrugations of the Allan lines. These were used to estimate slip direction by the matching of shapes across the fault. Several possible slip directions are indicated by arrows. (b) Top view of the fault cutout of a chalk horizon. The convex and concave shapes on both sides of the fault surfaces can be connected to estimate slip direction.

tips of the fault (Fig. 5), proposing that the obliquity of slip produced an asymmetry in the Allan map of an initially horizontal reflector. The parallelism of the slip arrows in Fig. 5 is an obvious simplification, as slip on normal faults becomes more oblique and rotated in the direction of the centre of the fault towards the tip lines (Roberts, 1996; Morewood and Roberts, 2000; Cowie and Roberts, 2001). Note that the analysis of the asymmetry of the Allan map can be e.g. used to support the slip interpretation presented in Fig. 4. In summary, a combination of these four approaches can be used directly for slip approximation of the youngest deformation phase. This deformation needs to be sequentially removed from deeper horizons, before Allan lines representing older tectonic phases can be established for these levels.

Structural reconstruction

The software package 3DMove was used for 3D retrodeformation and the measurement of the slip vectors. The tectonic reconstruction served two goals: (i) to measure and test the azimuth and plunge

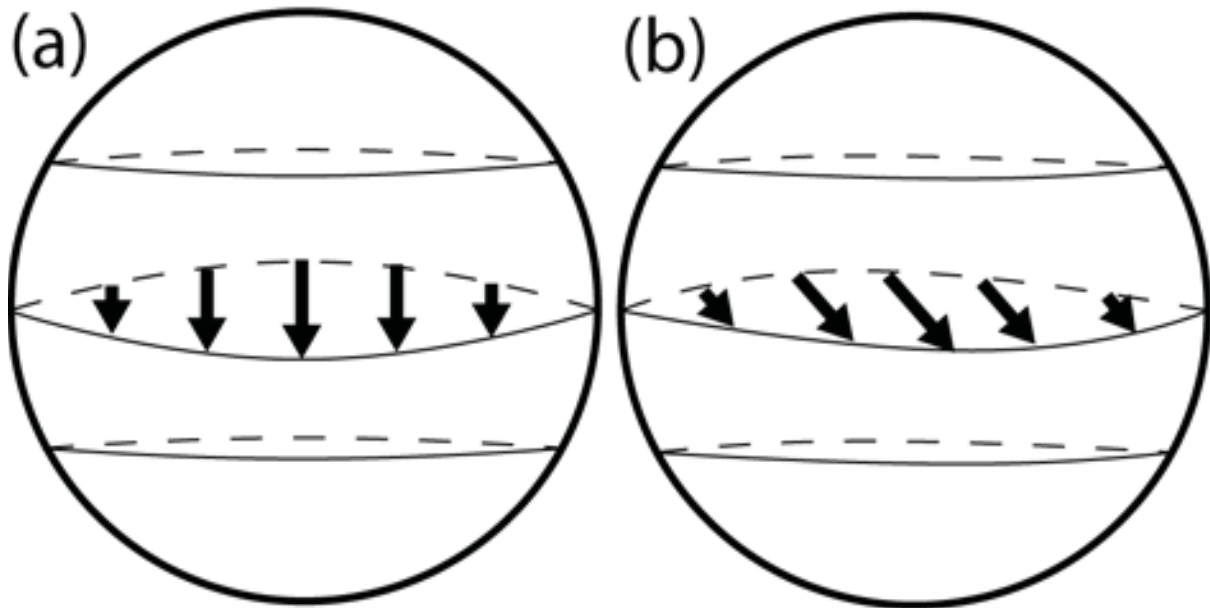


Figure 5: (a) Theoretical Allan Map of a circular fault with pure dip-slip displacement cutting three horizontal horizons. Dashed line is the footwall cutoff, the continuous line is the hangingwall cutoff and the bold line is the tip-line (zero-displacement line) of the fault. (b) Theoretical Allan Map of a circular fault with oblique-slip displacement cutting three horizontal horizons. Note the asymmetry in the Allan map that can be used as an indication of fault slip.

of the proposed slip vector, and (ii) to remove younger deformation in order to estimate movement vectors on deeper horizons.

Throughout the study area, all interpreted horizons are sub-horizontal in all fault blocks, which justified a sequential restoration by inclined shear. This algorithm was used to move the respective hangingwall blocks to their original position, based on the shape of the associated fault. A restoration was accepted when hangingwall and footwall blocks fitted along the entire length of the fault surface, without significant rotation of the horizon. Since the reconstructed geometry depends on the general shape of the fault surface, an erroneous movement vector could produce rotations or gaps between the footwall and hangingwall, making this an important quality-control tool. Prior to reconstruction of deeper horizons, the deformation of the overlying horizons had to be removed. This was done using 3DMove's Unfold-to-Target/Inclined-Shear algorithm that unfolded a selected target horizon to a predefined datum surface by vertical shear, carrying all other objects (both horizons and faults) as passive objects along while maintaining the same vertical distance to the selected horizon. The assumption to justify this step is that all horizons were deposited horizontally. Frequently, an unexpected result after this restoration step was a small area of increased horizon dip on the footwall side of faults. This artefact was produced by an erroneous projection of the vertical restoration vectors across inclined faults. The resulting "pull-ups" were manually removed by deleting the area of increased dip and "snapping" the remaining horizon back to the fault. No decompaction was performed in this study, as estimates of the change in fault dip due to the removal of compaction indicated that these values were less than the uncertainty in orientation due to interpretation.

During the stepwise restoration of the study area down to the Base Chalk level, we collected data on the dip direction and dip of faults together with azimuth and plunge of the slip vector from each restoration step for the subsequent use in paleostress analysis. Because of the presence of the ductile Zechstein salts above the Top Rotliegend, it was not possible to reconstruct all the way down to Top Rotliegend level.

It should be noted that the uncertainty in slip direction determination of faults that resulted from the structural reconstruction described above was partly compensated by the fact that almost all horizons contained two types of fault; “Older” faults that penetrate multiple horizons and already underwent restoration, and “fresh” or “blind” faults terminating in the target horizon that remained unaffected by previous reconstructions. An example of the occurrence of these “fresh” faults is the marked increase of faults between the Base Upper North Sea and the Brussels Sandstone (Table 2).

Paleostress methods

A number of different methods have been previously developed to calculate paleostress from fault orientations and slip vectors, e.g. the Direct Stress Inversion (DSI, Angelier, 1990) is based on the inversion of the Wallace & Bott hypothesis (Wallace, 1951; Bott, 1959; Angelier, 1984, 1994). This hypothesis states that slip on a fault surface is in the simplest case parallel to the direction of the maximum resolved shear stress on that plane. Shear stress can be calculated using the shear tensor and the orientation of the plane. Therefore, knowledge of the orientation of a fault surface and the direction of fault slip on this fault allows one to inverse the Wallace & Bott hypothesis and to calculate the direction of shear stress on the fault. Combining data from multiple faults then allows the calculation of the paleostress tensor (e.g. Angelier, 1984, 1990). DSI uses a least square algorithm to calculate the stress tensor, by minimizing the sum of the angles between the measured slip vectors, and the calculated shear stress for all faults. The use of the least square criterion implies that the method is relatively sensitive to outliers and inhomogeneities in the input data.

The Numeric Dynamic Analysis (NDA, Turner, 1953; Spang, 1972; Sperner et al., 1993) is based on the Mohr-Coulomb criterion and was initially used to calculate stress from twin lamellae in calcite crystals. NDA calculates the kinematic axes that, assuming coaxial deformation, coincide with the stress axes (Sperner et al., 1993; Sperner, 1996; Ilic and Neubauer, 2005). This method involves the calculation of the orientation of the compression and tension axes for each fault. These axes, that are perpendicular to each other, lie in the plane normal to the fault and in the direction of the movement vector. The friction angle θ (Θ , the angle between the pressure axis and the fault surface) needs to be defined prior to calculation. In this study, the “best fit angle” was used. This angle is found by analyzing the alignment of the P- and T axes. A tensor is then calculated (in the coordinate system defined by the fault and slip vector) by assuming a value of +1 in the direction of the compression axis, and a value of -1 in the direction of the tension axis as relative values. A tensor rotation transforms this into a real-world coordinate system, where concentrations of P- and T-axes are then interpreted to represent the orientation of σ_1 and σ_3 respectively.

In this study, NDA was preferred over DSI because NDA was less sensitive to outliers, as shown several tests using synthetic data (Appendix 2-5), and discussed by Sperner et al. (1993). Therefore,

data with deviations in the fault-slip vector or faults with orientations caused by local stress heterogeneities did not strongly influence the results. A comparison of the calculated DSI-tensors from this study and the faults used to calculate these tensors, often showed that fault systems dominated by normal faults (see Table 2) resulted in the calculation of compressional stress tensors. Tensors calculated with NDA did not exhibit this discrepancy.

Neither NDA nor DSI calculate the absolute stress/strain tensor, but only the orientation and the ratio of the principle stresses. In this study, the stress ratio R was defined as

$$R = \frac{(\sigma_2 - \sigma_3)}{(\sigma_1 - \sigma_3)}$$

with σ_1 , σ_2 and σ_3 as the principle stresses of the stress tensor, calculated either using DSI or NDA. In this study we used the implementation of the DSI and NDA methods in the program TectonicsFP (Ortner et al., 2002).

Fault interpretation results

Supra-Zechstein Faults

The mapped faults above the Zechstein mainly define graben or half-graben structures, and there are three main trends visible (Fig. 6). In the SW, a clear NW-SE orientation prevails parallel to the Lauwerszee Trough and the Rotliegend fault pattern. Along the western border of the study area, the structural trend of the interpreted fault orientation is N-S. In the N part of the studied volume, the fault orientation is generally NE-SW (Fig. 6). In the central and eastern part of the volume, no faults extending into the Tertiary succession were observed and faults in the Cretaceous were only interpreted when they had a significant throw (>50 m).

Many faults in the Upper Cretaceous Chalk and Tertiary clastics show indications of growth such as increased sediment thickness in the hangingwall (see Fig. 2). The number of faults in the Cretaceous is larger than the number of faults in the Cenozoic.

The supra-Zechstein faults in this dataset have a length between 1 and 6 km, with throws generally ranging between 50 and 200 m. Their location correlates in many cases with underlying Zechstein salt structures. In 3D the faults are slightly elliptical to rectangular, with a concave upward shape. Many of these fault surfaces, particularly in the Cretaceous

section, are undulated, with the corrugations being independent of the orientation of the interpretation cross section (see Fig. 3). Segmented faults were only observed in the Upper Rotliegend. For Mesozoic and Cenozoic faults that were not undulated we used the other methods described above to determine fault slip (Fig. 4 and 5). Additionally, complex fault assemblages, antithetic fractures and the geometries of splays were mapped as a secondary slip direction indicator.

Reactivation of a fault during later deformation may change the shape of the undulations on the fault surface. Therefore, we only used data on the direction of undulations for faults that were not reactivated.

Rotliegend faults

The Rotliegend faults consist of a number of linked concave and convex fault segments, with some relay ramps. These segmented faults directly indicate fault slip direction. The segments are an indication of the first stage of faulting before the fault was formed by subsequent fault linkage (e.g. Needham et al., 1996; Walsh et al., 1999; Schöpfer et al. 2007; Lohr, 2007; Lohr et al., 2008). The Rotliegend faults generally are longer than the survey, and have a NW-SE orientation. In Fig. 6 and Table 2 the orientation of the Rotliegend faults are shown. The ductile overlying salt makes it difficult to accurately time the deformation of the Top Rotliegend reflector. Well data showed that the strong reflector directly above the Top Rotliegend reflector (Fig 2), represents Zechstein deposits up to and including the Z2 Basal Anhydrite Member (267.5 Ma, Van Adrichem-Boogaert and Kouwe, 1993-

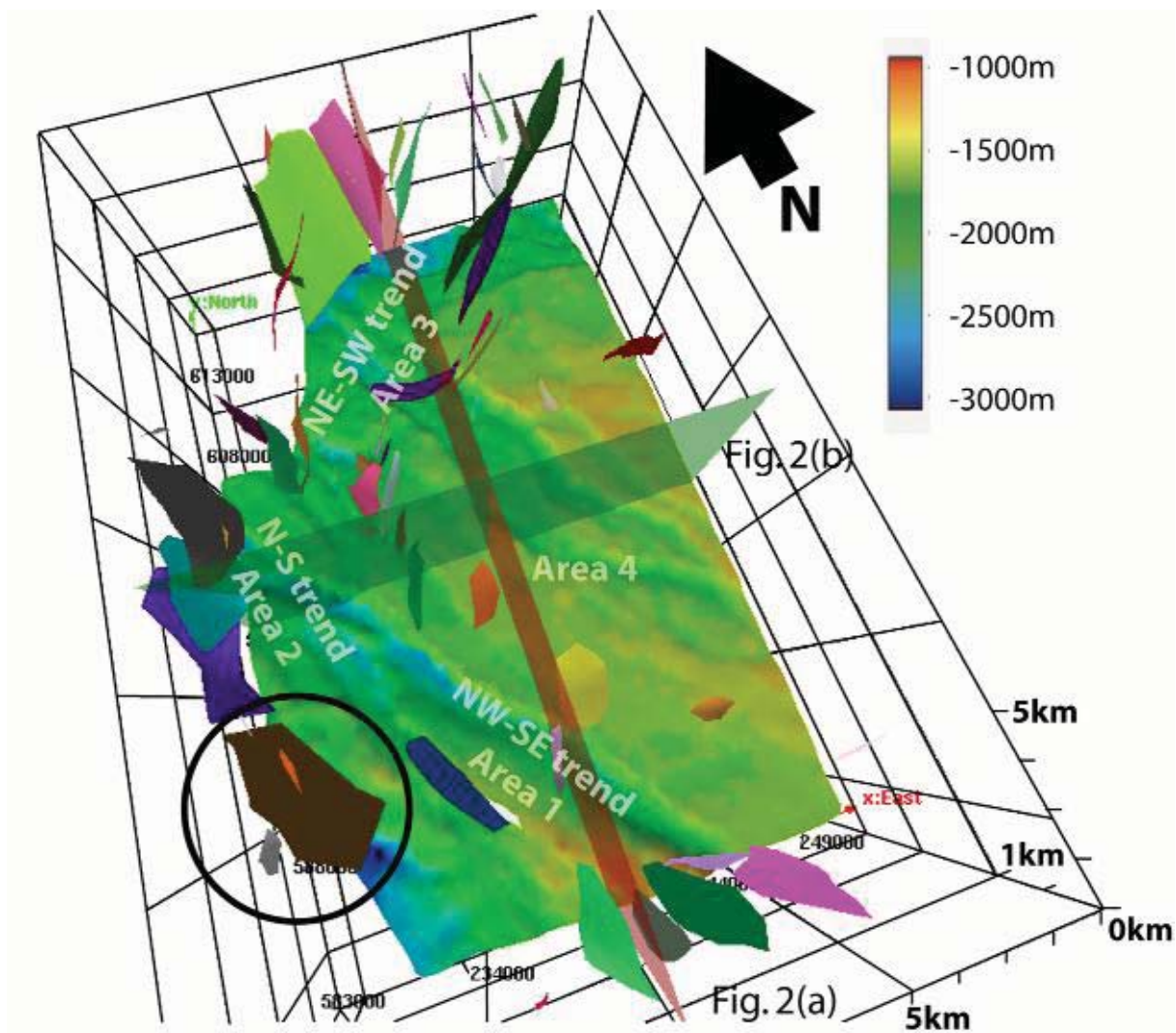


Figure 6: Oblique view of the model with all supra-Zechstein faults and the Top Rotliegend horizon. Note the agreement of the NW-SE fault trend with the general Top Rotliegend fault orientation. N-S oriented plane indicates position of inline cross section in Fig. 2 (a); the E-W oriented plane is the position of crossline (b). The circle encloses the fault shown in Fig. 3. The vertical exaggeration of the model is 3x.

1997). This Zechstein reflector is clearly faulted by the same event as the Top Rotliegend, and no syntectonic deposition is observed, documenting that the studied faulting of Top Rotliegend did not start before mid-Zechstein time.

Retro-deformation and paleostress results

After retro-deformation, from the 7 Cenozoic and Upper Cretaceous horizons only the two top Tertiary and the two top Upper Cretaceous horizons exhibited sufficient fault displacement (>50 m) for further

Paleostress axes:	Histogram:	Paleostress axes:	Histogram:
	Θ - angle	R-value	Θ - angle
			R-value
Top Middle North Sea	48°	0.40	NWGronn_CK_inside1.cor
			54°
			0.38
Brussels Sandstone	50°	0.12	Chalk_inside2
			48°
			0.38
All North Sea data	52°	0.20	All Chalk Data
			52°
			0.38
<ul style="list-style-type: none"> = σ_1 = σ_2 = σ_3 			
			Top Rotliegend
			32°
			0.40

Table 3: Paleostress results for the horizons reconstructed in this study showing the principle stress orientations and histograms of residuals together with the best fit Θ -angle and the R-value (ratio of the principle stresses). Stereonets are lower hemisphere, equal-area projections with North at the top of the circle.

analysis. The Top Rotliegend Horizon was not reconstructed due to the uncertainties in the timing of faulting due to by the decoupling effect of the Zechstein salts. The segmented faults, however, provided a slip direction for the time of fault formation. The orientation and slip direction of the retro-deformed Post-Zechstein faults in the reconstructed horizons and the Rotliegend faults are given in Table 2.

Table 3 shows the paleostress results calculated using the NDA-method. The stereoplot provides the estimated orientations of the principal stress axes. The R-value is the ratio between the principle stresses. In the histogram of residuals the difference between calculated and measured lineations is depicted. A homogeneous dataset (data from a single tectonic event and reasonably homogeneous stress field) may be assumed to have normally distributed residuals. Residuals with bimodal or skewed distribution indicate a stress field that is heterogeneous or that faults moved during different phases.

Top Rotliegend

Results from the 23 reconstructed faults at Top Rotliegend indicate a near-vertical σ_1 , with σ_2 oriented NW-SE (Table 3). R has a value of 0.40. The best-fit theta angle for this horizon is 32°.

Upper Cretaceous

Results from the 18 reconstructed faults of the first horizon in the Cretaceous shows a vertical σ_1 and a NNE-SSW oriented σ_2 (Table 3). The second reflector of the Cretaceous Chalk also has a near vertical σ_1 and a NNE-SSW oriented σ_2 . For both horizons, the minimum stress σ_3 is oriented WNW-ESE. At Base Chalk, fault displacement became zero when the overlying deformation was removed. This indicates that deformation of this horizon started after the deposition of the succeeding Chalk horizon. This period of tectonic quiescence in the early Late Cretaceous in the Netherlands is also observed in other studies (Ziegler, 1982; Van Wijhe, 1987; De Jager, 2003). R-values of both horizons are 0.38. The stress results for the two Upper Cretaceous horizons are similar, and are interpreted to reflect the same tectonic phase. The combined data from these horizons shows a stress tensor with a vertical σ_1 , a NNE-SSW oriented σ_2 , and σ_3 at WNW-ESE (Table 3). The R-value for the combined data is 0.38.

Tertiary

In the Tertiary succession only few faults have sufficient throw for reconstruction. The faults in the Base Upper North Sea Group horizon show a near vertical σ_1 , and a NW-SE σ_2 after the paleostress inversion (Table 3). The R-value for the Base Upper North Sea is 0.29. The Brussels Sandstone also has a near vertical σ_1 , and near NNW-SSE oriented σ_2 (Table 3), with an R-value of 0.17. The undefined Lower North Sea horizon and Base North Sea horizon were flat after the removal of the deformation of the overlying horizons. This indicates that after the deposition of these horizons no tectonic activity occurred until after the Brussels Sandstone member was deposited and deformed. This period of tectonic quiescence clearly separates the deformation of the Upper Cretaceous horizons from the deformed Tertiary horizons. The Upper Cretaceous deformation thus most likely represents a different tectonic phase than the phases that deformed the Base Upper North Sea and Brussels

Sandstone horizons. On basis of the differences in stress axis orientation and R-value, the Base Upper North Sea and Brussels Sandstone paleostress results were also interpreted as two different phases of deformation.

Discussion

Methodology

A basic assumption of nearly all paleostress methods is that of a homogeneous stress field on the scale of the study. The first order validity of this assumption is based on consistent results of field studies (e.g. Bergerat and Geysant, 1983; Bergerat, 1987; Larroque and Laurant, 1988; Bles et al., 1989; Sperner et al., 1993; Hibsich et al., 1995; Vandycke, 2002; Hinzen, 2003; Reicherter and Peters, 2005), but also on the basis of numerical studies for the case of the lack of fault interaction (Dupin et al., 1993; Pollard et al., 1993). Nevertheless, there are a number of possible situations where these assumptions do not hold. Stress fields are generally not homogeneous, and fault tips, fault irregularities and fault bends, as well as anisotropies such as deep rooted structural elements, sedimentary inhomogeneities and batholiths may result in local stress deflections on different scales (e.g. Dupin et al., 1993; Angelier, 1994; Gruenthal and Stromeyer, 1994; Maerten et al., 2002).

An important issue in this respect is the large size of the study area (25 km by 35 km) whilst the scale of outcrops is typically 5 to 50 m. Paleostress analyses based on field measurements can be considered as point datasets, whereas this study calculates the paleostress for an area of 750 km². Therefore, we needed to test the assumption of a homogeneous stress field. This was done in a bootstrapping study of the data (Appendix 3), subdividing the study area in 4 parts as shown in Fig. 6, and re-calculating the paleostress for these individual parts, using only those faults that were present in that part. The results from these analyses were internally very similar and compared well with the original data of the entire survey. This supports the assumption of homogeneous stress at the scale of the study area.

In this study, slip direction was established by analysis of fault surface undulations, interpretation of Allan maps, and matching of irregularities in the horizons on both sides of a fault. Faulted channels and unconformities (Back et al., 2006) were absent in this dataset. Segmented faults (Cartwright et al., 1995; Roberts, 1996; Marchal et al., 2003; Lohr, 2007; Lohr et al., 2008) are only observed in the Rotliegend horizon. The mechanism by which the undulations used in this work to constrain paleoslip are formed however remains unclear. The coalescence of older faults (sensu Schöpfer et al. 2007; Lohr et al., 2008) is a possibility, or it could reflect an inherent roughness of fault planes which forms during initial failure. Irrespective of the formation, corrugations in the most recent slip direction have the highest potential to be preserved or even amplified (Lee and Bruhn, 1996; Renard et al., 2006; Kokkalas et al., 2007).

Gartrell and Lisk (2005) have published paleostress results based on 3D seismic data from the Neogene deposits of the Timor Sea. They unfolded horizons to remove ductile deformation effects and bed rotations, after which both the flattened hangingwall and footwall horizons were restored to a specified level. In a following step, a rigid body translation was used for the restoration of the remaining horizontal separation. This two-stepped approach does not differ much from the restoration

used in this work. However, the flexural slip unfolding might introduce errors during restoration, especially at fault tips and relay ramps, and when fold axes are non-parallel (Gartrell and Lisk, 2005). This unfolding step was not part of this study as horizons within all studied fault blocks were almost horizontal.

It is important to discuss the effect of errors in slip direction determination from seismic data. Although interpretation uncertainties are more than compensated by the large volume of structural data available for the study, individual determinations are less accurate than those measured in the field using slickensides. Therefore, we carried out a Monte Carlo analysis with the slip direction in three datasets (see Appendix 2). We introduced normally distributed errors with a standard deviation of 2°, 9° and 20° in a set of 20 randomly selected faults from the present data set, as well as a homogeneous set of fault measurements based on field data from the Mammendorf Quarry (Southern Inverted Margin of the Southern Permian Basin, Germany, Sippel et al., in press, this volume) and an artificial dataset from Shan et al. (2003). The slip vector was rotated around the normal vector of the fault surface. This way, 50 modified datasets were prepared for every combination of data source and standard deviation. Results show that with increasing standard deviation of the introduced errors, the NDA method produced results where the average orientations of the principle stresses and the stress ratio remained roughly constant, but the variance increased significantly with increasing standard deviation. Using the same data with DSI produced similar results, but with an even higher variance. For about 5% of the Mammendorf results and 10% of the data set of this study, a completely different stress tensor was calculated, which did not fit the observed faults. We believe this results from the least squared criterion based calculation of the DSI, where outliers strongly influence the result. This might also be the reason why the DSI method did not produce internally consistent tensors in this study.

Discussions of the validity of the basic paleostress assumptions by e.g. Dupin et al. (1993), Pollard et al. (1993) and Gapais et al. (2000) focus on outcrop scale studies. It is reasonable to assume that the same features that cause problems in field-based paleostress analyses (closely spaced parallel faults, fault interaction, fault-bend rigidity, proximity to other faults, faults with a high length-to-width ratio and proximity to the earth surface) also influence paleostress analysis in the presented scale. Stress deflections occurring on a scale larger than that of a field study (e.g. stress deflection at the tips of a multi-kilometre fault zone, or around crustal fault zones or batholiths) may be documented in a densely sampled field study where many sites are investigated, while on the seismic scale presented here, these deflections are not apparent. It is clear that the validity of the basic stress inversion assumptions on the scale of this study need further evaluation, which can be achieved by a direct comparison of our results with known data from the same area.

For NW Europe, two different kinds of stress fields are generally recognized for the Meso- and Cenozoic (Bergerat and Geysant, 1983; Bergerat, 1987; Bles et al., 1989; Hibsich et al., 1995; Vandycke, 2002); an extensional stress field, interrupted by short, compressional stress states associated with the Alpine tectonic phases. Numerical modelling has shown that the present-day stress field of NW Europe is the result of the combined forces exerted by the European-African collision and ridge push at the Mid Atlantic Ridge (Gruenthal and Stromeyer, 1994, Gölke and Coblentz, 1996). When comparing the temporarily closely spaced, but tectonically very different,

extensional and inversion stress fields for the Cretaceous (Vandycke, 2002), it is common to find the maximum horizontal compressive stress (SH) to have the same orientation (see also Fig.7). This can be explained by that the stress ellipsoid during the Cretaceous is almost purely constrictional ($\sigma_1 \approx \sigma_2 > \sigma_3$, and σ_3 is horizontal, oriented NW-SE) so that small changes in the horizontal stress σ_H result in a switch or permutation (sensu Larroque and Laurant, 1988) in the principle stress directions. These changes might result from a variation in the contributions of tectonic forces and ridge push on the stress field of NW Europe. Our Cretaceous paleostress results show values of R of roughly 0.4, more representing a stress state with $\sigma_1 > \sigma_2 > \sigma_3$. The fact that we do not find R values supporting this model might be explained by the inherent uncertainty in slip direction determination, as suggested by our Monte Carlo analysis (Appendix 2).

Geology

Rotliegend

Hibsch et al (1995) and Bles et al. (1989) describe an earliest Zechstein NS extension in the UK and France. However, the coeval faulting of Z2 Basal Anhydrite member and the Top Rotliegend Horizon shows that the oldest tectonic phase interpreted in the Groningen dataset did not start before the Mid Zechstein, but its upper limit is not well constrained. A thickness analysis between the Top Rotliegend and the Z2 Anhydrite reflectors show that the EW trending faults in the survey were not active between the deposition of these strata (Table 2). Paleostress data from Southern Germany, Southern France (Reicherter et al., 2008 and references cited therein), and the UK (Hibsch et al., 1995) (Fig. 7) shows that the late Triassic to Jurassic stress field is described by a vertical σ_1 and a NW-SE oriented σ_2 (since σ_1 is vertical, σ_2 is equal to the maximum horizontal compressive stress, SH). The paleostress analysis of the Top Rotliegend horizon in this study is therefore interpreted to represent Triassic extension (Fig. 7). Lohr (2007) published a paleostress state based on 3D seismic data from the Aller Lineament with comparable orientation.

Late Cretaceous

As mentioned above, the tectonic state during the Cretaceous in NW Europe was characterized by prolonged extensional periods that were interrupted periodically by strike-slip/compressional events (Vandycke, 2002). Paleostress results from Sussex and Kent (UK), Boulonnais (N France) and the Mons Basin (Belgium) showed E-W to NW-SE extension (Vandycke, 2002), very similar to the results of the present study. The studied Upper Cretaceous Chalk reflectors are below the Subhercynian unconformity (see Fig. 7) but no evidence is found for tectonic inversion or fault reactivation within the seismic volume. Vandycke (2002) and De Jager (2003) showed furthermore that the effects of inversion events in the Upper Cretaceous were restricted to a few areas. Effects of the Subhercynian

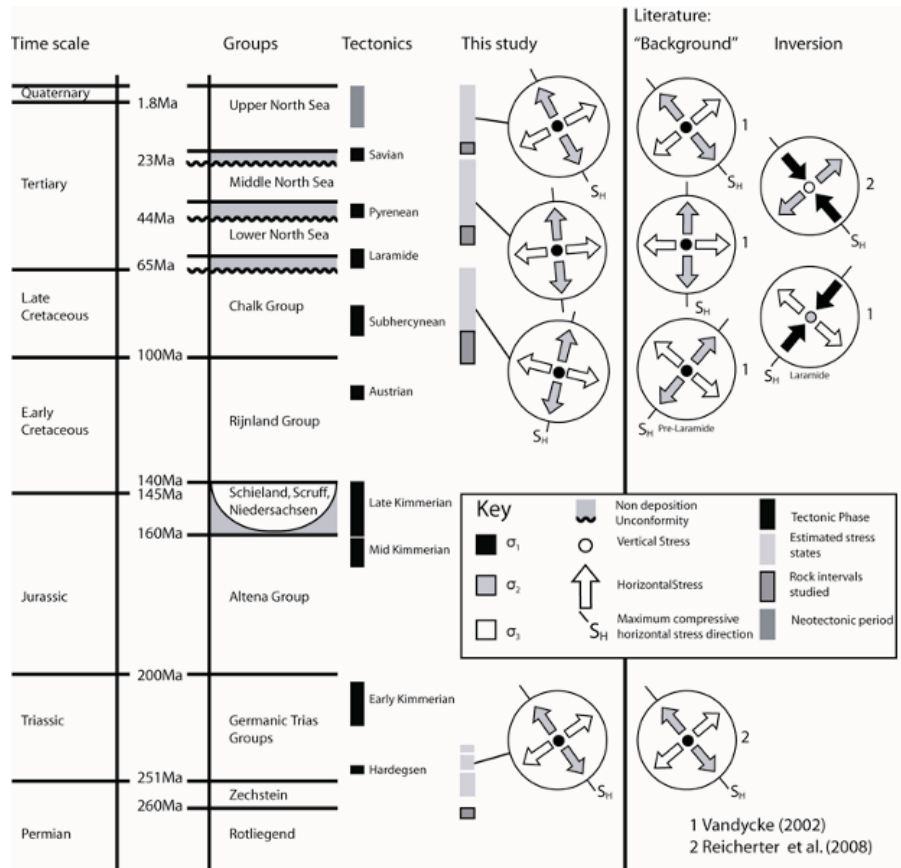


Figure 7: General overview of the stratigraphy in the Netherlands, including the tectonic phases (based on Van Adrichem-Boogaert and Kouwe, 1993-1997; Duin et al., 2006) and the paleostress results of this study, compared with outcrop-based data from (1) Vandycke (2002) and (2) Bergerat (1987), Bles et al. (1989), Becker (1993), and Reicherter et al. (2008). The general consistence of subsurface-based stress reconstruction and surface data emphasizes the value of detailed 3D seismic structural analysis in areas lacking rock exposure.

inversion phase are only documented in Kent and Boulonnais, while in the other studied areas E-W to NW-SE extension prevailed (Fig. 7). In Sussex, Kent and Boulonnais, Vandycke (2002) did not observe any effects of Laramide inversion.

During the Jurassic and Early Cretaceous, the stress field in Southern Germany and France was controlled by rifting in the Central Atlantic (Ziegler, 1982). Rifting in the South Atlantic and building of the Pyrenees began during the Late Cretaceous (Ziegler, 1982). These events corresponded to a stress field with a vertical σ_1 and an N-S oriented S_H that rotated to a NW-SE S_H , and shifted from extension to compression (Bergerat, 1987; Bergerat and Geyssant, 1983; Hibsich et al., 1995; Reicherter et al. 2008) (Fig. 7). Note that the S_H from this study corresponds both to the pre-Laramide extension as published by Vandycke (2002) for the Mons Basin, Kent, Boulonnais and Sussex, as well as to the S_H of the Laramide inversion phase in the Mons Basin, although the tectonic setting of the later is completely different.

Tertiary

The Brussels Sandstone (52Ma) paleostress shows a near E-W extensional stress field, very similar to the Late Paleogene extensional deformation observed by Vandycke (2002) (Fig. 7). In Sussex and the Isle of Wight, coeval strike-slip and thrust tectonics are respectively described by Vandycke (2002), with a N-S oriented compression direction. Also Hibschi et al. (1995) published "Post-Paleocene" N-S-oriented thrusting in England and Wales. Hibschi et al. (1995) describe a W-E stress permutation is observed in Europe, during the Late Paleogene. This transition with N-S thrust/strike-slip deformation to the west and E-W extensional faulting to the east runs roughly N-S through France. The Groningen area was on the extensional side of this pan-European trend, as only extension is observed here. In this study we have no evidence that the reconstructed North Sea Group horizons were subject to the documented major inversion; however, minor depositional gaps are observed between the different North Sea Groups in Groningen (Duin et al., 2006).

The start of the neotectonic period for central and northern Europe is estimated to have occurred around 10Ma (e.g. Becker, 1993 and Van Balen et al., 2005). The Base Upper North Sea Group was deposited around 19Ma (Van Adrichem-Boogaert and Kouwe, 1993-1997). Despite the obvious gap between the deposition of this horizon and the start of the Neotectonic period, we have compared the paleostress result of the Base Upper North Sea with the present day stress field, as published in the World Stress Map (WSM, Reinecker et al., 2005, Fig. 8). Becker (1993) notes that the onset of the Neotectonic period is not strict but a range. The line symbols in Fig. 8 represent the orientation of the maximum horizontal compressive stress (SH). Since in our study σ_1 is observed to be near vertical, we assume the orientation of σ_2 to be parallel to SH. The general present day stress trend for the Netherlands is an NW-SE SH. In the north of the Dutch offshore (Central Graben area) the SH is oriented roughly E-W, as well as in parts of the southern Netherlands and Belgium. These different stress orientations might result from stress deflections around the London Brabant Massif and the Central Graben (Gruenthal and Stromeyer, 1994). The data from this study are quite similar to the general trend of the neotectonic data of the WSM (Reinecker et al., 2005) in the Netherlands. However, the WSM data point closest to the study area (Lauwerszee Trough, Fig. 8) shows a NE-SW oriented maximum horizontal stress (SH). This data point is clearly an outlier if compared to the general regional trend. This data point is located between the Lauwerszee Trough bounding faults, and local stress deviations often occur over faults (Dupin et al., 1993; Pollard et al., 1993; Gapais et al., 2000).

Vandycke (2002) showed that for 6 locations in the southern UK, France and Belgium, NE-SW dominated during the Quaternary (equal to the minimum horizontal stress, σ_h). This trend fits very well with the observed NW-SE σ_H from the Upper North Sea Group studied in this study. Furthermore, based on borehole hydraulic fractures Frikken (1999) shows that the present day maximum compressive horizontal stress (σ_H) on the Friesland platform (roughly 60km to the west of the Groningen area, Fig. 8) is oriented at 152°. This measure is a 7° clockwise deviation with respect to the σ_H of the Base Upper North Sea horizon measured in this study.

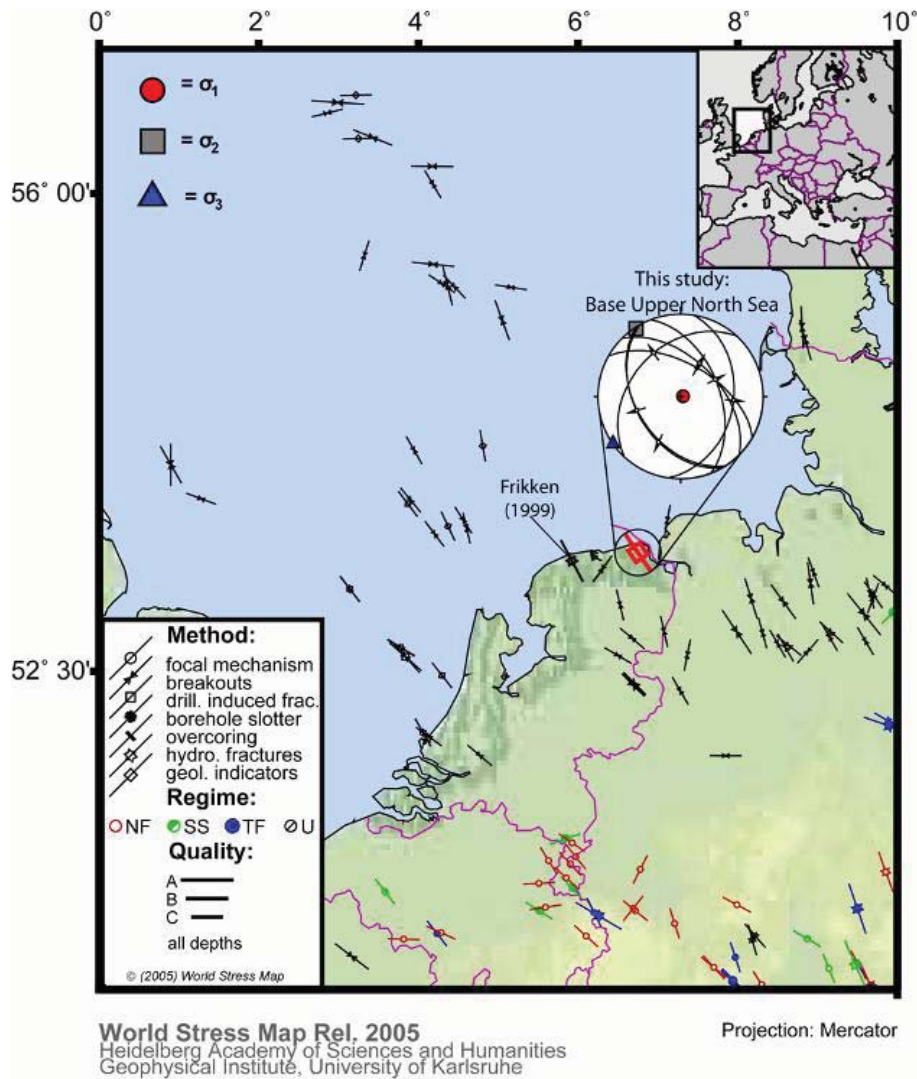


Figure 8: Data from the World Stress Map compared to results of this study and data from Frikken (1999). Lines represent the orientation of the present-day maximum horizontal compressive stress (σ_H). Shape of the data point indicates method, point fill indicates tectonic regime (NF = normal faulting; SS = strike slip; TF = Thrust faulting; U = undefined). Modified from Reinecker et al. (2005).

A stress permutation is observed in the Late Neogene stress axes in Fig. 7 and the European present-day stress maps (www.wsm.physik.uni-karlsruhe.de, Reinecker et al., 2005). While this study and Vandycke (2002) calculate a normal faulting stress state in Groningen and Belgium, France and the United Kingdom. The stress state described by Reicherter et al 2008, based on e.g. Bergerat and Geysant, 1983; Bergerat, 1987; Becker, 2003) is a strike slip stress tensor, with a similar maximum horizontal stress (σ_H). This stress tensor is based on field observations in the south of Europe, close to the African Indentor. Further north, the strike slip fault setting changes into normal faulting, while maintaining a NW-SE oriented σ_H (see also Gruenthal and Stromeyer, 1994).

The lack of tectonic inversion on the study area

In the study area, no tectonic, fault-related effects for Meso- and Cenozoic inversion phases are observed in the data. Erosional features represented by reflector truncations are present, showing that

these phases did affect the study area. As discussed by Stäuble and Milius (1970), Van Wijhe (1987) and De Jager (2003), the bulk of the Tertiary and Cretaceous inversion events are found in the West Netherlands Basin, Lower Saxony Basin and Central Netherlands Basin, the Broad Fourteens Basin and Dutch Central Graben, and to a lesser degree in the basins surrounding the Groningen area. The Groningen High was predominantly uplifted as homogenous rigid block, and only slightly eroded, but that the faults within the Groningen High were not reactivated. With the exception of erosional features, the post-Zechstein deposits of the studied region of the Groningen High exhibits only deformation related to extensional events during the Upper Cretaceous and Tertiary.

Salt

Van Balen et al. (2005) points out that in the northern and eastern Netherlands most of the faults are associated with salt movements. In this NW-Groningen case study there is also a clear link between the Top Zechstein topography and the general fault locations and orientations. Many of the faults detected are located directly above changes in the Top-Zechstein topography. The orientation of salt structures immediately N and E of the study area is N-S, a trend that is parallel to the Mesozoic graben structures of the Dutch-Central Graben, the Horn Graben and the Glückstadt Graben (e.g. Scheck et al., 2003; Mohr et al., 2005). However, without further detailed kinematic and mechanical analysis of the salt tectonic processes in this area (e.g. Mohr et al., 2005), it is not clear at which stage of the salt movement the faults formed.

Conclusions

The application of a novel, three-stepped workflow utilizing seismic data of the Groningen High, the Netherlands, and structural reconstruction techniques for paleostress restoration produced results that were in agreement with classic paleostress estimates based on extensive outcrop studies throughout Western Europe. In detail, the subsurface-based paleostress calculation delivered the following stress states in the study area; the earliest phase is characterized by a NE-SW directed extension probably of Latest Permian/ Early Triassic age. Between Triassic and Early Cretaceous no observations were made. In the latest Cretaceous the development of an approximately E-W extension (σ_h) is observed, that follows a phase of tectonic quiescence (early Late Cretaceous). In the Tertiary, two stress states are observed that are separated from the Late Cretaceous stress states by a phase of tectonic quiescence. Between 52 Ma and 19 Ma a roughly E-W extension is archived in sediments of the Lower North Sea Group, while after 19 Ma the stress state corresponds to an approximately NE-SW extension persisting until the present-day.

Bootstrapping (Appendix 3) of the dataset documented that the initial assumptions of the stress reconstruction with respect to the scale of stress homogeneity are justified. Before the paleostress-reconstruction method described in this paper can be universally applied, further critical evaluations are necessary. These should particularly focus on questions regarding the scale of homogenous stress field, critical issues of the basic assumptions of stress inversion and discussions on the ambiguity of the extraction of fault-slip indicators from 3D seismic data.

Acknowledgements

The authors like to thank the Nederlandse Aardolie Maatschappij (NAM); a Shell operated 50:50 joint-venture between Shell and ExxonMobil, and particularly Rien Herber, Jürgen Grötsch, Frank Pardoel, Jos Terken, Kees van Ojik, Joris Steenbrink, Rene Villafuerte and Martin de Keijzer for the use of the extensive 3D seismic database and discussion. Judith Sippel, Tina Lohr and Mauro Cacace (GFZ Potsdam) offered kind assistance in this project and fruitful discussions. Judith Sippel is also thanked for providing the data from the Mammendorf Quarry for quality control.

Midland Valley Exploration Ltd., Glasgow is thanked for providing 3DMove under an academic license. Schlumberger is acknowledged for granting an academic license for Petrel seismic interpretation and modelling software.

Final the reviewers are acknowledged. Their suggestions and critical reading significantly improved this paper.

References

- ◇ Allan, U. S. 1989. Model for Hydrocarbon Migration and Entrapment Within Faulted Structures. AAPG Bulletin 73(7), 803-811.
- ◇ Anderson, E. M. 1942. The Dynamics of Faulting. Oliver & Boyd, Edinburgh, First edition, pp. 206.
- ◇ Angelier, J. 1984. Tectonic analysis of fault slip data sets. Journal of Geophysical Research 89, 5838-5848.
- ◇ Angelier, J. 1990. Inversion of field data in fault tectonics to obtain the regional stress-III. A new rapid direct inversion method by analytical means. Geophysics Journal International 103, 363-376.
- ◇ Angelier, J. 1994. Fault Slip Analysis and Paleostress Reconstruction. In: Hancock, P. L. (Ed.), Continental Deformation. Pergamon Press, Oxford, 53-100.
- ◇ Back, S., Höcker, C., Brundiers, M. B., Kukla, P. A. 2006. Three-dimensional-seismic coherency signature of Niger Delta growth faults: integrating sedimentology and tectonics. Basin Research 18, 323-337.
- ◇ Becker, A. 1993. An attempt to define a "neotectonic period" for central and northern Europe. Geologische Rundschau 82, 67-83.
- ◇ Bergerat, F. 1987. Stress Fields in the European platform at the time of Africa-Eurasia collision. Tectonics 6(2), 99-132.
- ◇ Bergerat, F., Geysant, J. 1983. Fracturation tertiaire et evolution des contrantes en Baviere orientale: le Jura franconien et la foret bavaroise. Geologische Rundschau 72, 935-954.
- ◇ Bles, J. L., Bonijoly, D., Castaing, C., Gros, Y. 1989. Successive post-Variscan stress fields in the French Massif Central and its borders (Westerns European plate): comparison with geodynamic data. Tectonophysics 169, 79-111.
- ◇ Bott, M. H. P. 1959. The mechanics of oblique slip faulting. Geological Magazine 96(2), 109-117.
- ◇ Breunse, J. N., Rispens, F. B. 1996. Natural gas in the Netherlands: exploration and development in historic and future perspective. In: Rondeel, H. E., Batjes, D. A. J. & Nieuwenhuijs, W. H. (Eds.), Geology of Gas and Oil under the Netherlands. Kluwer Academic Publishers, Dordrecht, 19-30.

- ◇ Caiazza, C., Ascione, A., Cinque, A. 2006. Late Tertiary–Quaternary tectonics of the Southern Apennines (Italy): New evidences from the Tyrrhenian slope. *Tectonophysics* 421, 23-51.
- ◇ Cartwright, J. A., Trudgill, B. D., Mansfield, J. M. 1995. Fault growth by segment linkage: an explanation for scatter in maximum displacement and trace length data from the Canyonlands Grabens of SE Utah. *Journal of Structural Geology* 9, 1319-1326.
- ◇ Cowie, P. A., Roberts, G. P., 2001. Constraining slip rates and spacings for active normal faults. *Journal of Structural Geology* 23, 1901-1915.
- ◇ De Jager, J. 2003. Inverted basins in the Netherlands, similarities and differences. *Netherlands Journal of Geosciences / Geologie en Mijnbouw* 82(4), 355-366.
- ◇ Dronkers, A. J., Mrozek, F. J., 1991. Inverted basins of The Netherlands. *First Break* 9(9), 409-425.
- ◇ Du Rouchet, J. 1981. Stress Fields, A key to Oil Migration. *AAPG Bulletin* 65(1), 74-85.
- ◇ Duin, E. J. T., Doornenbal, J. C., Rijkers, R. H. B., Verbeek, J. W., Wong, T. E. 2006. Subsurface structure of the Netherlands - results of recent onshore and offshore mapping. *Netherlands Journal of Geosciences / Geologie en Mijnbouw* 85(4), 245-276.
- ◇ Dupin, J. M., Sassi, W., Angelier, J. 1993. Homogeneous stress hypothesis and actual fault slip: a distinct element analysis. *Journal of Structural Geology* 15, 1033-1043.
- ◇ Frikken, H. W., 1999. Reservoir-geological aspects of productivity and connectivity of gasfields in the Netherlands. PhD thesis, Technical University Delft.
- ◇ Gapais, D., Cobbold, P. R., Bourgeois, O., Rouby, D., de Urreiztieta, M. 2000. Tectonic significance of fault slip data. *Journal of Structural Geology* 22, 881-888.
- ◇ Gartrell, A. P., Lisk, M. 2005. Potential New Method for Paleostress estimation by Combining Three-dimensional Fault Restoration and Fault Slip Inversion Techniques: First Test on the Skua Field, Timor Sea. In: Boulton, P. & Kaldi, J. (Eds.), *Evaluating fault and cap rock seals*. AAPG Hedberg Series 2, 23-26.
- ◇ Gölke, M., Brudy, M. 1996. Orientation of crustal stresses in the North Sea and Barents Sea inferred from borehole breakouts. *Tectonophysics* 266, 25-32.
- ◇ Gölke, M., Coblenz, D. 1996. Origins of the European regional stress field. *Tectonophysics* 266, 11-24.
- ◇ Gras, R., Geluk, M. C., 1999. Late Cretaceous - Early Tertiary sedimentation and tectonic inversion in the southern Netherlands. *Geologie en Mijnbouw* 78, 1-79.
- ◇ Gruenthal, G., Stromeyer, D. 1986. Stress Pattern in Central Europe and Adjacent Areas. *Gerlands Beitrage zur Geophysik* 95, 443-452.
- ◇ Gruenthal, G., Stromeyer, D. 1994. The recent crustal stress field in Central Europe sensu lato and its quantitative modelling. *Geologie en Mijnbouw* 73, 173-180.
- ◇ Henk, A. 2005. Pre-drilling prediction of the tectonic stress field with geomechanical models. *First Break* 23, 53-57.
- ◇ Hibscher, C., Jarrige, J.-J., Cushing, E. M., Mercier, J. 1995. Paleostress analysis, a contribution to the understanding of basin tectonics and geodynamic evolution. Example of the Permian/Cenozoic tectonics of Great Britain and geodynamic implications in Western Europe. *Tectonophysics* 252, 103-136.

- ◇ Hinzen, K.-G. 2003. Stress field in the Northern Rhine area, Central Europe, from earthquake fault surface solutions. *Tectonophysics* 377, 325-356.
- ◇ Ilic, A., Neubauer, F., 2005. Tertiary to recent oblique convergence and wrenching of the Central Dinarides: Constraints from a palaeostress study. *Tectonophysics* 410, 465-484.
- ◇ Kettel, D., 1983. The east Groningen Massif - Detection of an Intrusive body by means of coalification. In: Kaasschieter, J. P. H. & Reijers, T. J. A. (Eds.), *Petroleum geology of the southeastern North Sea and adjacent onshore areas*. *Geologie en Mijnbouw* 62, The Hague, 203-210.
- ◇ Kokkalas, S., Jones, R. R., McCaffrey, K. J. W., Clegg, P., 2007. Quantitative fault analysis at Arkitsa, Central Greece, using terrestrial Laser-Scanning ("LiDAR"). *Bulletin of the Geological Society of Greece* XXXVII, 1-14.
- ◇ Larroque, J. M., Laurant, P., 1988. Evolution of the stress field pattern in the south of the Rhine Graben from the Eocene to the present. *Tectonophysics* 148, 41-58.
- ◇ Lee, J.-J., Bruhn, R. L., 1996. Structural anisotropy of normal faults. *Journal of Structural Geology* 18(8), 1043-1059.
- ◇ Lohr, T., 2007. Seismic and sub-seismic deformation on different scales in the NW German Basin. PhD thesis, Freie Universität Berlin.
- ◇ Lohr, T., Krawczyk, C. M., Oncken, O., Tanner, D. C., 2008. Evolution of a fault surface from 3D attribute analysis and displacement measurements. *Journal of Structural Geology* 30(6), 690-700.
- ◇ Maerten, L., Gillespie, P., Pollard, D. D. 2002. Effects of local stress perturbation on secondary fault development. *Journal of Structural Geology* 24, 145-153.
- ◇ Marchal, D., Guiraud, M., Rives, T. 2003. Geometric and morphologic evolution of normal fault planes and traces from 2D and 4D data. *Journal of Structural Geology* 25, 135-158.
- ◇ McBride, J. H., 1989. Remarks on the derivation of the paleostress system from inferred faults on deep seismic reflection records. *Tectonophysics* 168, 275-282.
- ◇ Michon, L., van Balen, R. T., Merle, O., Pangnier, H. 2003. The Cenozoic evolution of the Roer Valley Rift System integrated at a European scale. *Tectonophysics* 367, 101-126.
- ◇ Mohr, M., Kukla, P. A., Urai, J. L., Bresser, G. 2005. Multiphase salt tectonic evolution in NW Germany: seismic interpretation and retro-deformation. *International Journal of Earth Sciences (Geologische Rundschau)* 94, 914-940.
- ◇ Morewood, N. C., Roberts, G. P., 2000. The geometry, kinematics and rates of deformation within an en échelon normal fault segment boundary, central Italy. *Journal of Structural Geology* 22, 1027-1047.
- ◇ Needham, D. T., Yielding, G., Freeman, B. 1996. Analysis of fault geometry and displacement patterns. In: Buchanan, P. G. & Nieuwland, D. A. (Eds.), *Modern Developments in Structural Interpretation, Validation and Modelling*. Geological Society Special publication 99, 189-199.
- ◇ Ortner, H., Reiter, F., Acs, P., 2002. Easy handling of tectonic data: the programs TectonicVB for Mac and Tectonics FP for Windows(tm). *Computers & Geosciences* 28, 1193-1200, see also <http://www.tectonicsfp.com/>.
- ◇ Pollard, D. d., Saltzer, S. D., Rubin, A. M. 1993. Stress inversion methods: are they based on faulty assumptions? *Journal of Structural Geology* 15(8), 1045-1054.

- ◇ Reicherter, K., Froitzheim, N., Jarosinski, M., Badura, J., Franzke, H.-J., Hansen, M., Hübscher, C., Müller, R., Poprawa, P., Reinecker, J., Stackebrandt, W., Voigt, T., von Eynatten, H., Zuchiewicz, W., 2008. Alpine Tectonics north of the Alps. In: McCann, T. (Ed.), *Geology of Central Europe*. Special Publication Geological Society of London. The Geological Society, London, 53 pages..
- ◇ Reicherter, K. R., Peters, G. 2005. Neotectonic evolution of Central Betic Cordilleras (Southern Spain). *Tectonophysics* 405, 191-212.
- ◇ Reinecker, J., Heidbach, O., Tingay, M., Sperner, B., Müller, B. 2005. The release 2005 of the World Stress Map (available online at www.world-stress-map.org).
- ◇ Reinecker, J., Tingay, M., Müller, B. 2003. Borehole breakout analysis from four-arm caliper logs (guideline available online at www.world-stress-map.org).
- ◇ Renard, F., Voisin, C., Marsan, D., Schmittbuhl, J., 2006. High resolution 3D laser scanner measurements of a strike-slip fault quantify its morphological anisotropy at all scales. *Geophysical Research Letters* 33, L04305.
- ◇ Roberts, G. P., 1996. Variation in fault-slip directions along active and segmented normal fault. *Journal of Structural Geology* 18(6), 835-845.
- ◇ Scheck, M., Bayer, U., Lewerenz, B. 2003. Salt redistribution during extension and inversion inferred from 3D backstripping. *Tectonophysics* 373, 55-73.
- ◇ Schöpfer, M. P. J., Childs, C., Walsh, J. J., Manzocchi, T., Koyi, H., 2007. Geometrical analysis of the refraction and segmentation of normal faults in periodically layered sequences. *Journal of Structural Geology* 29, 318-335.
- ◇ Sippel, J., Scheck-Wenderoth, M., Reicherter, K., Mazur, S., accepted. Paleostress states at the south-western margin of the Central European Basin System - application of fault-slip analysis to unravel a polyphase deformation pattern. Submitted to *Tectonophysics*. This Volume.
- ◇ Shan, Y., Suen, H., Lin, G., 2003. Separation of polyphase fault/slip data: an objective-function algorithm based on hard division. *Journal of Structural Geology*, 25(6), 829-840.
- ◇ Spang, J. H. 1972. Numerical method for dynamic analysis of calcite twin lamellae. *Geological Society of America Bulletin* 83(1), 467-472.
- ◇ Sperner, B., 1996. Computer programs for the kinematic analysis of brittle deformation structures. In: Frisch, W. (Ed.), *Tübinger Geowissenschaftliche Arbeiten Reihe A*, 27, Tübingen.
- ◇ Sperner, B., Ratschbacher, L., Ott, R. 1993. Fault-striae analysis: a Turbo pascal program for graphical presentation and reduced stress tensor calculation. *Computers & Geosciences* 19(9), 1361-1388.
- ◇ Stäuble, A. J., Milius, G., 1970. Geology of Groningen Gas Field, Netherlands. In: Halbouty, M. T. (Ed.), *Geology of giant petroleum fields*. American Association of Petroleum Geologists, Tulsa, 359-369.
- ◇ TNO-NITG. 2004. *Geological Atlas of the Subsurface of the Netherlands - onshore*. TNO-NITG, Utrecht, pp. 103.
- ◇ Turner, F. J. 1953. Nature and dynamic interpretation of deformation lamellae in Calcite of three marbles. *American Journal of Science* 251, 276-298.

- ◇ Van Adrichem-Boogaert, H. A., Kouwe, W. F. P. 1993-1997. Stratigraphic Nomenclature of the Netherlands; revision and update by RGD and NOGEP. TNO-NITG, Mededelingen Rijks Geologische Dienst, Haarlem, 50, pp. 50.
- ◇ Van Balen, R. T., Houtgast, R. F., Cloetingh, S. A. P. L. 2005. Neotectonics of The Netherlands: a review. *Quaternary Science Reviews* 24, 439-454.
- ◇ Van Wijhe, D. H. 1987. Structural evolution of inverted basins in the Dutch offshore, Compressional Intra-Plate deformations in the Alpine Foreland. *Tectonophysics* 137, 171-219.
- ◇ Vandycke, S. 2002. Palaeostress records in Cretaceous formations in NW Europe: extensional and strike-slip events in relationships with Cretaceous–Tertiary inversion tectonics. *Tectonophysics* 357(1-4), 119-136.
- ◇ Wallace, R. E. 1951. Geometry of shearing stress and relation to faulting. *Journal of Geology* 59, 111-130.
- ◇ Walsh, J. J., Watterson, J., Bailey, W. R., Childs, C. 1999. Faults relays, bends and branch-lines. *Journal of Structural Geology* 21, 1019-1026.
- ◇ Wong, T. E., Batjes, D. A. J., de Jager, J. (Editors), 2007. *Geology of the Netherlands*. Editat-KNAW, Amsterdam, pp. 354.
- ◇ Worum, G., Michon, L., 2005. Implications of continues structural inversion in the West Netherlands Basin for understanding controls on Paleogene deformation. *Journal of the Geological Society* 162, 73-85.
- ◇ Ziegler, P. A. 1982. *Geological Atlas of Western and Central Europe*. Elsevier Scientific Publishing Company, The Hague, Amsterdam, pp. 130.

Chapter 2: Small-scale faulting in the Upper Cretaceous of the Groningen Block (The Netherlands): 3D seismic interpretation, fault plane analysis and regional paleostress¹

Abstract

Over the last years, field-based studies have shown that fault surfaces can exhibit a considerable self-affine topography. It is reasonable to assume that similar undulations are also present in fault interpretations from 3D reflection seismic data however both the interpretation uncertainty and geophysical resolution limits hinder their analysis. This study analyses a set of small-scale, non-reactivated faults in the Upper Cretaceous Chalk Group (Upper Ommelanden Formation) of the NW-part of the Groningen Block, the Netherlands, in a high quality Pre Stack Depth Migrated 3D seismic data set. The studied faults are fully contained inside the Chalk Group, in an area located between the major tectonic-bounding faults of the NW Groningen Block. Over 200 faults, with offsets in the order of 30-50 m, were interpreted across an area of ca. 150 km², showing a clear preferential orientation for strike, dip and dip-direction. Detailed interpretations and 3D fault plane analyses show undulations on the fault plane. We show that these undulations are not an interpretation or gridding artefact, and interpret these to indicate direction of fault slip. These results were used to calculate a paleostress tensor, using all faults to calculate a single stress tensor for the entire study area by Numerical Dynamic Analysis.

Based on the orientation, position and a thickness analysis, it is interpreted that these faults formed due to the tectonic reactivation of salt structures in the Latest Cretaceous. The calculated paleostress state shows a general NW-SE-extension, with a vertical maximum principle stress, and a stress ratio of about 0.3, indicating that the studied faults are not the result of dewatering. This interpretation agrees both with a nearby salt-tectonic reconstruction, as well as field-based paleostress results from the UK, Belgium and France. A first look at other surveys from the Dutch sector indicates that similar faults are present in other areas, with different orientations. We propose that a dedicated analysis of these faults across on- and offshore Europe would allow extending the stress map of the Late Cretaceous into areas where the Chalk is not outcropping.

Keywords: Upper Cretaceous Chalk; Paleostress; fault surface undulations; seismic interpretation; fault plane analysis

¹ Heijn van Gent, Stefan Back, Janos L. Urai, Peter Kukla. *Journal of Structural Geology* 32, 2010, 537-553

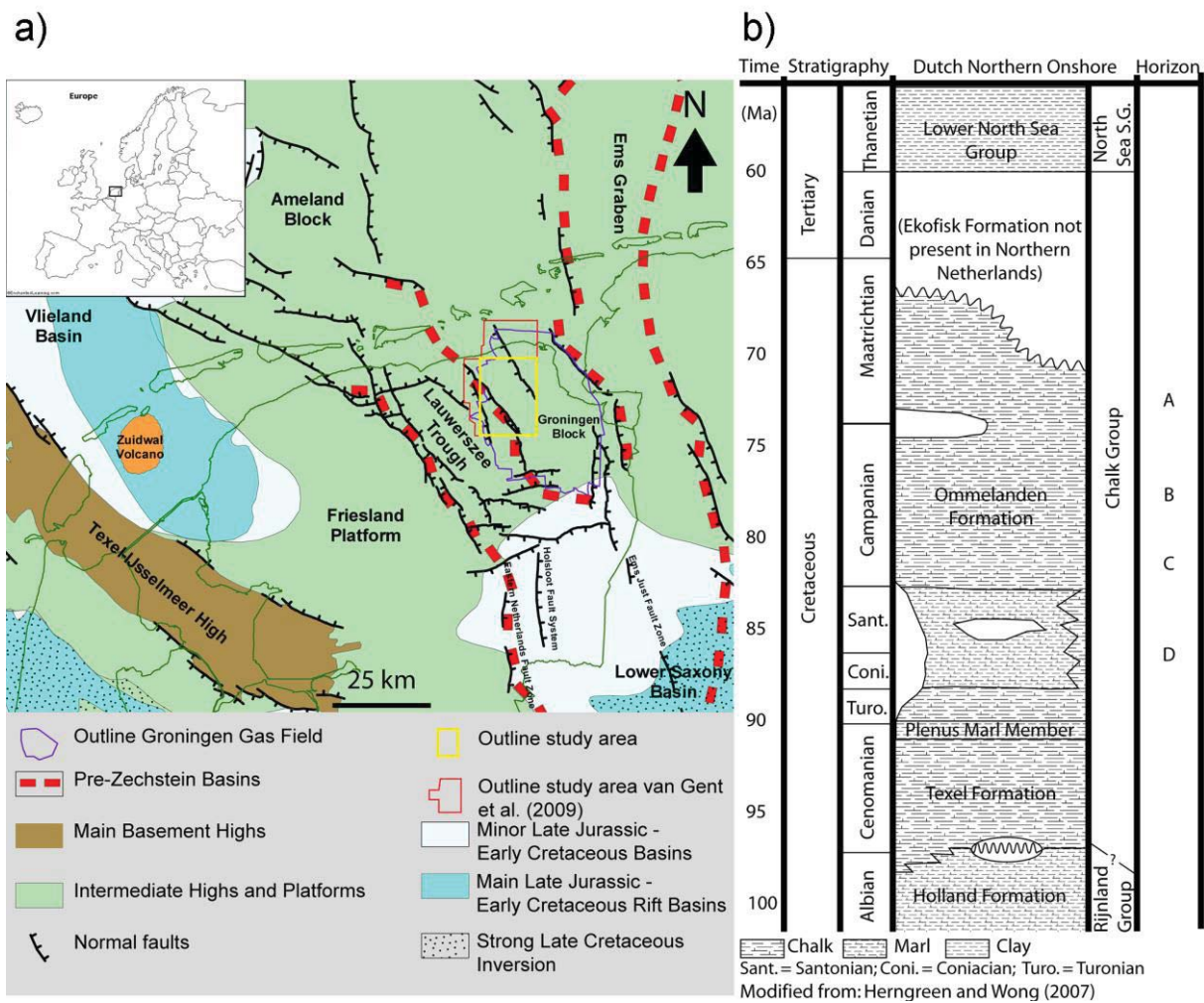


Figure 1: a) Location of the study area in the NW of the Groningen High, at the border of the Lauwerszee Trough. Image courtesy of NAM. b) Simple stratigraphic column for the northern Netherlands. Modified from Herngreen and Wong (2007). Also indicated are the approximate stratigraphic positions of the four internal reflectors (A-D), see table 1.

Introduction

This work presents a detailed analysis of a set of small-scale faults interpreted on high-quality 3D seismic data of the Upper Cretaceous Chalk Group of the NW Groningen Block, the Netherlands (Fig. 1a). The interpretation results are compared with existing analyses of faults in the chalk of NW Europe, and used for paleostress analysis. Previous studies on small-scale faults in chalk strata have been controversial concerning the interpretation of the origin of faulting. Hibschi et al. (1995) and Hibschi et al. (2003) interpreted intra-Chalk faults to have formed by compaction. In contrast, Vandycke (2002) argued for tectonic deformation as the main cause of faulting observed in Chalk outcrops. The study presented here will help to distinguish between the two models.

Paleostress analyses provide information on the tectonic evolution of the crust and help to predict the location and possible orientations of fracture and fault systems below the resolution of seismic observation. In hydrocarbon exploration, these fracture systems can have economically viable

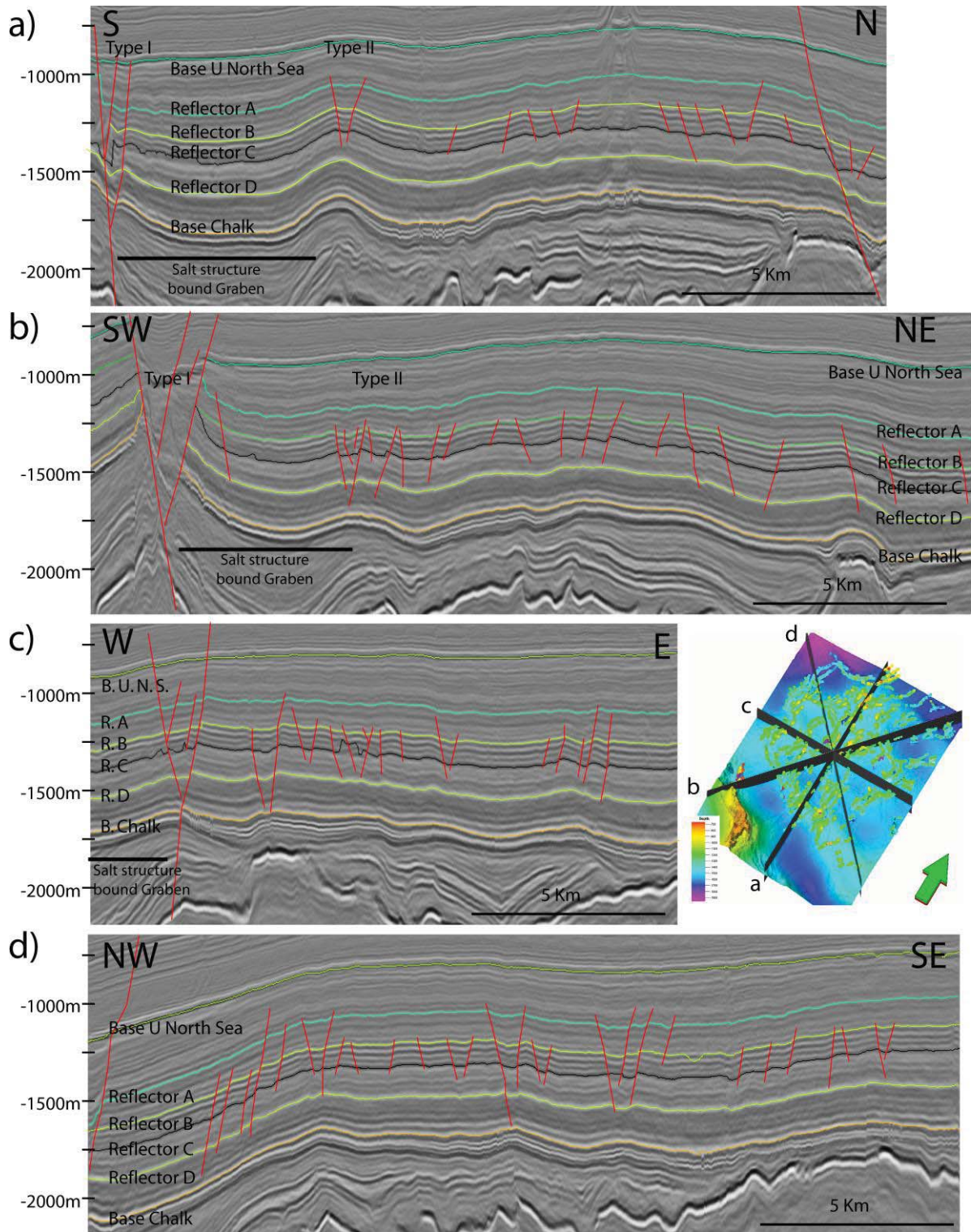


Figure 2: Four seismic crosssections (a-d) of part of the Groningen high. Although some meso-faults are interpreted, a high number of small-throw faults are observed between Base Upper North Sea and Base Chalk reflectors. Orientations of the crosssections are indicated in the inset. Indicated with “Salt structure bound Graben” is the Graben that is also indicated in Figures 3f and 5f and discussed in the text.

permeabilities (Koestler and Ehrmann, 1991; Arnott and van Wunnik, 1996; van Konijnenburg et al., 2000; Smith and McGarrity, 2001; Otrtuno-Arzate et al., 2003; Casabianca et al., 2007); thus, the seismic-based paleostress-analysis approach can potentially impact oil and gas exploration and production in carbonate provinces in general. Paleostress analyses can be used to estimate the timing of the opening and closing of faults and fractures, and for analyzing and modelling the migration of geofluids (du Rouchet, 1981; Sapra, 1997).

Paleostress analyses are usually based on maps of fault systems at km-scale (e.g. Anderson, 1942; Michon et al., 2003), on the detailed mapping of fault surfaces and slip directions in outcrops at m-scale (Bergerat, 1987; Kleinspehn et al., 1989; Angelier, 1994; Hibsich et al., 1995; Delvaux, 1997; Saintot and Angelier, 2002; Vandycke, 2002; Caiazza et al., 2006; Sippel et al., 2009), or on the analysis of calcite twins at mm-scale (Turner, 1953; Spang, 1972; Larroque and Laurant, 1988; Rocher et al., 2004). With the increased availability of industrial 3D seismic data for the scientific community, several attempts have been made to extract (paleo-) stress tensors from 3D seismic data (this does not include papers on seismic processing that constrain the orientation of either fractures and or the present-day stress tensor, such as for example Neves et al. 2003). Seismic extraction of paleostress has the advantage that direct access to rocks is no longer required, so that sedimentary cover, or seawater coverage in offshore settings does not hinder for paleostress analysis. Furthermore, the fact that seismic data is often available in areas of hydrocarbon exploration or production means that the results are directly applicable to aid the local exploration/production strategy (Du Rouchet, 1981; Gartrell and Lisk, 2005; Henk, 2005; Lohr et al. 2007 and Chapter 1). For example, Gartrell and Lisk (2005) have used 3D seismic data to calculate the present-day stress field in the Timor Sea (N Australia). Lohr (2007) used 3D seismic data to constrain the stresses that caused deformation of the Top Rotliegend in the Central European Basin. Finally we show in Chapter 1 how reactivated faults in reflection seismic data can be used to calculate paleostress stratigraphy in the NW part of the Groningen Block (Fig. 1) by using structural reconstructions, matching of horizon shapes across faults, and the analysis of undulations of fault planes.

In this study, a set of small-scale (on a seismic scale, the faults are actually roughly the same size as structures used in field-based paleostress study) faults (<50 m offset) of the Upper Cretaceous Chalk Group is interpreted and analyzed in detail (Fig. 2 and 3). These faults have low offset, are fully contained inside the Chalk Group, and not reactivated by later tectonic phases. To differentiate these small-scale faults from large, long-living, cross-formational faults, we use the term "Intra-Chalk faults". This term reflects that the studied faults do not penetrate Top or Base of the Chalk group; but is not meant to imply syn-sedimentary faulting. Using several overlapping and detailed interpretations of a number of these faults, it will be shown that these faults commonly have a down-dip oriented undulation, which is not the result of imaging or interpretation artefacts. These undulations can be used to constrain the slip direction in the down-dip-direction (pure normal faulting). Assuming that all faults in a similar fashion as the faults studies in detail, we used the orientation and related slip direction of all faults spread over the 10 x 15 km study area to calculate the regional paleostress tensor at the time of development of these faults. This approach differs from "normal" field-based paleostress studies in two important aspects: Firstly, this approach does not use direct fault observations from the field, where usually slickenlines or slickenfibers are used to constrain slip-

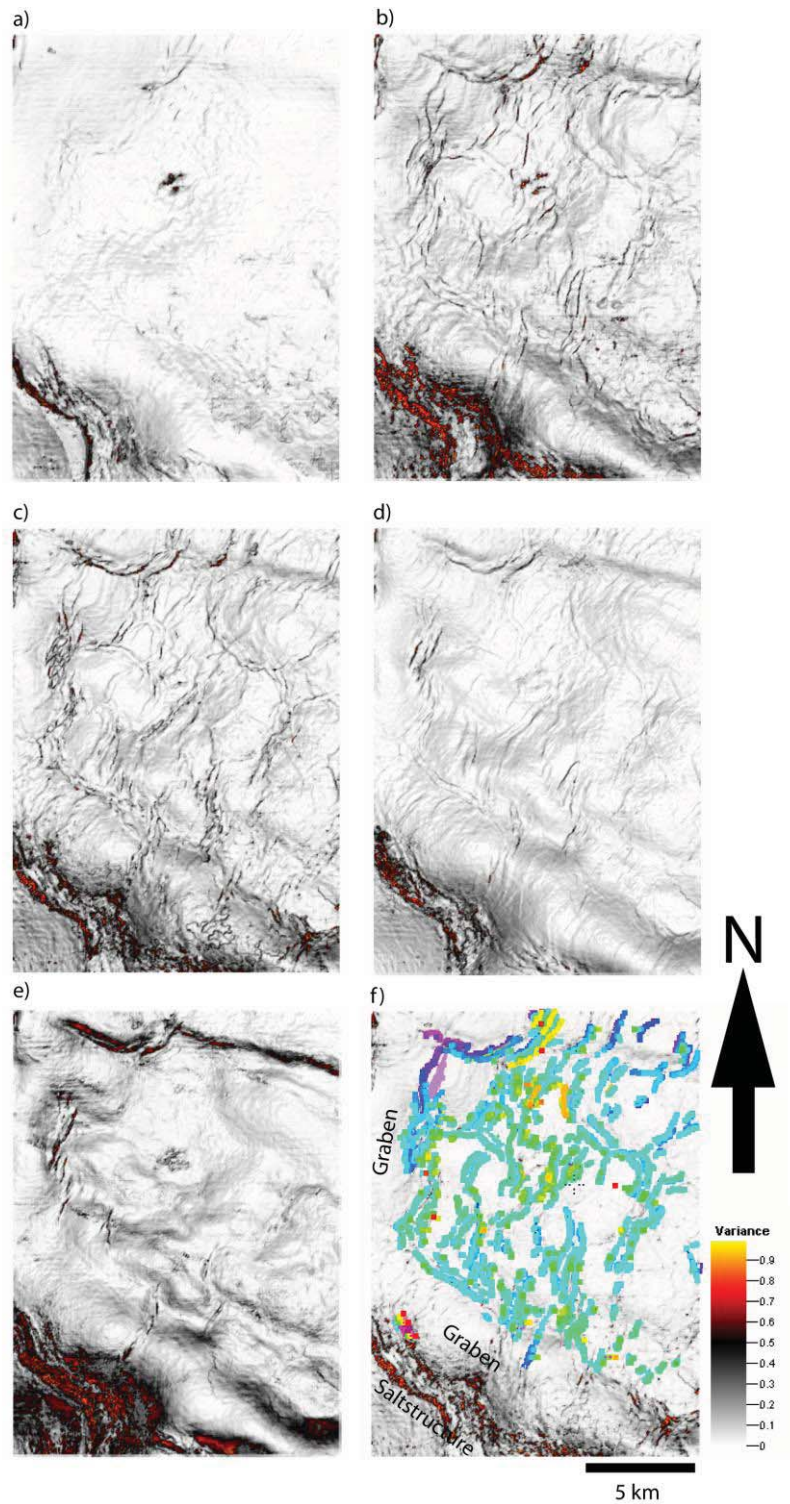


Figure 3: Variance maps of the five reflectors in Fig. 2. a) Variance map of the base of the North Sea Super-Group. b) Variance map of reflector B c) Variance map of reflector C, d) Variance map of reflector D. e) Variance map of the base of the Chalk Group. f) Variance map of reflector B with all interpreted fault sticks

direction (Means, 1987). Since these are much too small (in the order of 1-5 mm) to be observed in seismic data, a different approach of constraining the slip direction as is required (also see: Gartrell and Lisk, 2005; Lohr, 2007, Chapter 1). The second aspect deals with the size of the study area. In

field-based paleostress studies, it is a common approach to compare a number of outcrop-scale (3-300 m) paleostress tensors with each other to gain insight into the regional (10-100 km) differences in stress state. In this work we use all visible faults (faults above seismic resolution) in the study area to calculate a single regional paleostress tensor for this area. It must be noted that we use “regional” in this paper only as a comparative term, larger than the study area, but the exact size is not determined. The regional character of the stress tensor does not allow the observation of stress permutations on smaller scales (which is possible in comparative field paleostress studies), but gives the larger scale stress state. However, if one were to compare the paleostress results from several seismic blocks, an insight in the basin-wide stress changes, both over time and space, can be gained. The calculated stress tensor agrees well with that obtained also by (Chapter 1) for the same area and time from larger, reactivated faults. While the latter was also seismic derived, field studies from France, the UK and Southern Belgium show similar results (Vandycke et al., 2002).

Geological setting

The Groningen Block (Fig. 1a) contains one of the largest gas reservoirs of the world. It is part of the North Netherlands High (TNO-NITG, 2004; Wong et al., 2007), and has been a relatively stable block since the Late Kimmerian inversion phase (Latest Jurassic), when the North Netherlands High formed (Stäuble and Milius, 1970; Kettel, 1983; Duin et al., 2006; Wong et al., 2007). From Late Permian to Late Jurassic times, the Groningen Block was part of the Southern Permian Basin. The Rotliegend (Middle Permian) sandstones form the reservoir in the Groningen area, and are sealed by the Late Permian Zechstein evaporites and carbonates (Glennie, 1998; Wong et al., 2007). Triassic to Lower Cretaceous sequences of the Groningen area are only poorly developed on the Groningen Block (TNO-NITG, 2004; Duin et al., 2006; Wong et al., 2007), most likely reflecting a structurally elevated position of the area during this time. The thickness of the Triassic to Lower Cretaceous deposits is generally below 200 m in the study area, but reaches thicknesses between 400 m and 800 m in the surrounding sub-basins. Although many hydrocarbon reserves in the North Sea's Central Graben Area are in (fractured) Chalk Group reservoirs (Koestler and Ehrmann, 1991; Stewart and Clark, 1999; Mallon and Swarbrick, 2002; Casabianca et al., 2007; Mallon and Swarbrick, 2008), the Upper Cretaceous Chalk in the Netherlands is generally not productive (with the exception of the Harlingen Field; see van den Bosch, 1983). As a result, these deposits are relatively poorly studied (Van der Molen et al., 2005). The Chalk Group of the Dutch subsurface consists of Cenomanian to Danian (lowermost Paleocene), relatively deep marine, mostly bioclastic limestones with local marl interlayers (Herngreen and Wong, 2007). Along the basin fringes more clastic formations are found (e.g.: the Aken and Vaals Formations of Southern Limburg; Herngreen and Wong, 2007). The Dutch Chalk Group deposits generally display highly parallel, continuous, low-amplitude reflectors, characteristic of pelagic, autochthonous chalks (Fig. 2 and 3, Gras and Geluk, 1999; Van der Molen et al., 2005).

In the Groningen Block the Chalk Group lies concordantly on top of the Rijnland Group (Fig. 1b and 2, TNO-NITG, 2004; Herngreen and Wong, 2007). The thickness of the Chalk Group deposits varies between 600 m and 1000 m. Although in the surrounding areas the Laramide inversion (Latest Cretaceous) caused intense uplift, truncation, erosion, faulting and inversion (Ziegler, 1982; Dronkers

and Mrozek, 1991; Gras and Geluk, 1999; De Jager, 2003; TNO-NITG, 2004; Worum and Michon, 2005; Wong et al., 2007), the North Netherlands High remained relatively stable with only minor uplift of a local to regional character (Stäuble and Milius, 1970; TNO-NITG, 2004; Van der Molen, 2004; Herngreen and Wong, 2007). Only the uppermost Cretaceous shows signs of erosion of probably less than 100 m (Van der Molen, 2004). Post-Cretaceous sedimentation lead to a burial of the Chalk Group sequences in the study area ranges of 800 m to 1800 m.

In the Netherlands, three formations are recognized in the Chalk Group; the Texel Formation, the Ommelanden Formation and the Ekofisk Formation (Fig. 1b; Van Adrichem-Boogaert and Kouwe, 1993-1997, Oakman, and Partington, 1998 Herngreen and Wong, 2007). In the study area and its surroundings, the Lower Chalk Texel Formation is 50-70 m thick. The Ommelanden Formation is up to 1000 m thick, and consists of white, chalky limestones with occasional flint layers (Herngreen and Wong, 2007). While the Turonian part of the formation consists of relatively dense limestones, the Coniacian to Santonian deposits are generally more marl-rich. These are overlain by less marly Campanian and Maastrichtian deposits (Herngreen and Wong, 2007). The hard and dense limestones (informally called Upper Ommelanden deposits) have at their base consolidated calcarenites which grade into massive chalk with flint layers (Van Adrichem-Boogaert and Kouwe, 1993-1997; Herngreen and Wong, 2007). The Ekofisk Formation that forms the Tertiary (Danian) continuation of Cretaceous chalk deposition is not present on the Groningen Block. Studies of non-reservoir Chalk Group deposits (in the Dutch offshore and in the Central North Sea) have shown a high porosity and relatively low permeability (Brasher and Vagle, 1996; Mallon and Swarbrick, 2002; Van der Molen, 2004). The onset of overpressure occurs when the Chalk Group is buried below 1 km, coinciding with a change in compaction mechanism (Van der Molen, 2004). Above the Chalk interval, the clastic Cenozoic North Sea Super-Group consist of predominantly siliciclastic rocks that were deposited from the Thanetian (Early Paleocene) onwards.

Salt tectonics

Movement of the Late Permian Zechstein evaporite deposits has influenced the younger deposits and tectonics in the Dutch subsurface (Van Adrichem-Boogaert and Kouwe, 1993-1997; TNO-NITG, 2004; Wong et al., 2007). Mohr et al. (2005) showed that salt movement in the nearby Ems Graben was a multiphase process. Three distinct pulses of salt movement, coupled to distinct tectonic phases are recognized. The first phase started almost immediately after salt deposition and lasted to the Middle Keuper (Late Triassic); a second phase occurred from Middle Keuper to Lower Cretaceous. For the Lower Cretaceous no salt movement was recorded, but during the Upper Cretaceous to Lower Tertiary, salt movement was reactivated by compressional tectonics indicated by salt rise and small amounts of horizontal shortening of salt diapirs.

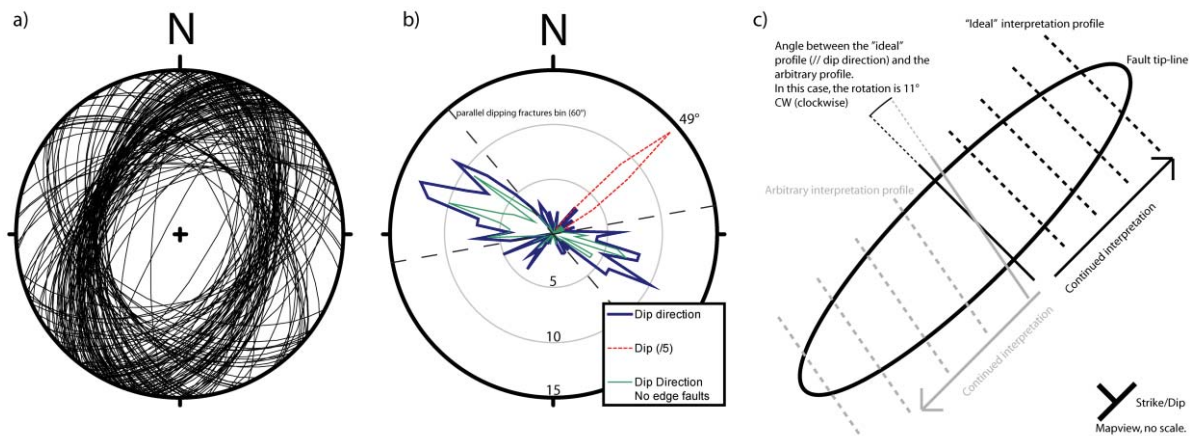


Figure 4: a) Stereoplot of the 213 faults interpreted in the Chalk interval. A plot of the Pi-poles are shown in Table 2. b) Rose diagram, showing the dip-direction (in blue) and the dip angle (in red). The green dip-direction plot shows the orientation of the faults when the faults on the edge of salt structure bound grabens are not taken into account. For dip-direction the concentric gridlines are spaced 5 counts, with a maximum of 15. For dip the concentric gridlines are spaced 25 counts, with a maximum of 75. Orientation bins are 5° wide. c) Sketch to illustrate the concept of “ideal” interpretation profile and a single arbitrary interpretation profile. The ideal profile is parallel to the down-dip-direction, while an arbitrary profile can have any angle to the fault. Since the same fault is sampled with both profiles, the resultant fault plane should have the same geometry (excluding aliasing effects), but since the profiles are slightly different, the different profile represent independent interpretations of the same fault. Here only two profiles are shown, but in Fig. 6 three to four different profiles per fault are shown. The directions of continued interpretation in this figure are arbitrary.

Methods

Seismic data and fault-interpretation workflow

The seismic data used in this study is part of a large, merged, 3D pre-stack depth migrated seismic data set, provided by the Nederlandse Aardolie Maatschappij BV. (NAM, a Shell operated 50-50 joint venture with ExxonMobil). The entire survey covers about 20 x 25 km, but the study area covers roughly 10 x 15 km large seismic cube (see Figure 1). The horizontal and vertical resolution of the seismic data is 25 m. Well control is provided by about 40 production and exploration wells. We used the interpretation package Petrel 2007 from Schlumberger for our interpretation work.

The Chalk Group of the study area exhibits numerous small-scale faults (see Fig. 2), close to the limit of seismic resolution (Hesthammer and Henden, 2000), that occur predominantly between areas of significant Post-Zechstein faulting (i.e. faults with throws between 50 m and 500 m, usually penetrating from Top Zechstein to middle Tertiary). The intra-Chalk faults can be seen in all crosssection directions (Fig. 2), exhibiting throws between 30 and 50 m.

Horizon:	Group:	Age:
Base North Sea	Lower North Sea	Tertiary; Thanetian (60 Ma)
Reflector A	Chalk	Early Maastrichtian
Reflector B	Chalk	Campanian
Reflector C	Chalk	Early Campanian
Reflector D	Chalk	Santonian-Coniacian
Base Chalk	Chalk	L. Cretaceous; (E) Cenomanian (97 Ma)

Table 1: Ages of the reflectors interpreted on Fig. 2. Stratigraphy is based on Van Adrichem-Boogaert and Kouwe (1993-1997), ages of reflector A-D are constrained with well data (Van Ojik, personal communication 2008).

To constrain possible activity phases of the intra-Chalk faults, four auxiliary reflectors (A to D) were mapped (Fig. 1b and 2), which were subsequently used for a thickness analysis. The ages for reflectors A, B C, and D are constrained by biostratigraphic data (see Table 1 as well as Fig. 1b, van Ojik, personal communication, 2008).

Fault interpretation using amplitude, variance, dip and fault enhancement attributes (e.g. Cox and Seitz, 2007) resulted in the interpretation of 213 individual intra-Chalk faults (Fig. 3f and Fig. 4 a and b). These faults were interpreted in vertical display with a line spacing of 1 to 5 (25-125 m), and on depth slices in intervals of 50-200 m. Vertical spacing depended on the size and complexity of the fault. Vertical fault interpretations were preferentially oriented perpendicular to the strike of the faults. As a rule, (i) faults were picked only where the fault was clearly defined in the hanging wall of the fault block, and (ii) the fault was preferentially picked where a change in fault dip occurred to avoid picking artefacts. In Fig. 2, a zone in the centre of the Chalk interval is visible where the faults are most clearly imaged (between reflector B and C).

To exclude that the fault-mapping procedure produced artificial fault undulations, four faults were interpreted at 25 m horizontal line spacing, using several different arbitrary and fully independent interpretation profiles, at an angle to the down-dip-direction (Fig. 4c). In general, a fault interpretation plane can cut the fault at any angle, but ideally a plane perpendicular to the fault (parallel to the down-dip-direction, and perpendicular to the strike) results in the “best” interpretation. By choosing a different “down-dip deviation” (angle between the down-dip-direction and the interpretation plane) for each of these interpretations, we ensured that the interpretation were completely independent. Subsequently, a series of independent surfaces of the same fault were constructed from the interpretations using the Petrel algorithm “Convergent Gridder” (see Petrel 2007 Help), with a grid increment of 10 m and smoothed with a Briggs biharmonic minimum curvature algorithm (Briggs, 1974). The resulting planes of the different fault interpretation directions were then visualized using a look-up table, colour-coded

according to dip-direction, and finally compared for structural similarity or dissimilarity either verifying fault undulations if persistent, or dismissing undulations as artefacts if incoherent in the different interpretation approaches.

Paleostress analysis

Following their interpretation, the fault surfaces of the study area were used for a paleostress analysis. The existing methods for paleostress calculation can be subdivided into those that are based on the Wallace and Bott criterion of minimum misfit angles (Wallace, 1951; Bott, 1959; Angelier, 1990), and those based on the Mohr-Coulomb Criterion (Coulomb, 1776; Mohr, 1900), with a high shear-to-normal-stress ratio. All methods require as input the combination of both the orientation and slip direction of faults. Here the different methods will only be discussed briefly, for a more extensive and technical discussion the reader is referred Angelier (1990), Ramsay and Lisle (2000) and Sippel et al. (2009).

Wallace (1951) and Bott (1959) showed that the direction of slip on any plane can be predicted, based on the stress tensor and the plane orientation, when slip is assumed to be parallel to the maximum resolved shear stress on the plane. Inverting this principle allows one to calculate the stress tensor, based on fault orientations and observed slip direction. Methods that employ this method are for example the Direct Stress Inversion (DSI) (Angelier, 1979, 1984, 1990) and the Multiple Inversion Method (MIM) (Yamaji, 2000), a modification of DSI for separating inhomogeneous data sets. In Wallace and Bott-based methods, the orientation of the principle stresses and their ratio (R) are varied until a minimum is found in the sum of the squared misfit angles for all faults (i.e. a least square criterion). The misfit angle is the difference between the observed slip direction and the calculated shear stress on the fault. The stress ratio is

$$R = \frac{(\sigma_2 - \sigma_3)}{(\sigma_1 - \sigma_3)}$$

with σ_{1-3} being the principle stresses of the in-situ stress tensor.

Methods based on the Mohr-Coulomb Criterion (Coulomb, 1776; Mohr, 1900) treat all faults as being newly formed and require a high shear stress- to normal stress – ratio on a fault to form. A further requirement is that the contraction and extension axis lie in the plane defined by the slip direction and the fault plane normal. This makes this method unsuitable for the use with faults with oblique striae (Sperner, 1996). Methods based on the Mohr-Coulomb Criterion include Numeric Dynamic Analysis (NDA; Spang, 1972; Sperner et al., 1993; Sperner, 1996) and the P-T-B axes Method (PTB; Turner, 1953; PTB; Sperner et al., 1993). These methods assume an angle of internal friction (Θ , generally assumed as 30° for neo-formed faults, and 45° for reactivated faults, Sperner et al., 1993; and Sperner, 1996), neglecting the natural variability of this parameter (Sperner et al., 1993). Both PTB and NDA calculate the orientation of the kinematic axes and the kinematic ratio, but in the case of coaxial, upper crustal deformation these can be considered to coincide with the stress axes and the stress ratio (R) (Anderson, 1942; Huang, 1988; Sperner et al., 1993; Sperner, 1996; Ilic and Neubauer, 2005; Sippel et al., 2009). Several workers combine the Wallace and Bott and Mohr-Coulomb- based

methods to calculate solutions that are as realistic as possible (Reches, 1987; Celerier, 1988; Angelier, 1990; Zolohar and Vrabec, 2007; Sippel et al., 2009).

In this study, the paleostress reconstruction program Tectonics FP (Ortner et al., 2002, see also <http://www.tectonicsfp.com/>) was used, with implementations of several methods. We used the NDA (Spang, 1972; Sperner et al., 1993; Sperner, 1996) and the Right Dihedra Method (Angelier and Melcher, 1977) for our analyses. NDA is preferred for a number of reasons: firstly, DSI fails in cases with a single predominant fault orientation or in conjugate faults, as it requires 4 independent slip directions for the least squared calculation to work properly (Sperner, 1996). The fault set discussed here shows a high degree of conjugation. NDA is specifically suited for neo-formed, conjugate faults, but less for (reactivated) faults with oblique slip (Sperner, 1996). Secondly, earlier tests have shown that NDA is significantly more robust when a modified Monte Carlo analysis was preformed (Appendix 2). We believe this results from the least squares algorithm used in DSI, which is very sensitive to outliers and inhomogeneities in the data.

The Right Dihedra Method is a graphic method based on the assumption that when all faults move independently of each other within the same stress, then σ_1 is a part of the P-dihedra of all faults, and σ_3 is a part of all T-dihedra. By overlapping the P-T dihedra, orientation of σ_1 and σ_3 can be constrained, but the solution is not unique and does not include information regarding the relative size of the principal stresses (Angelier, 1979). Unlike NDA however, this method calculates the stress axes, so it was used to confirm the assumption of coinciding kinematic and stress axes.

Results

Thickness analysis and timing of faulting

The study area is surrounded on three sides by a set of sub-basins (see Figs. 2, 3 and 6). The structures are salt-structure bounded grabens, with two types of salt pillows on the flanks (see Fig. 2a and b; note that the crosssections are not ideally oriented for this purpose). On the western side of the graben system, salt pillows with a height of 1800 m are observed (Type I in Fig. 2a and b). The salt does not penetrate the Base Rijnland Group (Lowest Cretaceous). On top of these pillows (Fig. 3), collapse grabens have formed in the Upper Cretaceous and Tertiary deposits. On the eastern side of the graben, less prominent salt pillows (Type II in Fig. 2a and b) formed. As with the larger pillows, Triassic sediments on-lap on the sides and a collapse graben within the Cretaceous sediments are observed. The faults of the collapse graben however do not extend into the Tertiary. Inside the salt structure bounded grabens between the pillows, tilted Triassic sediments attain a thickness up to 400m. The symmetrical termination of the Triassic succession against the base of the Lower Cretaceous suggests that the grabens formed before or during the initiation of salt pillow formation. In the study area outside the graben, the Triassic sediments are generally less than 200 m thick. The thickness of the Lower Cretaceous does not change across the salt pillows and graben, and is about 50-90 m.

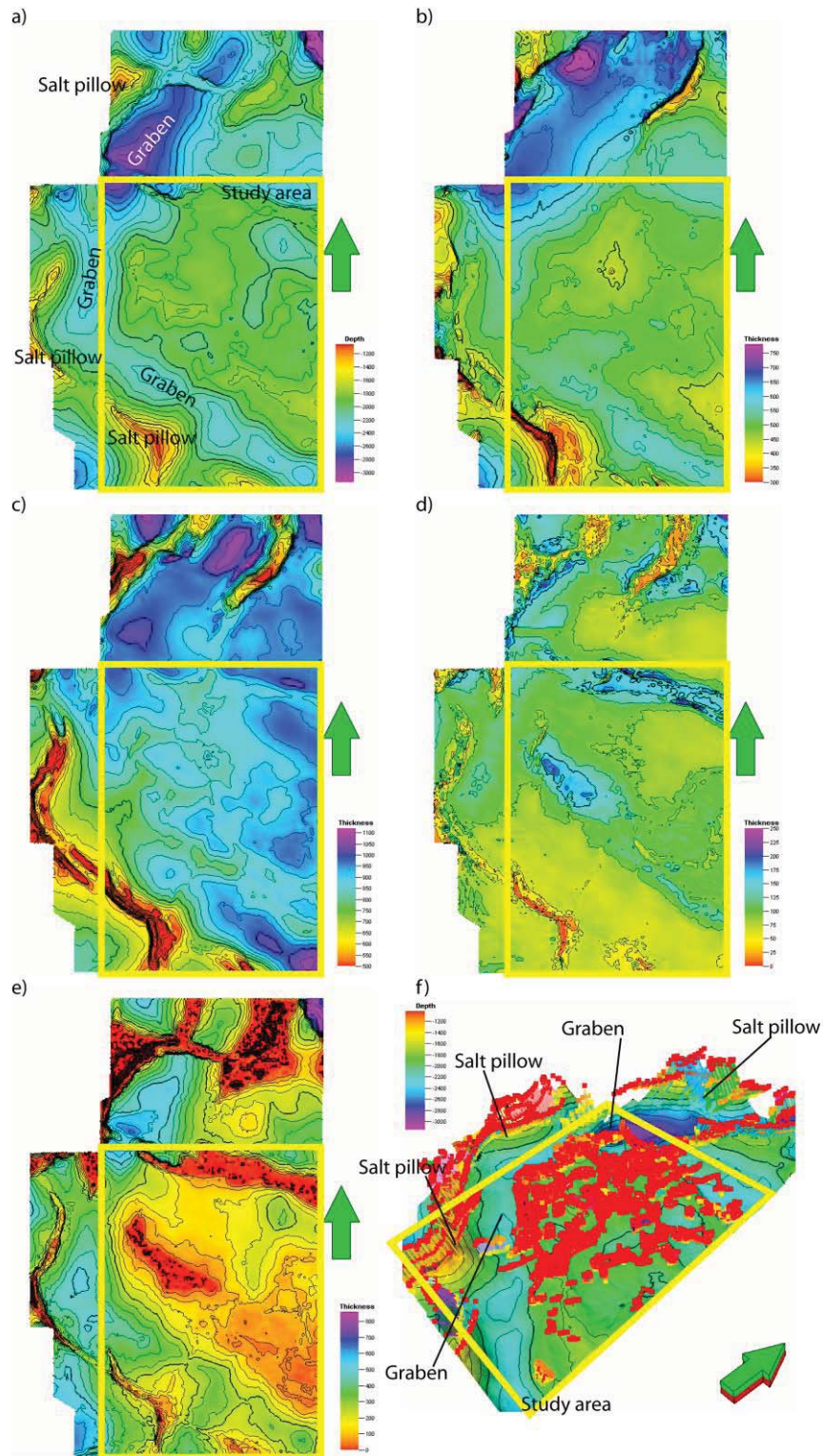


Figure 5: a) Top Zechstein depth map with grabens and salt structures indicated. Yellow box indicates present study area from figure 3. b) Thickness between Base Upper North Sea and Base North Sea. c) Thickness between base North Sea Supergroup and Base Chalk Group. d) Thickness between Base Chalk and Base Rijnland Formation (Upper Jurassic) e) Thickness between Base Rijnland and Top Zechstein f) Oblique view of the Top Zechstein Horizon. Faults within the yellow box are those studied in this study, while the faults along the crests of the salt structures are the meso-faults studied in Chapter 1.

An analysis of the Zechstein depth map (Fig. 5a) shows that the salt-structure bound grabens are between 400 m and 900 m deeper than the average of the study. Thickness maps show that the grabens were active between Base Upper North Sea and Base North Sea deposition (Fig. 5b), and to a lesser degree between Base North Sea and Base Chalk (Fig. 5c), with the NE-SW striking northern graben section receiving the largest amount of sediment. Between Base Chalk and Base Rijnland (Lowest Cretaceous), no significant differences are observed in the thickness between the graben and other parts of the study area (Fig. 5d), though differences are observed along faults.

Fault plane analysis

Figure 3 shows variance horizon maps for reflectors B to D and Top and Base Chalk. The variance maps of Fig. 3 are extracted at the reflector level, and faults appear as discrete, narrow zones of high variance (dark). In Figure 3a, the variance map of the base of the North Sea Group shows only major faults in the SW and NW corners. In the centre of the map, none of the intra-Chalk faults is seen to penetrate the level of the Base North Sea group (compare with Fig. 2). The variance maps of reflectors B and C (Fig. 3b and c) show of the predominantly NE-SW trending intra-Chalk faults, although some faults are observed in different orientations. The variance map of reflector D (Fig. 3d) shows mainly NE-SW oriented faults. In the Base Chalk variance map (Fig. 3e), traces of major faults are primarily observed in the N and SW of the survey. As suggested by Fig. 2, the intra-Chalk faults do not penetrate the base of the Chalk Group.

Figs. 4a and b shows that about 80% of the interpreted faults strike NE-SW and ca. 50% of the total numbers of faults (62% of the NE-SW striking faults) dip towards the NW, indicating a parallel-dipping fault array (sensu Buiter et al., 2008). Fault dips range between 45° and 65° , with an average of 49° (Fig. 4b). An oblique view of the interpreted fault sticks is provided in Fig. 5. Figure 6, shows series of different interpolated fault surfaces for different interpretation directions of four exemplary faults. In the following we use the following definitions: a fault pick is the node where the fault is “picked” during interpretation; a “fault stick” is the 3D representation of all fault picks interpreted in a single interpretation profile, connecting the picks with a bar; the interpretation profile is the 2D (usually vertical) crosssection through a fault on which the fault is picked. The horizontal angle between the down-dip-direction and the interpretation plane in the down dip direction (see Fig. 4c) is given for each fault. CW is a clockwise rotation away from the down-dip-direction; CCW is a counter clockwise rotation. The interpretation direction is also represented by the grey plane in the left of the fault. Fault undulations are defined as consistent, semi-linear changes in dip-directions in the fault plane, with respect to the overall dip-direction. These are interpreted and given as bold lines on the most ideally oriented interpretation of the fault plane (fault interpretation column a). This interpretation is then transposed to the same location on the other fault planes (columns b-d) for comparison. Successful transpositions (undulations that are clearly recognizable and can be independently interpreted on these planes) are black lines, mediocre transpositions (undulations are recognizable, but only with the

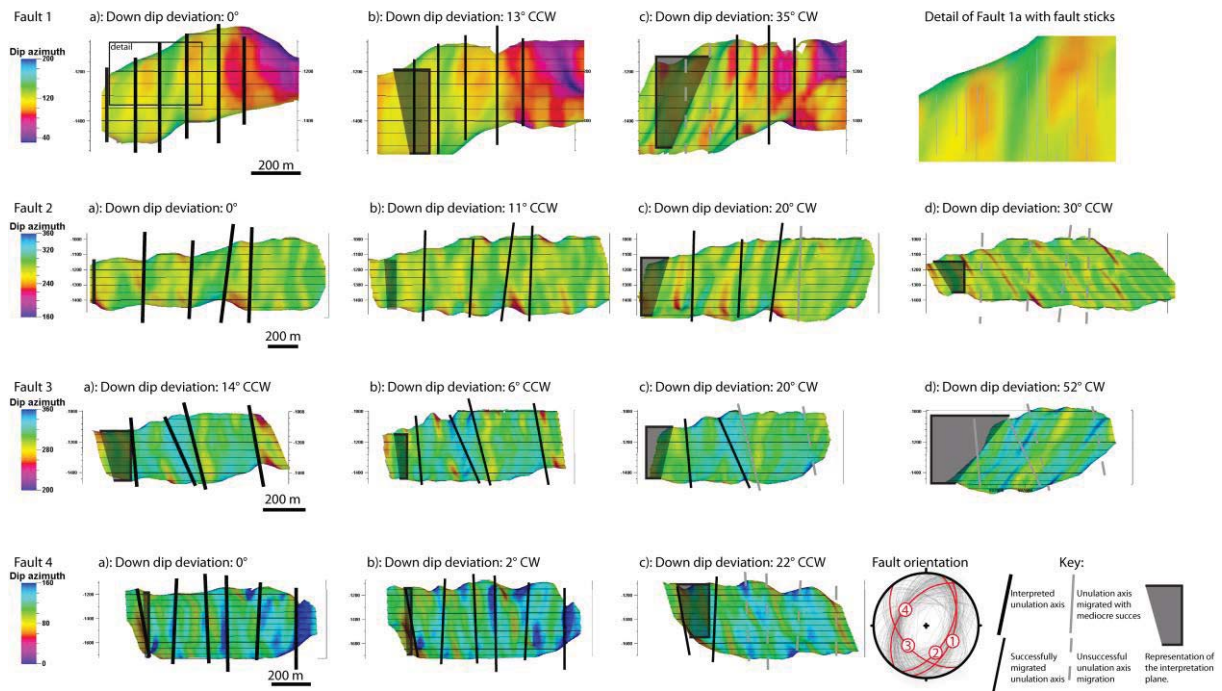


Figure 6: Overview of the fault surfaces, constructed from the detailed, independent interpretation of four faults from this study area, focussing on the fault undulations, see text for details. Fault 1 is the same fault as described in Chapter 1, figure 3, but in a different view. The fault orientations are given in the stereo net.. In the upper right a detail of fault 1a is shown, showing the number of fault sticks (purple lines) within an undulation.

a-priory interpretation on fault interpretation a) are grey lines. Unsuccessful transpositions (undulations are not recognizable) are grey dashed lines. The fault plane undulations observed in the first column (Fig. 6a) are recognizable in all of the different interpretations of the four faults shown in Fig. 6. Increasing the deviation of the interpretation profile (away from optimal) shows that the undulations are still recognizable, albeit with slightly different shapes. At higher deviations ($> 20^\circ$), new patterns appear with undulations parallel to the interpretation profile. Overall most undulations have a near down-dip orientation. The fact that in the detail of fault 1a, in the upper right of Fig. 6, multiple fault sticks are present in a single undulation shows that this is not the result of individual fault interpretations slightly out-of-line with the other fault sticks.

To further investigate the robustness of these undulations, Fig. 7a combines all the interpreted picks from all the different interpretations in a single plot. Several horizontal bands of high interpretation density can be distinguished (particularly in fault 4) which are the result of the choice to interpret faults at local dip changes (described above). Despite the presence of these bands, the overall spread of the interpretation points rules out the possibility that the fault surface undulations are an artefact of a longer average vertical distance between the points as compared to the average horizontal distance. Figure 7b shows the interpolated surface based on the combined data set of all interpreted points (Fig. 7a), with the interpreted undulation axes from (Fig. 6a) shown. This surface shows the main direction of undulations seen in Fig. 6, overprinted together with the undulations forming at high interpretation

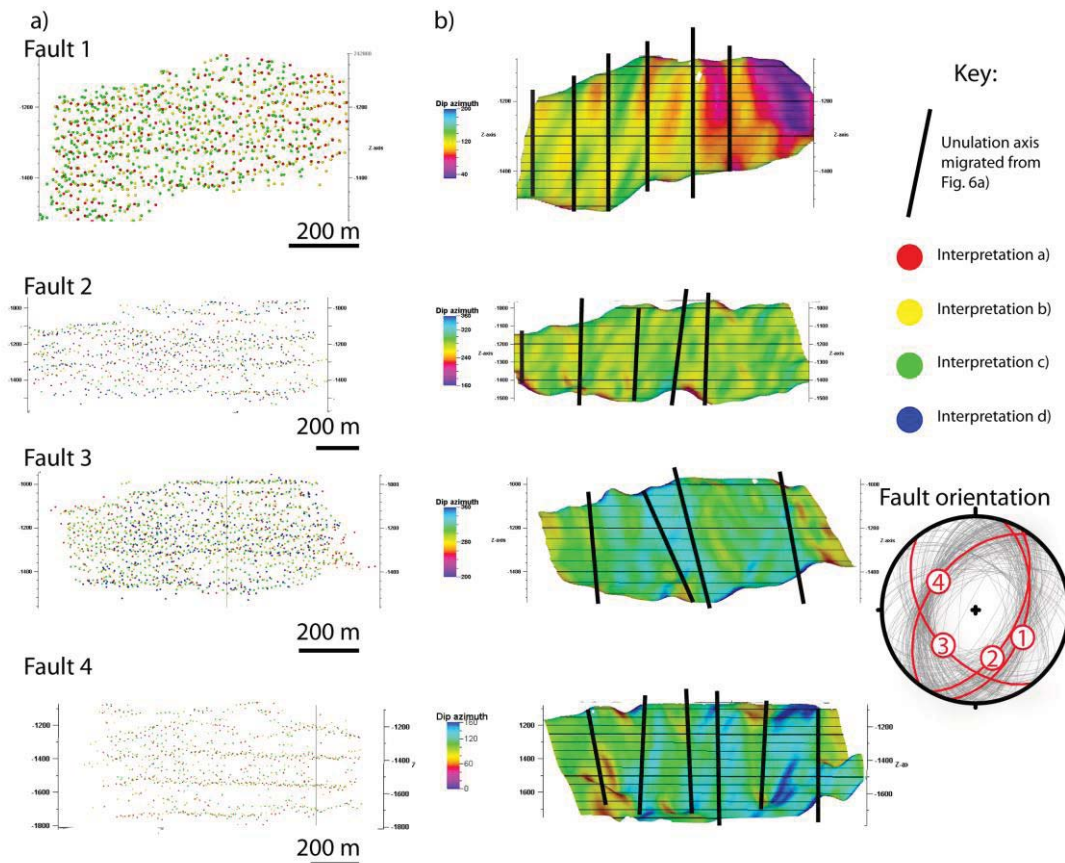


Figure 7: a) Original interpretation points for the four different interpretations in Fig. 6. The different colors denote the different interpretations, as in Fig. 6. b) Fault planes interpolated using the combined interpretations shown in the data from 7a). The undulation axes shown in the figure are taken from Fig. 6a).

angles (Fig. 6c-d). the main undulation directions however are still recognizable. Fig. 8 is an attempt to illustrate the spread of the actual fault picks around the fitted fault surfaces shown in Fig. 6a. The residuals between data and the surface (Fig. 8a) are the spread of interpretation picks around the interpolated fault surface. These are the result of “interpretation noise”. The spread of the data is maximum 30 m around the fault plane. Also shown is that (despite the inherent spread in points due to interpretation noise) the vertical bands of high interpretation density (Fig. 8b) show an undulation which has a larger wavelength than the spread in the data. Since the interpreted undulations and the interpolated fault surface are not coaxial (meaning that the undulations do not have linear and parallel axes, see Fig. 8b), it is not possible to find a projection which shows all residuals without parts of the data being obscured by the curved fault. For this reason, in Fig. 8c-g we show 100 m high, (nearly coaxial) ribbons cropped from the data set. Fig. 8c shows fault 4 (see Fig. 6), at 1400 ± 50 m depth (red arrows Fig. 8b), in a projection along the axis of the undulation in this slice. There are clear undulations in the fault pick data, reflected in the shape of the fault plane. Fig. 8d-g show other fault ribbons viewed in a similar way along the axis of undulations of the fault plane in a suitable slice, but without the fault plane to allow better visual interpretation of the undulations. The horizontal variance of

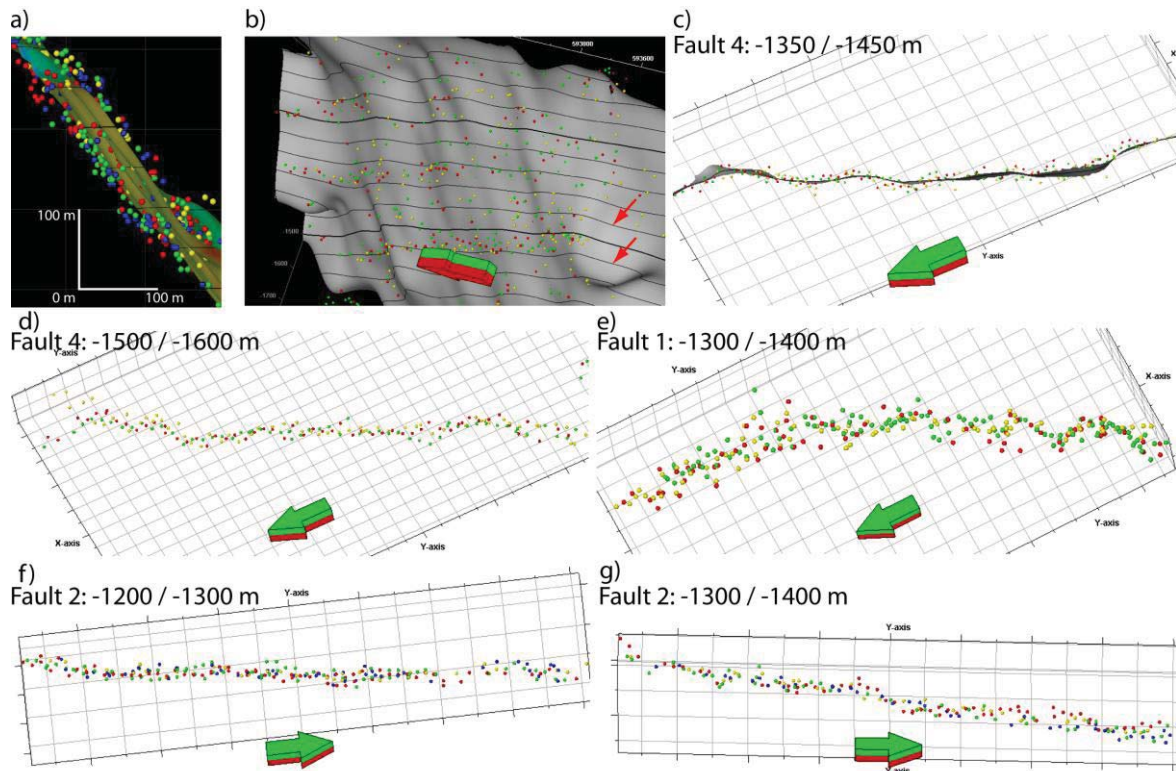


Figure 8: Detailed observations of the link between fault interpretation and fault surface undulations. For orientation and color key, see Fig. 6 and 7 A) a) Along-strike view of fault 2, showing the different interpretations as spheres (with color denoting the interpretation, and the letters corresponding to the position of the interpretation in Fig. 6) and the surface Fault 2 a-interpolation (Fig. 6) to indicate the residual distance of the interpretation points relative to the interpolated fault plane. b) updip, oblique view from the footwall block of fault 4 (For orientation; the arrow points north, green is up, red is down). This image shows the different interpreted points as spheres and fault plane 4a -interpolation (Fig. 6). Note the curving of the interpolated surface at the edges of the fault, due to interpolation artefacts. c) Along dip view of a cropped 100 m high ribbon of data from fault 4 around the -1400 m isochore (between red arrows in b). The fault surface is shown for clarity. d) A 100 m high ribbon of data from fault 4, around the -1550 m isochore. The fault surface is not shown, but was used to orientate the view in an optimal down-dip orientation. e) as d) but for fault 1, around the -1350 m isochore. f) as d) but for fault 2, around the -1250 m isochore. g) as d) but for fault 2, around the -1350 m isochore.

the interpreted points is much smaller than the wavelength of the undulations, which are clearly seen in all figures.

All surfaces in Fig. 6 and Fig. 7 are calculated using the default settings of the Taylor Series algorithm (Convergent Gridder in Petrel). To examine if the undulations are dependent on the surface-fitting algorithm, we used (with default settings) six different interpolation methods implemented in Petrel to calculate a fault surface interpretation 'a' of Fault 1 (Fig. 5). Fig. 9 shows the result of this comparison. As expected, some algorithms are less suited to fit a surface covering the whole range of data as they are not meant to interpolate this type of data, but the undulations of Fig. 6a can still be identified in all fault surfaces.

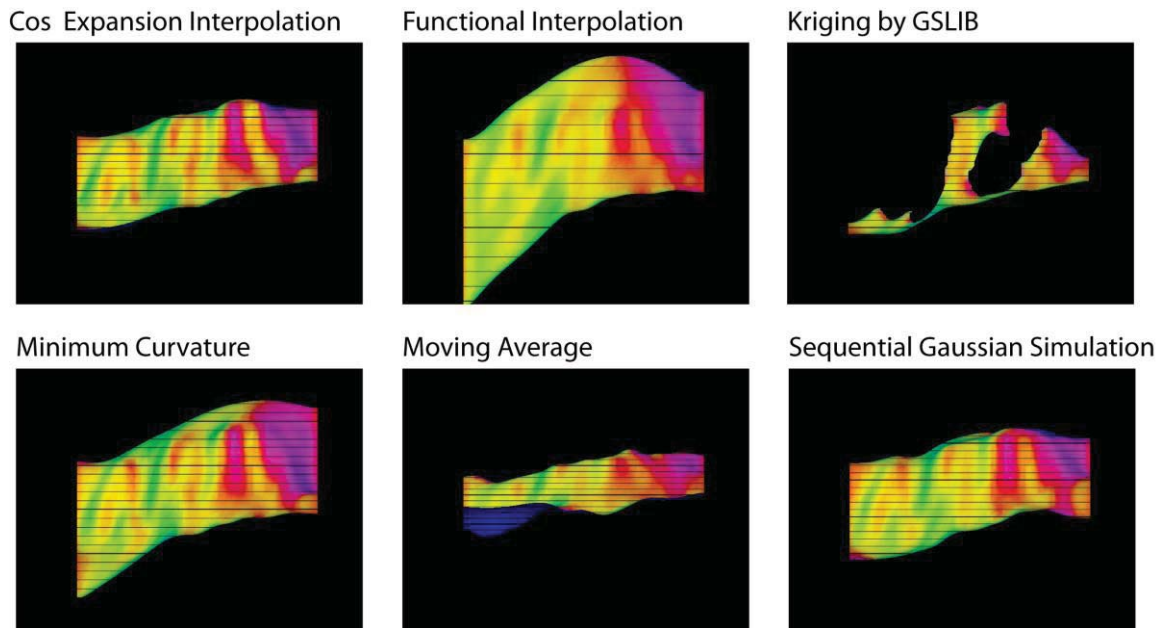


Figure 9: Comparison of fault planes built using different interpolation methods. The input data is fault 1a (Fig. 6). Fault surface colors denote dip-direction to show undulation as in Fig. 6 and Fig. 7. The names of interpolation method are taken from the Petrel 2007 version. Default calculation settings were used to calculate these fault planes

Interpretation of fault plane analysis results

All faults in Fig. 6 show fault undulation axes from different interpretation profiles can be successfully compared to each other. Whilst nearly all fault undulations are approximately down-dip oriented, Fault 3 seems to exhibit two different undulation orientations that are present in three of the four interpretation directions (Fig. 6, Fault 3, a-c). The reason for this could be that the oblique undulation results of two faults coalescing together (e.g. Lohr et al., 2008). The top tip-line of the fault is lower on the left compared to the right of this undulation, which supports this interpretation. However, it must be noted that the overall orientation of fault 3 does not correspond to the general trend of the faults in the study area (see stereoplot in Fig. 6). The comparison of fault planes in Fig. 9 shows that the undulations are independent of the gridding algorithm, thus that the undulations in Fig. 6 are not the result of processing artefacts.

A comparison of Figs. 6 and 7 shows consistent undulations of the fault plane. We interpret the observed fault plane undulations to be parallel to the direction of the slip on the fault (e.g. Brown and Scholz, 1985a; Power et al., 1987, Lee and Bruhn, 1996; Renard et al., 2006; Sagy et al., 2007). Slip on the faults studied here is thus interpreted to be dip-slip.

This interpretation is in line with studies of similar fault undulations from different settings and at a very wide range of length scales based on seismic data (see for example Needham et al., 1996; Marchal et al., 2003; Streit and Hillis, 2004; Lohr et al., 2008), laser measurements of exhumed fault surfaces

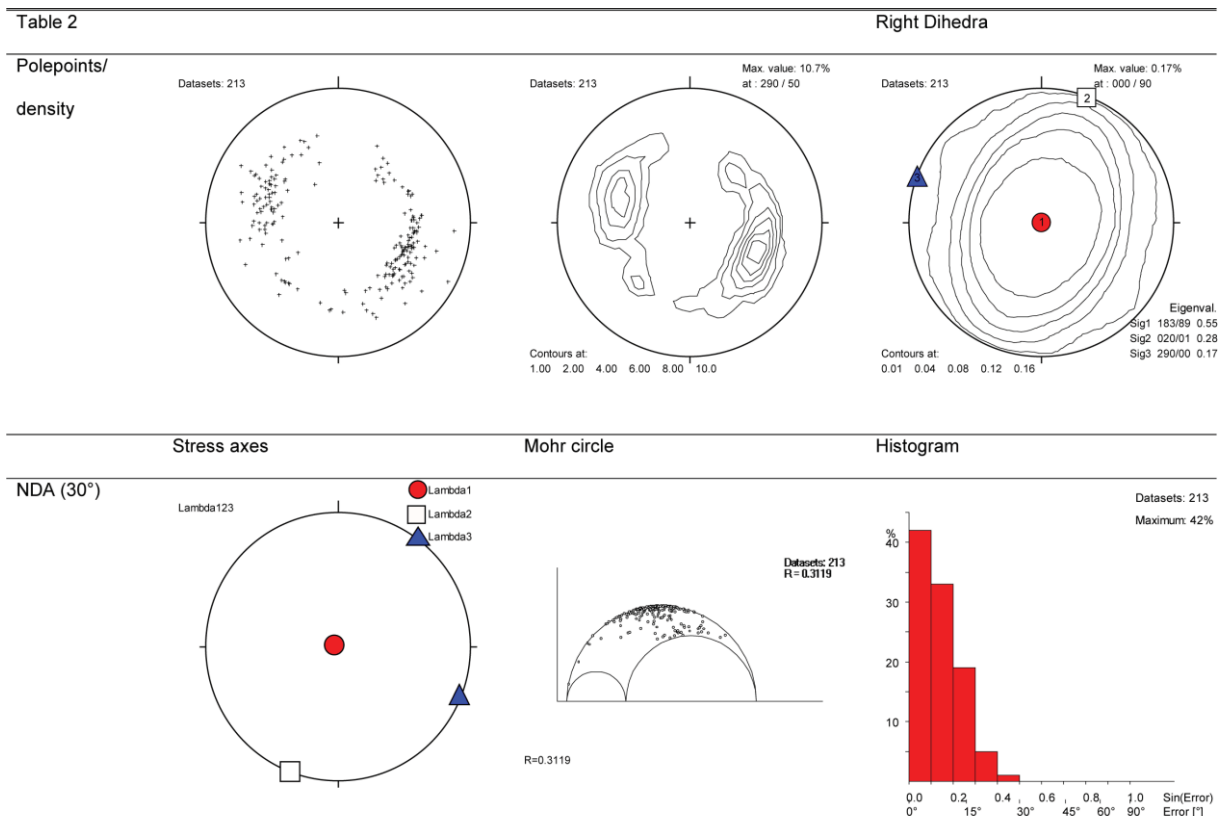


Table 2: Paleostress results calculated using a single dip-direction/ dip pair for every fault.

(Renard et al., 2006; Kokkalas et al., 2007; Sagy et al., 2007; Jones et al., 2009; Candela et al., 2009) and other field and laboratory data (e.g. Brown and Scholz, 1985b; Power et al., 1988; Lee and Bruhn, 1996; Van der Zee, 2001). These undulations of the fault plane are usually interpreted to result from the inherent random roughness of a fault at initial failure, which is selectively preserved or even amplified in the direction of the most recent slip (sensu: Brown and Scholz, 1985a; Power et al., 1987, Lee and Bruhn, 1996; Renard et al., 2006; Kokkalas et al., 2007; Sagy et al., 2007). Recent work suggests that faults with large slip are a lot smoother in the slip direction than small-scale faults (Sagy et al., 2007; Lohr et al., 2008).

Paleostress results

The fault plane analysis indicates that slip on the studied faults is dominantly dip-slip. For the subsequent paleostress analysis, the average orientation of each of the 213 interpreted faults was calculated by fitting an average plane to each fault, then assigning dip-slip movement vectors to each of surface. Table 2 shows the results for this paleostress calculation, together with stereographic projections of the 213 interpreted faults. Since the bulk of the faults are contained between Top and Base Chalk, and do not connect to any other structures, it can be inferred that all faults are neo-formed, non-inherited structures that were not reactivated during the Cenozoic. This supports our choice of the NDA paleostress technique. For NDA-based paleostress estimation, we used an angle of internal friction of 30°, an angle commonly used for neo-formed faults (Sperner et al., 1993; Sperner, 1996). The results from NDA and Right Dihedra give consistent kinematic and stress axes, supporting

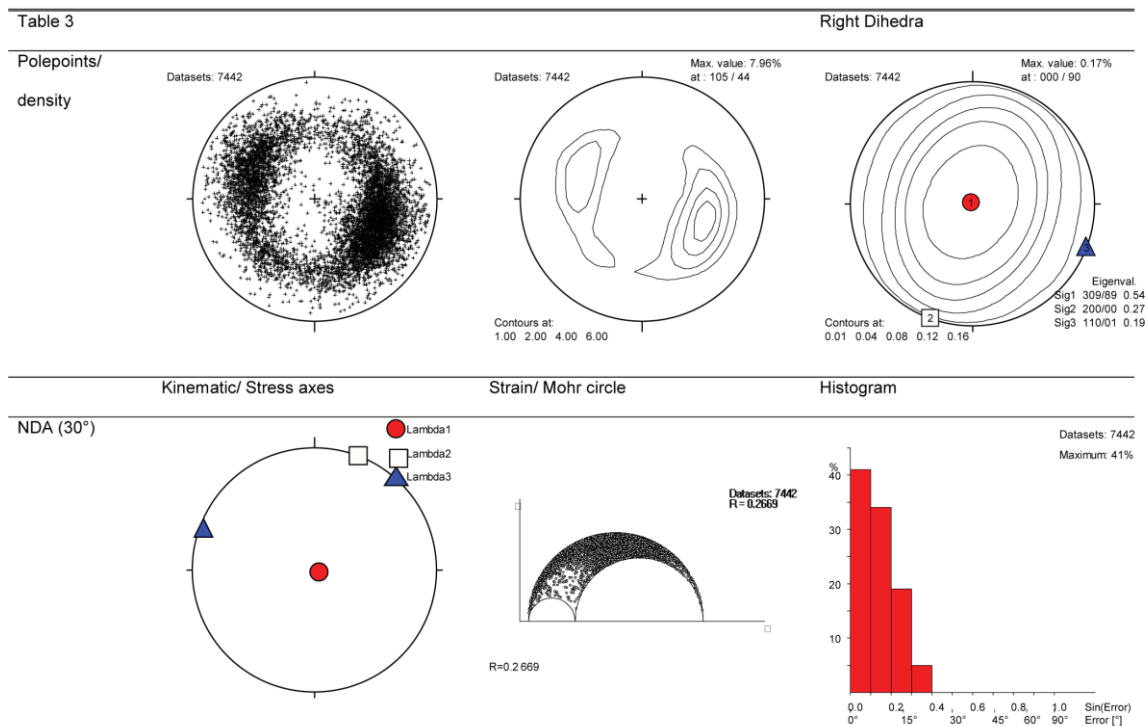


Table 3: Paleostress results calculated using dip-direction/ dip data from every triangle of the interpolated 3D surfaces.

the robustness of the results. The calculated paleostress axes show a vertical σ_1 and a NNE oriented σ_2 . This stress states represents NW-SE extension. The stress ratio for the NDA-calculation has a value of 0.31. The misfit histogram for the NDA-calculation has the half-bell-shape of a homogeneous data set (Sperner et al., 1993; Sperner, 1996).

The analysis described above uses a data set where the most of the shape information of individual faults is lost. In addition, faults are not weighed for their size or the detail of interpretation. To study the effect of this simplification, we have used each triangular segment of the electronic fault planes in combination with the corresponding dip-slip direction to calculate paleostress. This data set consist of 7442 orientation/slip pairs. Here we assume that slip is always dip-slip on every part of the fault, but this is an obvious simplification (see for example Roberts, 1996; Morewood and Roberts, 2000; Cowie and Roberts, 2001; Papanikolaou and Roberts, 2007; Maniatis and Hampel, 2008). Table 3 shows the results using this data set. The general shape of the pi-plot density contours is similar in both cases, showing that simplification of our first analysis is representative for the detailed fault shapes. Both the NDA and the Right Dihedra Method calculated a vertical σ_1 and a NNE oriented σ_2 . NDA gave an R-value of about 0.27. The NDA and Right Dihedra axes in Table 3 fit well with the axes calculated for Table 2 (the deviation is 1°) and the R-value is similar (0.31 vs. 0.27). Also the misfit histograms show a very good result, as 75% of the calculated slip directions have a misfit angle of 10° or less.

Discussion

Fault undulations

We interpret the consistent pattern of dip-direction variations on the fault plane (Figs. 6 and 7) as fault undulations that are not the result interpretation or interpolation artefacts. Fault undulations are observed on a wide range of length scales and are often described to be self affine (Brown and Scholz, 1985a; Power and Tullis, 1991; Lee and Bruhn, 1996; Develi and Babadagli, 1998; Van der Zee, 2001; Sagy et al., 2007; Candela et al., 2009). In this context it has to be kept in mind that “fault surfaces” in outcrops are formed by a combination of fracturing and erosion of a fault zone, and that fault surfaces studied here are representations of an entire zone of deformation with finite thickness and a complex internal structure (compare for example with: Koestler and Ehrmann, 1991, van der Zee et al., 2003). Also the number and particularly the spacing of data points, which are significantly smaller and larger respectively in this seismic study, need to be considered when comparing field and seismic studies.

The fault surface analysis presented in this paper documents that distinguishing “real” undulations from artefacts resulting from differences in the location of the pick in different crosslines, is a challenge. In addition, aliasing can occur if undulations exist at wavelength smaller than twice the sample point distance (Nyquist frequency; Campos and Tututi, 2007; Maxit, 2009). An additional complexity occurs when the interpretation plane has a large angle in respect to the down-dip-direction (Fig. 6, Fault 2d and Fault 3d). Here, the interpretation uncertainty in the interpretation direction creates an additional undulation, that overprints the (in this case) down-dip undulation. We suggest that keeping an interpretation profile at angles below 20° in respect to the down-dip-direction will help to avoid this. If discussing seismic-based fault surface analyses, detailed seismic interpretation is sensitive to “interpretation uncertainty”, but “conceptual uncertainty” can be another source of error (Bond et al., 2007), which is not entirely excluded here. In this study, no comparative analysis has been made on how “mis-picking” influences our results, but different interpreters are known to provide significantly different horizon interpretations (Rankey and Mitchell, 2003; Bond et al., 2007).

Figures 6, 7, 8 and 9 show that the fault plane undulations are consistent in interpretations in different profiles (Fig. 6, a-c/d) and have a wavelength greater than the inherent noise of interpretation (Fig. 8). They are also not the result of artefacts in the gridding algorithm (Fig. 9), of heterogeneous sampling or of spatial aliasing (Fig. 7). The amount of smoothing is, based on visual comparison in slices projected parallel to the axis of local undulations (Fig. 8c), a reasonable approximation to separate real undulations from noise.

Geology & regional paleostress

The presence of a large number of faults in the upper Cretaceous Chalk Group of the UK and France was previously interpreted to result of compaction and dewatering (Hibsch et al., 1995; Hibsch et al., 2003). These faults are described to be oriented highly heterogeneously in a single outcrop, contained entirely in the chalk succession, not connected to deeper or shallower structures and to display a pure dip-slip slickenside orientation. Dewatering related Chalk faults unsuitable for paleostress analysis as their formation is unrelated to tectonic events and due to their highly heterogeneous strike directions.

Polygonal faults were first described in the Cenozoic mudrocks of the North Sea and have been identified in over 50 sedimentary basins, predominantly in marine, fine-grained, smectite-rich mudrocks (Cartwright, 1994; Dewhurst et al., 1999; Goultly, 2001; Hansen et al., 2004; Goultly and Swarbrick, 2005). Polygonal faults only rarely occur in chalk (Goultly, 2001; Hansen et al., 2004). One polygonal fault set reported in the Upper Cretaceous Chalk of the Sable Subbasin, Canadian Atlantic Margin, might have been initiated in underlying mudrocks (Hansen et al., 2004).

On the other hand, Vandycke (2002) argues that the Chalk Group provides an excellent record for brittle tectonics using observations from several sites in Belgium, France and the UK to extract a paleostress stratigraphy spanning the Upper Cretaceous to the present time. Bevan and Hancock (1986) describe a system of NW-trending fractures in chalk deposits of southern England and northern France, which they attribute to Neotectonic movements in the Lower Rhinegraben system.

The faults of this study have several aspects in common with polygonal faulting. They are restricted to a specific depositional interval, appear to have no preferred strike direction in variance maps (Fig. 4) and low offsets. Detailed analysis of the interpreted faults however shows a clear preferential NW-SW orientation (Fig. 4), and the calculated R-value of 0.3 is too high for the radial extension associated with polygonal faulting (the R-value for polygonal faulting should approach 0; see Hibsich et al., 2003). Furthermore, a pressure-solutions study in reservoir chalk in the North Sea suggests that the chalk serves as an open system for fluid flow at the (paleo) depth of the Groningen Block (Safaricz and Davison, 2005; van der Molen 2005). Thus, it is most likely the faults of this study are tectonic in origin. The analysis of thickness maps (Fig. 5) shows two phases of activity of the major, salt-structure bound grabens; between the middle Upper Cretaceous and the present time, and during the Triassic. Because these grabens are decoupled from the underlying Rotliegend faults by the ductile Zechstein (Roth and Fleckenstein, 2001), and due to the mismatch in orientation of the fault structures across the salt, we infer that the growth of grabens is related to the growth of salt pillows. The thickness analysis then shows that no salt movement occurred in the Groningen Block between the Jurassic and the Campanian corresponding to the conclusion of Mohr et al. (2005). The fact that the salt structures on the western side of the graben extend further into the overburden is interpreted that during the second phase of salt movement, these structures were more active than those on the eastern side. Consequently, it seems most likely that the intra-Chalk faults described in this paper formed as a result of the (re-) activation of flow of salt to the salt pillows on the western side of the graben in the Upper Cretaceous, and the subsequent extension of the cover sediments towards the North West (Mohr et al., 2005).

The faults in this study preferentially dip in the direction of extension, the NW. In a 60° wide bin (stippled lines in Fig. 4b), placed over the average preferred orientation, 105 faults dip in the NW-direction and 64 dip to the SE. Buitter et al. (2008) indicated that parallel, basinward-dipping fault sets in the cover above a moving viscous layer will form when the basal shear on the brittle-viscous transition is "top-to-the-basin-centre". This means that in our case the basal shear was top-to-the NW. The intra-chalk faults directly bordering the main grabens (Fig. 5) are parallel to these grabens and do not correspond to the overall NW-orientation. A recalculation of the paleostress with 31 of these edge faults removed did not influence the paleostress result, and the interpreted faults still retained the preferential NW-SW strike and NNW dip (Fig. 4b). This suggests that the NW-SE extension was

relatively uniform in NW direction, and that the other grabens from Fig. 5 had little influence on this extension. The increase of the thickness of graben fill of the NE-SW striking graben in the NW corner of the study area (Fig. 5) also indicates that Chalk extension was predominantly in the NW direction. Smaller subsidence in the other grabens might have resulted in minor extension in different directions forming faults that do not correspond to the NW-SE extension.

The calculated paleostress results for the small faults in the Groningen area correspond well with the interpretation of the Late Cretaceous stress field derived from the analysis of large scale faults of the same area (Chapter 1). Despite a significant difference of the data sets used, a data set of 27 reactivated faults with a displacement larger than 50 m delivered stress tensors that are almost identical (both in orientation of the principle stresses and stress ratio, which is 0.38; Chapter 1) with faults analyzed in this study. Furthermore, Vandycke (2002) observed a very similar pre-Laramide extension phase in the chalks of Kent, Sussex (UK), Boulonnais (France) and the Mons Basin (Belgium). The R-Value for these tensors is between 0.2 and 0.5 (Vandycke, personal communication, 2008). This suggests that the Late Cretaceous phase of extension is of regional nature.

We have assumed in this study that the slip direction on the interpreted faults was entirely dip-slip. However, even if the movement on the faults was not exactly dip-slip, but rather normally distributed about pure dip-slip movement, a theoretical Monte Carlo study has shown for three different data sets (Appendix 2) that the introduction of a normally distributed, artificial measurement error in the slip direction, with a standard deviation of several degrees, only has a limited effect on the orientation of the stress axes.

A quick inventory of three additional seismic data sets spread over the entire Dutch sector, spread over 200 km, suggests that similar intra-Chalk faults are present in seismic surveys as well. All faults in these surveys (in one data set over 230 faults were identified and interpreted) show a preferential E-W orientation, rather than the NE-SW orientation in Groningen. The E-W oriented faults seem generally unaffected by the main tectonic trends of the area. The difference in orientation might result from a difference in timing of fault formation (e.g. Gauthier et al., 2000 observed a Tertiary N-S extension), a perturbation of the local paleostress field (these three additional surveys are west of the Lauwerszee Trough, a Pre-Permian structure, and the present study area is on the eastern side), or a difference in fault-formation mechanism or Zechstein decoupling (e.g. Scheck et al., 2003).

Mechanical stratigraphy

An important feature of the extensional faults of this study is that they are only visible in the Chalk deposits, and are best observed between auxiliary horizons B and C (Fig. 2). Above and below these horizons the studied faults seem to die out rather quickly. This interval corresponds to the Middle and Upper Campanian. Herngreen and Wong (2007) describe the Campanian and Maastrichtian “Upper” Ommelanden Formation as consisting of consolidated calcarenites in the lower parts that grade towards the top into massive chalks with flint layers. Below the Ommelanden Fm occur marlier Coniacian to Santonian deposits. This makes the Lower to Middle Campanian carbonates relatively competent in comparison with the surrounding Cretaceous chalks and the underlying Triassic rocks, which might explain why these faults predominantly formed in this interval.

Paleostress assumptions

An important assumption of paleostress analyses is that the sampled stress field is homogenous and constant on the scale of the study. In field studies, outcrop sizes do generally not exceed 50 to 100 m, though stress deflections are known to occur on this scale (e.g. Dupin et al., 1993; Angelier, 1994; Gruenthal and Stromeyer, 1994 and Maerten et al., 2002). Discussions of the validity of the basic paleostress assumptions by e.g. Dupin et al. (1993), Pollard et al. (1993) and Gapais et al. (2000) focus on outcrop scale studies. It is however reasonable to assume that the same features that cause problems in field-based paleostress analyses also influence paleostress analysis at the scale presented. The present study area is with 10 x 15 km much larger compared to outcrop paleostress studies.

However, it must be noted that this is probably one of the most important aspects in which this paleostress study differs from field-based paleostress analyses. The area or volume of rock over which the paleostress is calculated is significantly larger than that of field-based paleostress studies. This means that unlike in field studies where local stress states are calculated, a “regional”, or possibly, geodynamic stress state is calculated. This also has the effect that a considerable part of internal detail is lost in seismic-based paleostress studies. However, comparing different 3D seismic distributed over a basin will allow recognition of the regional or geodynamical stress changes and their controls. The second aspect in which seismic-based studies differ from field studies is that the slip direction is not directly observed, but inferred from geometrical information. However, we believe that the fault undulations described here form a reasonably proxy for the paleo-slip direction of faults. On the other hand, the three dimensional nature of seismic data unravels significantly more of the 3D geometry of fault system than outcrop studies.

To test this first order assumption of stress field homogeneity we sub-divided the study area in four zones (Appendix 3). Recalculating the stresses with only the faults enclosed in these subareas showed a first order validity of the assumption of stress homogeneity but the result was influenced by the reduction of the amount of faults in the subareas. The present study, with a high number of faults producing the same stress tensor as the large scale study (Chapter 1), shows the validity of this approach and indicates that stresses in the Groningen area during the Upper Cretaceous were relatively homogenous on the scale of the analysis. Compared with the Upper Cretaceous stress state calculated in (Chapter 1), the fact that here only a single set of non-reactivated, low displacement faults is present, makes the structural reconstruction step (in order to remove younger deformation, to obtain older geometries) unnecessary. This actually makes the results here more robust, as the reconstruction is assumed to introduce a lot of errors (Gartell and Lisk, 2005). This, combined with the observation of similar, but differently oriented intra-Chalk faults in other parts of the Dutch subsurface, leads us to propose that a detailed, NW Europe-wide study of Chalk in seismic data sets would allow for a detailed stress-map of the Upper Cretaceous in areas currently covered by post-Cretaceous sediments and/or water.

Conclusions and outlook

The workflow described in this paper uses small-scale, intra-Chalk faults, confined to the Cretaceous Chalk Group, to provide a way to estimate paleostress from seismic data for a specific time interval.

The relatively brittle nature of the Chalk Group makes it an excellent recorder of brittle deformation that might not be observed in softer deposits. The dominance of these faults in a specific interval might be related to variation of brittleness of chalk deposits.

A detailed interpretation of the fault and the seismic data shows that the fault surfaces studied show clear down-dip undulations that are not the result of interpretation or gridding effects. These undulations are interpreted to represent the paleo-slip direction of these faults.

The calculated paleostress of this study results in a stress for the Upper Cretaceous that corresponds well with stress fields described by Vandycke (2002) and Chapter 1, indicating that the studied faults are very likely to be influenced by a regional stress field.

Acknowledgement

The Nederlandse Aardolie Maatschappij BV (NAM, a Shell operated 50-50 joint venture with ExxonMobil) is thanked both for the use of the seismic data, and for discussion of the results.

Kees van Ojik (Argo Geosciences) is thanked for constraining the age of the chalk reflectors.

We further thank Judith Sippel for various discussions on paleostress and Sussane Buiter for discussing on the nature of parallel dipping fault sets. Schlumberger is thanked for providing Petrel 2007 under academic licence.

Charlotte Krawczyk and an anonymous reviewer are thanked for their comments that improved the manuscript considerably.

References

- ◇ Anderson, E. M., 1942. The dynamics of faulting and dyke formation with applications to Britain. Oliver&Boyd, Edinburgh, First edition, pp. 206.
- ◇ Angelier, J., 1979. Determination of the mean principle directions of stresses for a given fault population. *Tectonophysics* 3-4, T17-T27.
- ◇ Angelier, J., 1990. Inversion of field data in fault tectonics to obtain the regional stress-III. A new rapid direct inversion method by analytical means. *Geophysics Journal International* 103, 363-376.
- ◇ Angelier, J., 1994. Fault Slip Analysis and Paleostress Reconstruction. In: Hancock, P. L. (Ed.), *Continental Deformation*. Pergamon Press, Oxford, 53-100.
- ◇ Angelier, J., Melcher, P., 1977. Sur une methode graphique de recherche des contraintes principales egalement utilisable en tectonique et en seismologie: la methode des diedres droits. *Bull. Soc. geol. Fr.* 7, 1309-1318.
- ◇ Arnott, S. K., van Wunnik, J. N. M., 1996. Targeting Infill Wells in the Densely fractured Lekhwaier Field, Oman. *GeoArabia* 1(3), 405-416.
- ◇ Bergerat, F., 1987. Stress Fields in the European platform at the time of Africa-Eurasia collision. *Tectonics* 6(2), 99-132.

- ◇ Bevan, T. G., Hancock, P. L., 1986. A late Cenozoic regional mesofracture system in southern England and northern France. *Journal of the Geological Society* 143, 355-362.
- ◇ Bond, C. E., Gibbs, A. D., Shipton, Z. K., Jones, S., 2007. What do you think this is? "Conceptual uncertainty" in geoscience interpretation. *GSA Today* 11, 4-10.
- ◇ Bott, M. H. P., 1959. The mechanics of oblique slip faulting. *Geological Magazine* 96(2), 109-117.
- ◇ Brasher, J. E., Vagle, K. R., 1996. Influence of lithofacies and diagenesis on Norwegian North Sea chalk reservoirs. *AAPG Bulletin* 80(5), 746-769.
- ◇ Briggs, I. C., 1974. Machine contouring using minimum curvature. *Geophysics* 39, 39-48.
- ◇ Brown, S. R., Scholz, C. H., 1985a. Broad Bandwidth Study of the Topography of Natural Rock Surfaces. *Journal of Geophysical Research* 90(B14), 12575-12582.
- ◇ Brown, S. R., Scholz, C. H., 1985b. Closure of Random Elastic Surfaces in Contact. *Journal of Geophysical Research* 90(B7), 5531-5545.
- ◇ Buiter, S., Schreurs, G., Ellis, S., 2008. The formation of parallel-dipping faults at passive margins. *Geo2008 – Resources and Risks in the Earth System, Aachen, Germany, Schriftreihe der Deutschen Gesellschaft für Geowissenschaften*, 60, 68.
- ◇ Caiazza, C., Ascione, A., Cinque, A., 2006. Late Tertiary–Quaternary tectonics of the Southern Apennines (Italy): New evidences from the Tyrrhenian slope. *Tectonophysics* 421, 23-51.
- ◇ Campos, R. G., Tututi, E. S., 2007. Aliasing modes in the lattice Schwinger model. *Physics Letters A* 36, 1-5.
- ◇ Candela, T., Renard, F., Bouchon, M., Marsan, D., Schmittbuhl, J., Voisin, C., 2009. Characterization of Fault Roughness at Various Scales: Implications of Three-Dimensional High Resolution Topography Measurements. *Pure and Applied Geophysics* 166(10-11), 1817-1851.
- ◇ Cartwright, J. A., 1994. Episodic basin-wide hydrofracturing of overpressured Early Cenozoic mudrock sequences in the North Sea Basin. *Marine and Petroleum Geology* 11(5), 587-607.
- ◇ Casabianca, D., Jolly, R. J. H., Pollard, R., 2007. The Machar Oil Field: waterflooding a fractured chalk reservoir. In: Lonergan, L., Jolly, R. J. H., Rawnsley, K. & Sanderson, D. J. (Eds.), *Fractured reservoirs*. Geological Society, London, Special Publications 270, 171-191.
- ◇ Celerier, B., 1988. How much does slip on a reactivated fault plane constrain the stress tensor? *Tectonics* 7(6), 1257–1278.
- ◇ Coulomb, C. A., 1776. Sur une application des règles maximis et minimis à quelques problèmes de statique à l'architecture. *Acad. Sci. Paris Mém. Math. Phys.*, 343-382.
- ◇ Cowie, P. A., Roberts, G. P., 2001. Constraining slip rates and spacings for active normal faults. *Journal of Structural Geology* 23, 1901-1915.
- ◇ Cox, T., Seitz, K., 2007. Ant Tracking Seismic Volumes for Automated Fault Interpretation. CSPG CSEG Convention, Calgary, Alberta, Canada.
- ◇ De Jager, J., 2003. Inverted basins in the Netherlands, similarities and differences. *Netherlands Journal of Geosciences / Geologie en Mijnbouw* 82(4), 355-366.
- ◇ Delvaux, D., 1997. Post-Variscan right-lateral wrench faulting in the Ardenne Allochton and Variscan Front (Belgium). *Belgian Symposium on Structural Geology and Tectonics, Aardkundige Mededelingen*, 8, 57-60.

- ◇ Develi, K., Babadagli, T., 1998. Quantification of Natural Fracture Surfaces Using Fractal Geometry. *Mathematical Geology* 30(8), 971.
- ◇ Dewhurst, D. N., Cartwright, J. A., Lonergan, L., 1999. The development of polygonal fault systems by syneresis of colloidal sediments. *Marine and Petroleum Geology* 16, 793-810.
- ◇ Dronkers, A. J., Mrozek, F. J., 1991. Inverted basins of The Netherlands. *First Break* 9(9), 409-425.
- ◇ du Rouchet, J., 1981. Stress Fields, A key to Oil Migration. *AAPG Bulletin* 65(1), 74-85.
- ◇ Duin, E. J. T., Doornenbal, J. C., Rijkers, R. H. B., Verbeek, J. W., Wong, T. E., 2006. Subsurface structure of the Netherlands - results of recent onshore and offshore mapping. *Netherlands Journal of Geosciences / Geologie en Mijnbouw* 85(4), 245-276.
- ◇ Dupin, J. M., Sassi, W., Angelier, J., 1993. Homogeneous stress hypothesis and actual fault slip: a distinct element analysis. *Journal of Structural Geology* 15, 1033-1043.
- ◇ Gapais, D., Cobbold, P. R., Bourgeois, O., Rouby, D., de Urreiztieta, M., 2000. Tectonic significance of fault slip data. *Journal of Structural Geology* 22, 881-888.
- ◇ Gartrell, A. P., Lisk, M., 2005. Potential New Method for Paleostress estimation by Combining Three-dimensional Fault Restoration and Fault Slip Inversion Techniques: First Test on the Skua Field, Timor Sea. In: Boulton, P. & Kaldi, J. (Eds.), *Evaluating fault and cap rock seals*. AAPG Hedberg Series 2, 23-26.
- ◇ Gauthier, B. D. M., Franssen, R. C. W. M., Drei, S., 2000. Fracture networks in Rotliegend gas reservoirs of the Dutch offshore: implications for reservoir behaviour. *Geologie en Mijnbouw/ Netherlands Journal of Geosciences* 79(1), 45-57.
- ◇ Glennie, K. W. (Editor), 1998. *Petroleum Geology of the North Sea. Basic Concepts and Recent Advances* (fourth edition). Blackwell Science, Oxford, pp. 464.
- ◇ Gouly, N. R., 2001. Polygonal fault networks in fine-grained sediments - an alternative to the syneresis mechanism. *First Break* 19(2), 69-73.
- ◇ Gouly, N. R., Swarbrick, R. E., 2005. Development of polygonal fault systems. a test of hypotheses. *Journal of the Geological Society* 162, 587-590.
- ◇ Gras, R., Geluk, M. C., 1999. Late Cretaceous - Early Tertiary sedimentation and tectonic inversion in the southern Netherlands. *Geologie en Mijnbouw* 78, 1-79.
- ◇ Gruenthal, G., Stromeyer, D., 1994. The recent crustal stress field in Central Europe sensu lato and its quantitative modelling. *Geologie en Mijnbouw* 73, 173-180.
- ◇ Hansen, D. M., Shimeld, J. W., Williamson, M. A., Lykke-Andersena, H., 2004. Development of a major polygonal fault system in Upper Cretaceous chalk and Cenozoic mudrocks of the Sable Subbasin, Canadian Atlantic margin. *Marine and Petroleum Geology* 21, 1205-1219.
- ◇ Henk, A., 2005. Pre-drilling prediction of the tectonic stress field with geomechanical models, *First Break* 23, 53-57.
- ◇ Herngreen, G. F. W., Wong, T. E., 2007. Cretaceous. In: Wong, T. E. (Ed.), *Geology of the Netherlands*. Edita-KNAW, Amsterdam, 127-150.
- ◇ Hesthammer, J., Henden, J. O., 2000. Closing the gap between theory and practice in seismic interpretation of small-scale faults. *Petroleum Geoscience* 6, 107-111.

- ◇ Hibsich, C., Cartwright, J. A., Hansen, D. M., Gaviglio, P., André, G., Cushing, M., Bracq, P., Juignet, P., Benoit, P., Allouc, J., 2003. Normal faulting in chalk: tectonic stresses vs. compaction-related polygonal faulting. In: Van Rensbergen, P., Hillis, R. R., Maltman, A. J. & Morley, C. K. (Eds.), *Subsurface Sediment Mobilization*. Geological Society of London, Special Publications 216, 391.
- ◇ Hibsich, C., Jarrige, J.-J., Cushing, E. M., Mercier, J., 1995. Paleostress analysis, a contribution to the understanding of basin tectonics and geodynamic evolution. Example of the Permian/Cenozoic tectonics of Great Britain and geodynamic implications in western Europe. *Tectonophysics* 252, 103-136.
- ◇ Huang, Q., 1988. Computer-based method to separate heterogeneous sets of fault-slip data into sub-sets. *Journal of Structural Geology*, 10(3): 297-299.
- ◇ Ilic, A., Neubauer, F., 2005. Tertiary to recent oblique convergence and wrenching of the Central Dinarides: Constraints from a palaeostress study. *Tectonophysics* 410, 465-484.
- ◇ Jones, R. R., McCaffrey, K. J. W., Clegg, P., Wilson, R. W., Holliman, N. S., Holdsworth, R. E., Imber, J., Waggott, S., 2009. Integration of regional to outcrop digital data: 3D visualisation of multiscale geological models. *3D GIS and 3D visualisation* 35(1), 4-18.
- ◇ Kettel, D., 1983. The east Groningen Massif - Detection of an Intrusive body by means of coalification. In: Kaasschieter, J. P. H. & Reijers, T. J. A. (Eds.), *Petroleum geology of the southeastern North Sea and adjacent onshore areas*. *Geologie en Mijnbouw* 62, The Hague, 203-210.
- ◇ Kleinspehn, K. L., Pershing, J., Teyssier, C., 1989. Paleostress stratigraphy: A new technique for analyzing tectonic control on sedimentary-basin subsidence. *Geology* 17, 253-256.
- ◇ Koestler, A. G., Ehrmann, W. U., 1991. Description of brittle extensional features in chalk on the crest of a salt ridge (NW Germany). In: Roberts, A. M. & Yielding, G. (Eds.), *The Geometry of Normal Faults*. Geological society Special Publication 56, 113-123.
- ◇ Kokkalas, S., Jones, R. R., McCaffrey, K. J. W., Clegg, P., 2007. Quantitative fault analysis at Arkitsa, Central Greece, using terrestrial Laser-Scanning ("LiDAR"). *Bulletin of the Geological Society of Greece XXXVII*(Proceedings of the 11th International Congress, Athens, May, 2007), 1-14.
- ◇ Larroque, J. M., Laurant, P., 1988. Evolution of the stress field pattern in the south of the Rhine Graben from the Eocene to the present. *Tectonophysics* 148, 41-58.
- ◇ Lee, J.-J., Bruhn, R. L., 1996. Structural anisotropy of normal faults. *Journal of Structural Geology* 18(8), 1043-1059.
- ◇ Lohr, T., 2007. Seismic and sub-seismic deformation on different scales in the NW German Basin. PhD thesis, Freie Universität Berlin.
- ◇ Lohr, T., Krawczyk, C. M., Oncken, O., Tanner, D. C., 2008. Evolution of a fault surface from 3D attribute analysis and displacement measurements. *Journal of Structural Geology* 30(6), 690-700.
- ◇ Maerten, L., Gillespie, P., Pollard, D. D., 2002. Effects of local stress perturbation on secondary fault development. *Journal of Structural Geology* 24, 145-153.
- ◇ Maniatis, G., Hampel, A., 2008. Along-strike variations of the slip direction on normal faults: Insights from three-dimensional finite-element models. *Journal of Structural Geology* 30(1), 21.

- ◇ Mallon, A. J., Swarbrick, R. E., 2002. A compaction trend for non-reservoir North Sea Chalk. *Marine and Petroleum Geology* 19, 527-539.
- ◇ Mallon, A. J., Swarbrick, R. E., 2008. Diagenetic characteristics of low permeability, non-reservoir chalks from the Central North Sea. *Marine and Petroleum Geology*, 25, 1097-1108
- ◇ Marchal, D., Guiraud, M., Rives, T., 2003. Geometric and morphologic evolution of normal fault planes and traces from 2D and 4D data. *Journal of Structural Geology* 25, 135-158.
- ◇ Maxit, L., 2009. Wavenumber space and physical space responses of a periodically ribbed plate to a point drive: A discrete approach. *Applied Acoustics* 70, 563-578.
- ◇ Means, W. D. 1987. A newly recognized type of slickenside striation. *Journal of Structural Geology* 9(5-6), 585.
- ◇ Michon, L., van Balen, R. T., Merle, O., Pangnier, H., 2003. The Cenozoic evolution of the Roer Valley Rift System integrated at a European scale. *Tectonophysics* 367, 101-126.
- ◇ Mohr, M., Kukla, P. A., Urai, J. L., Bresser, G., 2005. Multiphase salt tectonic evolution in NW Germany: seismic interpretation and retro-deformation. *International Journal of Earth Sciences (Geologische Rundschau)* 94, 914-940.
- ◇ Mohr, O., 1900. Welche Umstände bedingen die Elastitätsgrenze und den Bruch eines Materials? *Zeitschrift de Vereins Deutscher Ingenieure* 44, 1524-1530, 1572-1577.
- ◇ Morewood, N. C., Roberts, G. P., 2000. The geometry, kinematics and rates of deformation within an en échelon normal fault segment boundary, central Italy. *Journal of Structural Geology* 22, 1027-1047.
- ◇ Needham, D. T., Yielding, G., Freeman, B., 1996. Analysis of fault geometry and displacement patterns. In: Buchanan, P. G. & Nieuwland, D. A. (Eds.), *Modern Developments in Structural Interpretation, Validation and Modelling*. Geological Society Special Publication 99, 189-199.
- ◇ Neves, F. A., Al-Marzoug, A., Kim, J. J., Nebrija, A. L., 2003. Fracture characterization of deep tight gas sands using azimuthal velocity and AVO seismic data in Saudi Arabia. *The Leading Edge*, 469-475.
- ◇ Oakman, C. D., Partington, M. A., 1998. Chapter 9: Cretaceous. In: Glennie, K. W. (Ed.), *Petroleum Geology of the North Sea. Basic Concepts and Recent Advances (fourth edition)*. Blackwell Science, Oxford, 294-349.
- ◇ Ortner, H., Reiter, F., Acs, P., 2002. Easy handling of tectonic data: the programs TectonicVB for Mac and Tectonics FP for Windows(tm). *Computers & Geosciences* 28, 1193-1200, see also <http://www.tectonicsfp.com/>.
- ◇ Otrtuno-Arzate, S., Ferket, H., Cacas, M.-C., Swennen, R., Roure, F., 2003. Late cretaceous Carbonate Reservoirs in the Cordoba Platform and Veracruz Basin, Eastern Mexico. In: Bartolini, C., Buffler, R. T. & Blickwede, J. (Eds.), *The Circum-Gulf of Mexico and the Caribbean: Hydrocarbon habitats, basin formation, and plate tectonics*. AAPG Memoir 79, 476-514.
- ◇ Papanikolaou, I. D., Roberts, G. P., 2007. Geometry, kinematics and deformation rates along the active normal fault system in the southern Apennines: Implications for fault growth. *Journal of Structural Geology* 29(1), 166.
- ◇ Pollard, D. d., Saltzer, S. D., Rubin, A. M., 1993. Stress inversion methods: are they based on faulty assumptions? *Journal of Structural Geology* 15(8), 1045-1054.

- ◇ Power, W. L., Tullis, T. E., 1991. Euclidean and Fractal Models for the Description of Rock Surface Roughness. *Journal of Geophysical Research* 96(B1), 415-424.
- ◇ Power, W. L., Tullis, T. E., Weeks, J. D., 1988. Roughness and Wear During Brittle Faulting. *Journal of Geophysical Research* 93(B12), 15268-15278.
- ◇ Power, W. L., Tullis, T. E., Brown, S. R., Boitnott, G. N., Scholz, C. H., 1987. Roughness of natural fault surfaces. *Geophysical Research Letters* 14(1), 29-32.
- ◇ Ramsay, J. G., Lisle, R. J., 2000. *The Techniques of modern structural geology Volume 3: Applications of continuum mechanics in structural geology*. Academic Press, London, pp. 700-1061.
- ◇ Rankey, E. C., Mitchell, J. C., 2003. That's why it's called interpretation: Impact of horizon uncertainty on seismic attribute analysis. *The Leading Edge* 22(9), 820.
- ◇ Reches, Z. E., 1987. Determination of the tectonic stress tensor from slip along faults that obey the Coulomb yield condition. *Tectonics* 6(6), 849–861.
- ◇ Renard, F., Voisin, C., Marsan, D., Schmittbuhl, J., 2006. High resolution 3D laser scanner measurements of a strike-slip fault quantify its morphological anisotropy at all scales. *Geophysical Research Letters* 33, L04305.
- ◇ Roberts, G. P., 1996. Variation in fault-slip directions along active and segmented normal fault. *Journal of Structural Geology* 18(6), 835-845.
- ◇ Rocher, M., Cushing, M., Lemeille, F., Lozac'h, Y., Angelier, J., 2004. Intraplate paleostresses reconstructed with calcite twinning and faulting: improved method and application to the eastern Paris Basin (Lorraine, France). *Tectonophysics* 387, 1-21.
- ◇ Roth, F., Fleckenstein, P., 2001. Stress orientations found in north-east Germany differ from the West European trend. *Terra Nova* 13(4), 289-296.
- ◇ Safaricz, M., Davison, I., 2005. Pressure solution in chalk. *AAPG Bulletin* 89(3), 383–401.
- ◇ Sagy, A., Brodsky, E. E., Axen, G. J., 2007. Evolution of fault surface roughness with slip. *Geology* 35(3), 283-286.
- ◇ Saintot, A., Angelier, J., 2002. Tectonic paleostress fields and structural evolution of the NW-Caucasus fold-and-thrust belt from Late Cretaceous to Quaternary. *Tectonophysics* 357, 1 –31.
- ◇ Sapra, A., 1997. Geological analysis of early water production in horizontal wells in the Middle East. AAPG international conference and exhibition., Vienna, Austria, Sept. 7-10, 1997, AAPG Bulletin, American Association of Petroleum Geologists: Tulsa, OK, United States, 81, 1410.
- ◇ Scheck, M., Bayer, U., Lewerenz, B., 2003. Salt redistribution during extension and inversion inferred from 3D backstripping. *Tectonophysics* 373, 55-73.
- ◇ Sippel, J., Scheck-Wenderoth, M., Reicherter, K., Mazur, S., 2009. Paleostress states at the south-western margin of the Central European Basin System - Application of fault-slip analysis to unravel a polyphase deformation pattern. *Tectonophysics - Progress in understanding sedimentary basins* 470(1-2), 129-146.
- ◇ Smith, R. L., McGarrity, J. P., 2001. Cracking the fractures—seismic anisotropy in an offshore reservoir. *The Leading Edge* 20, 18-26.
- ◇ Spang, J. H., 1972. Numerical method for dynamic analysis of calcite twin lamellae. *Geological Society of America Bulletin* 83(1), 467-472.

- ◇ Sperner, B., 1996. Computer programs for the kinematic analysis of brittle deformation structures. In: Frisch, W. (Ed.), *Tübinger Geowissenschaftliche Arbeiten Reihe A*, 27, Tübingen.
- ◇ Sperner, B., Ratschbacher, L., Ott, R., 1993. Fault-striae analysis: a Turbo pascal program for graphical presentation and reduced stress tensor calculation. *Computers & Geosciences* 19(9), 1361-1388.
- ◇ Stäuble, A. J., Milius, G., 1970. Geology of Groningen Gas Field, Netherlands. In: Halbouty, M. T. (Ed.), *Geology of giant petroleum fields*. American Association of Petroleum Geologists, Tulsa, 359-369.
- ◇ Stewart, S. A., Clark, J. A., 1999. Impact of salt on the structure of the Central North Sea hydrocarbon fairways. In: Fleet, A. J. & Boldy, S. A. R. (Eds.), *Petroleum Geology of Northwest Europe: Proceedings of the 5th Conference: Geological Society* 65, London, 179-200.
- ◇ Streit, J. E., Hillis, R. R., 2004. Estimating fault stability and sustainable fluid pressures for underground storage of CO₂ in porous rock. *Energy* 29, 1145-1456.
- ◇ TNO-NITG. 2004. *Geological Atlas of the Subsurface of the Netherlands - onshore*. TNO-NITG, Utrecht, pp. 103.
- ◇ Turner, F. J., 1953. Nature and dynamic interpretation of deformation lamellae in Calcite of three marbles. *American Journal of Science* 251, 276-298.
- ◇ Van Adrichem-Boogaert, H. A., Kouwe, W. F. P., 1993-1997. *Stratigraphic Nomenclature of the Netherlands; revision and update by RGD and NOGEP*. TNO-NITG, Mededelingen Rijks Geologische Dienst, Haarlem, 50, pp. 50.
- ◇ van den Bosch, W. J., 1983. The Harlingen Field, the only gas field in the Upper Cretaceous Chalk of the Netherlands, *Petroleum geology of the southeastern North Sea and the adjacent onshore areas*. *Geologie en Mijnbouw. Netherlands Journal of Geosciences* 62, 145-156.
- ◇ Van der Molen, A. S., 2004. *Sedimentary development, seismic stratigraphy and burial compaction of the Chalk Group in the Netherlands North Sea area*. PhD. thesis, Utrecht University.
- ◇ Van der Molen, A. S., Dudok, H. W., Wong, T. E., 2005. The influence of tectonic regime on chalk deposition: examples of the sedimentary development and 3D-seismic stratigraphy of the Chalk Group in the Netherlands offshore area. *Basin Research* 17, 63-81.
- ◇ Van der Zee, W., 2001. *Dynamics of fault gouge development in Layers sand-clay sequences*. Shaker Verlag, Aachen, PhD thesis
- ◇ van der Zee, W., Urai, J. L., Richard, P. D., 2003. Lateral clay injection into normal faults. *GeoArabia* 8(3), 501-522.
- ◇ van Konijnenburg, J.-H., Massaferrò, J. L., Mauduit, T., Richard, P., Willemse, M., Droste, H., Fenton, M., 2000. Explaining early water breakthrough in a tough carbonate reservoir: the Natih E formation, Al Ghubar Field, Oman. *AAPG Annual Meeting, New Orleans, Louisiana, April 16-19, 2000*.
- ◇ Vandycke, S., 2002. Paleostress records in Cretaceous formations in NW Europe: extensional and strike-slip events in relationships with Cretaceous-Tertiary inversion tectonics. *Tectonophysics* 357, 119-136.

- ◇ Wallace, R. E., 1951. Geometry of shearing stress and relation to faulting. *Journal of Geology* 59, 111-130.
- ◇ Wong, T. E., Batjes, D. A. J., de Jager, J. (Editors), 2007. *Geology of the Netherlands*. Edited by KNAW, Amsterdam, pp. 354.
- ◇ Worum, G., Michon, L., 2005. Implications of continuous structural inversion in the West Netherlands Basin for understanding controls on Palaeogene deformation. *Journal of the Geological Society* 162, 73-85.
- ◇ Yamaji, A., 2000. The multiple inverse method: a new technique to separate stresses from heterogeneous fault-slip data. *Journal of Structural Geology* 22, 441-452.
- ◇ Zolohar, J., Vrabec, M., 2007. Paleostress analysis of heterogeneous fault-slip data: the Gauss method. *Journal of Structural Geology* 29(11), 1798-1810.
- ◇ Ziegler, P. A., 1982. *Geological Atlas of Western and Central Europe*. Elsevier Scientific Publishing Company, The Hague, Amsterdam, pp. 130.

Chapter 3: The internal geometry of salt structures - a first look using 3D seismic data from the Zechstein of the Netherlands¹

Abstract

We present a first look at the large scale, complexly folded and faulted internal structure of Zechstein salt bodies in NW-Europe, using 3D reflection seismic data from two surveys, on the Groningen High and the Cleaver Bank High. We focus on a relatively brittle, folded and boudinaged, claystone, carbonate, anhydrite layer (the Z3 stringer), enclosed in ductile salt. A first classification of the structures is presented, and compared with observations from salt mines and analogue and numerical models.

Z3 stringers can be reservoirs for hydrocarbons but also present a serious drilling problem in some areas. Results of this study could provide the basis for better prediction of zones of drilling problems. More generally, the techniques presented here can be used to predict the internal structure of salt bodies, to estimate the geometry of economic deposits of all kinds and locate zones suitable for storage caverns.

Structures observed include an extensive network of zones with increased thickness of the stringer. These we infer to have formed by early diagenesis, karstification, gravitational sliding and associated local sedimentation. Later, this template was deformed into large scale folds and boudins during salt tectonics. Salt flow was rarely plane-strain, producing complex fold- and boudin geometries. Deformation was further complicated by the stronger zones of increased thickness, which led to strongly non-cylindrical structures. We present some indications that the thicker zones also influence the locations of later supra-salt structures, suggesting a feedback between the early internal evolution of this salt giant and later salt tectonics.

This study opens the possibility to study the internal structure of the Zechstein and other salt giants in 3D using this technique, exposing a previously poorly known structure which is comparable in size and complexity to the internal parts of some orogens.

Keywords: Zechstein; Salt tectonics; 3D reflection seismic; Folding; Boudinage.

Introduction

The sedimentary basins of NW Europe are classic areas of salt tectonics (Fulda, 1928; Richter-Bernburg, 1953a; Ziegler, 1982; Taylor, 1998; Mohr et al., 2005; Geluk, 2007; Geluk et al., 2007; Hübscher et al., 2007). The Dutch part of the Central European Basin contains five evaporite cycles of the Late Permian Zechstein Group (Z1-Z5, see: Fulda, 1928; Ziegler, 1982; Best, 1989; Taylor, 1998; Geluk, 2000; De Mulder et al., 2003; TNO-NITG, 2004; Wong et al., 2007), including a relatively brittle layer consisting of anhydrite, carbonate and clay (the “Z3 stringers” 2).

1 Heijn van Gent, Janos L. Urai, Martin de Keijzer. *Journal of Structural Geology*. In press: Doi: 10.1016/j.jsg.2010.07.005.

2 The terms raft or floater are sometimes used to specify layered, competent inclusions in salt. The names raft and floater imply buoyancy, but carbonate, dolomite and anhydrite have a higher density than halite and are expected to sink under the influence of gravity over geological timescales.

On the importance of stringers

A large part of the world's hydrocarbon reserve is associated with evaporitic deposits (Warren, 2006), for example in the Central European Basin, the Caspian Sea, the Gulf of Mexico, offshore Brazil, and the basins the Middle East. Prediction of the thickness, porosity, geometry and fluid fill of stringers is of significant economic importance. In some settings in Europe as well as in Oman, stringers enclosed in the salt are hydrocarbon reservoirs (Mattes and Conway Morris, 1990; Geluk, 1997, 2000; Peters et al., 2003; Al-Siyabi, 2005; Reuning et al., 2007; Reuning et al., 2009; Schoenherr et al., 2009a; Schoenherr et al., 2009b). Better understanding stringers in NW Europe can help the interpretation of the complex geometry and history of the hydrocarbon-bearing stringers in the Ara Salt in Oman.

In addition, in most cases the Z3 stringer is considered a drilling hazard by operators in the Central European Basin. The Carbonate Member of Z3 stringer can be significantly overpressured, with pressures up to lithostatic (Williamson et al., 1997). Overpressures in stringers are difficult to predict. When planning the well path, stringers are avoided where possible, and not drilled when strongly folded and/or faulted. Zechstein salt is also used for different kinds of geological storage or solution mining (Hofrichter, 1974; Coelewij et al., 1978; Bornemann, 1991; Fokker et al., 1995; Geluk et al., 2000; Van Eijs and Breunse, 2003; Evans and Chadwick, 2009) and prediction of internal structure is of major relevance in these fields (see Bornemann, 1991; Koyi, 2001; Chemia et al., 2008).

Internal and external salt tectonics

In the literature, salt structures are typically shown in two strikingly different ways. In studies using 3D seismic and well data that focus on the sub- or suprasalt sediments and are typically hydrocarbon-related, the evaporites are invariably shown as structureless bodies (for example: Jackson and Vendeville, 1994; Jackson, 1995; Scheck et al., 2003; Mohr et al., 2005; Maystrenko et al., 2006).

On the other hand, studies of the internal structure of salt are typically salt-mining or storage-related and are based on observations from mine galleries and borehole data (for example: Krische, 1928; Richter-Bernburg, 1953a; Siemeister, 1969; Hofrichter, 1974; Richter-Bernburg, 1980; Jackson, 1985; Richter-Bernburg, 1987; Bornemann, 1991; Smith, 1996; Behlau and Mingerzahn, 2001; Schléder et al., 2008). These studies show the extremely complex internal geometry with less attention to the structure of the surrounding sediments.

Detailed observations of salt mines and drill holes (with cm- to m-resolution) display a variety of deformation structures in the salt on a wide range of scales (Krische, 1928; Richter-Bernburg, 1953a; Lotze, 1957; Borchert and Muir, 1964; Kupfer, 1968; Muehlberger, 1968; Richter-Bernburg, 1980; Schwerdtner and Van Kranendonk, 1984; Richter-Bernburg, 1987; Talbot and Jackson, 1987; Best, 1989; Jackson et al., 1990; Bornemann, 1991; Zirngast, 1991; Geluk, 1995; Burliga, 1996; Smith, 1996; Zirngast, 1996; Behlau and Mingerzahn, 2001; Siemann and Ellendorff, 2001; Schléder et al., 2008). Observations (typically 2D to 3D in salt mines and 1D in storage or solution mining) include boudins and folds together with shear zones (Bornemann, 1991; Geluk, 1995; Burliga, 1996; Taylor 1998, Behlau and Mingerzahn, 2001; Geluk, 2000). The folds have curved, open to isoclinal fold axes, and boudins from mm- (Schléder et al., 2008) to km-scale (Burliga, 1996) are common. Cross sections through the Zechstein in the Gorleben and Morsleben salt domes (Bornemann, 1991; Behlau

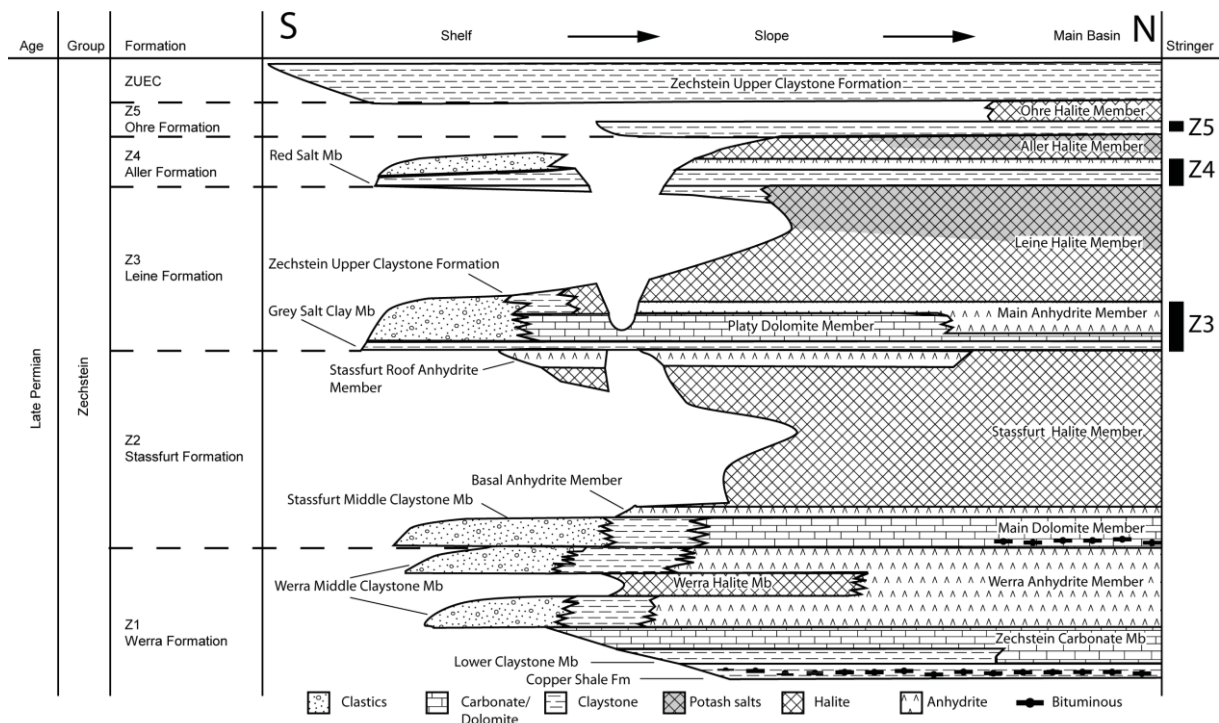


Figure 1: Zechstein stratigraphy in the Netherlands (based on Van Adrichem-Boogaert and Kouwe, 1993-1997, Geluk, 2000 and TNO-NITG, 2004). In the right column the position of the three brittle intervals in the evaporites is indicated. Only the Z3 stringer is visible in seismic reflection data, and is fully encased in halite.

and Mingerzahn, 2001) show isoclinal folding of the Z3. Richter-Bernburg (1980) further describes several examples of fold structures with amplitudes over half the height of the salt structures. Field studies, from Iran and Oman have also shown the internal complexities of surface-piercing salt domes, such as the distribution of different age salt, the position and internal deformation of solid inclusions, the microstructures and, by inference, the deformation mechanisms (among others: Jackson et al., 1990; Talbot and Aftabi, 2004; Talbot, 2008; Reuning et al., 2007; Reuning et al., 2009; Schoenherr et al., 2009a; Schoenherr et al., 2009b; Desbois et al., 2010).

Numerical as well as analogue centrifuge and extrusion models of salt tectonics tend to assume relatively homogeneous rheological properties (although mechanical stratigraphy is used), and consequently produce relatively simple salt structures (for example: Jackson and Talbot, 1989, Van Keken et al., 1993; Koyi, 2001; Schultz-Ela and Walsh, 2002; Talbot and Aftabi, 2004; Chemia et al., 2008). It must be noted however that most of these models, do provide a way to study structural evolution due to deforming meshes or the use of multicoloured analogue materials. Despite the relatively simple rheological models, analogue and numerical models with mechanical stratigraphy have shown the complex deformation associated with (brittle) inclusions in deforming ductile media (see for example: Escher and Kuenen, 1929; Koyi, 2001; Goscombe and Passchier, 2003; Goscombe et al., 2004; Zulauf and Zulauf, 2005; Chemia et al., 2008; Zulauf et al., 2009, Schmid et al. 2009).

Aim of this work

In this paper we aim to contribute to the understanding of the structural style and geometry of the Z3 stringer, by describing detailed interpretations of two 3D reflection seismic surveys from the Dutch on-

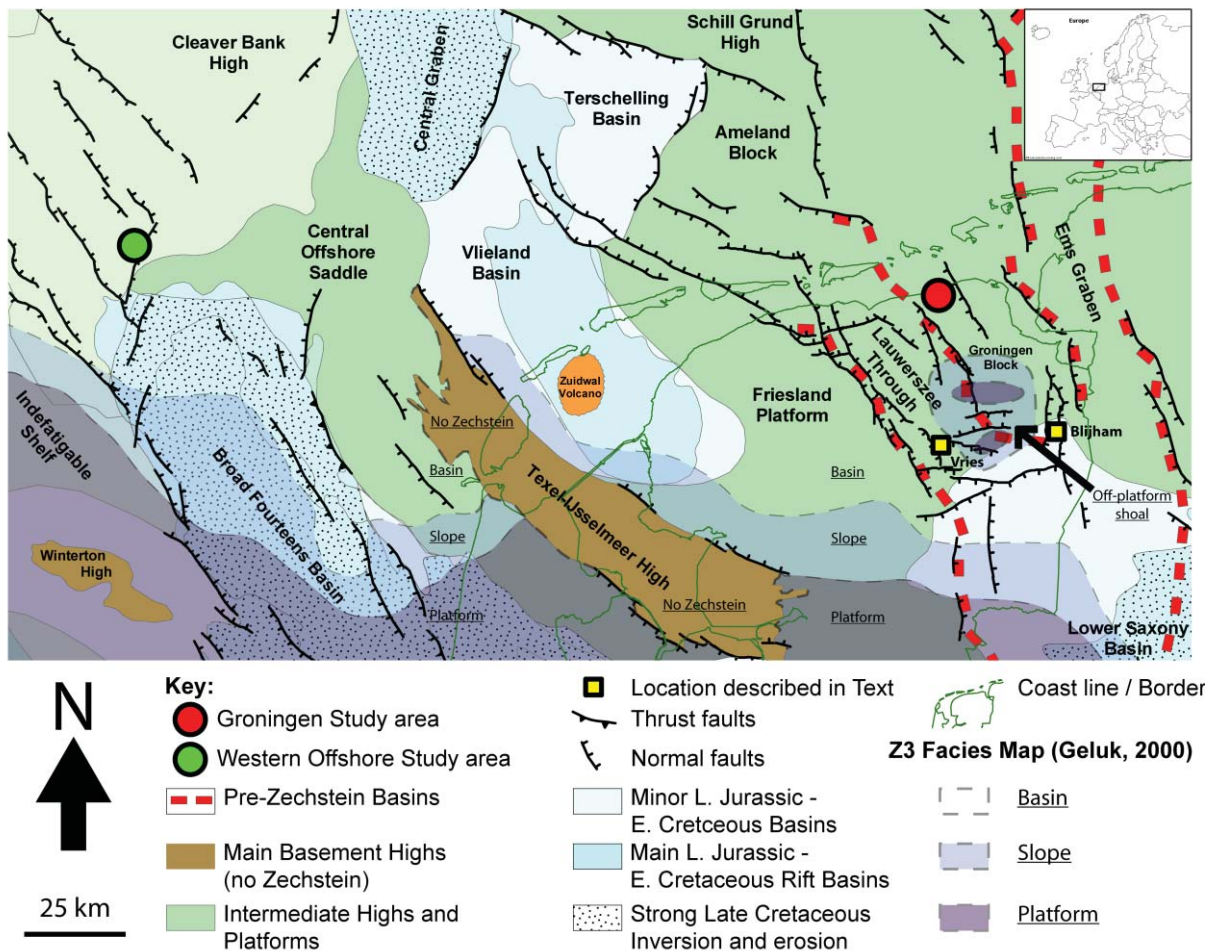


Figure 2: Location map of the study areas with the structural elements (image courtesy of Nederlandse Aardolie Maatschappij) and Z3 paleogeography (after Geluk, 2000). On the Texel-IJsselmeer High and the Winterton High no salt is present. The NW-Groningen High study area is indicated with a red dot and the offshore study area with a green dot. Locations discussed in the text are indicated with yellow dots.

and offshore. We focus on thickness variations and structural style at the scale of 30 m to 20 km, to draw inferences about sedimentary and diagenetic evolution and salt tectonic processes.

The stratigraphy of the Zechstein

In the Dutch subsurface, the Zechstein can be subdivided in a marine lower part (Z1-Z3) and a playatype upper part (Z4 and Z5) with more clastic deposits (Geluk, 1997, 2000). Z1 to Z3 follow the classic carbonate-evaporite cycle: claystone- carbonate- gypsum- halite - and potassium- magnesium salts (Warren, 2006; Geluk, 2000). The cycles correspond to major transgressions from the Arctic and evaporation of sea water in the arid Southern Permian Basin (Fig. 1 and 2, Taylor, 1998). In the

northern Netherlands deposition was relatively continuous, but the sedimentary sequence has major periods of non-deposition in the south (TNO-NITG, 2004; Geluk, 2007, see also Fig. 1).

Z1 halite is absent in both areas studied in this paper (Taylor, 1998; Wong et al., 2007). The Z2 Main Dolomite member and Z2 Basal Anhydrite Member (Stassfurt Formation) are deposited directly on top

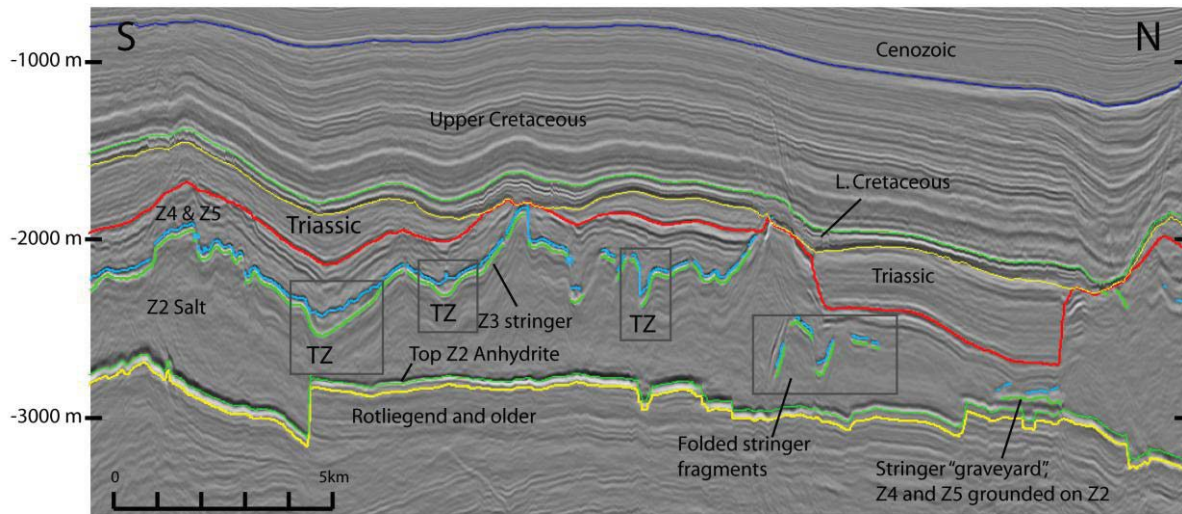


Figure 3: N-S seismic cross sections through the Groningen area. The main formation bounding reflectors are indicated, as well as the top and base Z3 stringer. The Z3 stringer is relatively continuous here, although breaks in the reflector are observed. Also note the roughly 500-700 m of Z2 halite below the Z3 stringer (chaotic, weak reflectors), while above the stringer a few tens to 200 m of Z3 halite are observed between stringer and top Zechstein. The continuous, parallel reflectors directly below top Zechstein are the Playa-type deposits of the Z4-cycles. Thicker Zones are indicated with TZ.

of the Z1 anhydrite in both study areas. Therefore, up to the top of Z2 Anhydrite, all rocks are brittle and coupled to the Rotliegend and underlying basement. The top Z2 Anhydrite reflector is therefore used in this study to define top of mechanical basement (Fig. 3 and 4). The Z2 halite reaches a primary thickness between 500 and 600 m in both study areas, which was later strongly modified by salt tectonics (Taylor, 1998; Geluk, 2007; Geluk et al., 2007). Near the top of Z2 locally (not in the study areas) thick deposits of potassium-magnesium salt layers are found (Geluk, 2007). The Z3 Leine Formation starts with an approximately 1 m thick grey shale (Grey Salt Clay) with a high Gamma-ray signal in wireline logs (Taylor, 1998). The overlying Platy Dolomite ("Plattendolomit") reaches thicknesses of 30 m (Smith, 1995) to 75-90 m (Taylor, 1998) on the shelf, considerably more than in the basin where it reduces to a few meters (Taylor, 1998). On top of the Platy Dolomite the Main Anhydrite ("Hauptanhydrit") is found (Taylor, 1998; Siemann and Ellendorff, 2001). In the Dutch part of the basin the thickness of the Main Anhydrite increases from 3 m on the shelf to 45 m in the basin, with local excursions to 100 m and complex changes in thickness (Rijks Geologische Dienst, 1991, 1993, 1995; Taylor, 1998; TNO, 1998; Geluk, 2000). Local variations in the Z3 anhydrite thickness were first described by Fulda (1928) and were subsequently interpreted to result from a type of gypsum diapirism or sedimentary swells, although some were interpreted to be tectonic in nature (Langbein, 1987; Williams-Stroud and Paul, 1997; Bäuerle et al., 2000).

The Z3 Leine halite is overlain by two thick potassium-magnesium salt layers, with bischofite, kieserite, carnallite and sylvite (Coelewij et al., 1978). Primary thickness of the Z3 halite is 200-300 m in the Groningen and about 100 m in the offshore study area (Wong et al., 2007).

The Aller (Z4) and Ohre (Z5) formations consist of sabkha deposits and are quite thin (Geluk, 2007). The Z6 and Z7 (Best 1989) are not found in the Netherlands. The youngest Zechstein unit is the Upper Claystone Formation (ZUEC) which is between 10 and 50 m thick and is present in large portions of the Dutch subsurface (Van Adrichem-Boogaert and Kouwe, 1993-1997; TNO-NITG, 2004; Geluk, 2007).

The Zechstein Carbonate facies (Z1, Z2, Z3).

Zechstein carbonates in the Netherlands are subdivided in shelf, slope and basin facies (Taylor, 1998; Geluk, 2000; Wong et al., 2007, see also Fig. 1). The platform carbonates consist of shallow water deposits with occasional karst features (Scholle et al., 1993; Southwood and Hill, 1995; Strohmenger et al., 1996). The carbonate members are thickest in the slope, where individual reefs and off-platform highs, as well as gravity flows are found (Geluk, 2000). The basin facies was deposited in water depths up to 200 m and can contain high Total Organic Carbon (Geluk, 2000).

Z3 Stringers in Seismic Data

The high acoustic impedance contrast between the stringer and surrounding halite makes the Z3 stringer image reasonably well in seismic data (Fig. 1, Fig. 3). The stringer is visible as a pair of parallel loops in the relatively transparent halite. Imaging limitations are related to frequency content and noise level of the seismic data, to the thickness of the layer and to the local high dip of the layer (Sleep and Fujita, 1997). If the thickness of the stringer is below the tuning thickness of about 30-35 m, exact thickness determination from seismic data is not possible (and thickness will be overestimated). Sections of the stringer with thicknesses below ca. 10 m are not resolved. However, the majority of stringers in the study area are typically 40-50 m thick, with local excursions up to 150 m or more (see below). The internal structure of the stringer generally is not resolved, probably because of the low impedance contrast between anhydrite and carbonate.

Study areas and methodology

We studied stringers in two areas: the Groningen High, and the Cleaver Bank High (Fig. 2).

The Groningen High

The first study area is 20 by 30 km and is located on the Groningen High (NE Dutch onshore, Fig. 2, Chapter 1). The Groningen Gas Field (Fig. 2) contains one of the largest gas reservoirs of the world (Stäuble and Milius, 1970; Wong et al., 2007). Mohr et al. (2005) showed that salt tectonics in the nearby Ems Graben initiated during the Early Triassic with subsequent phases in the Late Triassic and the Upper Cretaceous/Lower Tertiary. There was little or no activity between the Jurassic to Lower Cretaceous. The stringer is clearly visible in the seismic volume (Fig. 3). The data from this area is part of a large, merged, 3D pre-stack depth migrated seismic data set, provided by the Nederlandse

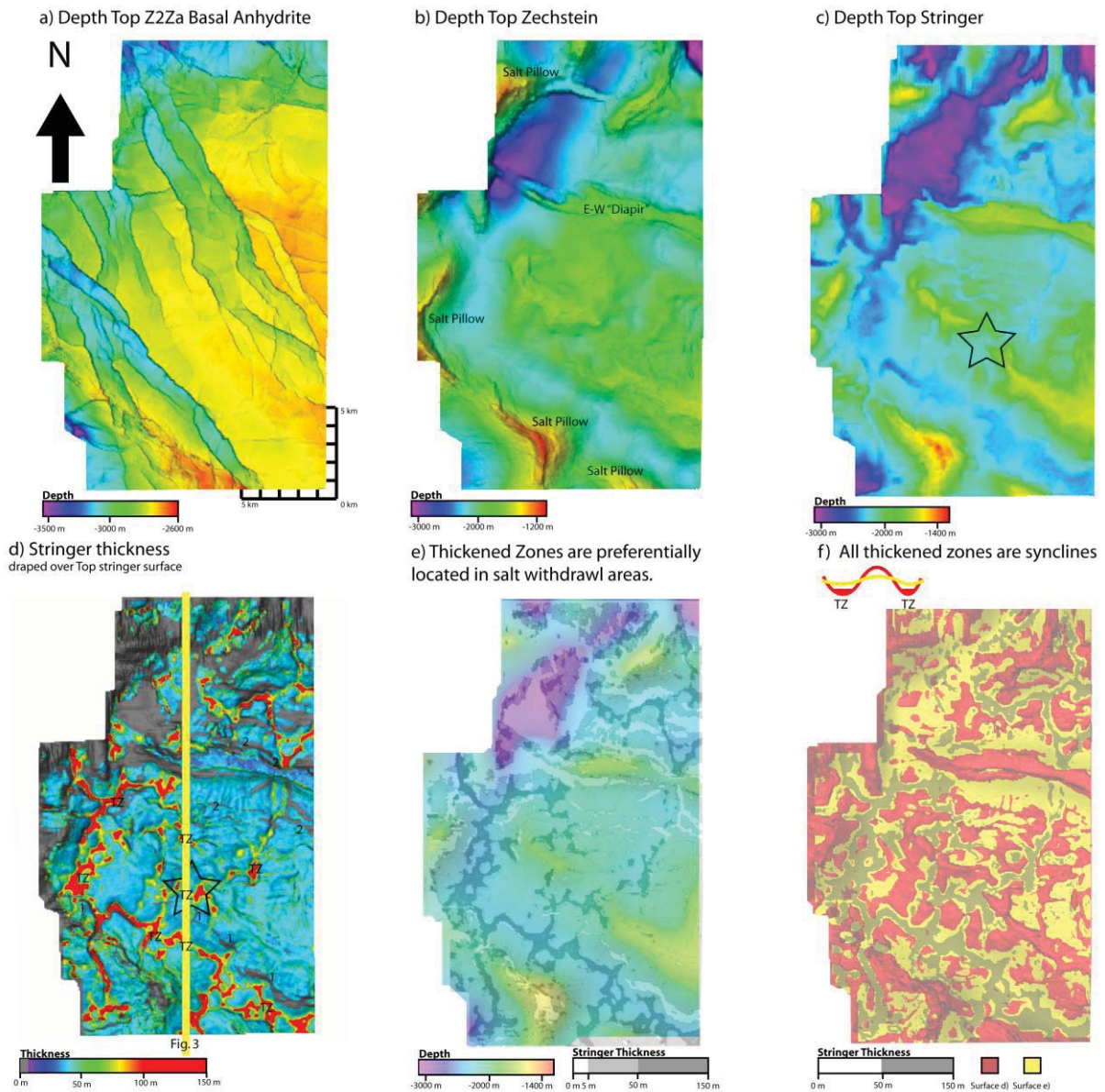


Figure 4: a) Depth top Z2 Anhydrite map, which assumed here to be the top of the mechanical basement. b) Depth top Zechstein. Note the structures indicated. c) Depth top Stringer map. Star denotes location where a large scale harmonic fold is disturbed by a TZ (see section 5.4.1.3 for description). d) Thickness of the Zechstein Z3 stringer, draped over the obliquely lit top stringer surface. Note the variations in thickness and the distribution of the grey areas where the stringer is less than 5m thick (and assumed to be absent). e) Smoothed top stringer depth map, with a discrete stringer thickness map draped over it. Dark grey means stringer is thicker than 50 m, grey is between 5 and 50 m and white is thinner than 5 m (assumed to be absent). Note that the thicker zones always lie in the large scale synclinal (deeper) sections of the stringer. f) Comparison of the present, detailed geometry of the top stringer depth map (c, red) and the smoothed depth map (e, yellow) and the thicker sections (above 50 m). Note that the stringer is always thicker in those areas where the original depth map lies below the smoothed surface - i.e. the TZ are dominantly found in local synclinal structures. The inset shows in cross section how the overlapping of the original (red) and smoothed (yellow) surface shows that TZ only occur in synclines.

Aardolie Maatschappij BV (NAM, a Shell operated 50–50 joint venture with ExxonMobil). The horizontal resolution and seismic positioning uncertainty are around 50-75 m, with the seismic bin size being 25 m. Vertical sampling is 2 to 4 milliseconds. In total over 250 wells were drilled in the Groningen area.

The Western Offshore

The second study area, a 20 by 20 km survey, is located in the Dutch offshore (Fig. 2), on the Cleaver Bank High (CBH), directly north of the Broad Fourteens basin, and is in close proximity to the Sole Pit Basin and the Central Graben. During the Late Carboniferous, Saalian tectonic phase, the CBH was tectonically active and uplifted. Between the Permian and the Middle Jurassic the CBH was quiet, but during the Late Jurassic to Early Cretaceous the CBH was uplifted and deeply eroded (Ziegler, 1982; Van der Molen, 2004; Duin et al., 2006). However, the study area is located outside the most important zone of erosion (Fig. 2, Van Hoorn, 1987; Van Wijhe, 1987; De Jager, 2003; Wong et al., 2007).

Top Zechstein is dominated by a NNE striking salt wall with minor grabens on both sides in the suprasalt deposits. The salt wall has a listric fault and asymmetric graben above its crest, (Fig. 7, cf. Remmelts, 1996). The sub-salt top Rotliegend horizon shows three fault trends (Fig. 8). The first, NW striking trend is associated with Variscan wrench faulting (Ziegler, 1982). The second, NNE trend, is parallel to the salt structure and may be related to the Central Graben / Broad Fourteens Basin fault system (see Fig.2). The third trend is a minor, approximately E-W fault system, which is related to the northern border of the Broad Fourteens basin.

Depth and thickness maps of the suprasalt deposits show that the faults parallel to the NW trend clearly influenced the younger deposits (cf. Fig. 8 and 9).

The seismic data used for this area was also provided by NAM. The horizontal resolution and seismic positioning uncertainty are typically around 50-75 m (as the seismic bin size is 25 m). Vertical sampling is 2 to 4 milliseconds. Well control is provided by a dozen production and exploration wells.

The workflow

In addition to the interpretation of the Z3 stringer, sub- and supra-salt reflectors and major faults were used to establish a geological framework. We used the seismic interpretation package Petrel 2005 and Petrel 2007 (Schlumberger).

Starting from an existing interpretation (Joris Steenbrink, personal communication, 2007) in the Groningen area, the complex geometry of the stringers was studied by detailed manual interpretation. The stringers were interpreted on a 100 x 100 m seed grid, followed by seeded autotracking with a very low level of tolerance. This means in practice that the interpretation software only extends the manual interpretation a few lines away from the seed. In Groningen the Z3 stringer can be mapped with high confidence (Fig. 3). The occurrence of overlapping stringers in the offshore area (Fig. 7) provides a challenge when interpreting horizons because of the limitation of a single z-value at any x-y- location in the interpretation software.

In both areas the stringer is locally less clearly defined or absent: either only one loop is visible or there is no reflector visible at all. A stringer was only interpreted in locations where both loops were

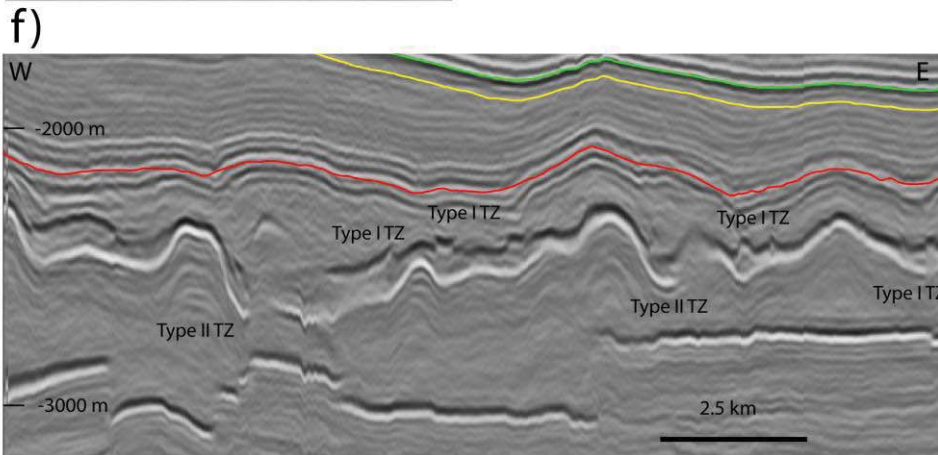
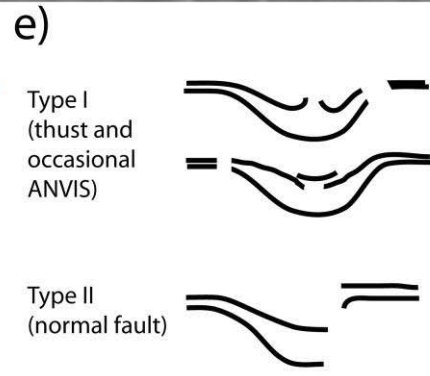
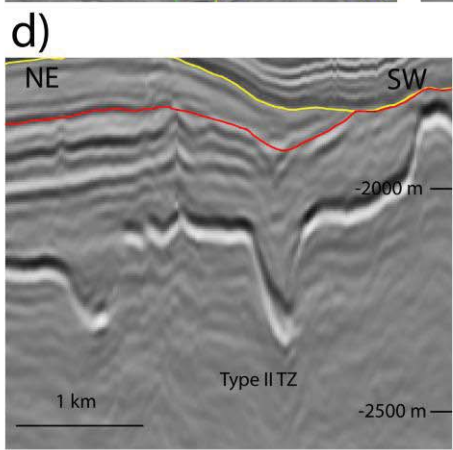
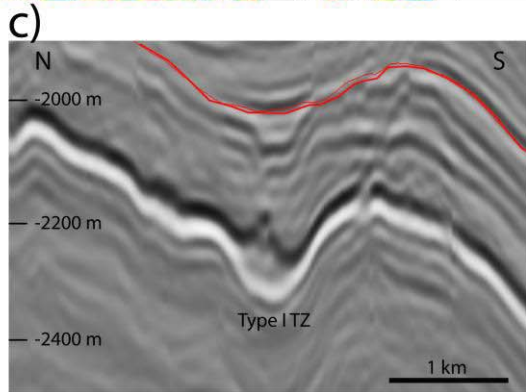
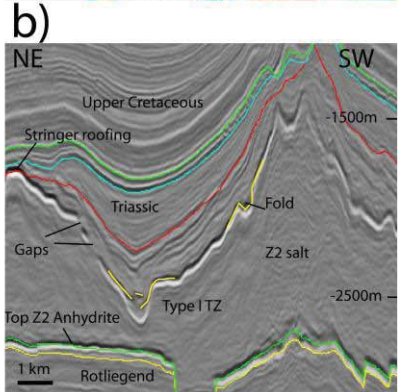
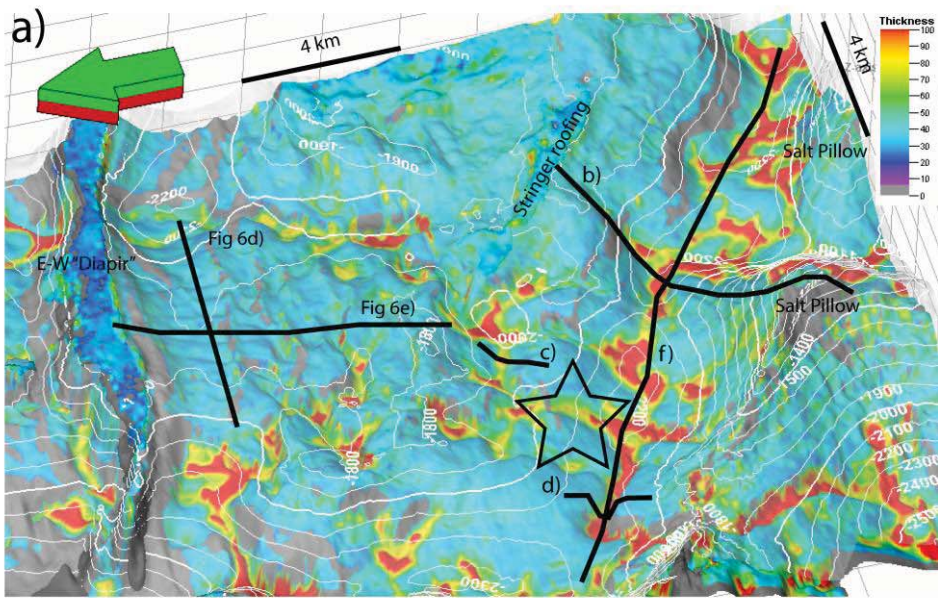


Figure 5 (previous page): (a) Observations of the Z3 stringer in the Groningen area, based on a shaded oblique view of the top stringer (arrow points north, green is up, red is down). The stringer thickness (Fig. 4d) is projected on the surface, with thickness less than 10 m is gray. Also shown is the top Zechstein (white contours), and locations of cross sections shown in b – f as well as those in Fig. 6. Vertical exaggeration is 2x. Star is in the same location as in Fig. 4 and 5. Note how the TZ in all cross sections are always in a syncline (Fig. 4f).

b): Cross section of internal thrusts (Type I), gaps and folds in a cross section through the TZ. Note that the TZ is located where the stringer is low. Reflectors have the same colours in the following cross sections.

c) Close-up cross section of an internal thrust in the stringer (Type I).

d) Cross section of Type II TZ

e) Conceptual sketch of Type I and Type II TZ.

e) Cross section showing Type I and Type II TZ in the same profile.

visible. In the surface- building interpolation step this resulted in two continuous and overlapping surfaces in the areas without a reflector. In the Groningen area, we used the imaging resolution to define a threshold value (5 m) for the distance between these surfaces to locate “holes” in the stringer (Fig. 4d and 5a). The exact value of this threshold is not critical because the transition from seismically visible stringer to zones without visible stringer is abrupt. These holes correspond closely to the areas without well-defined stringer reflectors in cross section (compare for example Fig. 3 and 4d, as well as Fig. 5).

In the offshore area we completed two different interpretations of the stringers. First, stringers were interpreted as a horizon, with very low tolerance auto tracking around the manual picks. Here we consistently chose the higher stringer in case of overlap. A continuous surface was thus created over gaps in the interpretation.

In addition, we manually interpreted stringers using the "Fault Interpretation" routine of Petrel in cross sections, at 100 - 200 m spacing to define a point cloud of 54000 points. Although no realistic surface can be created in the interpretation software from these data points, this allowed interpretation of overlapping and near-vertical parts of the visible stringers, and was used to study more complex 3D structures (see sections 5.2 and 5.3).

Stringer geometry

Groningen

The Base Zechstein map (top Z2 Anhydrite, Fig. 4a) shows a number of basement faults with offsets up to 300 m, while the top Zechstein map (Fig. 4b) shows a few salt pillows flanked by a graben, and a central area where top Zechstein is relatively horizontal at 2000 – 2200 m. Thickness of Zechstein is about 1000 m, increasing up to 2000 m in the salt pillows.

Although the original stratigraphic position of the Z3 stringer is about 200 to 300 m below top Zechstein, in its present geometry (Fig. 3, 4d, 5 and 6) its position varies from very close to top Zechstein, to very close to top Z2 Anhydrite. In the central area (away from the salt pillows) the enveloping surface of the stringer is sub-horizontal and approximately in its original stratigraphic position (Fig. 4c). In what follows, we focus on areas with anomalously thick stringers, on areas where

stringers are not visible, and on folds of different wavelengths, orientation and amplitudes (Figs. 3, 5 and 6).

Stringer thickness distribution

The observed stringers usually have a rather constant thickness of around 40 m, with areas of increased thickness (up to 150 m). We call these TZ (Thicker Zones; Fig. 3). A stringer thickness distribution map is shown in Fig. 4d and 5a (areas with no visible stringers - as defined above - are grey).

We studied 7 wells that penetrate the visible Zechstein stringer. In those wells that penetrate a TZ, the stringers are 80-125 m thick with two strong Gamma Ray peaks: one in the basal claystone and a second peak at the top. In all wells penetrating seismically visible stringers outside the TZ, stringer thickness is around 50 m with only one GR peak in the basal claystone.

In the stringer thickness map (Fig. 4d), a clearly defined regional network of up to 400 m wide, long, branching TZ are seen throughout the area (red and yellow colour in Fig. 4d and Fig. 5a, dark grey in Fig. 4e and 4f). These zones are curved, and are connected at triple (rarely quadruple) junctions. TZ are synclinal (never anticlinal) in shape and lie below the stringers' enveloping surface (Fig. 4e, 4f and 5).

In more detail, in cross section, TZ can be (I) symmetric, with two overlapping top stringer reflectors (top Main Anhydrite), and top stringer slightly raised in the thickest section (Fig. 5a, b, c and e and 6c) and a continuous base (Fig. 5 a, b, c, and e), or (II) asymmetric, with the stringer invisible on one side of the TZ (Fig. 5d, e, f). In the Type I TZs, structures that appear to be internal thrusts are interpreted (Fig. 5c), but it can not be ruled out that this is an imaging effect.

There is at best a weak correlation between Rotliegend faults and TZ. In the south of the study area TZ is only roughly parallel to the Rotliegend fault trend, while the NE-SW oriented TZ along the western edge of the survey is perpendicular to this trend (compare Fig. 4a and 4d). There is however a clear correlation between TZ and the topography of top Zechstein (compare Fig. 4b and 4e), as well as in local depressions of the stringer (Fig. 4e and 4f): TZ are dominantly found in areas where top Zechstein is deep.

Folds

The enveloping surface of ZE3 forms 10 km-scale fold structures which are harmonic with the top Zechstein (Fig. 3 and 4). TZ are located in the synclinal hinges of these large scale folds. In the area marked with a star in Fig. 4c, d, and Fig 5, (also visible in Fig. 6a), a TZ crosses an anticlinal structure. Here the amplitude of the anticline is much lower than in the rest of the fold.

On a smaller (km) scale, fold structures also exist, most clearly expressed in areas away from the TZ. The seismic section in Fig. 6d is parallel to the E-W diapir (see Fig. 5 and 6b). A number of low wavelength (200 m) folds are observed in the stringer, while the Z2, Z4 and Z5 are not folded in the same way. Since the latter are mechanically coupled to the basement and top salt respectively, this suggests that the folding of the Z3 solely results from movements in the salt. These folds have fold axes perpendicular to the axis of the diapir (Fig. 6b). Fig. 6c shows a similar structure of folds in an area

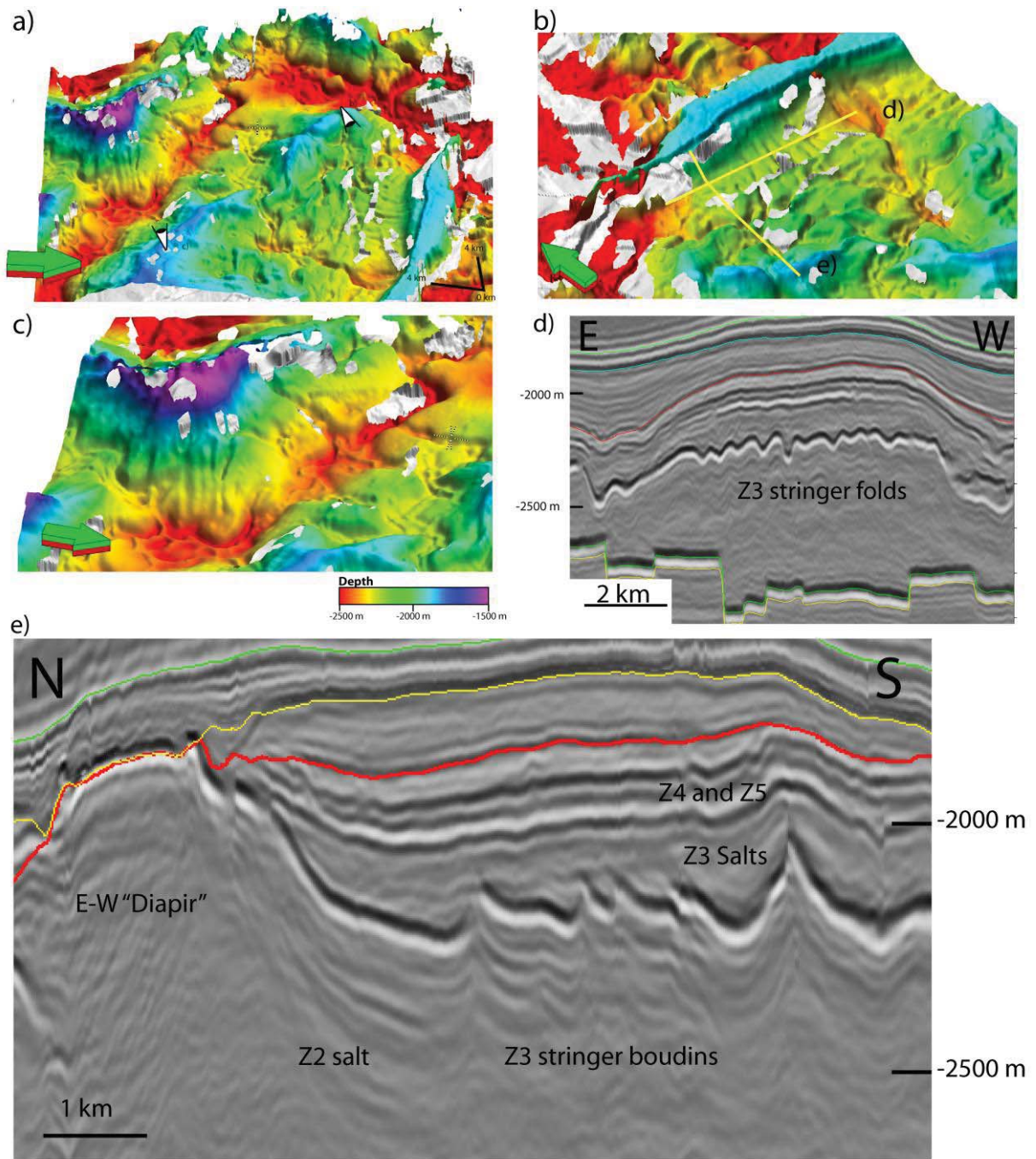


Figure 6: Observations of folds and boudins in the Groningen Area.

- a) Oblique view of the top Stringer horizon with zones thinner than 5 m made transparent to show top basement (grey) below. View directions of b) and c) are indicated in a).
- b) Oblique view of the constriction folds south of the EW diapir. Note how the TZ crossing the diapir influences the orientation of the holes in top stringer. Width of image about 10 km.
- c) View of constriction folds on the flank of a salt structure in the south of the study area. Also note the slightly raised centre of the TZ in the valley at the base of the pillow. Width of image about 8 km.
- d) Cross section perpendicular to the fold axes, location shown in yellow in b) showing open folds (note vertical exaggeration). Also note the TZ in the most Western part of the cross section.
- e) Cross section parallel to the fold axes, location shown in yellow in b), cutting the diapir. The profile shows a series of broken, asymmetric monoclines with wavelengths between 250 and 1000 m. See discussion for interpretation of these structures.

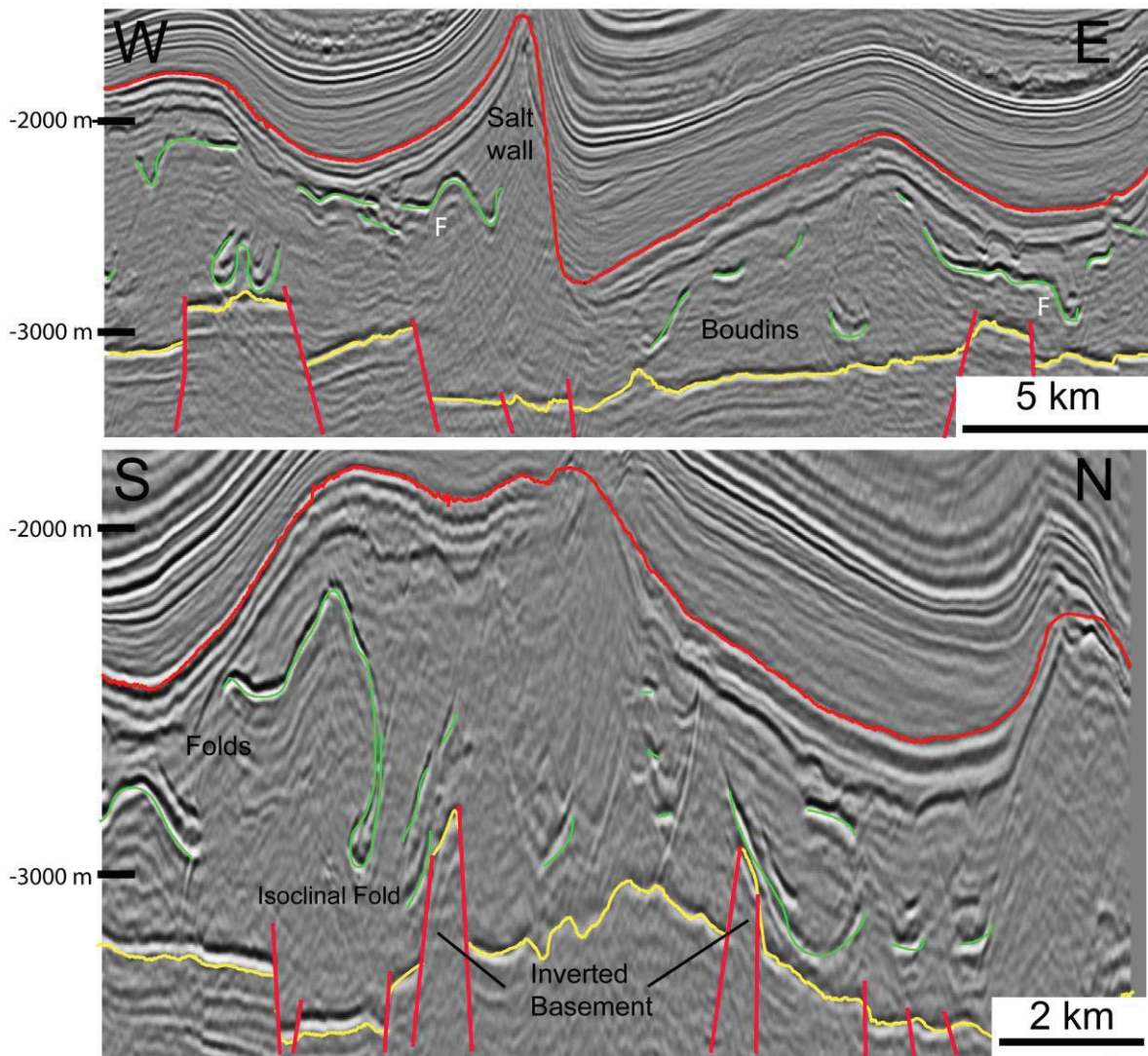


Figure 7: Cross sections through the Western Offshore area. For locations see Fig. 8d. Note the boudins (see discussion) and that the isoclinally folded stringers are located close to the inverted basement blocks. The isoclinal fold in the N-S cross section is also shown in Fig. 11a and d.

with fold axes running up the crest of a salt pillow and wavelengths of a few 100 m. The observed fold axes in Fig. 4, 5 and 6 generally are in the dip direction of the Z3 enveloping surface.

Areas with no visible stringer

Areas with No Visible Stringer reflector - called ANVIS - are common in the Groningen study area. In some cases, TZ is spatially related to ANVIS in sub-parallel, occasionally en-echelon, zones (ANVIS, key 1 in Fig 4d, Fig. 5 a, b and c and Fig. 6e). In other areas, ANVIS have no apparent relationship with TZ but are related to the E-W striking salt diapir in the north of the area (key 2 in Figure 4d). These ANVIS are clearly elongated and sub-parallel to the axis of the diapir on its southern side, most clearly expressed where no TZ is present. On the northern side of the diapir ANVIS are also present but here the presence of TZ do not allow a clear attribution to TZ or the diapir. The cross section in Fig. 6e cuts through these gaps showing a series of asymmetric monoclines with lengths between 250

and 1000 m. The Z4 and Z5 reflectors in this area do not show the same structure, suggesting once again that the Z3 salts serve as a decoupling layer.

In 4 wells penetrating ANVIS, 2 wells encountered no stringer. In one case a very thin (10-20 m) stringer was encountered. Finally, one well in an ANVIS penetrated a 100 m long, steeply dipping stringer section, this shows that the stringers' visibility can be limited by their dip.

In the east of the survey, the roughly N-S oriented TZ intersects the E-W diapir (Fig. 4d and Fig. 6d). Here the ANVIS which is sub-parallel to the diapir crest further west curves towards the diapir and the diapir is also narrower here. This may suggest that TZ are older than ANVIS.

Western Dutch offshore

Compared to the Groningen area, the Z3 stringer in the offshore study area has a much more complex structure. In seismic cross sections (Fig. 7, indicated in Fig. 8d) the visible Z3 stringer is less continuous and varies strongly in depth over short distances. The stringer is more intensely folded and frequently offset vertically over more than half of the total Zechstein thickness. The Mesozoic tectonic inversion of the Broad Fourteens basin is manifested in several inverted basement blocks in the area (Fig. 7).

The individual interpreted stringer fragments in this area are relatively chaotic, with a weak trend of their long axis parallel to the axis of the salt wall in the east (Fig. 8c and d). Additional trends are recognized, for example the alignment of stringer fragments along the NW-trend of basement faults in the NW of the study area (Fig. 8) and along the NW-SE trending faults in the overburden (Fig. 9).

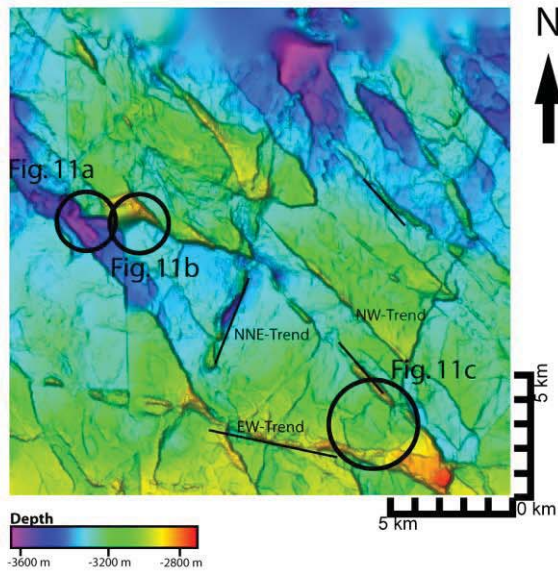
The stringer surface which was created by horizon interpretation, autotracking and surface interpolation, is, as expected, quite similar to the point cloud interpretation which was created using the fault interpretation routine (in areas with no overlapping stringers - compare Fig. 8c and Fig. 10). The point cloud however, shows locally a high level of additional complexity (Fig 11). TZ were not observed in this survey; where the stringer could be interpreted, the top and bottom reflector was about 40 m apart. ANVIS occurred in a larger fraction of the area than in Groningen.

At the regional scale, top Rotliegend shows several inverted blocks (Fig. 8a) and top Zechstein shows the NE-SW striking salt wall with two secondary, NW-SE striking graben structures which are all clearly associated with fault systems in the overburden (Fig. 8b and 9). On average the stringer is several hundreds of meters higher on the west-side of the salt wall than on the east side. The Z3 stringer is very close to the top of the inverted basement blocks in almost every case studied (see also Figs. 7 and 11).

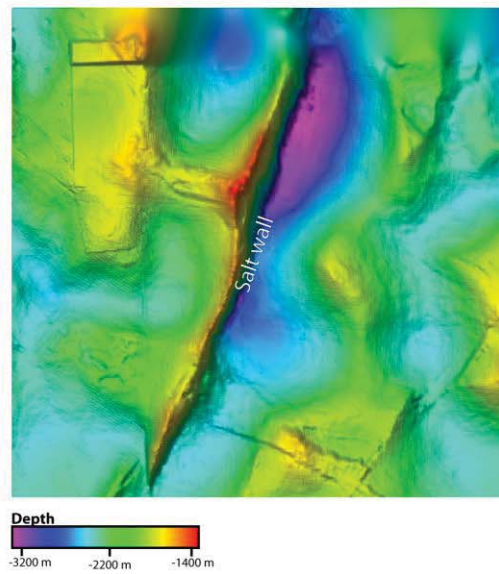
Stringer surface geometry

The base stringer is shown in Fig. 8e and Fig. 10. There are a number of clearly defined structural elements. Firstly, the enveloping surface of the stringers follows the large scale salt wall (Fig. 7a en 8b). In the areas where the stringers can be auto-tracked and dip less than 30 degrees (areas with bright colours and grey dots in Fig. 10) the surface shows gentle, open folds (F in Fig 7 and 8e) with a wavelength of around 400 m and amplitude less than 200 m. Fold axes are usually curved and do not show a clear preferred orientation. Second, the surface is frequently offset (O in Fig. 8, see also Fig.

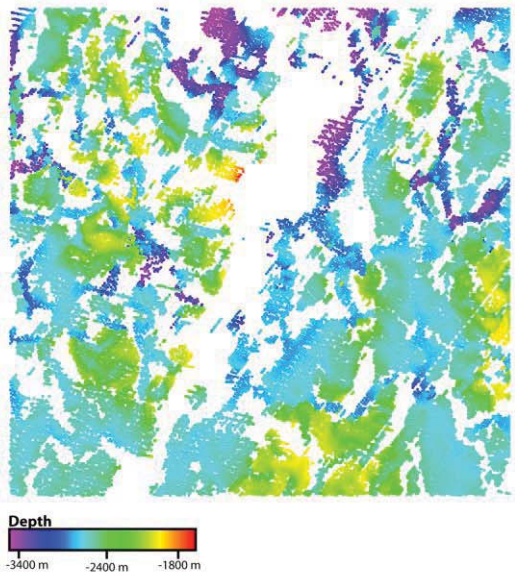
a) Depth Top Rotliegend



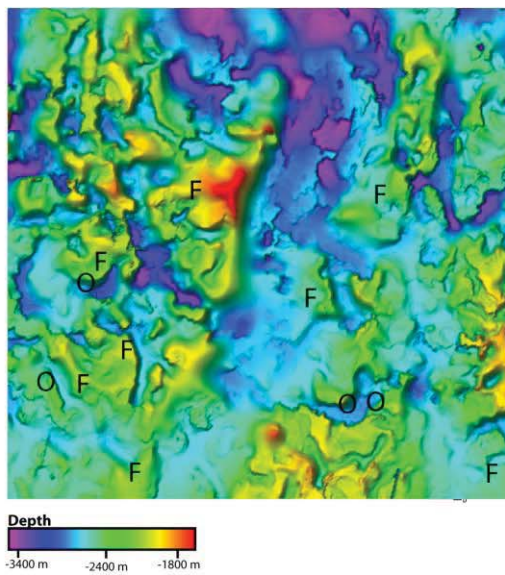
b) Depth Top Zechstein



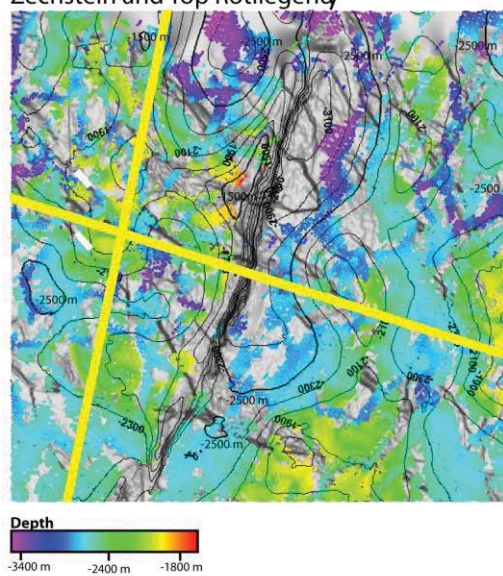
c) Depth Base Stringer (fault interpretation)



e) Depth Base Stringer Horizon



d) Depth Base Stringer, combined with Top Zechstein and Top Rotliegend/



f) Discrete Dip plot of the Base Stringer Horizon

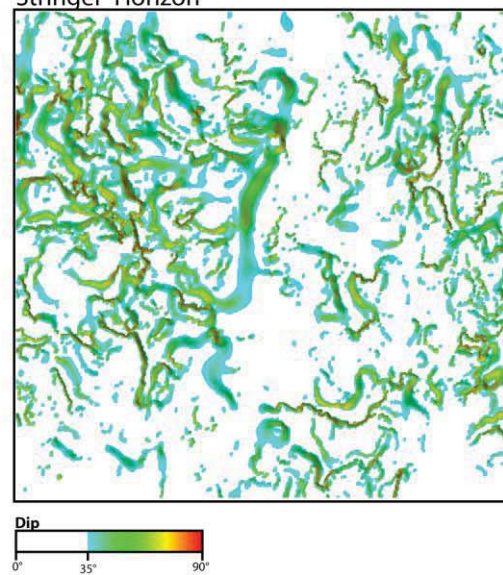


Figure 8 (previous page): Maps from the Western Offshore area. a) Depth map top Rotliegend, note the different structural trends and the inverted blocks. b) Depth map of top Zechstein. c) Depth of the point cloud of the manually interpreted Base Stringer. d) Same as c) but overlaid on depth top Rotliegend surface and with contour lines of depth top Zechstein. e) Depth of interpolated base stringer surface, based on autotracking plus interpolation interpretation. F denotes fold axes, O means vertical offsets, see also Fig. 12. f) Only displaying the offset-parts of the autotracked and interpolated base stringer surface with a dip higher than 35°, marked O in e). Sections are coloured for dip value. Note the extremely complex pattern of offsets. A movie of the comparison of the autotracked and manual interpretations of the stringer can be found on our website and YouTube Channel (www.ged.rwth-aachen.de)

12) along steep (steeper than 35°, grey in Fig. 10 and steeper than 45°, grey in Fig. 12) discontinuities. This offset can be more or less symmetric (graben like, G in Fig. 8 and 12) or monoclinical (M in Fig. 12). The offsets can be small and become zero towards the tip of the steep zone, but also up to 1000 m vertically, offsetting the stringer across almost the whole Zechstein. In map view, these discontinuities have a peculiar, curved morphology (Fig. 8f) with no clearly defined preferred orientation. In the point cloud some of these offsets resemble ductile ruptures (Fig. 11c). Fold axes are often at right angles to these offsets.

Areas with no visible stringer in the Western Offshore

Stringers are usually not visible in the steeply dipping discontinuities described above (see Fig. 10 and Fig. 12). However, in relatively flat-lying parts the stringers are also frequently not visible. Some of these ANVIS can be shown to be related to the basement structures (Fig. 8) or to structures in the overburden (Fig. 9). Other ANVIS like those in the east of the survey (Fig. 8c and d) are parallel to the salt wall.

Folds

The open folds (Fig. 7, 8 and 12), in the area have been described above. More striking are parts of the stringers which form complex, three dimensional, tight to isoclinally folded surfaces defined by the interpreted point cloud (Fig. 11). Visualization of these surfaces is difficult because of software limitations, and analysis of the structures was best done by interactively rotating the point cloud and defining the folded surfaces by visual inspection. In Fig. 11a, b and d some of these structural elements are shown as the raw point cloud together with a basic interpretation. It is striking that these structures have been only observed in direct proximity of inverted basement blocks.

Movies where of the point clouds shown in Fig. 11 are rotated to get a better feel for the 3D structure are available on our website and YouTube Channel (www.ged.rwth-aachen.de & www.youtube.com/user/StrucGeology). Here also a direct comparison between the horizon and fault interpretation of the offshore study area can be found.

General description of observed fold types

Both in the Groningen area and Offshore study area, folds are observed at different scales and with different morphologies. The structures can be classified in the following four different groups: (1) diapir

scale folds, (2) “constriction” folds, (3), strongly non-cylindrical structures and (4) isoclinal folds inside the salt structures. We will now discuss the interpretation of these in detail. We note here that our descriptions follow the “classical” fold description methods, focusing on 3D extrapolations of essentially 2D observations (Lisle and Toimil, 2007, Schmid, et al, 2009). Defining the folded surfaces using differential geometry (Lisle and Toimil, 2007, Mynatt et al., 2007) will be used in a follow-up project.

Diapir-scale folds

At the regional scale of the salt structures the Z3 stringer resembles the top Zechstein surface (Figs. 3, 4, 7 and 8). This produces large, regional folds in the stringer’s enveloping surface which are harmonic with the large scale salt structures and are therefore interpreted to reflect the large scale flow paths during salt tectonics. The other three types of structures are disharmonic to this movement, and interpreted to result from local deviations from the relatively simple deformation pattern expected (see Fig. 13a and d).

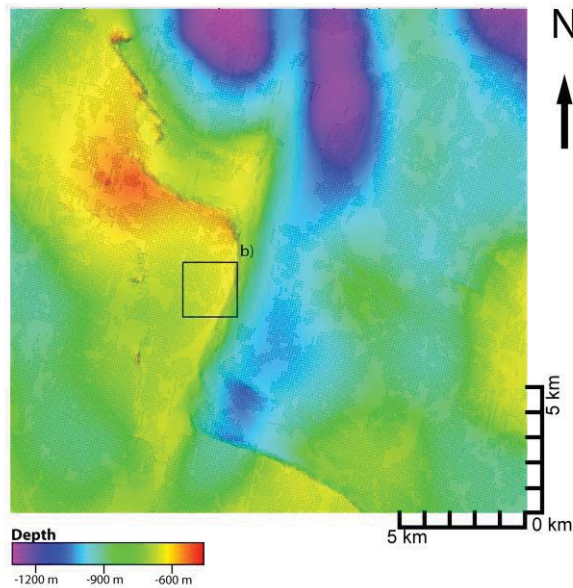
“Constriction” folds

When the fold axes are steeply dipping, folds in the Groningen area (Fig. 6) are interpreted as “constriction folds” similar to “curtain folds” (but the latter have vertical fold axes). These reflect simultaneous shortening and extension in the surrounding salt (cf. Zulauf and Zulauf, 2005, see also Fig. 13d) and implies that stringers underwent significant internal deformation and do not deform in a fully brittle fashion. Similar structures were described in many other studies in salt mines (see for example: Lotze, 1957; Richter-Bernburg, 1980; Talbot and Jackson, 1987; Bornemann, 1991; Jackson et al., 1996) and in experiments (Escher and Kuenen, 1929; Jackson and Talbot, 1989; Koyi, 2001; Goscombe and Passchier, 2003; Goscombe et al., 2004; Zulauf and Zulauf, 2005; Chemia et al., 2008; Zulauf et al., 2009). Particularly the results of Callot et al. (2006) are very similar to the observed structure in Groningen directly south of the E-W diapir (here the pattern of holes in the stringer around the E-W diapir is similar to the pattern of ruptures in the analogue models, see also Fig. 13d). The open folds with subhorizontal fold axes (Fig. 8e and Fig. 9) in the Western Offshore study area can also be interpreted to result from a constrictional process as the stringer moved along with the salt into the salt structure, (see Fig. 13c).

Strongly non-cylindrical structures

Two types of non-cylindrical folds (see Pollard and Fletcher, 2005 for definitions) are observed. The first type is illustrated in Fig. 5 and 6a with a relatively large anticlinal stringer fold, harmonic to top salt, which is bisected by a TZ at a high angle to the fold axis. The axial surface of this fold is (approximately) planar, but the fold hinge is lower where the TZ crosses this structure. We infer that TZ had a mechanical effect which influenced the buckling process and locally led to a longer wavelength, lower amplitude fold structure (Fig. 13 b, Ramsay, 1967). Experimental and numerical modeling of the development of folds in layers with strongly variable initial thickness (Grujic, 1993; Grujic et al., 2002) is in agreement with this, but much more work is needed to allow a full interpretation.

a) Base North Sea and Stringer distribution



b) Detail of a) showing un-aliased interpretation

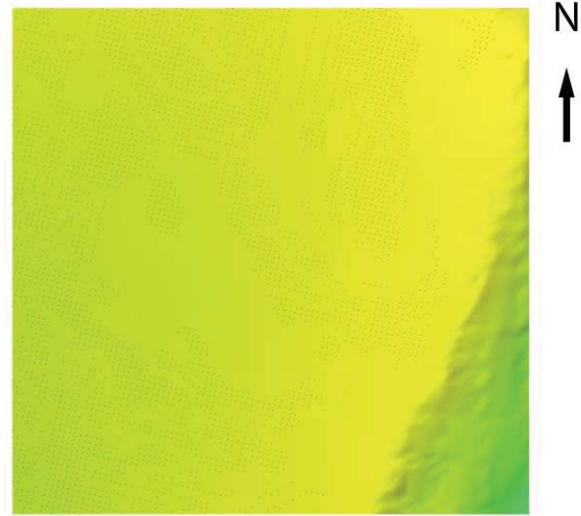


Figure 9: Correlation between the stringer distribution and overburden structures. a) Base North Sea Super Group (Base Cenozoic) reflector depth map, overlain by map showing where stringer interpretation is present (black points). Note the correlation between the NW-SE oriented structures in the depth map and the ANVIS in the stringer. b) Detail of a) showing interpretation of the stringer as individual points.

The second type of non-cylindrical folds is observed in the offshore area. Here large areas of low amplitude folding with con-cylindrical axial planes, but relatively horizontal fold hinges (Fig. 13 c, Pollard and Fletcher, 2005), are found (Fig. 8e and Fig. 9). These are very similar to structures formed in deformation of a constricted layer (Schmid et al., 2009) and constrictional plasticine experiments (Zulauf and Zulauf, 2005).

Isoclinal folds inside the salt structures

Although reliable interpretation of steeply dipping, complex structures is difficult, it is tempting to interpret tight to isoclinal folds in the stringers in a number of areas in the western offshore (Figs. 7 and 11). The structures shown in Fig. 11 closely resemble those documented in large salt structures by underground studies (cf. Krische, 1928; Richter-Bernburg, 1953a; Bornemann, 1991; Burliga, 1996; Behlau and Mingerzahn, 2001; Schléder et al., 2008) and experiments (Koyi, 2001; Callot et al., 2006; Chemia et al., 2008), and we propose that the high quality of the seismic data allows the 3D mapping of these structures in our study areas. These folds show strongly curved axial planes and fold axes, and are associated with ruptures in the stringer (see below). In the regions where these structures dominate, deformation at the scale of the salt dome was clearly much more heterogeneous.

Discussion

Interpretation of the Thicker Zones

The thickness of the Z3 stringer in the Groningen area and in the Western Offshore is generally about 40 m. Similar Z3 units are between 30-50 thick in Poland, UK and Germany (Richter-Bernburg, 1980; Bornemann, 1991; Burliga, 1996; Smith, 1996). This shows that the thickness of the undisturbed Z3 stringer is relatively constant over large areas of the Zechstein basin, but local deviations are present like in the Blijham area (south of the Dollard Bay, Fig. 2) where the stringer is 80-90 m thick, perhaps related to the proximity of the off-platform shoal (Fig. 2). Complex thickness variations are observed on the hydrocarbon field-scale. Examples include the Vries area, south of Groningen (see Fig. 2 for location) and several other locations in the Netherlands (Rijks Geologische Dienst, 1991, 1993, 1995; TNO, 1998; Geluk, 2007; Geluk et al., 2007, this study).

Thickened zones (TZ) in this study were only observed in the Groningen study area and their increased thickness in seismic data is consistent with well data. They form a branching network (Fig. 4d-e and Fig.5) of approximately in 4-5 km wide synclines (never anticlines), where the TZ is about 400 m wide and 300 m deeper than the surrounding stringer (Fig. 4f). In synclinal areas between salt pillows where the present-day top Zechstein is deep, TZ are more frequent than in areas where this horizon is shallow (Fig. 5 & 4f). In cross section at smaller scale, we observe internal overlapping reflectors and clear geometrical difference with respect to the surrounding thinner stringer (Fig. 5). In many cases, there is an ANVIS zone parallel to the TZ where the stringer is not visible.

The pattern of TZ and the peculiar internal structure can not be explained by salt tectonics and basement-related faulting alone. In the following section we present one possible interpretation of the events leading to the development of the observed structures, other interpretations are certainly possible. We assert the formation of these structures to be the product of sedimentary and diagenetic processes, modified by deformation in the flowing salt. Keeping in mind the fact that the seawater during deposition of the Z3 stringer (clay, carbonate, anhydrite) is undersaturated with respect to the underlying Z2 Halite, it is clear that any pathway for circulation of this seawater into the underlying Z2 halite will lead to strong dissolution, a system of karst caves and collapse structures which enhance further dissolution. Several authors describe sinkholes and collapse breccias related to karst in Z1 platform carbonates (Scholle et al., 1993; Southwood and Hill, 1995; Strohmenger et al., 1996). The early evolution of salt giants is still enigmatic (Hübscher et al., 2007), particularly with respect to karstification (Langbein, 1987). It is also possible that subtle (tectonic) movements during Zechstein times (Geluk, 2005) played a role in the development of the regional depressions and the incipient rupture of the Z3 clay, allowing solution of the Z2 evaporites.

Our preferred scenario involves the formation of 4-5 km wide depressions after deposition of the Grey Salt Clay (otherwise a thicker clay would later prevent groundwater circulation and formation of karst). In these depressions, during or after the deposition of the Z3 Anhydrite (but before the start of deposition of Z3 Halite from hypersaline brines), minor salt deformation led to the formation of an open fracture system in the Z3, allowing NaCl-under-saturated brines to circulate into the Z2 Halite. This led to the formation of an extensive network of dissolution channels and collapse of overlying Z3. Sections of the Z3 stringer on the edges of the collapse zones ruptured and slid down the slope forming the

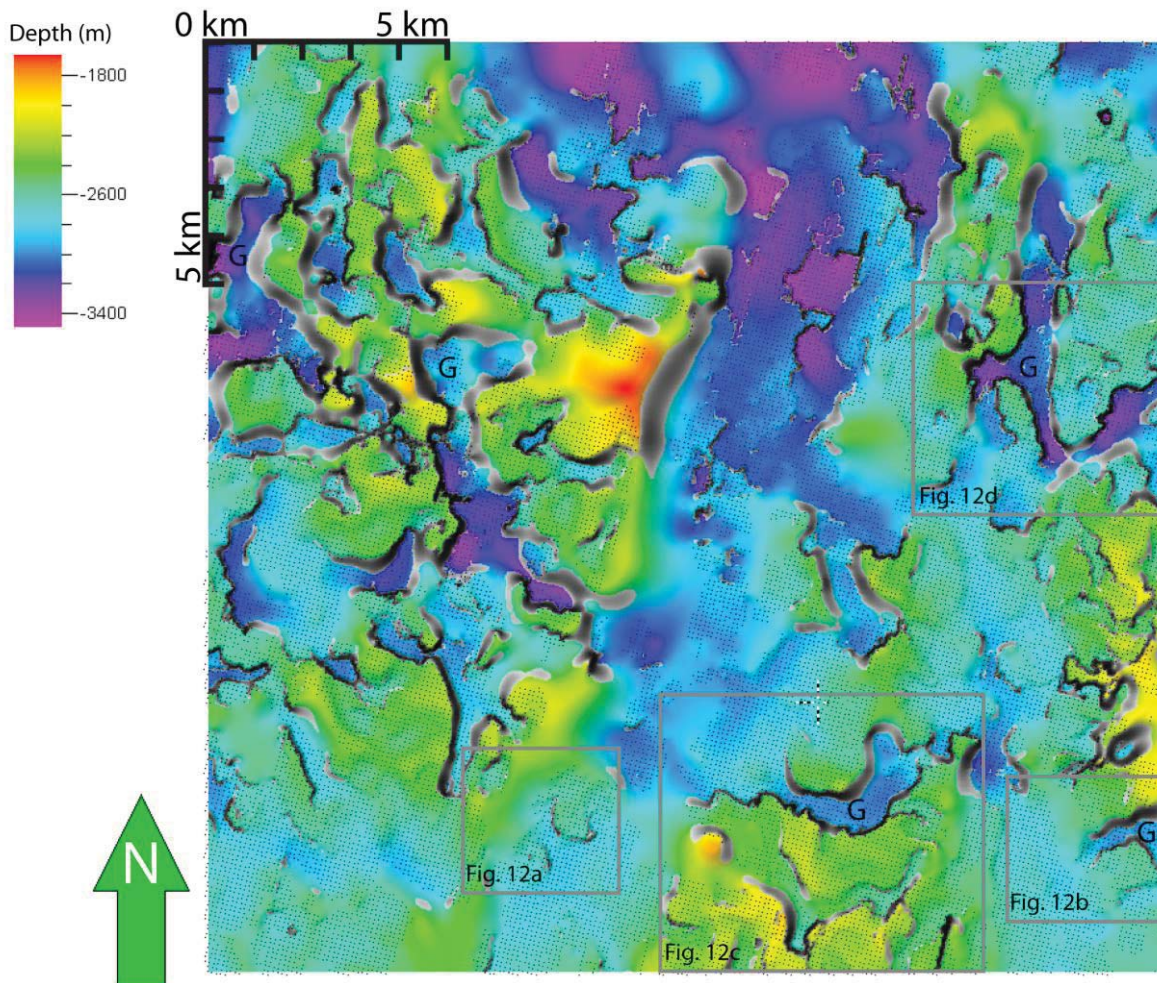
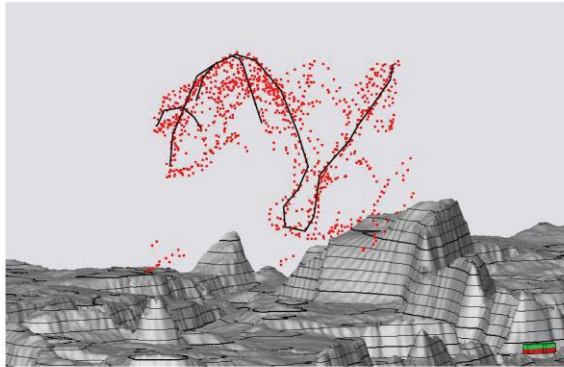


Figure 10: Depth interpolated base stringer surface, based on autotracking and interpolation and the autotracked interpretation (as black points). Also shown are those areas where the dip of this surface is larger than 45° (ANVIS, grey, compare with 8e and 8f). ANVIS in areas where the surface is relatively flat-lying is shown by the absence of points in the coloured map. We interpret these ANVIS to represent boudin-necks in the stringer (see Fig. 10b). Also shown are several locations of the graben-type offsets (G) and the locations of detailed views in Fig. 12.

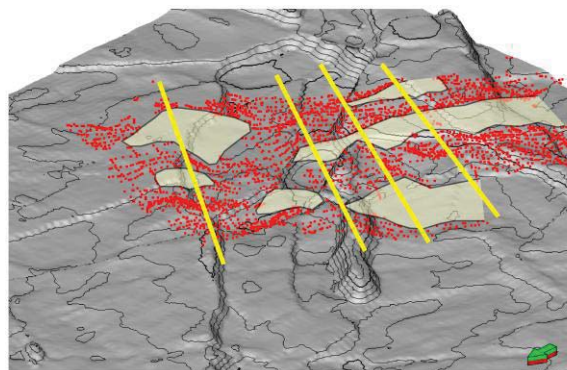
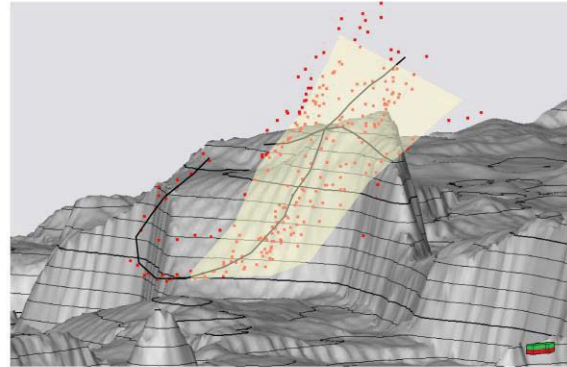
ANVIS sub-parallel to TZ (Fig. 4 and 5). The slides collect at the base of the valleys resulting in the strongly deformed and tectonically thickened Z3 (TZ) observed in cross sections (Fig. 5). In the Groningen area, the presence of what appears to be internal thrusts in seismic cross sections and the presence of TZ in synclines rules out the interpretation that TZ are anhydrite diapirism, as these structures generally have a flat base (Fulda, 1928; Langbein, 1987; Williams-Stroud and Paul, 1997; Bäuerle et al., 2000). The observed structures are more compatible with early sliding structures (Richter-Bernburg, 1953b; Evrard et al., 2008).

The incursion of sea water into the Southern Permian Basin that is related to the deposition of the Z3 Stringer, represents the most important Zechstein transgression and flooding of the Southern Permian Basin (Geluk, 2007). Little is known of structures formed during the re-flooding of the centre of large salt basins, as most information is from the edge of the basins (Barber, 1981; Blanc, 2002; Rouchy and Caruso, 2002; Loget et al., 2005; Cornée et al., 2006). It is however easy to imagine currents

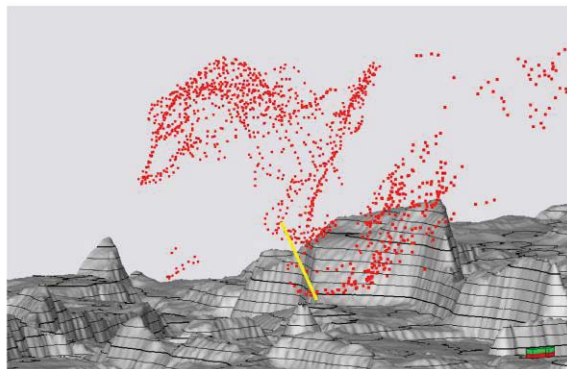
a) vx2



b) vx2



c) vx1



d) vx2

Figure 11: Detailed observations of selections of the manual (point cloud) interpretation of the Z3 stringer in the western offshore study area. See Fig. 8 for locations. a) Large scale isoclinal fold, connected to a stringer with a dome-like shape. Black lines are manually drawn to illustrate the general shape. Note the proximity of this structure to the inverted basement (grey surface). Vertical exaggeration 2 x. b) Isoclinal fold close to inverted basement. Black lines and yellow surface indicate rough shape of the stringer. Vertical exaggeration 2 x. c) Detailed view of overlapping stringers in the Western Offshore area. Yellow planes are ANVIS, yellow lines are parallel to fold-axes in this part of the stringer. No vertical exaggeration. d) Combined point clouds of a) and b). Note how the fold hinges align (yellow line).

Movies of the rotating point clouds of fig. 11 a, b and c can be found on our website and YouTube Channel (www.ged.rwth-aachen.de).

(perhaps from the off- platform high; Fig. 2 and Bäuerle et al., 2000; Geluk, 2000) during Z3 carbonate deposition having formed erosional or karst structures when (halite- undersaturated) sea water was flowing over a halite substrate covered by a thin Grey Salt Clay layer. Sub-areal karst in salt forms the same structures as carbonate karst, but at faster rates (Bosá et al., 1999). In fact, the shape of the water-filled caves mapped by Bosá et al. (1999) including triple junctions, is remarkably similar to TZ in Groningen.

The formation of thicker zones in a deforming layer has significant implications for the evolution during salt tectonic deformation. Since the stringer is more competent than the surrounding host, the thicker zones of these layers represent stronger zones in this layer and will therefore be more difficult to deform. This will for example lead to different dominant wavelengths in folds (Ramsay, 1967; Grujic,

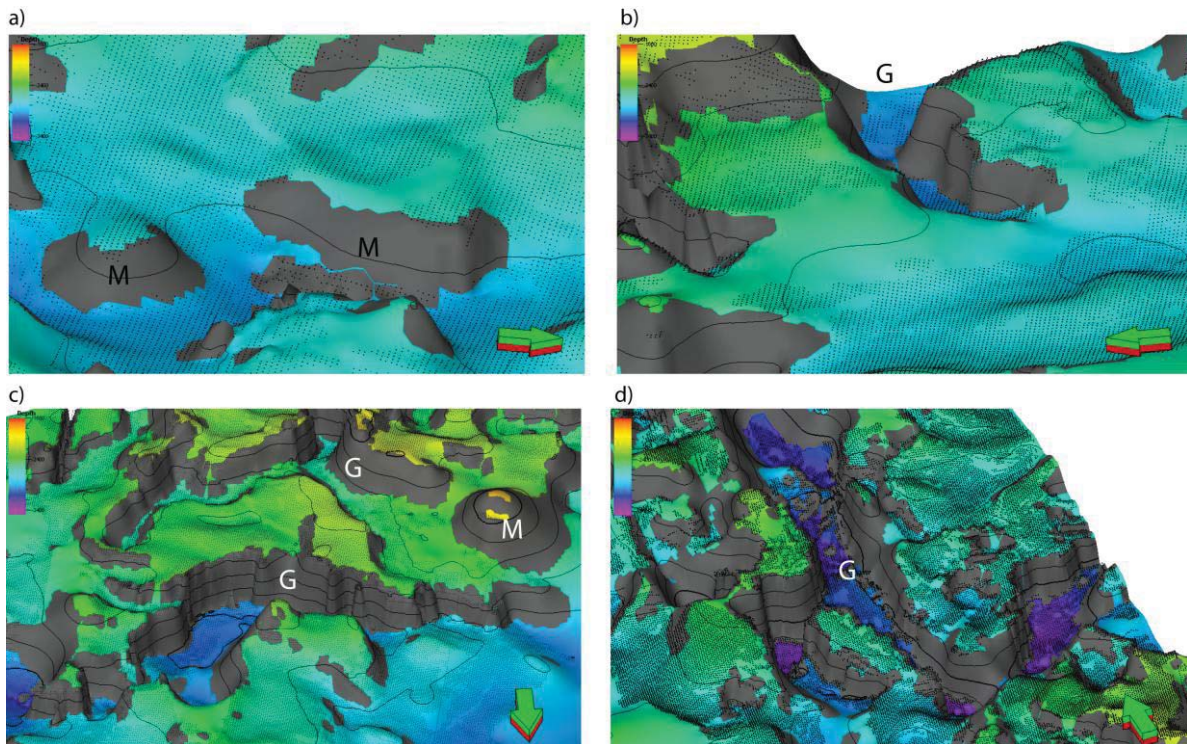


Figure 12: Detailed observations of the auto tracked base stringer interpretation (points), overlain by the interpolated surface (as in Fig. 8e and 9). Those sections of this surface that dip steeper than 45° are grey. Locations of detailed views are shown in Fig. 9. Indicated are monocline like offsets (M) in a) and c) and graben like offsets (G) in b) and d). Note the differences in ANVIS where the stringer is quite flat (no points on coloured surface), like in a) and b) and those steeper than 30° (no points where the surface is grey). Note the curved shape of all ANVIS in map view. The vertical exaggeration is 2 x.

1993; Grujic et al., 2002). The thicker zones clearly influence the patterns of ANVIS and fold geometry in the study area (Fig. 5 and Fig. 13b).

Gravity-induced sinking

The density of natural halite is about 2200 kg/m^3 , that of anhydrite is about 2900 kg/m^3 , and dolomite has a density of 2850 kg/m^3 (Lide, 1995; Koyi, 2001; Chemia et al., 2008; Li et al., 2009). This density difference makes the stringers negatively buoyant and they tend to sink if the rheology of the surrounding salt allows this to happen at geologically significant rates.

The question of gravity-induced sinking of stringers has been a subject of much controversy (Gansser, 1992; Koyi, 2001; Callot et al., 2006; Chemia et al., 2008; Urai et al., 2008). Analogue and numerical models show that dense blocks in diapirs sink when the diapiric rise velocity is not sufficiently high to keep the blocks in the diapir (Koyi, 2001; Callot et al., 2006; Chemia et al., 2008). However, estimates of the in-situ rheology of salt vary widely (cf. Urai et al., 2008), and consequently there is much uncertainty about the expected in-situ sinking rates. It would therefore be useful to obtain additional constraints based on our results on this process. Diagnostic structures which allow separating salt tectonics-related and gravitational sinking-related processes are difficult to define but could consist of a correlation between vertical position of the stringer and stringer size (Li et al., 2009). Such a

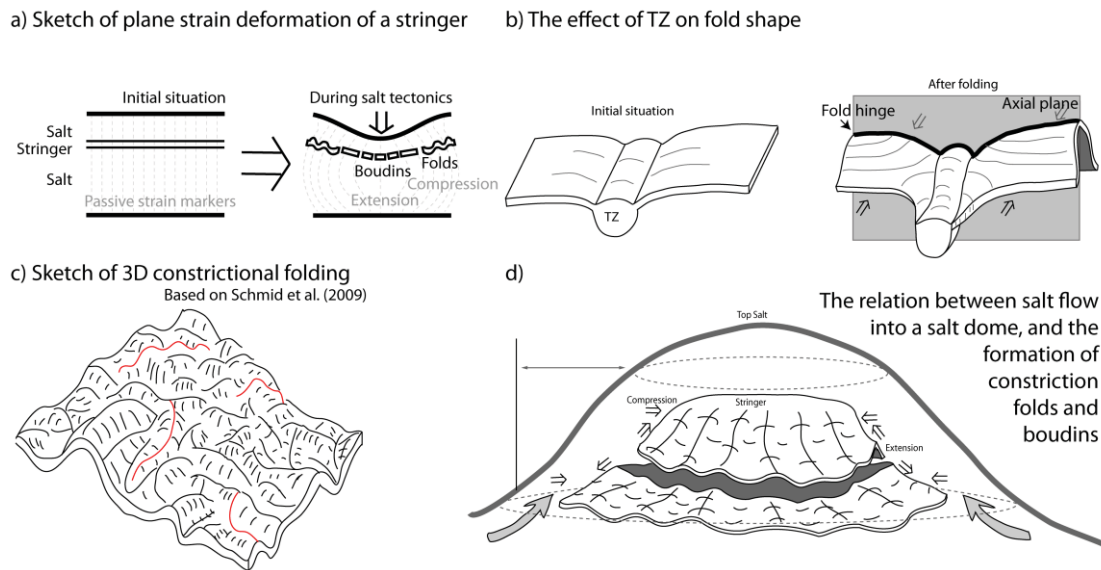


Figure 13: Sketches of the structures observed in this study.

a) First order, plane strain structural evolution in a salt pillow, showing areas of layer-parallel extension and shortening and the corresponding boudinage in areas of top salt subsidence and folding in the salt pillows. Note that the shape of the stringer should resemble top Zechstein as a harmonic fold. b) The effect of a thicker zone perpendicular to the folding is a depressed fold hinge while the axial plane is roughly planar. The TZ is stronger and this influences the shape of the fold. c) In a constrictionaly folded layer, the resulting fold structures have non-cylindrical axial planes. This is a different kind of “non-cylindrical folds” as those described in b). d) The formation of constriction folds and concentric boudins due to flow into a salt dome (compare with the concentric boudins in Fig. 4d and 6). The combined effect of the tensile forces due to vertical extension, and coeval horizontal compression due to the decrease in salt dome diameter result in the contemporary formation of contradicting structural styles.

correlation is not apparent in our dataset. Keeping in mind that the major salt tectonic movements occurred before the end of the Cretaceous, the fact that many of our stringers are located high in the Zechstein (about 250 m from top Zechstein), can be used to calculate an upper bound of sinking velocity. Considering the case that these stringers were first ruptured into individual bodies, tectonically displaced to top Zechstein and then started to sink 65 Ma, the upper bound velocity is around 4 m/Myr. This is much lower than the rates suggested by some analogue and numerical models, and in agreement with the wide variation of salt rheologies used by the different studies, calling for more work to resolve this question.

Folding

In salt mines (see for example Krische, 1928; Richter-Bernburg, 1953a; Lotze, 1957; Talbot and Jackson, 1987; Schlöder, 2006; Schlöder et al., 2007) isoclinal folds are common even in apparently flat-lying salt. The folded layers are often associated with boudins (Ramsay and Huber, 1987; Schlöder, 2006). High strain, folded intervals are often located close to less strongly deformed salt. This indicates that flow in evaporites can be strongly partitioned, possibly associated with the strong

topography of the inverted basement blocks (compare with: Talbot and Jackson, 1987). Also the presence of shear zones in salt can add to the complexity (Kupfer, 1976; Schlöder, 2006).

Interpretation of ANVIS

There are four possible explanations for the absence of a stringer in seismic sections. First, it may not have been deposited in this location. Second, the layer may be too thin to be imaged. Third, it may be discontinuous after being disrupted by tectonic deformation. Fourth, it may be in an orientation, which is too steep to produce a seismic reflection (Sleep, 1995; Geluk et al., 2000). The first explanation is rejected considering regionally constant thickness of the Z3. The well data from the Groningen area which was available for this study (see above) do not allow a clear distinction between alternatives two, three and four. However, it is not possible to explain all ANVIS by steep orientation only, because they also occur in areas where the surrounding stringer is shallow-dipping and has no vertical offset. Keeping in mind that a full explanation of ANVIS in the Zechstein requires additional data from many wells, and that in some ANVIS steeply dipping stringers were found by drilling, in what follows, we make the reasonable assumption that in areas where the stringers' enveloping surface dips less than 30 degrees, ANVIS correspond to the absence of a stringer due to tectonic disruption (boudinage). In areas where the stringers' enveloping surface dips more than 30 degrees, ANVIS can either correspond to the absence of a stringer due to tectonic disruption (boudinage or faulting), or a tectonically tilted stringer which is not imaged seismically.

Boudinage in salt – observations in mines

We interpret some of the fracturing of the stringer in the data to result from boudinage. The best examples of boudinage in our study areas are shown in Fig. 4d, 6b, 6e, 7, 8c and 11c, but the data quality does not allow a detailed description. We will compare our results with published examples of boudinage in this section. The process of boudinage is the “disruption of layers, bodies or foliation planes within a rock mass in response to bulk extension along the enveloping surface” (Goscombe et al., 2004), and a boudin can be described as “a fractured sheet of rock situated between non-fractured (...) rocks” (Lohest, 1909; Ramberg, 1955; see also Sintubin, 2008).

There is large variety of boudin geometries which can be subdivided both according to their kinematics as well as to the shape of the boudin blocks (see Goscombe and Passchier, 2003, Goscombe et al. 2004). Boudinage of brittle inclusions in salt is described by several authors. Lotze (1957, page 294; Smith, 1996; Davison, 1996; Roth, 1953; Borchert and Muir, 1964; Siemeister, 1969; Burliga, 1996; Schlöder, 2006; Schlöder et al., 2007; 2008). The six published wells of the Gorleben salt structure (Bornemann, 1991) penetrate the Z3 stringer in total eight times in four wells. In three of these penetrations the stringer is interpreted to be disrupted, faulted or fractured, showing the high fracture density in the Z3 stringer.

Boudinage in 3D

Studies of boudins to date have almost exclusively been in 2D profiles, and although there is a reasonable understanding of the range of structures occurring in profile view, there is a striking lack of understanding of the 3D morphology of boudins.

A 3D exposure of pegmatite boudins in marble (Schenk et al., 2007) shows boudins that are bound by a set of normal faults formed by reactivation of Mode-I fractures. The most extensive study to date of how boudins evolve in 3D is provided by the model experiments of G. Zulauf and coworkers (Zulauf et al., 2003; Zulauf and Zulauf, 2005, Zulauf et al., 2009). These experiments employ plasticine and natural anhydrite as strong layer. Here the plasticine is sufficiently ductile to fold when shortened parallel to the layering, but at the same time sufficiently brittle to rupture if extended parallel to the layers, much like natural anhydrite. The patterns of this “ductile rupture” are much more complicated than brittle fracture patterns. It is clear that the deviation from plane strain deformation results in the formation of very complex structures.

Boudin dimensions

Since the thickness of the stringer in Groningen (Fig. 3 and 6e) is between 40 and 50 m, the observed boudins have unusually high aspect ratios, in the order of 5 to 20, much larger than the largest mean aspect ratios described by Goscombe et al. (2004) in siliciclastic and carbonate rocks. In the Kłodawa salt mine, aspect ratios of around 20 are observed in the larger boudins (Burliga, 1996). The exceptional torn halite boudins in a carnallite matrix (Borchert and Muir, 1964; Siemeister, 1969), have aspect ratios in the order of 2.5-5 (assuming the view is perpendicular to the extension direction) and also the experimental D1-boudins of Zulauf and Zulauf (2005) have aspect ratios around 5. Observations of boudins of sand in viscous putty (Callot et al., 2006) also indicate a high aspect ratio. On the other hand, Zulauf et al. (2009) produced experimental boudins of very brittle anhydrite in halite with aspect ratios of 1.5 ± 1.0 . This difference in aspect ratio between the boudins of Goscombe et al. (2004) and “evaporitic” boudins may originate from the different rheologies, but more work is needed to resolve this question.

The rheology of salt and anhydrite during salt tectonic deformation

The rheology of anhydrite at shallow depth in the crust is not well known (Urai et al., 2008). We note that during shortening, anhydrite layers in salt domes commonly form concentric folds (see above), which means that the viscosity ratio is rather high, but at the same time boudins (brittle structures) are formed in extension. Corresponding to the present state of research (Urai et al., 2008), our present preferred model is that rheology of anhydrite is controlled by pressure solution and is Newtonian in layer parallel shortening. However, the high, near lithostatic, fluid pressures commonly observed in stringers (Williamson et al., 1997), allow tensile failure in layer parallel extension in the anhydrite encased in sealing salt. This model explains why the stringer forms ductile folds as well as brittle boudins at the same time. A similar model has already been proposed for pegmatites encased in marble (Schenk et al., 2007). Alternatively, brittle fracturing may be initiated in the underlying, more brittle limestone and claystone (*sensu* Hansen et al., 2004).

Folds formed under plane strain can be used to approximate the relative viscosity of the two layers (Sherwin and Chapple 196), using the Biot-Ramberg equations (Ramsay and Huber, 1987) for Newtonian fluids, or those Smith (1977) for non-Newtonian fluids. It is tempting to apply a similar method here, and to compare for example this normalized arc length of folds to the aspect ratio of boudins to calculate the relative viscosity. However, conventional folding theory is based on plane strain deformation and this is not the case in our field area, so a simple analysis may lead to errors (Stefan Schmalholz, personal communication). In future work we will attempt to constrain the relative rheologies of halite and anhydrite by 3D numerical modeling (Schmid et al 2009; Schmalholz and Podladchikov, 2001).

The early life of a salt giant

In summary, this study has shown early karst-related thickness variations overprinted by complex folding and boudinage, producing the complicated present-day geometry of the Z3 stringer. Possible effects of early karst, diagenesis or gravitational deformation, probably augmented by a local increase in sedimentation of the stringer, formed a network of ruptures and slide-related folds. This resulted in a series of thicker zones in the stringer. During the Early Mesozoic salt flow, the salt moved into the narrow stems of salt walls and diapirs (Fig. 13d). This resulted in the coeval folding and boudinage in the stringer, leading to significantly more complex structures than in plane strain. This complexity is further increased by the thicker zones which are significantly stronger than the surrounding stringer and might form preferred instabilities for folding and boudinage. When the growth of salt structures was halted, the possible sinking of the broken anhydrite blocks added even further complexity, although we do not expect this sinking to have geologically significant velocities.

A useful conceptual model for the displacement and deformation of stringers is that of passive and active processes. Passive means that the stringers are displaced by the flowing salt as passive objects and active means that the contrast in mechanical properties causes local instabilities, resulting in deformation, folding and boudinage of the stringers. It is also clear that the temporal evolution of the position or orientation of a stringer in a salt dome has a large effect on the strain history (Weijermars, 1988; Zulauf et al., 2003; Chemia et al., 2008).

An interesting observation of this study is the apparent correlation of the position of the TZ between the salt pillows. This is surprising because the TZ are thought to be older than the main phase of salt tectonics and also much smaller than the first-order structures. If this correlation can be shown to be real by additional observations of the same correlation in different areas, it would point to a subtle feedback mechanism in which the early internal structure of the salt basin can have a large effect on the evolving structures. In previous work, the main drivers for this were thought to be deformation on basement faults, regional tilt of the basin and lateral differences in overburden stress (Hudec and Jackson, 2007) but not the internal structure. An interesting concept emerging from this project is then, that active deformation of the stringers during the early life of the Zechstein salt giant can initiate feedback processes which control the evolution of the later instabilities and the growth of large scale salt structures (Hübscher et al., 2007). One mechanism for this could be that weak early deformation

of TZ affects the topography of the top of the salt, creating a small topography which controls sediment architecture and evolution of overburden load (cf Ings and Beaumont, 2010).

A toolbox to predict internal structure of salt bodies

The Zechstein of the Central European Basin has a fascinating, complexly folded structure which is known only in a few cases based on mining data. The methods outlined in this study can be used at a regional scale because the Z3 reflector is present almost everywhere and can be mapped in 3D using seismic reflection data which is available over very large areas (TNO-NITG, 2004).

Using the same 3D seismic data, the kinematics of the suprasalt sequence can be relatively accurately reconstructed using palinspastic reconstruction techniques (e.g. Mohr et al., 2005). Rheology of the Zechstein salt is not completely understood, but is constrained by a large amount of data. It is clear that even relatively pure halite can have strain rates variable by two orders of magnitude at the same differential stress and temperature (Urai et al., 2008) making the mechanical structure of the Zechstein strongly layered.

This dataset can now be combined into geomechanical models starting from the reconstructed original structure of the Zechstein including stringers, with the palinspastically reconstructed kinematics of top salt as kinematic boundary conditions, and the final structure compared with the interpretation of the Z3 stringer from 3D seismic. In addition, differential stress can be measured by subgrain size piezometry in drill cores. This method therefore produces models which can be tested against observations and, if the test is passed, can predict the internal structure of the salt body in the whole volume.

Conclusions

- ◇ We mapped complex internal structure of salt domes using 3D seismic reflection data. This opens the possibility to study the internal structure of the Zechstein and other salt giants in 3D using this technique, exposing a previously poorly known structure which is comparable in size and complexity to the internal parts of some orogens.
- ◇ The evolutionary sequence of sedimentary and diagenetic processes, followed by deformation at different scales results in early thickness variations, overprinted by a range of fold and of boudin structures.
- ◇ Flow heterogeneities in salt caused by presence of thickness variations in stringers are interpreted to lead to subtle topography of top salt, which in turn influenced sedimentation and deformation of overburden.
- ◇ Our observations show no conclusive evidence for significant gravity-induced sinking of stringers.
- ◇ The methods used in this study can be combined with numerical modeling to predict the internal structure of salt bodies without extensive drilling or construction of galleries.

Acknowledgements

JLU and MdK would like to express their gratitude to Paul Williams for his mentoring and many discussions on the geometry and kinematics of folding.

The authors thank the Nederlandse Aardolie Maatschappij (NAM, a Shell operated 50-50 joint venture with ExxonMobil) for providing the data. We gratefully acknowledge discussions with Peter Kukla and Stephan Back on stringer geology and seismic interpretation. This paper benefited considerably from discussion with Jos Terken, Joris Steenbrink and Daan den Hartog Jager (Shell). We also thank Mark Geluk for his discussion and comments.

Schlumberger is thanked for providing Petrel 2005 and 2007 seismic interpretation software under academic licence. The editor, Shoufa Lin, and the reviewers Gernold Zulauf and Charlotte Krawczyk are thanked for their comments which considerably improved the manuscript. Janneke IJmker is thanked for critical notes in the early stages of the MS.

References

- ◇ Al-Siyabi, H. A., 2005. Exploration history of the Ara intrasalt carbonate stringers in the South Oman Salt Basin. *GeoArabia* 10(4), 39-72.
- ◇ Barber, P. M., 1981. Messinian subaerial erosion of the proto-Nile Delta. *Marine Geology* 44(3-4), 253.
- ◇ Bäuerle, G., Bornemann, O., Mauthe, F., Michalzik, D., 2000. Turbidite, Breccien und Kristallrasen am top des Hauptanhydrits (Zechstein 3) des Salzstocks Gorleben. *Zeitschrift der Deutschen Geologischen Gesellschaft* 151(1-2), 99-125.
- ◇ Behlau, J., Mingerzahn, G., 2001. Geological and tectonic investigations in the former Morsleben salt mine (Germany) as a basis for the safety assessment of a radioactive waste repository. *Engineering Geology* 61, 83-97.
- ◇ Best, G., 1989. Die Grenze Zechstein/Buntsandstein in Nordwest-Deutschland nach Bohrlochmessungen. *Zeitschrift der Deutschen Gesellschaft für Geowissenschaften* 140, 73-85.
- ◇ Blanc, P. L., 2002. The opening of the Plio-Quaternary Gibraltar Strait: assessing the size of a cataclysm. *Geodynamica Acta* 15, 303-317.
- ◇ Borchert, H., Muir, R. O., 1964. *Salt Deposits. The Origin, Metamorphism and Deformation of Evaporites*. D. Van Nostrand Company, Ltd., London, New York, Toronto, pp. 338.
- ◇ Bornemann, O., 1991. Zur Geologie des Salzstocks Gorleben nach den Bohrergebnissen. *BfS-Schriften* 4, 1-67.
- ◇ Bosá, P., Bruthans, J., Filippi, M., Svoboda, T., Šmíd, J., 1999. Karst and caves in salt diapirs, SE Zagros Mts (Iran). *Acta Carsologica* 28(2), 41-75.
- ◇ Burliga, S., 1996. Kinematics within the Klodawa salt diapir, central Poland. In: Alsop, G. I., Blundell, D. J. & Davison, I. (Eds.), *Salt tectonics*. Geological Society Special Publication 100. Geological Society, London, 11-21.
- ◇ Callot, J.-P., Rondon, D., Rigollet, C., Letouzey, J., Pillot, D., Mengus, J.-M., 2006. Stringers and evolution of salt diapirs, insight from analogue models. 2006 AAPG International Conference and Exhibition, Perth, Australia.
- ◇ Chemia, Z., Koyi, H., Schmeling, H., 2008. Numerical modelling of rise and fall of a dense layer in salt diapirs. *Geophysical Journal International* 172, 798-816.

- ◇ Coelewijn, P. A. J., Haug, G. M. W., Kuijk, H. v., 1978. Magnesium-salt exploration in the Northeastern Netherlands. *Geologie en Mijnbouw* 57(4), 487-502.
- ◇ Cornée, J. J., Ferrandini, M., Saint Martin, J. P., Münch, P., Moullade, M., Ribaud-Laurenti, A., Roger, S., Saint Martin, S., Ferrandini, J., 2006. The late Messinian erosional surface and the subsequent reflooding in the Mediterranean: New insights from the Melilla-Nador basin (Morocco). *Palaeogeography, Palaeoclimatology, Palaeoecology* 230(1-2), 129.
- ◇ Davison, I., 1996. Deformation and sedimentation around active Miocene salt diapirs on the Tihama Plain, Northwest Yemen. *Geological Society Special Publications* 100, 23.
- ◇ De Jager, J., 2003. Inverted basins in the Netherlands, similarities and differences. *Netherlands Journal of Geosciences / Geologie en Mijnbouw* 82(4), 355-366.
- ◇ Desbois, G., Zavada, P., Schléder, Z., Urai, J. L., 2010. Deformation and recrystallization mechanisms in actively extruding salt fountain: Microstructural evidence for a switch in deformation mechanisms with increased availability of meteoric water and decreased grain size (Qum Kuh, central Iran). *Journal of Structural Geology* 32 (4), 580-594.
- ◇ Duin, E. J. T., Doornenbal, J. C., Rijkers, R. H. B., Verbeek, J. W., Wong, T. E., 2006. Subsurface structure of the Netherlands - results of recent onshore and offshore mapping. *Netherlands Journal of Geosciences / Geologie en Mijnbouw* 85(4), 245-276.
- ◇ Escher, B. G., Kuenen, P. H., 1929. Experiments in connection with salt domes. *Leidsche Geologische Mededeelingen* 3, 151-182.
- ◇ Evans, D. J., Chadwick, R. A. (Editors), 2009. *Underground Gas Storage: Worldwide Experiences and Future Development in the UK and Europe*. Geological Society, London, Special Publications, 313.
- ◇ Evrard, E., Sellier, N., Vendeville, B. C., Loncke, L., Loubrieu, B., Brosolo, L., Mascle, J., 2008. Physical Modelling of Thin-Skinned, Salt-Related Gravitational Deformation in Response to Active Crustal-Scale Tectonics: Examples from the Eastern Mediterranean. Third International Geomodelling Conference, Florence, Italy, September 24, 2008, *Bollettino di Geofisica, teorica ed applicata, Istituto Nazionale di Oceanografia e di Geofisica Sperimentale*, 49, 366-371.
- ◇ Fokker, P. A., Urai, J. L., Steeneken, P. V., 1995. Production-induced convergence of solution mined caverns in Magnesium salts and associated subsidence. *Proceedings of the 5th International Symposium on land subsidence, The Hague/The Netherlands*, A.A. Balkema, 281-289.
- ◇ Fulda, E., 1928. Die Geologie der Kalisalzlagerstätten. In: Krische, P. (Ed.), *Das Kali*, II. Teil. Enke's Bibliothek für Chemie und Technik unter Berücksichtigung der Volkswirtschaft 7. Ferdinand Enke, Stuttgart, Germany, 24-136.
- ◇ Gansser, A., 1992. The enigma of the Persian dome inclusions. *Eclogae Geologicae Helveticae* 85, 825-846.
- ◇ Geluk, M. C., 1995. Stratigraphische Gliederung der Z2-(Staßfurt-) Salzfolge in den Niederlanden: Beschreibung und Anwendung bei der Interpretation von halokinetisch gestörten Sequenzen. *Zeitschrift der deutschen Gesellschaft für Geowissenschaften* 146, 458-465.

- ◇ Geluk, M. C., 1997. Peleogeographic maps of Moscovian and Artinskian; contributions from the Netherlands. In: DSoleau, S. & De Wever, P. (Eds.), Peri-Thetys stratigraphic correlations. *Geodiversitas* 19, 229-234.
- ◇ Geluk, M. C., 2000. Late Permian (Zechstein) carbonate-facies maps, the Netherlands. *Geologie en Mijnbouw/ Netherlands Journal of Geosciences* 79(1), 17-27.
- ◇ Geluk, M. C., 2005. Stratigraphy and tectonics of Permo-Triassic basins in the Netherlands and surrounding areas, Utrecht University.
- ◇ Geluk, M. C., 2007. Permian. In: Wong, T. E., Batjes, D. A. J. & De Jager, J. (Eds.), *Geology of the Netherlands*. Royal Netherlands Academy of Arts and Sciences, Amsterdam, 63 - 84.
- ◇ Geluk, M. C., Arts, R., Duin, E. J. T., Van Wees, J.-D., Oldenziel, C., Paar, W. A., 2000. The Zuidwending salt dome: A multidisciplinary mapping project. *TNO-NITG – INFORMATION* 5, 5-7.
- ◇ Geluk, M. C., Paar, W. A., Fokker, P. A., 2007. Salt. In: Wong, T. E., Batjes, D. A. J. & De Jager, J. (Eds.), *Geology of the Netherlands*. Royal Netherlands Academy of Arts and Sciences, Amsterdam, 283 - 294.
- ◇ Goscombe, B. D., Passchier, C. W., 2003. Asymmetric boudins as shear sense indicators--an assessment from field data. *Journal of Structural Geology* 25(4), 575 - 589.
- ◇ Goscombe, B. D., Passchier, C. W., Hand, M., 2004. Boudinage classification: end-member boudin types and modified boudin structures. *Journal of Structural Geology* 26, 739-763.
- ◇ Grujic, D., 1993. The influence of initial fold geometry on type 1 and type 2 interference patterns: an experimental approach. *Journal of Structural Geology* 15(3-5), 293.
- ◇ Grujic, D., Walter, T. R., Gärtner, H., 2002. Shape and structure of (analogue models of) refolded layers. *Journal of Structural Geology* 24(8), 1313.
- ◇ Hansen, D.M., Shimeld, J.W., Williamson, M.A., Lykke-Andersena, H., 2004. Development of a major polygonal fault system in Upper Cretaceous chalk and Cenozoic mudrocks of the Sable Subbasin, Canadian Atlantic margin, *Marine and Petroleum Geology* 21, 1205–1219
- ◇ Hofrichter, E., 1974. Speicherkavernen im Salzstoecken Nordwestdeutschlands -Geologische Probleme, Bemerkungen zur selektiven Aufloessing von Kalisalzen. *Erzmetall* 65(5), 219-226.
- ◇ Hübscher, C., Cartwright, J., Cypionka, H., De Lange, G., Robertson, A., Suc, J. P., Urai, J. L., 2007. Global look at Salt Giants. *Eos* 88(16), 177-179.
- ◇ Hudec, M. R., Jackson, M. P. A., 2007. Terra infirma: Understanding salt tectonics. *Earth Science Reviews* 82(1-2), 1-28.
- ◇ Ings, S. J., Beaumont, C., 2010. Shortening viscous pressure ridges, a solution to the enigma of initiating salt 'withdrawal' minibasins *Geology* , 38, 339-342,
- ◇ Jackson, M. P. A., 1985. Natural Strain in Diapiric and Glacial Rock Salt, with Emphasis on Oakwood Dome, East Texas, Bureau of Economic Geology/The University of Texas at Austin/Texas.
- ◇ Jackson, M. P. A., 1995. Retrospective salt tectonics. In: Jackson, M. P. A., Roberts, D. G. & Snelson, S. (Eds.), *Salt tectonics: a global perspective: AAPG Memoir* 65, 1-28.
- ◇ Jackson, M. P. A., Cornelius, R. R., Craig, C. H., Gansser, A., Stocklin, J., Talbot, C. J., 1990. Salt Diapirs of the great Kavir, central Iran. *Geological Society of America, Boulder, Memoir* 177, pp. 139 + Karte.

- ◇ Jackson, M. P. A., Roberts, D. G., Snelson, S. (Editors), 1995. Salt tectonics - A global perspective. AAPG Memoir, 65. AAPG Bulletin, Tulsa, U.S.A., pp. 454.
- ◇ Jackson, M. P. A., Talbot, C. J., 1989. Anatomy of mushroom-shaped diapirs. *Journal of Structural Geology* 11(1/2), 211-230.
- ◇ Jackson, M. P. A., Vendeville, B. C., 1994. Regional extension as a geologic trigger for diapirism. *Geological Society of America Bulletin* 106, 57-73.
- ◇ Koyi, H., 2001. Modeling the influence of sinking anhydrite blocks on salt diapirs targeted for hazardous waste disposal. *Geology* 29(5), 387-390.
- ◇ Krische, P. (Editor), 1928. Das Kali (parts I and II). Enke's Bibliothek für Chemie und Technik unter Berücksichtigung der Volkswirtschaft, 7. Ferdinand Enke, Stuttgart, Germany, pp. 768.
- ◇ Kupfer, D. H., 1968. Relationship of internal to external structure of salt domes, Diapirism and diapirs; a symposium. *Memoir - American Association of Petroleum Geologists* 8, 78-89.
- ◇ Kupfer, D. H., 1976. Shear Zones Inside Gulf Coast Salt Stocks Help to Delineate Spines of Movement. *AAPG Bulletin* 60(9), 1434-1447.
- ◇ Langbein, R., 1987. The Zechstein sulphates: The state of the art. In: Peryt, T. M. (Ed.), *The Zechstein Facies in Europe. Lecture Notes in Earth Sciences.* Springer, Berlin/ Heidelberg, 143-188.
- ◇ Li, S., Abe, S., Urai, J. L., Van Gent, H. W., 2009. Sinking of carbonate and anhydrite stringers in rock salt: insights from numerical simulations. *EGU General Assembly 2009, Vienna, Austria, 19 – 24 April 2009, Geophysical Research Abstracts*, 11.
- ◇ Lide, D. R. (Editor), 1995. *CRC Handbook of Chemistry and Physics. A Ready Reference Book of Chemical and Physical Data.* CRC Press, Boca Raton, New York, London, Tokio.
- ◇ Lisle, R. J., Toimil, N. C., 2007. Defining folds on three-dimensional surfaces. *Geology* 35, 519-522.
- ◇ Loget, N., Van Den Driessche, J., Davy, P., 2005. How did the Messinian Salinity Crisis end? *Terra Nova*, 414-419.
- ◇ Lohest, M., 1909. De l'origine des vienes et des géodes des terrains primaires de Belgique. *Soc. géol. Belgique Annales* 36B, 275-282.
- ◇ Lotze, F., 1957. *Steinsalz und Kalisalze, 1. Teil (Allgemein-geologischer Teil).* Gebrueder Borntraeger, Berlin, 1, pp. 465.
- ◇ Mattes, B. W., Conway Morris, S., 1990. Carbonate/evaporite deposition in the late Precambrian-Early Cambrian Ara Formation of southern Oman. In: Robertson, A. H. F., Searle, M. P. & Ries, A. C. (Eds.), *The geology and tectonics of the Oman region.* Geological Society (London) Special Publication 49, 617-636.
- ◇ Maystrenko, Y., Bayer, U., Scheck-Wenderoth, M., 2006. 3D reconstruction of salt movements within the deepest post-Permian structure of the Central European Basin System – the Glueckstadt Graben. *Netherlands Journal of Geosciences - Geologie en Mijnbouw* 85(3), 181 - 196.
- ◇ Mohr, M., Kukla, P. A., Urai, J. L., Bresser, G., 2005. Multiphase salt tectonic evolution in NW Germany: seismic interpretation and retro-deformation. *International Journal of Earth Sciences (Geologische Rundschau)* 94, 914-940.

- ◇ Muehlberger, W. R., 1968. Internal structures and mode of uplift of Texas and Louisiana salt domes, Saline deposits 88. Special Paper - Geological Society of America, 359-364.
- ◇ Mynatt, I., Bergbauer, S., Pollard, D. D., 2007. Using differential geometry to describe 3-D folds. *Journal of Structural Geology* 29, 1256-1266.
- ◇ De Mulder, E. F. J., Geluk, M. C., Ritsema, I. L., Westerhoff, W. E., Wong, T. E., 2003. *De ondergrond van Nederland*. Wolters-Noordhoff, Gronningen/Houten, pp. 379.
- ◇ Peters, J. M., Filbrandt, J. B., Grotzinger, J. P., Newall, M. J., Shuster, M. W., Al-Siyabi, H. A., 2003. Surface-piercing salt domes of interior North Oman, and their significance for the Ara carbonate "stringer" hydrocarbon play. *GeoArabia* 8(2), 231-270.
- ◇ Pollard, D. D., Fletcher, R. C., 2005. *Fundamentals of Structural Geology*. Cambridge University Press, Cambridge, pp. 500 pp.
- ◇ Ramberg, H., 1955. Natural and experimental boudinage and pinch-and-swell structures. *Journal of Geology* 63, 512-526.
- ◇ Ramsay, J. G. (Editor), 1967. *Folding and Fracturing of Rocks*. McGraw-Hill Book Company, New York San Francisco St.Louis Toronto London Sydney, pp. 568.
- ◇ Ramsay, J. G., Huber, M. I., 1987. *Folds and Fractures, The Techniques of modern Structural Geology*. 2. Academic Press, London.
- ◇ Remmelts, G., 1996. Salt tectonics in the southern North Sea, the Netherlands. In: Rondeel, H. E., Batjes, D. A. J. & Nieuwenhuijs, W. H. (Eds.), *Geology of Gas and Oil under the Netherlands*. Kluwer Academic Publishers, Dordrecht, 19-30.
- ◇ Reuning, L., Schoenherr, J., Heimann, A., Kukla, P. A., Urai, J. L., Littke, R., 2007. The salt domes of the Ghaba Salt Basin: An analogue of the hydrocarbon play of the south Oman Salt Basin? 13th Bathurst Meeting of Carbonate Sedimentologists, Norwich, UK, 16. - 18. Juli 2007.
- ◇ Reuning, L., Schoenherr, J., Heimann, A., Urai, J. L., Littke, R., Kukla, P. A., Rawahi, Z., 2009. Constraints on the diagenesis, stratigraphy and internal dynamics of the surface-piercing salt domes in the Ghaba Salt Basin (Oman): A comparison to the Ara Group in the South Oman Salt Basin. *GeoArabia* 14(3), 83-120.
- ◇ Richter-Bernburg, G. (Editor), 1953a. *Salzlagerstätten (Proceedings of the Frühjahrstagung der Deutschen Geologische Gesellschaft, Goslar, May 13-16 1953)*. *Zeitschrift der Deutschen Geologischen Gesellschaft*, 105, pp. 589-908.
- ◇ Richter-Bernburg, G., 1953b. *Stratigraphische Gliederung des deutschen Zechsteins*. *Zeitschrift der deutschen geologischen Gesellschaft* 105, 593-645.
- ◇ Richter-Bernburg, G., 1980. Salt Tectonics, Interior structures of Salt Bodies. *Bull. Cent. Rech. Explor.-Prod. Elf-Aquitaine* 4(1), 373-393.
- ◇ Richter-Bernburg, G., 1987. Deformation within salt bodies. In: Lerche, I. & O'Brien, J. J. (Eds.), *Dynamical Geology of Salt and Related Structures*. Academic Press, Inc., 39-75.
- ◇ Rijks Geologische Dienst (RGD), 1991. Map sheet II Ameland-Leeuwarden, Explanation to map sheet II Ameland-Leeuwarden. Rijks Geologische Dienst (RGD), Haarlem, the Netherlands, 87.
- ◇ Rijks Geologische Dienst (RGD), 1993. Map sheet V Sneek-Zwolle, Explanation to map sheet V Sneek-Zwolle. Rijks Geologische Dienst (RGD), Haarlem, the Netherlands, 126.

- ◇ Rijks Geologische Dienst (RGD), 1995. Map sheet III Rottumeroog-Groningen, Explanation to map sheet III Rottumeroog-Groningen. Rijks Geologische Dienst (RGD), Haarlem, the Netherlands, 113.
- ◇ Roth, H., 1953. Ausbildung und Lagerungsformedn des Kalifözes "Hessen" im Fuldagebiet. *Zeitschrift der Deutschen Geologischen Gesellschaft* 105, 674-684.
- ◇ Rouchy, J. M., Caruso, A., 2002. Review: The Messinian salinity crisis in the Mediterranean basin: A reassessment of the data and an integrated scenario. *Sedimentary Geology* 188–189, 35–67.
- ◇ Scheck, M., Bayer, U., Lewerenz, B., 2003. Salt redistribution during extension and inversion inferred from 3D backstripping. *Tectonophysics* 373, 55-73.
- ◇ Schenk, O., Urai, J. L., Van der Zee, W., 2007. Evolution of Boudins under progressively decreasing pore pressure - a case study of pegmatites enclosed in marble deforming at high grade metamorphic conditions, Naxos, Greece. *American Journal of Science* 307, 1009-1033.
- ◇ Serra, O., 1984. Fundamentals of well-log interpretation, 1. The acquisition of logging data. *Developments in Petroleum Science*, 15A Elsevier, Amsterdam. 218 pages.
- ◇ Sherwin, J.-A., Chapple, W.M., 1968. Wavelengths of single layer folds. A comparison between theory and observation. *American Journal of Science* 266, 167-178
- ◇ Schlöder, Z., 2006. Deformation mechanisms of naturally deformed rocksalt. PhD thesis, Rheinisch-Westfälischen Technischen Hochschule Aachen.
- ◇ Schlöder, Z., Burliga, S., Urai, J. L., 2007. Dynamic and static recrystallization-related microstructures in halite samples from the Kłodawa salt wall (central Poland) as revealed by gamma-irradiation. *Neues Jahrbuch für Mineralogie und Petrologie* 184(1), 17-28.
- ◇ Schlöder, Z., Urai, J. L., Nollet, S., Hilgers, C., 2008. Solution-precipitation creep and fluid flow in halite: a case study of Zechstein (Z1) rocksalt from Neuhof salt mine (Germany). *International Journal of Earth Sciences* 97(5), 1045-1056.
- ◇ Schmalholz, S.M., Podladchikov, Y.Y., 2001. Strain and competence contrast estimation from fold shape., *Tectonophysics* 340 (2001) 195–213
- Schmid, D. W., Dabroski, M., Krotkiewski, M., 2009. Structure of fold traps. *Physics of hydrocarbon bearing systems. The 22nd Kongsberg seminar*, Kongsberg, Norway, 6-8 May.
- Schoenherr, J., Reuning, L., Kukla, P. A., Littke, R., Urai, J. L., Siemann, M., Rawahi, Z., 2009a. Halite cementation and carbonate diagenesis of intra-salt reservoirs from the Late Neoproterozoic to Early Cambrian Ara Group (South Oman Salt Basin). *Sedimentology* 56(2), 567-589.
- ◇ Schoenherr, J., Schlöder, Z., Urai, J. L., Littke, R., Kukla, P. A., 2009a (online first). Deformation mechanisms of deeply buried and surface-piercing Late Pre-Cambrian to Early Cambrian Ara Salt from interior Oman. *International Journal of Earth Sciences*, DOI 10.1007/s00531-009-0443-3.
- ◇ Scholle, P. A., Stemmerik, L., Ulmer-Scholle, D., Di Liegro, G., Henk, F. H., 1993. Palaeokarst-influenced depositional and diagenetic patterns in Upper Permian carbonates and evaporites, Karstryggen area, central East Greenland. *Sedimentology* 40, 895-918.
- ◇ Schultz-Ela, D. D., Walsh, P., 2002. Modeling of grabens extending above evaporites in Canyonlands National Park, Utah. *Journal of Structural Geology* 24 (2), 247-275

- ◇ Schwerdtner, W. M., Van Kranendonk, M., 1984. Structure of Stolz Diapir; a well-exposed salt dome on Axel Heiberg Island, Canadian Arctic Archipelago. *Bulletin of Canadian Petroleum Geology* 32(2), 237-241.
- ◇ Siemann, M. G., Ellendorff, B., 2001. The composition of gases in fluid inclusions of late Permian (Zechstein) marine evaporites in Northern Germany. *Chemical Geology* 173, 31-44.
- ◇ Siemeister, G., 1969. Primärparagenese und Metamorphose des Ronnenbergslagers nach Untersuchungen im Grubenfeld Salzdettfurth. Bundesanstalt für Bodenforschung und den Geologischen Landesämtern der Bundesrepublik Deutschland, Hannover, 62, pp. 122.
- ◇ Sintubin, M., 2008. Photograph of the month: Boudin centennial. *Journal of Structural Geology* 30, 1315-1316.
- ◇ Sleep, N. H., 1995. Ductile creep, compaction, and rate and state dependent friction within major fault zones. *J. Geophys. Res.* 100(B7), 13,065-13,080.
- ◇ Sleep, N. H., Fujita, K., 1997. *Principles of Geophysics*. Blackwell Science, USA,
- ◇ Smith, R.B., 1977. Formation of folds, boudinage, and mullions in non-Newtonian materials. *Geological Society of America Bulletin* 88, 312-320.
- ◇ Smith, D. B., 1995. Chapter 3: North-east England (Durham Province), Marine Permian of England. *Geological Conservation Review* 8, 205.
- ◇ Smith, D. B., 1996. Deformation in the Late Permian Boulby Halite (EZ3Na) in Teesside, NE England. *Geological Society Special Publications* 100, 77-88.
- ◇ Southwood, D. A., Hill, W. O. R., 1995. The origin and distribution of porosity in the Zechsteinkalk (Upper Permian) of Hewett Field, Southern North Sea. *Petroleum Geoscience* 1, 289-302.
- ◇ Stäuble, A. J., Milius, G., 1970. Geology of Groningen Gas Field, Netherlands. *Geology of Giant Petroleum Fields AAPG A009*, 359-369.
- ◇ Strohmenger, C., Voigt, E., Zimdars, J., 1996. Sequence stratigraphy and cyclic development of Basal Zechstein carbonate-evaporite deposits with emphasis on Zechstein 2 off-platform carbonates (Upper Permian, Northeast Germany). *Sedimentary Geology* 102(1-2), 33.
- ◇ Talbot, C. J., 2008. Photograph of the Month. *Journal of Structural Geology* 30(7), 810.
- ◇ Talbot, C. J., Aftabi, P., 2004. Geology and models of salt extrusion at Qum Kuh, central Iran. *Journal of the Geological Society* 161, 321-334.
- ◇ Talbot, C. J., Jackson, M. P. A., 1987. Internal kinematics of salt diapirs. *AAPG Bulletin* 71(9), 1068-1093.
- ◇ Taylor, J. C. M., 1998. Upper Permian - Zechstein. In: Glennie, K. W. (Ed.), *Petroleum Geology of the North Sea. Basic Concepts and Recent Advances (fourth edition)*. Blackwell Science, Oxford, 174-211.
- ◇ TNO-NITG. 2004. *Geological Atlas of the Subsurface of the Netherlands - onshore*. TNO-NITG, Utrecht, pp. 103.
- ◇ TNO. 1998. Map sheet X Almelo-Winterswijk, *Geological Atlas of the Subsurface of The Netherlands*. Netherlands Institute for Applied Geoscience TNO - National Geological Survey, Haarlem, 142.
- ◇ Urai, J. L., Schlöder, Z., Spiers, C. J., Kukla, P. A., 2008. Flow and Transport Properties of Salt Rocks. In: Littke, R., Bayer, U., Gajewski, D. & Nelskamp, S. (Eds.), *Dynamics of complex*

- intracontinental basins: The Central European Basin System. Springer-Verlag, Berlin Heidelberg, 277-290.
- ◇ Van Adrichem-Boogaert, H. A., Kouwe, W. F. P., 1993-1997. Stratigraphic Nomenclature of the Netherlands; revision and update by RGD and NOGEP. TNO-NITG, Mededelingen Rijks Geologische Dienst, Haarlem, 50, pp. 50.
 - ◇ Van der Molen, A. S., 2004. Sedimentary development, seismic stratigraphy and burial compaction of the Chalk Group in the Netherlands North Sea area. PhD. thesis, Utrecht University.
 - ◇ Van Eijs, R., Breunse, J., 2003. Evidence for two different creep mechanisms in rocksalt - Solution mining in the Barradeel concession. TNO-NITG – INFORMATION, 5-9.
 - ◇ Van Hoorn, B., 1987. Structural evolution, timing and tectonic style of the Sole Pit inversion. In: (Editor). P. A. Z. (Ed.), Compressional Intra-Plate Deformations in the Alpine Foreland. Tectonophysics 137, 239-284.
 - ◇ Van Keken, P. E., Spiers, C. J., Van den Berg, A. P., Muzyert, E. J., 1993. The effective viscosity of rocksalt: implementation of steady-state creep laws in numerical models of salt diapirism. Tectonophysics 225(4), 457-476.
 - ◇ Van Wijhe, D. H., 1987. Structural evolution of inverted basins in the Dutch offshore, Compressional Intra-Plate deformations in the Alpine Foreland. Tectonophysics 137, 171-219.
 - ◇ Warren, J. K., 2006. Evaporites: Sediments, Resources and Hydrocarbons. Springer, pp. 1035.
 - ◇ Weijermars, R., 1988. Convection experiments in high Prandtl number silicones, Part 2. Deformation, displacement and mixing in the Earth's mantle. Tectonophysics 154(1-2), 97.
 - ◇ Williams-Stroud, S. C., Paul, J., 1997. Initiation and growth of gypsum piercement structures in the Zechstein Basin. Journal of Structural Geology 19(7), 897.
 - ◇ Williamson, M. A., Murray, S. J., Hamilton, T. A., Copland, M. A., 1997. A review of Zechstein drilling issues. SPE Drilling & Completion 13(3), 174-181.
 - ◇ Wong, T. E., Batjes, D. A. J., de Jager, J. (Editors), 2007. Geology of the Netherlands. Editat-KNAW, Amsterdam, pp. 354.
 - ◇ Ziegler, P. A., 1982. Geological Atlas of Western and Central Europe. Elsevier Scientific Publishing Company, The Hague, Amsterdam, pp. 130.
 - ◇ Zirngast, M. (Editor), 1991. Die Entwicklungsgeschichte des Salzstocks Gorleben, Ergebnis einer strukturgeologischen Bearbeitung. Geologisches Jahrbuch. Reihe A: Allgemeine und Regionale Geologie BR Deutschland und Nachbargebiete, Tektonik, Stratigraphie, Palaeontologie, Heft 132. Herausgegeben von der Bundesanstalt für Bodenforschung und den Geologischen Landesämtern der Bundesrepublik Deutschland, Hannover, pp. 31.
 - ◇ Zirngast, M., 1996. The development of the Gorleben salt dome (northwest Germany) based on quantitative analysis of peripheral sinks. In: Alsop, G. I., Blundell, D. J. & Davison, I. (Eds.), Salt Tectonics. Geological Society Special Publications 100, 203-226.
 - ◇ Zulauf, G., Zulauf, J., Hastreiter, P. & Tomandl, B., 2003. A deformation apparatus for three-dimensional coaxial deformation and its application to rheologically stratified analogue material. J. Struct. Geol., 25: 469-480

- ◇ Zulauf, G., Zulauf, J., Bornemann, O., Kihm, N., Peinl, M., Zanella, F., 2009. Experimental deformation of a single-layer anhydrite in halite matrix under bulk constriction. Part 1: Geometric and kinematic aspects. *Journal of Structural Geology* 31(4), 460.
- ◇ Zulauf, J., Zulauf, G., 2005. Coeval folding and boudinage in four dimensions. *Journal of Structural Geology* 27, 1061-1068.

Concluding remarks

"...as the great philosopher Jagger said: 'you can't always what you want'" (...)

"But as it turns out, if you try sometimes, you get what you need."

- *House MD* - Pilot episode

Faults in outcrop vs. seismic faults

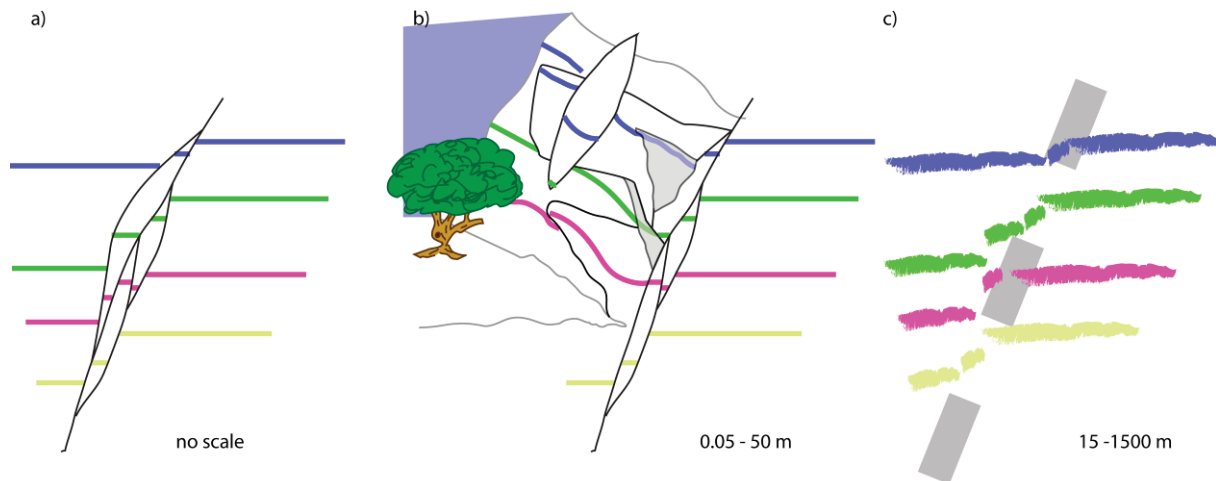


Fig. 1: There are several fundamental differences in observing fault structures (a) in outcrop (b) and seismic data (c).

There are several fundamental differences between studying faults surfaces in outcrop and the fault surfaces constructed by interpolation of seismic picks in a seismic dataset (see Chapter 2). Natural faults consist of a complex of set superimposed fractures and faults with multiple slip surfaces (Fig. 1a, and e.g.: Koestler and Ehrmann, 1991; Van der Zee, 2001; Storti et al., 2003; Van der Zee et al., 2003; Van der Zee and Urai, 2005; Bussolotto et al., 2007). The exposed fault plane in outcrop (Fig. 1b) actually is only one of these slip surfaces, with most likely, several planes removed by erosion, and several other planes buried below the present exposure. Erosion and fracturing can form “windows” to other slip planes, but detailed observations of slip planes over large distances is generally not possible. In seismic interpretation on the other hand (Fig.1c), the fault zone is reconstructed by discretely picking the locations of reflector termination in seismic cross section, or zones of high fault likelihood, as indicated by dip, curvature or other fault enhancement attributes (Cox and Seitz, 2007). Seismic fault analysis is restricted by the limit of seismic resolution (Hesthammer and Henden, 2000) and is complicated by the effects of diffraction at the reflector terminations. This diffraction makes the reflectors (which are often actually quite discrete surfaces, for example bedding planes) appear fuzzy and extend further laterally into the fault zone than the actual reflecting surface. On the other hand, seismic interpretation does provide an excellent 3D representation of the fault zone, provided the fault is picked with enough density.

Several works have shown that the power spectra of 1D profiles from natural fault roughness at different scales plot as a scale invariant property. The roughness scaling factor is about 0.8 perpendicular to the striations, and thus are essentially fractal (e.g.: Power et al., 1988; Power and Tullis, 1991; Lee and Bruhn, 1996; Power and Durham, 1997; Renard et al., 2006; Candela et al., in press). When the undulations from faults picked on 3D seismic reflection data have the same fractal dimension, they are very likely to be “real” and not an imaging or interpolation effect.

So, while outcrops allow high detail observations of single slip-surfaces at a time (or in crosssections observations of fault zones, only a 2D representation of this zone), seismic fault surfaces actually represent the geometry of the fault zone up to a certain resolution limit, and generally fail to observe individual slivers of host rock inside fault zones. Nevertheless, very important observations, for example the roughness of the slip plane/fault zone can be assumed to be scale invariant.

Multiple kinematic indicators on a single movement plane

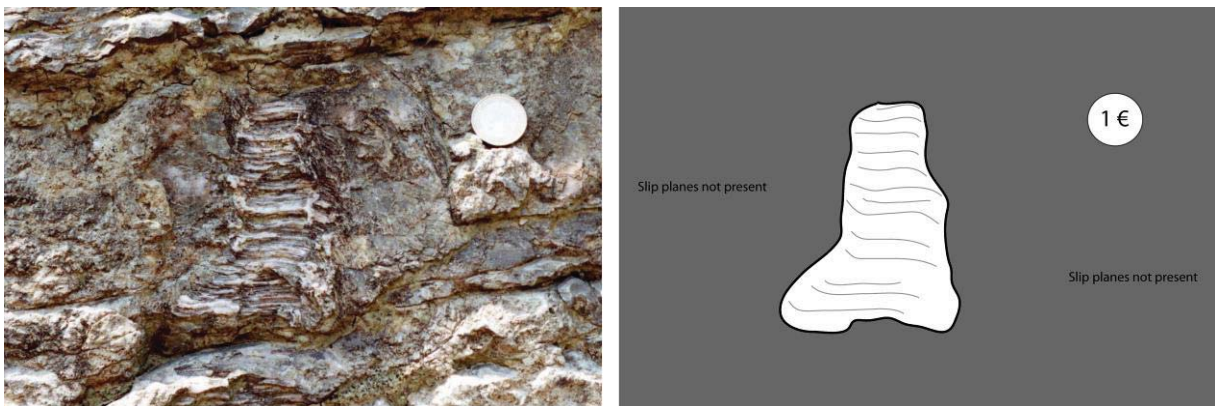


Fig. 2: A patch slickenside with curved movement striations. Does this indicate a continued movement with changing movement direction? Picture is taken on the same fault in Fig. 1 Fig. 2 of the introduction.

The overprinting of different kinematic indicators (like in Fig.1 of the Introduction) is often used to establish a relative chronology of movement events on a fault plane, and thus to calculate a paleostress stratigraphy (see: Chapter 1; Kleinspehn et al., 1989; Vandycke, 2002; Sippel, 2008; Sippel et al., 2009). Changes in the tectonic setting or continued tectonic evolution are assumed to reactivate faults according to the new stress state, and thus with a different slip direction. The calculation of paleostress stratigraphy involves separation of heterogeneous fault slip events on a single fault, and combining this separated data with faults that only recorded a single slip event/direction in order to build internally consistent and homogenous datasets. These are assumed to have formed due to the different tectonic events, and allow determining the different paleostress states through time.

Faults generally have several slip planes (for example, but not exclusively: Van der Zee, 2001; Agosta and Aydin, 2006), which can have such a small spacing, that the kinematic indicators can become overprinted, similar to Fig. 1 in the Introduction. This figure however provides no means to (relatively) date these, as one phase of slickenside formation does not affect (erode, damage or reorientate) the

other phase. Since it is not possible to determine which slip plane was active the latest from this picture, cross-cutting slickensides like these are not suited for relative dating of the events.

Furthermore, sometimes curved slickenside fibers are observed on a single fault plane (Fig. 2, and Twiss and Gefell, 1990), showing that slip on faults is not as simple, or linear as is often assumed, but is complicated by for example rigid body rotation (Twiss and Gefell, 1990). Furthermore, detailed field observations and numerical modeling have shown that in pure dip-slip normal faults, slip directions rotate towards the middle of the fault when moving away from the centre of the fault (Roberts, 1996; Morewood and Roberts, 2000; Cowie and Roberts, 2001; Papanikolaou and Roberts, 2007; Maniatis and Hampel, 2008). Movement indicators can be rotated away from the average slip on faults by up to 40° on a 40 km long normal fault (Maniatis and Hampel, 2008). This means that the location of the measurement of a movement indicator along strike (but also vertically) of a fault controls the exact orientation of the movement indicator. In seismic studies this effect can be controlled since one can see the entire fault, but in the field one hardly ever knows ones exact location relative to the fault centre.

There is an additional complication in the way faults rupture. Slip on faults generally is not the result of a single event, but the combination of multiple seismic events on sections of the fault (I. Papanikolaou, personal communication 2009), and faults often consist of multiple segments (for example: Cartwright et al., 1995; Lohr et al., 2008). Individual seismic slip events on a larger fault can be assumed to have the same convergent slip profile as the fault as a whole. Slickensides are observed on co-seismic

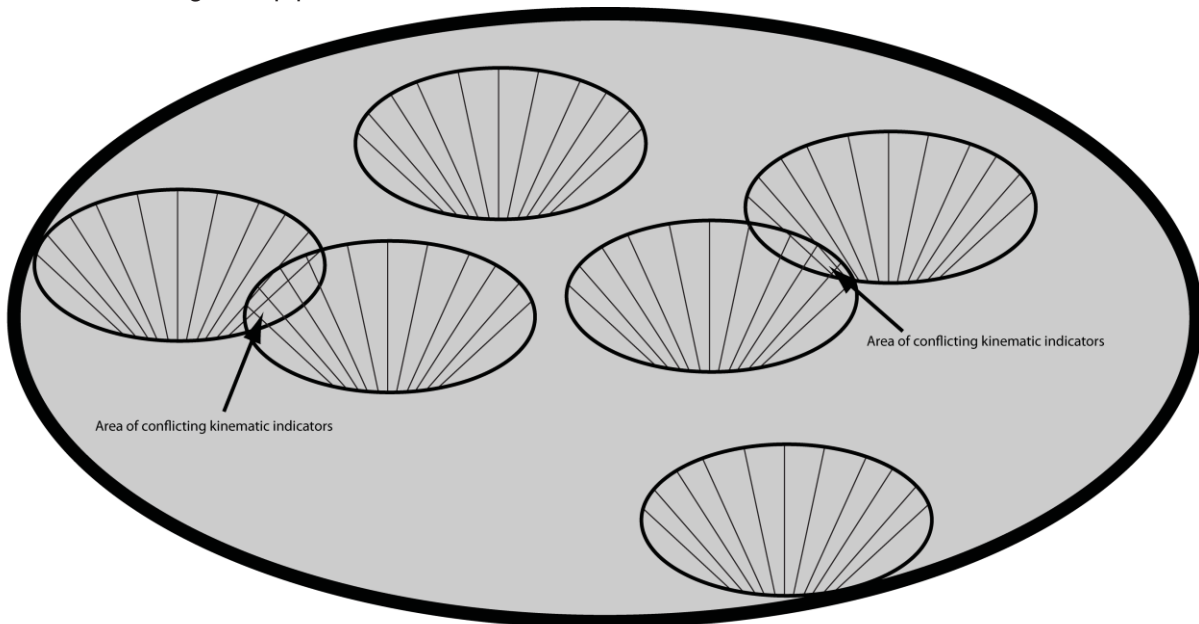


Fig. 3: Sketch of an idealized normal fault, with 6 “seismic slip events” drawn randomly on it. The lines inside the seismic events represent a simplified slip pattern, and the lines are parallel to the slip direction. All seismic events are formed during the same tectonic phase, but areas where the seismic events overlap shows overprinted, conflicting kinematic indicators

surface ruptures, showing that they can form due to a single event (Lin et al., 2001; Lin et al., in press). This means that the subsequent occurrence of seismic events on different sections of a single fault under the same stress conditions can result in overprinted, conflicting kinematic indicators of different

orientations where these sections overlap (Fig. 3). Also in segmented faults, conflicting kinematic indicators are to be expected, as the fault segment boundaries can be expected to exhibit strongly diverging slip directions (Maniatis and Hampel, 2008).

Slip directions deduced from the geometrical determination of slip or by fault plane analysis on the basis of fault plane undulations represent the cumulative slip on the fault plane. In fact the fault plane undulations, such as those described in Chapter 2 and for example Sagy et al (2007) and Lee and Bruhn (1996), are formed over longer time periods and multiple slip events. Also, the 3D seismic data allow the centre of the fault (the area of “un-affected slickenlines”) and any fault segments (Lohr et al., 2008) to be identified. As a result, these methods might be more applicable to determine slip directions and stress tensors from fault measurements than kinematic indicators measured in the field.

The integration of salt structure knowledge

Many papers on salt deformation that focus on large scale processes, such as salt diapir initiation and sedimentary basin development, show salt as a rather homogenous body (e.g.: Hecht et al., 2003; Scheck et al., 2003; TNO-NITG, 2004; Mazur et al., 2005; Maystrenko et al., 2006). Observations in mines and well data on the other hand show extremely complex structures forming in deforming salt (Ahlborn, 1953; Ahlborn and Richter-Bernburg, 1953; Dietz, 1953; Herrmann and Richter-Bernburg, 1953; Martini, 1953; Richter-Bernburg, 1953; Roth, 1953; Wagner, 1953; Siemeister, 1969; Hofrichter, 1974; Richter-Bernburg, 1980; Jackson, 1985; Richter-Bernburg, 1987; Bornemann, 1991; Smith, 1996; Behlau and Mingerzahn, 2001; Schlöder et al., 2008). One of the most exciting conclusions of Chapter 3 is that early sedimentary/diagenetic structures could (co-)control the position of salts structures, while previously this control was attributed to extra-salt influences, such as basement faults. The understanding of these feedbacks will only be completed when the different views of salt structures are integrated.

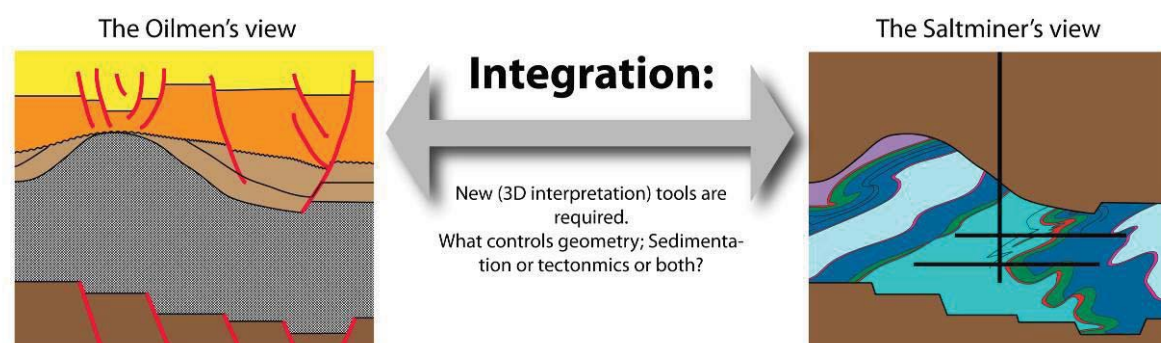


Fig. 4: While in the oil industry salt is often treated as rather homogenous, but extensive knowledge of the over-and underburden structure is available, the salt miner often has an unprecedented knowledge of the complex structures inside deforming salt.

Conclusions

Given a sufficiently detailed dataset, the calculation of paleostress-stratigraphy from 3D reflection seismic data is possible. The resultant stress tensors show good correspondence with tensors calculated using the “classic”, field based paleostress calculation methods.

Faults from the Upper Cretaceous faults show in 3D reflection seismic features which are very similar to the slip parallel fault plane undulations observed in LiDAR, laboratory and field data.

Although significantly more difficult to observe and interpret, the geometrical and fault plane analysis methods of fault slip determination are less sensitive to the convergent slip patterns and conflicting slip indicators as field observations.

When artificial random measurement errors are introduced in fault slip data, the Direct Stress Inversion can potentially produce two different stress tensors from what is essentially the same dataset.

The brittle inclusion of the Zechstein evaporite deposits shows evidence of a very complex structural and depositional history, with compressional and extensional structures. Constrictional salt flow is most likely responsible for the complex deformation pattern.

It seems that depositional and diagenetic structures formed early in the history of salt giants can play a significant role in salt structure development. Only the full integration of knowledge from seismic interpretation and observations from salt mines will allow these feedbacks to be understood.

Outlook: Is seismic paleostress determination worth the effort?

"By understanding many things, I have accomplished nothing."

- *Hugo de Groot*

The original aim of this study was to establish the paleostress stratigraphy (up to six time steps per location) for a number (up to 12) of basins. This way, a number of paleostress maps for large parts of the Dutch subsurface were to be constructed. This aim was however not fulfilled, as the work did involve considerably more seismic interpretation as originally anticipated. The construction of such maps however is still possible.

More work is required to better quantify the fault undulations described in this work, for example also in thrust or strike-slip faults. We note that a seismic dataset of exceptional “crispness” is required and a sufficient amount of picks is required for the correct representation of these undulations. We however have shown that these undulations are most likely not the result of the interpretation direction or the interpolation, but to date these structures were only observed in (near) dip-slip normal faults. A possible geophysical effect or geophysical processing has not been completely excluded. Nevertheless, the fault plane analysis presented in Chapter 1 and Chapter 2 describes a fault plane morphology which is very similar to observations using LiDAR and laboratory measurements, in that the fault plane seems to be undulated on all scales, and that these undulations are self-similar. There is no reason to doubt that the calculation of the roughness scaling exponent of the 3D seismic surfaces would not fit with that of LiDAR and laboratory measurements. This certainly is a very interesting avenue of research for a future project

Although it does not produce a paleostress stratigraphy as described in Chapter 1, the workflow described in Chapter 2 has the potential to constrain the Upper Cretaceous stress field over large areas relatively quickly. A similar interpretation can be performed in a number of surveys in the Central European Basin. In fact, similar workflows can also be used to establish the paleostress in other relatively brittle lithologies, using 3D reflection seismic data in any setting.

The methods described in the introduction, that is, connecting objects on two sides of the fault surface is a potentially very potent method to reconstructing slip direction. However, it only works in areas which have for example faulted channels. For this, a data set such as that described by Back et al. (2006) would be very interesting, as it contains channels that are cut by faults.

In Chapter 3, for the first time, the complex 3D strain patterns in the ductile Zechstein evaporites is hinted on, using a 3D seismic reflection interpretation of the brittle Z3 stringer. However, based on a quick review of other seismic datasets in the Central European Basin, it was found that the two datasets used in this study are relatively complicated. In the offshore study area, the NE-SW salt wall dominates the study area, where deformation is further complicated by the inversed basement blocks. In the Groningen area, the salt structures are less pronounced, but the deformation seems to be influenced considerably by the network of thicker zones, which result in a sedimentary and/or diagenetic network of stronger and weaker zones in the brittle layer. Also the geophysical properties of the stringer are not fully understood yet, so what the reflection of a steeply dipping stringer looks like is still not known. Nevertheless, this is a very interesting topic which should be pursued further.

References

- ◇ Agosta, F., Aydin, A., 2006. Architecture and deformation mechanism of a basin-bounding normal fault in Mesozoic platform carbonates, central Italy. *Journal of Structural Geology* 28, 1445-1467.
- ◇ Ahlborn, O., 1953. Die Flöze "Thüringen" und "Hessen" der Werraserie und ihre wechselseitigen Beziehungen. *Zeitschrift der Deutschen Geologischen Gesellschaft* 105(IV), 655-673.
- ◇ Ahlborn, O., Richter-Bernburg, G., 1953. Exkursion zum Salzstock von Benthe (Hannover), mit Befahrung der Kaliwerke Ronnenberg und Hansa. *Zeitschrift der Deutschen Geologischen Gesellschaft* 105(IV), 855-865.
- ◇ Back, S., Höcker, C., Brundiers, M. B., Kukla, P. A., 2006. Three-dimensional-seismic coherency signature of Niger Delta growth faults: integrating sedimentology and tectonics. *Basin Research* 18, 323-337.
- ◇ Behlau, J., Mingerzahn, G., 2001. Geological and tectonic investigations in the former Morsleben salt mine (Germany) as a basis for the safety assessment of a radioactive waste repository. *Engineering Geology* 61, 83-97.
- ◇ Bornemann, O., 1991. Zur Geologie des Salzstocks Gorleben nach den Bohrergebnissen. *BfS-Schriften* 4, 1-67.
- ◇ Bussolotto, M., Benedicto, A., Invernizzi, C., Micarelli, L., Plagnes, V., Deiana, G., 2007. Deformation features within an active normal fault zone in carbonate rocks: The Gubbio fault (Central Apennines, Italy). *Journal of structural Geology* 29-(12), 2017-2037.

- ◇ Candela, T., Renard, F., Bouchon, M., Marsan, D., Schmittbuhl, J., Voisin, C., in press. Characterization of Fault Roughness at Various Scales: Implications of Three-Dimensional High Resolution Topography Measurements. HAL: hal-00326981, version 1, available online at: <http://hal.archives-ouvertes.fr/hal-00326981/en/>.
- ◇ Cartwright, J. A., Trudgill, B. D., Moore, J. M., 1995. Fault growth by segment linkage: an explanation for scatter in maximum displacement and trace length data from the Canyonlands Grabens of SE Utah. *Journal of Structural Geology* 9, 1319-1326.
- ◇ Cowie, P. A., Roberts, G. P., 2001. Constraining slip rates and spacings for active normal faults. *Journal of Structural Geology* 23, 1901-1915.
- ◇ Cox, T., Seitz, K., 2007. Ant Tracking Seismic Volumes for Automated Fault Interpretation. CSPG CSEG Convention, Calgary, Alberta, Canada.
- ◇ Dietz, C., 1953. Exkursion zu den Tagesaufschlüssen im Bereich des Sarstedt-Lehter Salzstockes. *Zeitschrift der Deutschen Geologischen Gesellschaft* 105(IV), 872-875.
- ◇ Hecht, C. A., Lempp, C., Scheck, M., 2003. Geomechanical model for the post-Variscan evolution of the Permocarboneous–Mesozoic basins in Northeast Germany. *Tectonophysics* 373, 125-139.
- ◇ Herrmann, A., Richter-Bernburg, G., 1953. Frühdiagenetische Störungen der Schichtung und Lagerung im Werra-Anhydrit (Zechstein 1) am Südwestharz. *Zeitschrift der Deutschen Geologischen Gesellschaft* 105(IV), 689-702.
- ◇ Hesthammer, J., Henden, J. O., 2000. Closing the gap between theory and practice in seismic interpretation of small-scale faults. *Petroleum Geoscience* 6, 107-111.
- ◇ Hofrichter, E., 1974. Speicherkavernen im Salzstoecken Nordwestdeutschlands -Geologische Probleme, Bemerkungen zur selektiven Aufloessung von Kalisalzen. *Erzmetall* 65(5), 219-226.
- ◇ Jackson, M. P. A., 1985. Natural Strain in Diapiric and Glacial Rock Salt, with Emphasis on Oakwood Dome, East Texas, Bureau of Economic Geology/The University of Texas at Austin/Texas.
- ◇ Kleinspehn, K. L., Pershing, J., Teyssier, C., 1989. Paleostress stratigraphy: A new technique for analyzing tectonic control on sedimentary-basin subsidence. *Geology* 17, 253-256.
- ◇ Koestler, A. G., Ehrmann, W. U., 1991. Description of brittle extensional features in chalk on the crest of a salt ridge (NW Germany). In: Roberts, A. M. & Yielding, G. (Eds.), *The Geometry of Normal Faults*. Geological society Special Publication 56, 113-123.
- ◇ Lee, J.-J., Bruhn, R. L., 1996. Structural anisotropy of normal faults. *Journal of Structural Geology* 18(8), 1043-1059.
- ◇ Lin, A., Ouchi, T., Chen, A., Maruyama, T., 2001. Co-seismic displacements, folding and shortening structures along the Chelungpu surface rupture zone occurred during the 1999 Chi-Chi (Taiwan) earthquake. *Tectonophysics* 330(3-4), 225.
- ◇ Lin, A., Ren, Z., Jia, D., Wu, X., in press. Co-seismic thrusting rupture and slip distribution produced by the 2008 Mw 7.9 Wenchuan earthquake, China. *Tectonophysics* In Press, Corrected Proof.
- ◇ Lohr, T., Krawczyk, C. M., Oncken, O., Tanner, D. C., 2008. Evolution of a fault surface from 3D attribute analysis and displacement measurements. *Journal of Structural Geology* 30(6), 690-700.

- ◇ Maniatis, G., Hampel, A., 2008. Along-strike variations of the slip direction on normal faults: Insights from three-dimensional finite-element models. *Journal of Structural Geology* 30(1), 21.
- ◇ Martini, H. J., 1953. Salzsättel und Deckgebirge. *Zeitschrift der Deutschen Geologischen Gesellschaft* 105(IV), 823-836.
- ◇ Maystrenko, Y., Bayer, U., Scheck-Wenderoth, M., 2006. 3D reconstruction of salt movements within the deepest post-Permian structure of the Central European Basin System – the Glueckstadt Graben. *Netherlands Journal of Geosciences - Geologie en Mijnbouw* 85(3), 181 - 196.
- ◇ Mazur, S., Scheck-Wenderoth, M., Krzywiec, P., 2005. Different modes of the Late Cretaceous–Early Tertiary inversion in the North German and Polish basins. *International Journal of Earth Sciences (Geologische Rundschau)* 94, 782–798.
- ◇ Morewood, N. C., Roberts, G. P., 2000. The geometry, kinematics and rates of deformation within an en échelon normal fault segment boundary, central Italy. *Journal of Structural Geology* 22, 1027-1047.
- ◇ Papanikolaou, I. D., Roberts, G. P., 2007. Geometry, kinematics and deformation rates along the active normal fault system in the southern Apennines: Implications for fault growth. *Journal of Structural Geology* 29(1), 166.
- ◇ Power, W. L., Durham, W. B., 1997. Topography of Natural and Artificial Fractures in Granitic Rocks: Implications for Studies of Rock. *International Journal of Rock Mechanics and Mining Sciences* 34(6), 979-989.
- ◇ Power, W. L., Tullis, T. E., 1991. Euclidean and Fractal Models for the Description of Rock Surface Roughness. *Journal of Geophysical Research* 96(B1), 415-424.
- ◇ Power, W. L., Tullis, T. E., Weeks, J. D., 1988. Roughness and Wear During Brittle Faulting. *Journal of Geophysical Research* 93(B12), 15268-15278.
- ◇ Renard, F., Voisin, C., Marsan, D., Schmittbuhl, J., 2006. High resolution 3D laser scanner measurements of a strike-slip fault quantify its morphological anisotropy at all scales. *Geophysical Research Letters* 33, L04305.
- ◇ Richter-Bernburg, G., 1953. Über salinare Sedimentation. *Zeitschrift der Deutschen Geologischen Gesellschaft* 105(IV), 593-645.
- ◇ Richter-Bernburg, G., 1980. Salt Tectonics, Interior structures of Salt Bodies. *Bull. Cent. Rech. Explor.-Prod. Elf-Aquitaine* 4(1), 373-393.
- ◇ Richter-Bernburg, G., 1987. Deformation within salt bodies. In: Lerche, I. & O'Brien, J. J. (Eds.), *Dynamical Geology of Salt and Related Structures*. Academic Press, Inc., 39-75.
- ◇ Roberts, G. P., 1996. Variation in fault-slip directions along active and segmented normal fault. *Journal of Structural Geology* 18(6), 835-845.
- ◇ Roth, H., 1953. Ausbildung und Lagerungsformedn des Kalifözes "Hessen" im Fuldagebiet. *Zeitschrift der Deutschen Geologischen Gesellschaft* 105, 674-684.
- ◇ Sagy, A., Brodsky, E. E., Axen, G. J., 2007. Evolution of fault-surface roughness with slip. *Geology* 35(3), 283-286.
- ◇ Scheck, M., Bayer, U., Lewerenz, B., 2003. Salt redistribution during extension and inversion inferred from 3D backstripping. *Tectonophysics* 373, 55-73.

- ◇ Schlöder, Z., Urai, J. L., Nollet, S., Hilgers, C., 2008. Solution-precipitation creep and fluid flow in halite: a case study of Zechstein (Z1) rocksalt from Neuhof salt mine (Germany). *International Journal of Earth Sciences* 97(5), 1045-1056.
- ◇ Siemeister, G., 1969. Primärparagenese und Metamorphose des Ronnenberglagers nach Untersuchungen im Grubenfeld Salzdetfurth. Bundesanstalt für Bodenforschung und den Geologischen Landesämtern der Bundesrepublik Deutschland, Hannover, 62, pp. 122.
- ◇ Sippel, J., 2008. The Paleostress History of the Central European Basin System. Dr. rer. nat. thesis, Freien Universität.
- ◇ Sippel, J., Scheck-Wenderoth, M., Reicherter, K., Mazur, S., 2009. Paleostress states at the south-western margin of the Central European Basin System - Application of fault-slip analysis to unravel a polyphase deformation pattern. *Tectonophysics - Progress in understanding sedimentary basins* 470(1-2), 129-146.
- ◇ Smith, D. B., 1996. Deformation in the Late Permian Boulby Halite (EZ3Na) in Teesside, NE England. *Geological Society Special Publications* 100, 77-88.
- ◇ Storti, F., Billi, A., Salvini, F., 2003. Particle size distributions in natural carbonate fault rocks: insights for non-self-similar cataclasis. *Earth and Planetary Science Letters* 206, 173-186.
- ◇ TNO-NITG. 2004. Geological Atlas of the Subsurface of the Netherlands - onshore. TNO-NITG, Utrecht, pp. 103.
- ◇ Twiss, R. J., Gefell, M. J., 1990. Curved slickenfibers: a new brittle shear sense indicator with application to a sheared serpentinite. *Journal of Structural Geology* 12(4), 471.
- ◇ Van der Zee, W., 2001. Dynamics of fault gouge development in layered sand-clay sequences. Shaker Verlag, Aachen, PhD thesis
- ◇ Van der Zee, W., Urai, J., 2005. Processes of normal fault evolution in a siliciclastic sequence: a case study from Miri, Sarawak, Malaysia. *Journal of Structural Geology* 27(12), 2281-2300.
- ◇ Van der Zee, W., Urai, J., Richard, P. D., 2003. Lateral clay injection into normal faults. *Geo-Arabia* 8(3), 501-522.
- ◇ Vandycke, S., 2002. Paleostress records in Cretaceous formations in NW Europe: extensional and strike-slip events in relationships with Cretaceous-Tertiary inversion tectonics. *Tectonophysics* 357, 119-136.
- ◇ Wagner, W., 1953. Die tertiären Salzlagerstätten im Oberrheintal-Graben. *Zeitschrift der Deutschen Geologischen Gesellschaft* 105(IV), 705-728.

Appendix 1: Excel applets

"Don't worry about the future; or worry, but know that worrying is as effective as trying to solve an algebra equation by chewing bubblegum."

- *Baz Luhrmann - Everybody's Free (To Wear Sunscreen)*

Summary

Two Excel applets were written for angle calculation in 3D and the plotting of stress field and faults in Schmidt's and Wulfs nets as well as the effects of these stress fields on the planes with two different material properties. Modifications of these applets were used when azimuth dip data needed to be converted to strike/dip, rake into plunge and pitch into dip (or vice versa) for input in the different paleostress programs that were tested (see next appendices). The original applets can be found on www.ged.rwth-aachen.de.

Similar applets and/or programs have been written numerous times. However here we use Excel to program this, as Excel is a relatively widely-used program. These applets can thus be understood and adopted relatively easy. Since Excel is however an essentially 2D program (at least, regarding the production of figures), several tricks are needed to create stereographic projections. Also the calculation of eigenvectors in Excel proved to be a rather complicated venture. In the Excel workbook *Stereogram_v2.2*, the user is allowed to calculate all the angles between two different planes and two different lines, as well as the intersection line between two planes. The workbook *StressTensor_v2.6* is written to define a stress tensor and up to 18 different planes. The applet then calculates the total, normal and shear stress on the different planes. To calculate whether material would fail on these planes, two different material properties can be provided (e.g. intact rock and fault rock). For the stress tensor the size and orientation of the principle stresses (and their ratio R) are established. All data is combined in a Mohr diagram.

A detailed description of the mathematical rationale of these applets will be given below. The implementation of these calculations in Excel is not described, only the general mathematics. No references are given in the text, but most mathematical background has been taken from MathWorld.com, while information to the stress on a plane and the projection types was taken from Meschede (1994).

Acknowledgements

Sven Lentzen of the Institut für Allgemeine Mechanik, RWTH-Aachen is thanked for his help in solving the eigenvector problem.

References

◇ [Mathworld.com http://mathworld.wolfram.com/](http://mathworld.wolfram.com/)

Meschede, M., Ratschbacher, L., Frisch, W., Herrman, U. R., 1994. The relation between plate convergence and paleostress fields: fault-slip analyses in southern Mexico and along the Motagua-

Polochic fault system in Guatemala. TSK 5, Göttingen, 6.4.1994, Göttinger Arbeiten Geologie und Paläontologie, 252-255.

„Stereogram_v2.2.xls“

Aim of the applet

The aim of this applet is to plot planes and lineation in a lower hemisphere Schmidt Net using the Lambert (Equal area) projection, and a Wulffs Net (Equal angle). Also, it can be used to calculate the angles between two planes, between a plane and a lineation, between two lineations and between a lineation and a plane intersection line.

Input

The applet can plot two planes and two lineations. The input consists therefore of the dip direction and dip of planes 1 and 2, and the azimuth and the plunge of lineation 1 and 2.

Output

The output consists of the projection of the lineation 1 and 2 and both the pole and the great circle of planes 1 and 2 on a lower hemisphere Schmidt Net as well as in a lower hemisphere Wulffs Net. The output further exists of the azimuth ($^{\circ}$) and plunge ($^{\circ}$) of the intersection of planes 1 and 2, as well as the angles between lineations, the angles between the planes and the lineations, the angle between the planes, and the angles between the lineations and the plane intersection line. All these angles are in degrees and are the smallest angles. This means that angles between lineations never exceed 180° and angles between planes and lineations and planes never exceed 90° .

For example, the angle between a plane with orientation 000/10 and a lineation 180/10 is 20° and not 160° (see figure 1).

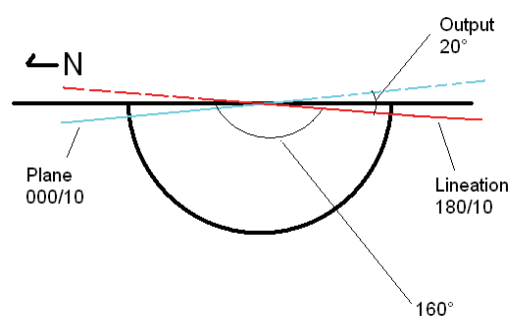


Figure 1: The applet output consists of the smallest angle between two objects

Coordinate systems

Different coordinate systems are used for the input, calculation and projection of the objects and angles in this applet. Input data in the polar coordinate system, with azimuth and plunge as the

components. The azimuth is the angle in degrees from north, which in this applet is defined as straight up in the diagrams. The plunge is the deviation in degrees from the horizontal. Note that when planes are concerned, the azimuth describes the dip direction and the plunge equals the dip of the plane.

For the calculations, the right-handed 3D Cartesian vector coordinate system is used, where the following rules apply; the vectors have three elements, (x,y,z), the Cartesian axes are orthogonal and the x direction is up (north), y is to the right (east) and z is down.

For the projection of the objects, a different, 2D Cartesian coordinate system is used, where x is to the right (east) and y is up (north).

Note to Excel

In Excel all angles are calculated as radian, while the output of the applet and in this script the angle will be described in degrees. Radians can be converted into degrees by dividing the radian value by ($\pi/180$).

Turning lineation and planes orientations into vectors

Being a line, a lineation can be transformed into a vector relatively easy. The vector is calculated using the formulas:

$$x = \cos \varphi * \cos \alpha$$

$$y = \cos \varphi * \sin \alpha$$

$$z = \sin \varphi$$

Where α is the azimuth in degrees, and φ is the plunge, in degrees.

In this applet, planes are initially characterized by their pole (a line which is perpendicular to the plane). Calculating the pole of the plane is done by:

$$\text{Pole azimuth} = \text{Plane azimuth} + 180$$

$$\text{Pole dip} = 90 - \text{Plane dip}$$

This line can then be turned into a vector using formulas (1.1).

Note that since all vectors are recalculated into unit vectors (vectors with magnitude 1) before they are used further in this applet.

Calculating angles between lines and planes

The scalar product of two vectors (A and B) is a number and is defined as

$$A \cdot B = |A| |B| \cos \theta$$

and as

$$A \cdot B = A_x B_x + A_y B_y + A_z B_z,$$

where $|A|$ is the length of vector, which equals:

$$A (= \sqrt{A_x^2 + A_y^2 + A_z^2}),$$

$|B|$ similarly is the length of vector B, and θ is the angle between vectors A and B. Combining these formulas produces:

$$\theta = \cos^{-1} \left(\frac{A \bullet B}{|A||B|} \right)$$

$$\theta = \cos^{-1} \left(\frac{A_x B_x + A_y B_y + A_z B_z}{\left(\sqrt{A_x^2 + A_y^2 + A_z^2} \right) \left(\sqrt{B_x^2 + B_y^2 + B_z^2} \right)} \right)$$

Using this formula allows the calculation of the angle between lines. For the calculation of the angle between two planes, the same formula can be used, but the poles to the plane needs to be used as input vector. For the calculation of the angle between a line and a plane, the pole vector needs to be used as input for the plane. Since the pole vector by definition has an angle of 90° to the plane, the angle between a line and a plane (θ') is defined as $\theta' = 90 - \theta$.

Calculating the intersection between two planes

The intersection line between two planes is an important object as it can be interpreted as a fold axis, if the planes represent the two sides of the fold. To calculate the plane intersection line, the vector product is used. The vector product is defined as:

$$A \times B = (iA_x + jA_y + kA_z) \times (iB_x + jB_y + kB_z)$$

$$A \times B = i(A_y B_z - A_z B_y) + j(A_z B_x - A_x B_z) + k(A_x B_y - A_y B_x)$$

Where i, j and k are unit vectors in the direction x, y and z respectively. These define the vector v, which is a vector perpendicular to both vector A and B, and therefore parallel to the intersection of these two planes.

To calculate the azimuth and plunge of the plane intersection line, the formulas are:

$$\alpha = \tan^{-1} \left(\frac{\hat{v}_y}{\hat{v}_x} \right)$$

$$\phi = \tan^{-1} \left(\frac{\hat{v}_z}{\sqrt{(\hat{v}_x)^2 + (\hat{v}_y)^2}} \right)$$

Here v_x , v_y and v_z are the components of the vector v.

Calculating and plotting the great circle of a plane

The determination of the great circle of a plane consists of two steps (see figure 2). First, the strike component of the plane needs to be determined. Then this vector needs to be rotated around the pole of the plane, describing a semicircle. Excel is essentially a 2D program, but a great circle is a

projection of a 3D plane intersecting a 3D hemisphere. The strike component is a horizontal vector parallel to the strike of the plane (that is, dip direction $\pm 90^\circ$). Since this vector is horizontal, the z-value of this vector is 0. To determine the strike component, the vector product of the pole of the plane and the vertical vector ($= 0*i, 0*j, 1*k$) was determined. Since the vector product always returns a vector perpendicular to the input vectors, the resultant vector will be parallel to the strike. When this vector is

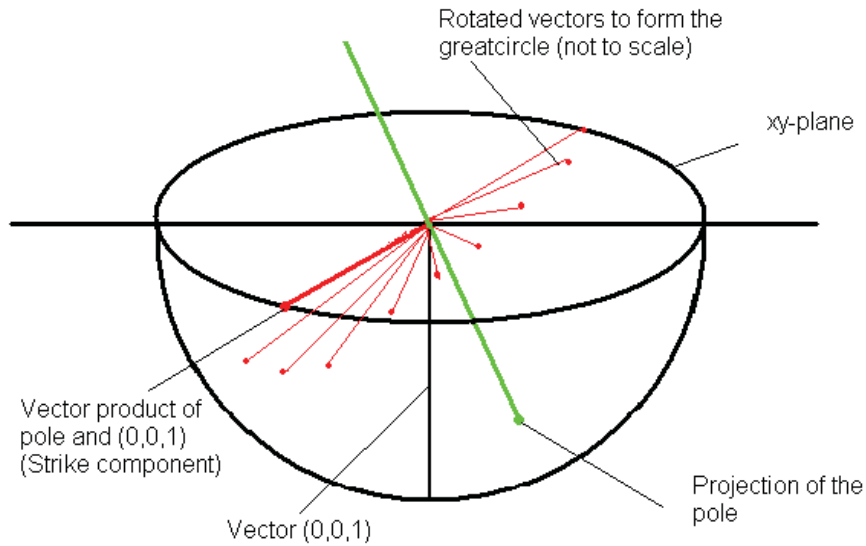


Figure 2: The construction of a great circle, see text for details.

normalized (when a unit vector with length = 1 is made of it), it represents the vector projection of the strike on a lower hemisphere projection with radius 1.

To create the great circle, this point is now rotated 180° around the pole to the plane in 3 degree increments. These 60 points are combined to form the great circle.

The strike vector is rotated using a rotation matrix (M). In 3D-space, M is a 3*3 matrix of the form:

$$M(\hat{\mathbf{v}}, \theta) = \begin{bmatrix} \cos \theta + (1 - \cos \theta) \hat{v}_x^2 & (1 - \cos \theta) \hat{v}_x \hat{v}_y - (\sin \theta) \hat{v}_z & (1 - \cos \theta) \hat{v}_x \hat{v}_z + (\sin \theta) \hat{v}_y \\ (1 - \cos \theta) \hat{v}_y \hat{v}_x + (\sin \theta) \hat{v}_z & \cos \theta + (1 - \cos \theta) \hat{v}_y^2 & (1 - \cos \theta) \hat{v}_y \hat{v}_z - (\sin \theta) \hat{v}_x \\ (1 - \cos \theta) \hat{v}_z \hat{v}_x - (\sin \theta) \hat{v}_y & (1 - \cos \theta) \hat{v}_z \hat{v}_y + (\sin \theta) \hat{v}_x & \cos \theta + (1 - \cos \theta) \hat{v}_z^2 \end{bmatrix}$$

Here θ is rotation angle, and v_x , v_y and v_z are the components of the vector \mathbf{v} about which the rotation needs to be performed (in this case, the pole vector of the plane). A new rotation matrix is required for each of the 60 points that define the great circle.

The formula to rotate a vector (for example the strike vector S) into its rotated equivalent (S') is:

$$S' = MS$$

Since this operation is simple rotation, the rotated vectors still have the magnitude 1, and therefore, in 3D define a semicircle.

Projection of the vectors

Because all the vectors in the great circle and the pole and lineation vectors are unit vectors, all together they describe a sphere with the diameter 1. Projection of these vectors on a horizontal plane (by simply plotting the x and y values of the vector in a xy-plane) is not what is wanted, as that represents neither the equal angle (Stereographic projection, Wulffs Net), or the equal area (Lambert Projection, Schmidt Net) projection (note the differences between the left and right panels of figure 5).

The principles of the equal area or Lambert projection are given in figure 3. Here point B represents the end point of a vector with unit length 1 as it intersects the hemisphere. The plane underneath the lower hemisphere represents the plane of the Lambert projection, and point X in this plane is the projection of point B on it. This is done in such a way that $AB = AX$. This means this is not a true projection, but rather a rotation of point B into point X. The distance AX is defined as:

$$AX = \sqrt{2R \sin\left(\frac{\pi - \varphi}{4} - \frac{\varphi}{2}\right)}$$

Here φ is the plunge and R is the radius of the projected sphere, in this case, $R = 1$

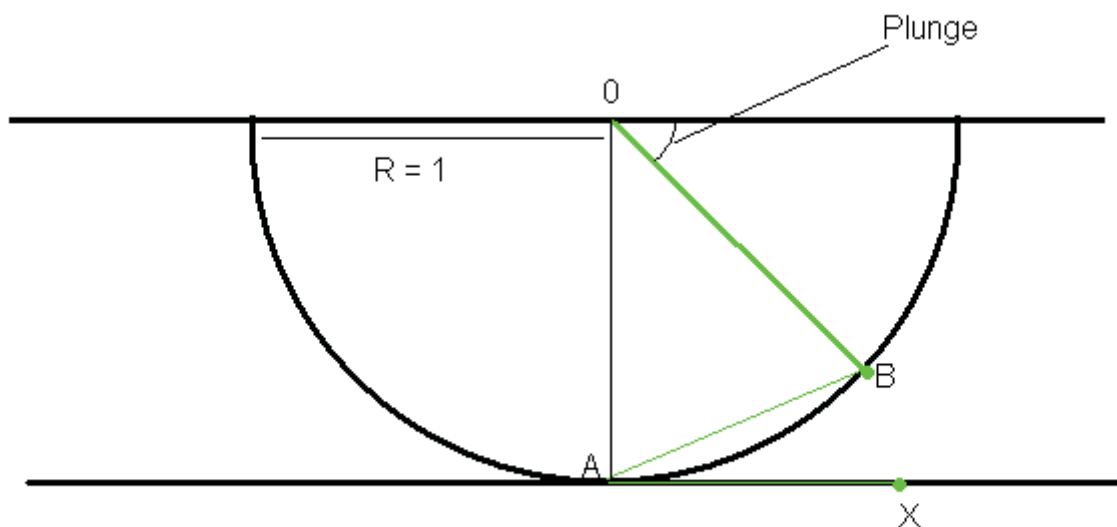


Figure 3: The principles of the Lambert projection, see text for details.

To project lineation and poles on the xy-plane, the azimuth and plunge of these objects are used in the formulas (note that the direction of x and y is different from those in the vector coordinate system):

$$x = \sin(\alpha) * \sqrt{2 \sin\left(\frac{\pi - \phi}{4} - \frac{\phi}{2}\right)}$$

$$y = \cos(\alpha) * \sqrt{2 \sin\left(\frac{\pi - \phi}{4} - \frac{\phi}{2}\right)}$$

Here α is the azimuth and ϕ is the plunge. These formulas are also used to plot the 60 points of the great circles and the intersection vector.

All data is also plotted in a Wulffs Net. The principles of the stereographic projection, on which the Wulffs Net is based, are given in figure 4.

Here A' is the projection of point A , and the distance OA' is defined as:

$$OA' = R \left(\tan \frac{90 - \phi}{2} \right)$$

R is the radius of the projection circle (1 in our case), and ϕ is the plunge.

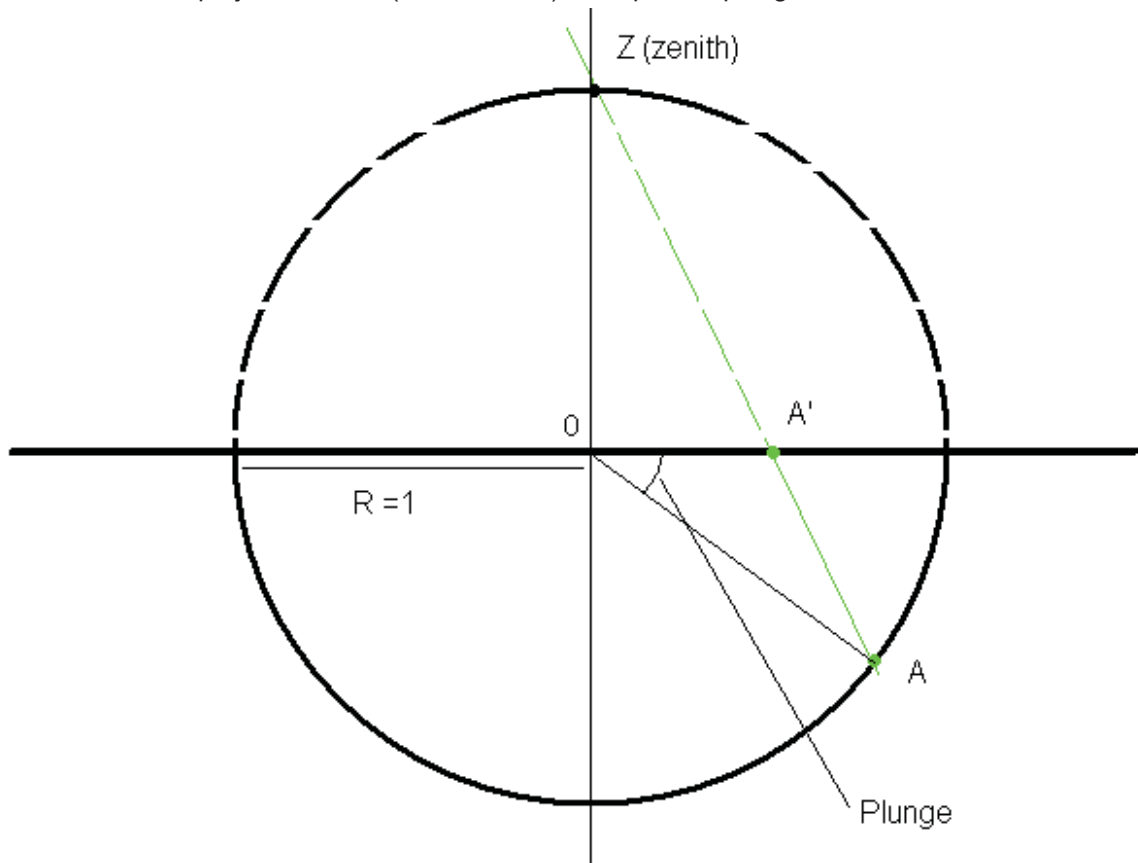


Figure 4: The principles of the stereographic projection.

To project lineation and poles on the xy -plane, the azimuth and plunge of these objects are used in the formulas (note that the direction of x and y is different in the vector coordinate system):

$$x = \sin(\alpha) * \left(\tan \frac{90 - \varphi}{2} \right)$$

$$y = \cos(\alpha) * \left(\tan \frac{90 - \varphi}{2} \right)$$

Where α is the azimuth and φ is the plunge. These formulas are also used to plot the points of the great circles and the intersection vector.

Note to projecting great circles in the applet:

If the vector S' has a negative x scalar, the calculation of the xy -projection-coordinates results in a great circle that does not enter into the negative y area of the Schmidt Net but projects an additional, conjugate great circle fragment (see figure 5, right panel). This results from the back calculation to azimuth and plunge, which is required before the projection coordinates can be plotted. The problem is solved by forcing Excel to adopt negative x and y projection coordinates, if the vector S' has a negative x -component.

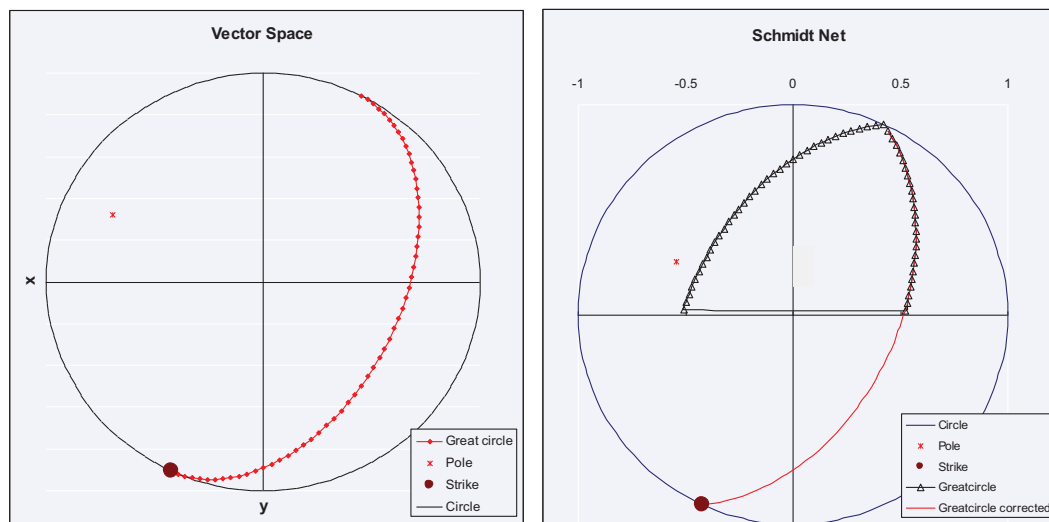


Figure 5: Panels from the Excel sheet showing the difference between vector projection (left) and Schmidt Net projection (red, right), as well as the result of a negative (black triangles) value for the vector x coordinate on the projection of the great circle.

„StressTensor_v2.4.xls“

Aim of the applet

The aim of this applet is to calculate the stress (the total, normal and shear stress) on 18 planes, given a plane and a stress tensor, as well as establishing the size and orientation of the principle stresses (and their ratio R) of the same stress tensor. It also calculates whether these planes would fail, given two sets of material properties (for example, intact rock and faults, to calculate the possibility of failure and when the plane is an old fault, reactivation). All data is combined in a Mohr diagram.

Input

The input of this applet consists of 18 planes (dip direction and dip angle), the six independent values of the symmetric stress tensor, and the properties of two materials.

Output

The output consists of the stress vector on the 18 planes, as well as the normal and shear stress components of this vector and the angles between the stress vector and the normal and shear components of this vector. Also the three principle stresses (σ_{1-3}) and their ratio (R) are given. The principle stresses and principle stress axis of the stress tensor are given. The applet also calculates whether the plane would fail and indicates this, both in text, as well as in a Schmidt Net. It further grid-searches the areas where failure occurs.

Since the principles of the coordinate systems, calculating angles between planes and lines and how to convert planes and lines into vectors are already discussed in the section on „Stereogram_v2.2.xls“, we will omit that here.

Stress on a plane

To calculate the stress on one of the 18 planes, the following tensor equation is used:

$$\sigma = Tn$$

Here σ is the stress vector on an arbitrary plane. This plane is defined by its pole vector; a unit vector normal to the plane, here called n . T is the stress tensor.

Note that these planes describe geometrical planes in an unfaulted sample, and therefore do not necessarily represent faults, joints or other discontinuities inside a volume.

The length of the vector σ ($|\sigma|$) is the scalar value of the stress on the plane and is defined as:

$$|\sigma| = \sqrt{x^2 + y^2 + z^2}$$

Where x , y and z are the x , y and z components of the vector.

The stress vector σ can be divided in two components, one parallel to the plane (the shear stress, τ), the other normal to the plane (the normal stress, v), see figure 1. Since v is parallel to n , and since also applies that: $\sigma = (\tau + v)$, we find that:

$$v = n\sigma$$

and

$$\tau = \sigma - n$$

$|v|$ and $|\tau|$ represent the length of these vectors and the scalar value of the normal and shear stress on the plane respectively.

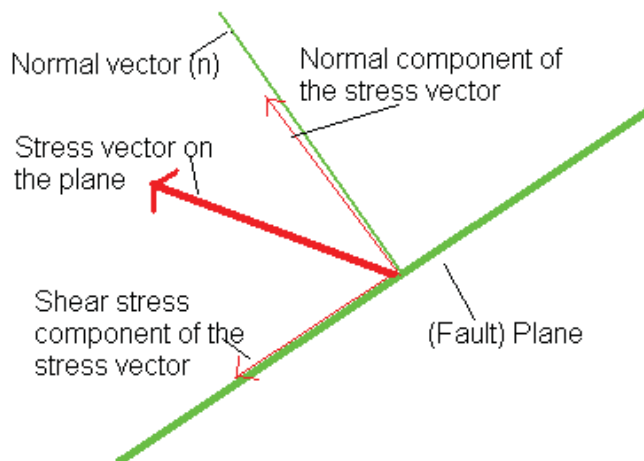


Figure 1: The components of a stress vector acting on a plane.

Calculating the eigenvalues of the stress tensor

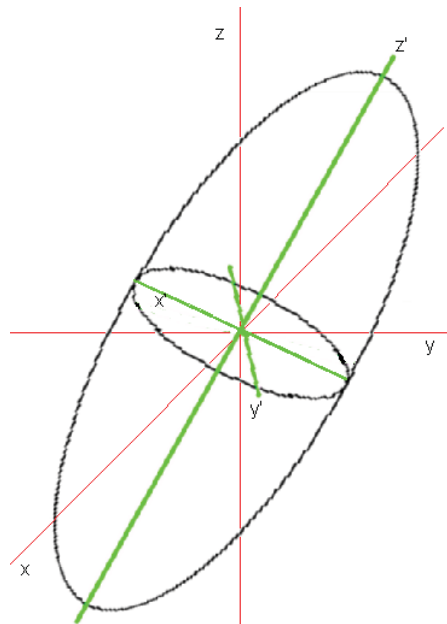


Figure 2: A stress ellipsoid with the initial (x, y, z) and transformed (x', y', z') coordinate systems.

A normal stress tensor is symmetrical and defines a so-called stress ellipsoid space. In the definition of any tensor there is the implicit reference to a coordinate system or axes-system. But this coordinate system may not necessarily be the most practical, as it does not cut the ellipsoid at its apexes.

This principle is illustrated in figure 2. The black ellipsoid is the stress ellipsoid defined by the stress tensor T , and the red coordinate system is the initial coordinate system. The green coordinate system cuts the stress ellipsoid where the radius is largest (on the z' -axis) and where the radius is smallest (in this case the ellipsoid is a prolate spheroid (cigar-shaped), so $x' = y'$). This coordinate system is called the transformed coordinate system.

The values on the axis of a coordinate system which cut the stress ellipsoid at the maximum, at the minimum and along an axis perpendicular to both these axes are called the principle stresses σ_{1-3} (where $\sigma_1 \geq \sigma_2 \geq \sigma_3$; and compressive vectors are positive), and the coordinate system is called the principal coordinate system (x' , y' and z').

The transformed stress tensor (T') defines the same ellipsoid as the original stress tensor T but using the transformed coordinate system. T' has non-zero values only along the diagonal, and these values are the principle stresses σ_{1-3} .

The principle stresses are equal to the eigenvalues of the stress tensor T . These eigenvalues are sometimes also called characteristic values or the roots of the tensor. The eigenvalues of stress tensor T are calculated by solving the equation.

$$\begin{aligned}
 & \mathbf{TX} = \mu\mathbf{X} \\
 & \begin{bmatrix} a & b & c \\ d & e & f \\ g & h & i \end{bmatrix} \begin{bmatrix} x \\ y \\ z \end{bmatrix} = \mu \begin{bmatrix} x \\ y \\ z \end{bmatrix} \\
 & \begin{bmatrix} a & b & c \\ d & e & f \\ g & h & i \end{bmatrix} \begin{bmatrix} x \\ y \\ z \end{bmatrix} - \begin{bmatrix} \mu x \\ \mu y \\ \mu z \end{bmatrix} = \begin{bmatrix} 0 \\ 0 \\ 0 \end{bmatrix} \\
 & \begin{vmatrix} a-\mu & b & c \\ d & e-\mu & f \\ g & h & i-\mu \end{vmatrix} = 0
 \end{aligned}$$

Here T is the stress tensor, X is a vector and μ is a constant (this equation describes a vector X which direction does not change when the deformation T is applied to it, but it's length changes with a factor μ). The last line in this equation shows that μ can be solved by solving $\det(T-\mu I)=0$ (I is the identity matrix, and $\det(T-\mu I)$ is the determinant of $(T-\mu I)$). Note that $a-i$ are the known components of T .

$\det(T-\mu I)=0$ is solved like:

$$\begin{vmatrix} a-\mu & b & c \\ d & e-\mu & f \\ g & h & i-\mu \end{vmatrix} = 0$$

$$a-\mu \begin{vmatrix} e-\mu & f \\ h & i-\mu \end{vmatrix} - d \begin{vmatrix} b & c \\ h & i-\mu \end{vmatrix} + g \begin{vmatrix} b & c \\ e-\mu & f \end{vmatrix} = 0$$

$$a-\mu((e-\mu)(i-\mu)-h*f) - d(b*(i-\mu) - h*c) + g(b*f - (e-\mu) * c) = 0$$

$$-\mu^3 + (i+a+e) \mu^2 + (-a*i-e*i-a*e+c*g+f*h+b*d) \mu + (a*e*i+b*f*g+c*d*h-c*g*e-f*h*a-b*d*i) = 0$$

$$\mu^3 - (i+a+e) \mu^2 - (-a*i-e*i-a*e+c*g+f*h+b*d) \mu - (a*e*i+b*f*g+c*d*h-c*g*e-f*h*a-b*d*i) = 0$$

$$\mu^3 + (a_2) \mu^2 + (a_1) \mu + (a_0) = 0$$

The last line in this equation can be solved using the cubic formula (similar to the quadratic or ABC-formula for solving quadratic equations). The three real solutions of the cubic formula equal the eigenvalues and are (from mathworld.wolfram.com/CubicFormula.html):

$$z_1 = 2\sqrt{-Q} \cos\left(\frac{\theta}{3}\right) - \frac{1}{3}a_2$$

$$z_2 = 2\sqrt{-Q} \cos\left(\frac{\theta+2\pi}{3}\right) - \frac{1}{3}a_2$$

$$z_3 = 2\sqrt{-Q} \cos\left(\frac{\theta+4\pi}{3}\right) - \frac{1}{3}a_2$$

where

$$\theta = \cos^{-1}\left(\frac{R}{\sqrt{-Q^3}}\right)$$

$$Q = \frac{3a_1 - a_2^2}{9}$$

$$R = \frac{9(a_2 a_1) - 27a_0 - 2a_2^3}{54}$$

There the largest value of z_1 , z_2 and z_3 is σ_1 and the smallest value of z_1 , z_2 and z_3 equals σ_3 . Of course the middle value then equals σ_2 .

The ratio R defines the relation between σ_1 , σ_2 and σ_3 is:

$$R = \frac{(\sigma_2 - \sigma_3)}{(\sigma_1 - \sigma_3)}$$

This ratio is often used in stress tensor calculation and stress tensor inversions to describe the shape of the principle stress tensor, because the absolute values of the tensor can not be calculated.

Calculating the eigenvectors of the stress tensor

The vectors defining the transformed coordinate system in the original coordinates can be found by solving the eigenvectors of the tensor T. For the different characteristic values (that is σ_1 , σ_2 and σ_3) the eigenvectors can be found by solving the following sets of equations:

$$\begin{array}{rcll} & (a-\sigma_1) x_1 & +by_1 & +cz_1 & =0 \\ \text{for } \sigma_1: & dx_1 & + (e-\sigma_1) y_1 & +fz_1 & =0 \\ & gx_1 & +hy_1 & + (i-\sigma_1) z_1 & =0 \end{array}$$

$$\begin{array}{rcll} & (a-\sigma_2) x_2 & +by_2 & +cz_2 & =0 \\ \text{for } \sigma_2: & dx_2 & + (e-\sigma_2) y_2 & +fz_2 & =0 \\ & gx_2 & +hy_2 & + (i-\sigma_2) z_2 & =0 \end{array}$$

$$\begin{array}{rcll} & (a-\sigma_3) x_3 & +by_3 & +cz_3 & =0 \\ \text{for } \sigma_3: & dx_3 & + (e-\sigma_3) y_3 & +fz_3 & =0 \\ & gx_3 & +hy_3 & + (i-\sigma_3) z_3 & =0 \end{array}$$

Here x, y and z define the eigenvectors for the appropriate characteristic values. Solving these sets of equations in Excel is complicated. Normally one would assume one value of x_j , y_j or z_j ($j = 1, 2$ or 3) to be 1, and solve the set of equations to calculate the other two values. It is possible that the selected value is 0, rendering the calculation useless and the user will select another value to be 1. It is however possible to ascertain a priori whether x_j , y_j or z_j is 0, using the subdeterminants; if the subdeterminant of x_j , y_j or z_j is 0, then x_j , y_j or z_j is also 0. The definition of the subdeterminant of x_j , y_j and z_j for σ_i (i is 1, 2 or 3) is shown below:

$$\begin{aligned}
 \text{The subdeterminant of } x_{ij} &= \begin{vmatrix} \cancel{(a-\sigma_i)} & \cancel{b} & \cancel{c} \\ \cancel{d} & (e-\sigma_i) & f \\ \cancel{g} & h & (i-\sigma_i) \end{vmatrix} \\
 &= \begin{vmatrix} (e-\sigma_i) & f \\ h & (i-\sigma_i) \end{vmatrix} \\
 &= ((e-\sigma_i) * (i-\sigma_i)) - (h * f)
 \end{aligned}$$

$$\begin{aligned}
 \text{The subdeterminant of } y_{ij} &= \begin{vmatrix} (a-\sigma_i) & \cancel{b} & c \\ \cancel{d} & \cancel{(e-\sigma_i)} & \cancel{f} \\ g & \cancel{h} & (i-\sigma_i) \end{vmatrix} \\
 &= \begin{vmatrix} (a-\sigma_i) & c \\ g & (i-\sigma_i) \end{vmatrix} \\
 &= ((a-\sigma_i) * (i-\sigma_i)) - (g*c)
 \end{aligned}$$

$$\begin{aligned}
 \text{The subdeterminant of } z_{ij} &= \begin{vmatrix} (a-\sigma_i) & b & \cancel{c} \\ d & (e-\sigma_i) & \cancel{f} \\ \cancel{g} & \cancel{h} & \cancel{(i-\sigma_i)} \end{vmatrix} \\
 &= \begin{vmatrix} (a-\sigma_i) & b \\ d & (e-\sigma_i) \end{vmatrix} \\
 &= ((a-\sigma_i) * (e-\sigma_i)) - (d*b)
 \end{aligned}$$

Using these subdeterminants, it is possible to establish a priori whether one of the x_{ij} , y_{ij} and z_{ij} are zero, and thus the process of solving the system of equations can be adopted accordingly. When for example, it is shown that x_{ij} is 0, then the system is solved by assuming y_{ij} is 1 and z_{ij} is calculated using this knowledge. The choices to establish which of the values of x_{ij} , y_{ij} and z_{ij} to assume as 1 and which of the x_{ij} , y_{ij} and z_{ij} –values is 0 is handled in the Excel sheet by a complex succession of IF-THEN and TRUE/FALSE arguments. First the subdeterminants are calculated and then is established which are zero. Parallel to this, a total of five possible sets of equations per σ_1 -value are solved, in which all possible variations are calculated. These four sets represent the case when none of the subdeterminants is 0 and three possibilities when one subdeterminants is 0. These four sets are supplemented by the case when two sub determinants are 0, then of course the third value is (assumed to be) 1. Using the IF-THEN and TRUE/FALSE arguments it is then established which of the five possible cases applies in this case, and the appropriate set of equations is printed as outcome. When calculating the x_{ij} , y_{ij} and z_{ij} for σ_i , there are three possible outcomes: i) all nine subdeterminants have the value 0, ii) all six subdeterminants of two principle stresses have the values 0, and at least one of the three subdeterminants of the other principle stress has a non-zero value and iii) for all three principle stresses at least one of the three subdeterminants is not zero.

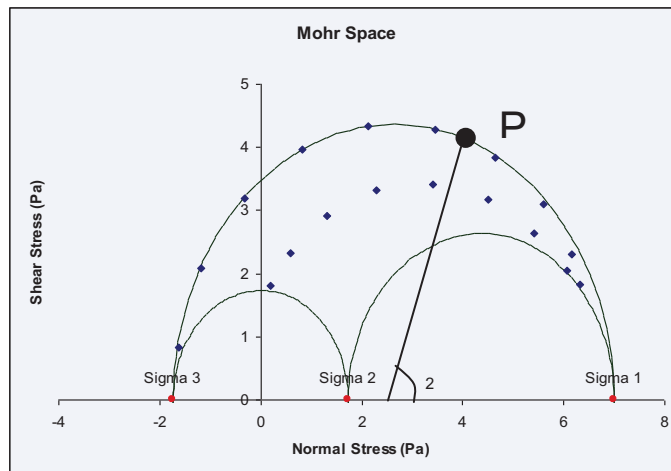


Figure 3: example Mohr diagram from StressTensor_v2.2.exl

A case where only one principle stress has all sub determinants zero is not possible in this applet. When all sub determinants are 0 (case i) this means that there is no principle stress axis; all possible vectors (an infinite amount) in the stress tensor define a perfect sphere and stress from all directions is the same. This stress state is called hydrostatic. It is defined by a stress tensor with non-zero, identical values only along the diagonal. Entering a stress tensor describing a hydrostatic stress state will not result in a successful calculation, as this applet is designed to calculate shear stresses, and a hydrostatic stress state is defined by its lack of shear stresses.

When all subdeterminants of two principle stresses are 0, and at least one of the sub determinants is non-zero (case ii) means that no direction of the principle vector of these two principle stresses have no fixed orientation. Together they describe a perfect circle in the stress ellipsoid, perpendicular to the orientation of the third principle value. In practice this means that the stress ellipsoid is a prolate ellipsoid, defining a uni-axial stress state. The principle values of the two undefined vectors are the same and a uni-axial matrix consist of no-zero values only occurring along the diagonal, and two of these values are identical. In case iii the stress tensor defines a triaxial state where all principle stresses can be established and there are three principle stresses with different values. The case with only one principle stress which three sub determinants are 0 is not possible, as this would imply that the other two vectors are defined. Since the three principle stress vectors are at angles of 90° relative to each other, knowing two axes will automatically result in knowing the orientation of the third vector.

Plotting all data in a Mohr-circle

The Mohr circle (named after Otto Mohr and first defined in 1882) is a powerful graphic tool to illustrate principle stresses and the normal/shear stress relations. The Mohr circle is plotted in a space defined by the shear stress (plotted along the y-axis) and the normal stress (along x-axis, see figure 3).

The principle stresses are plotted along the normal stress axis, because the principle stresses by definition do not have a shear stress component.

The circle connecting σ_1 and σ_3 represent the stresses on planes perpendicular to the $\sigma_1\sigma_3$ -plane, just as the circles between σ_1 and σ_2 and the circle between σ_2 and σ_3 represent the stresses on planes perpendicular to the $\sigma_1\sigma_2$ -plane and the $\sigma_2\sigma_3$ -plane respectively.

Remember from your basic Mohr circle knowledge that point P on the $\sigma_1\sigma_3$ circle represents the shear stress/normal stress relation of a plane at an angle of θ to the σ_1 -direction and that the line connecting point P and the normal stress axis is located at the average of σ_1 and σ_3 .

These circles were plotted by plotting a unit circle and then adding the appropriate components to change the diameter and the centre of the circle:

Plotting a circle with radius 1 and centred on the origin

$$x=\cos\theta \text{ and } y=\sin\theta.$$

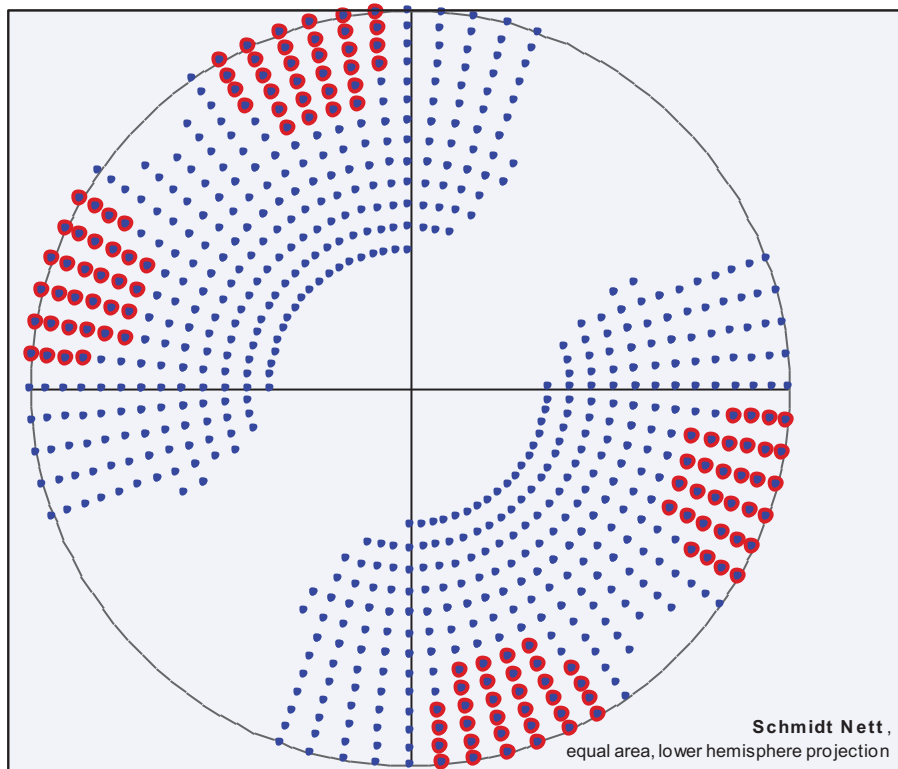
For Mohr circle between σ_1 and σ_3

$$x=\frac{\sigma_1-\sigma_3}{2}\cos\theta+\left(\frac{\sigma_1+\sigma_3}{2}\right) \text{ and } y=\frac{\sigma_1-\sigma_3}{2}\sin\theta$$

$$\left(\begin{array}{l} \frac{\sigma_1-\sigma_3}{2} = \text{the radius of the circle} \\ \frac{\sigma_1+\sigma_3}{2} = \text{the centre of the circle on the } \sigma_n \text{-axis} \end{array} \right)$$

Here θ is an angle used to plot the circle, between 0 and 360° (the number of increments defines the resolution of the circle).

The shear stress/ normal stress relations for the different planes can be plotted in the Mohr diagram as well. For all possible points applies that they can only plot on or inside the circle between σ_1 and σ_3 and on or outside the $\sigma_1\sigma_3$ - and $\sigma_2\sigma_3$ -circles. If a plane plots on for example on the $\sigma_1\sigma_2$ -circle this means that the pole of the plane lies within the plane defined by the $\sigma_1\sigma_2$ vectors (i.e. the pole is perpendicular to the σ_3 -vector). Ergo, planes that plot on the $\sigma_2\sigma_3$ -circle, have a pole perpendicular to the σ_1 -vector. Planes that plot between the circles have poles not perpendicular to any of the principle directions.



Failure in the sheet

Failure occurs when the calculated stress/strain data for a plane lie above the failure envelope.

In this applet, both Mohr-Coulomb failure and tensional failure can be modeled. The linear Mohr-Coulomb failure envelope is defined by

$$\tau = \tan\phi * \sigma_n + C$$

Where τ is shear stress, ϕ is the friction angle, σ_n is the normal stress and C is the cohesion. Tensile failure occurs at negative (tensional) normal stresses, and the tensional failure envelope curves down from the cohesion value on the shear stress axis, to the tensile force (T) on the negative normal stress axis. To simplify, I have programmed a linear tensile failure envelope between C and T .

One of the special features of this applet is that it predicts the orientations of failure, using the material properties and the stress tensor (see figure). This is done by calculating the normal/shear stress data for 1511 points distributed over the Schmidt Nett. These are compared with the failure envelopes for two materials. Failed planes are indicated in the plot with colored dots (red is material 1, blue is material 2).

Calculate your own stress tensor

The tab "Calculate own stress tensor", allows the user to calculate a stress tensor, in the case when one of the principle stresses is vertical (Andersons Theorem). Input consists of the size of the vertical stress (for example based on ρgh), the sizes of the largest and smallest horizontal stress, and the

azimuth of the largest horizontal stress. Output consists of the stress tensor and a stereoplot of the input values.

Appendix 2: Monte Carlo analysis of seismic based paleostress results of NW Groningen.

Introduction

Paleostress analyses have been used to decipher the stress evolution and tectonic evolution for several decades, either by studying faults in outcrop (Bergerat, 1987; Wojtal and Pershing, 1991; Hippolyte et al., 1993; Hibsich et al., 1995; Gapais et al., 2000; Fellin et al., 2002; Saintot and Angelier, 2002; Vandycke, 2002; Hecht et al., 2003; Michon et al., 2003; Reicherter and Peters, 2005; Caiazza et al., 2006) or in seismic data (McBride, 1989; Gartrell and Lisk, 2005, Chapter 1 and 2), as well as by studying various types of sub-grain piezometry, such as calcite twins (e.g.: Rocher et al., 2004).

Many different paleostress analyses have been proposed, but in general, paleostress analysis tools can be separated by those based on the Mohr-Coulomb failure criterion, for example the Numerical Dynamic Analysis (NDA) (Turner, 1953), while other analyses are based on the Wallace and Bott Criterion (Wallace, 1951; Bott, 1959), for example the Direct Stress Inversion (DSI) (Angelier, 1984, 1990, 1994). Both methods assume a homogenous stress field at the scale of the input data. Since much of the background of these methods is discussed in the individual Chapters of this thesis, as well as more extensively in for example Sippel (2008), this will not be discussed here.

To the best of our knowledge, no study has been published looking at the effect of the quality of the input data (with the possible exception of Shan et al. (2006), and Zalohar and Vrabec (2007) who apply it on their own paleostress calculation methods).

In this appendix, we will look at the effect of simulated measurement errors on the outcome of a paleostress analysis in three different datasets. For this, data published by Sippel et al. (2009), Shan (2003) and Chapter 1 are used to calculate the paleostress tensor using the NDA- and DSI-methods.

The original input data for these three datasets consist of the dip direction and dip of the fault, the azimuth and plunge of the slip vector (combined here in "fault/slip data", sensu: Shan et al., 2003) and a quality-indicator, which can be used to weigh the data.

In this work however, we will artificially modify the orientation of the slip vector, in order to introduce a synthetic measurement error in the data. The three original input data sets we have used are corrected data sets. This means that the displacement orientations are corrected for measurement errors that rotate the slip vector away from the fault plane. This was done using the program TectonicsFP (Ortner et al., 2002).

The datasets

The first dataset is taken from Shan et al. (2003). In this paper, the objective-function algorithm is introduced, which can be used to separate polyphase fault/slip data. Polyphase data in this case means a dataset of fault/slip data, collected at the same location, but containing the slip data from multiple, unrelated tectonic events. Separating polyphase datasets constitutes a considerable challenge in paleostress analyses (see also for example: Kleinspehn et al., 1989; Yamaji, 2000; Fellin et al., 2002; Zalohar and Vrabec, 2007; Sippel et al., 2009). Shan et al. (2003) have published two polyphase datasets (case 1 and case 2) of artificial fault /slip, consisting of three equally large sub-sets

of monophasic fault /slip data to represent different tectonic phases. Case 1 is an idealized dataset, with slip data being exactly parallel to the maximum resolved shear stress on the faults (exactly following the Wallace and Bott Criterion). In case 2 however a small, random rotation between -5° and 5° was applied to the slip vector. In this work we have used the 20 fault /slip data pairs of subset 1 of case 2, as this case most closely approaches a “natural” data-set measured in the field, while still ensuring that this data is from a single tectonic event. The dataset was constructed using a stress tensor with the σ_1 oriented 180/10, σ_2 has an orientation of 089/05.65, σ_3 is oriented 329.932/78.48 and the stress ratio R is 0.333 ($\Phi=2$), making it representing a phase of strike slip faulting (Shan et al., 2003).

The second dataset consists of 24 fault orientation/ slip vector data, measured in the field, provided by Judith Sippel (GFZ, Potsdam). They are part of a larger dataset, recorded in the Mammendorf Quarry, on the Flechtingen High, on the south-western margin of the Central European Basin System (Sippel et al., 2009). The larger dataset is polyphase in nature, but is separated in two homogenous datasets using the approach described by Sippel et al. (2009, dataset MAM1 in this paper). The dataset describes a phase of strike-slip/ reverse faulting, with σ_1 is oriented 185/10, σ_2 348/80 and σ_3 is 094/03 (R approaches 0, Φ approaches ∞) (Sippel et al., 2009).

The third data set is taken from Chapter 1, and contains all 23 faults in the North Sea interval from the Groningen High. The data set contains only normal faults, with movement vectors all close to dip slip. The stereographic projection of the three datasets are shown in table 1.

Table 1

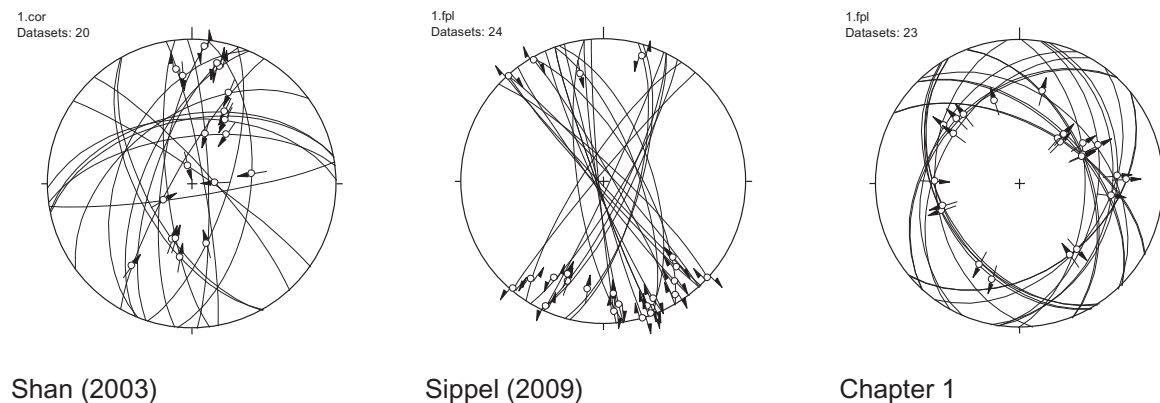


Table 1 The datasets used in this study.

Method

The program used to calculate the paleostress axes is TectonicsFP (Ortner et al., 2002). This program allows for the NDA method a Θ angle of $0-90^\circ$, and to estimate the effect of differences in this angle, paleostress were calculated with a fixed Θ angle of 45° and a best fit Θ angle calculated by TectonicsFP. The effect of artificial measurement errors was also tested on the DSI method.

In order to evaluate the effect of measurement errors, we performed a modified Monte Carlo analysis (Metropolis and Ulam, 1949). Although lacking a formal definition, Monte Carlo analysis is used as a collective term for a group of statistical analyses based on the repeated sampling of a small number of

parameters from a much larger database (Metropolis and Ulam, 1949). Large groups of data are often difficult to describe statistically, due to limitations in the calculation capacity. In a Monte Carlo analysis, a subset of random datapoints is taken from this large dataset and analyzed statistically. If the size of the subset is correctly chosen, the statistical parameters of this subset will be the same as those of the entire datagroup. Repeating the analysis with different random subset shows the robustness of the statistical analysis. In this work we use a slightly modified analysis. Instead of taking random subsets from our dataset, we modified our original dataset randomly in order to test the robustness of the paleostress calculation technique.

To introduce artificial measurement errors into the data, a method to change the original data in a consistent and logical way needed to be developed first. Since the slip of the fault can be thought of as a vector located in the fault plane, the azimuth and plunge data were converted into a vector. This vector can then be rotated this slip-vector by a specified amount of degrees around the normal vector (n) of the fault plane (see Fig. 1). To rotate the movement vector orientation and to change azimuth/plunge orientations into vectors and back, the excel sheet "StereogramHeijn_v.2.0.xls" (available online on http://www.ged.rwth-aachen.de/Ww/people/heijn/heijn_index.html, see also Appendix 1) was modified.

Once the original datasets were converted in vector data, the slip data was rotated around the fault plane normal vector using a random, normally distributed number of degrees. For each of the three input datasets we performed 3 analyses, by varying the original slipvector randomly, using three different standard deviations.

The normal distribution was a Gaussian distribution, with a standard deviation of either 2, 9 or 20° with a mean of 0. This way three new datasets were constructed from the original, with an additional, normally distributed artificial measurement error in the range of -2° and 2°, -9° and 9° and -20° and 20° respectively. The assignment of a specific error value within this range was controlled by a random number generator. Repeating the process 50 times created a large dataset containing 50 different versions of the three original datasets, with the slip vector modified by an artificial error with three different standard deviations (the total number of modified datasets therefore is 450). The fault orientations where not varied. These 450 datasets consisted of vector data, so they were consequently recalculated into azimuth/slip pairs. Due to rounding errors, these new orientations not always align perfectly with the fault plane, but TectonicsFP allows a correction step, to rotate these orientations into the fault plane.

In the second step (Fig. 1), the resultant nine (3 different input datasets times 3 different standard deviations) sets of 50 new datasets, were subsequently used to calculate the paleostress axes, using the NDA method with the best fit Θ (which can vary for every of the 50 datasets), the NDA method with a standard Θ angle of 45° and the DSI method, which requires no assumption of material properties.

The calculated groups of 50 paleostress orientations were subsequently plotted together in lower hemisphere (third step in Fig. 1), equal area projection (Schmitt Nett), to visualize the spread in output data. The calculated R value was also plotted in a histogram to visualize spread.

Results

The results are plotted in the tables below. The data is grouped in such a way that, the data from one set of modified data sets is displayed in one page. The three different stress reconstructions are plotted below each other, with first the NDA results with the best fit angle, below that the results of the NDA method with a fixed angle of 45° and lastly the results of the DSI method. The calculated paleostress axes of the original data are also shown.

For the Groningen data set (standard deviation 2°) there is an obvious discrepancy between the resultant stress axes of both NDA methods and the DSI method (as discussed in Chapter 1.

Step 1:

Step 2:

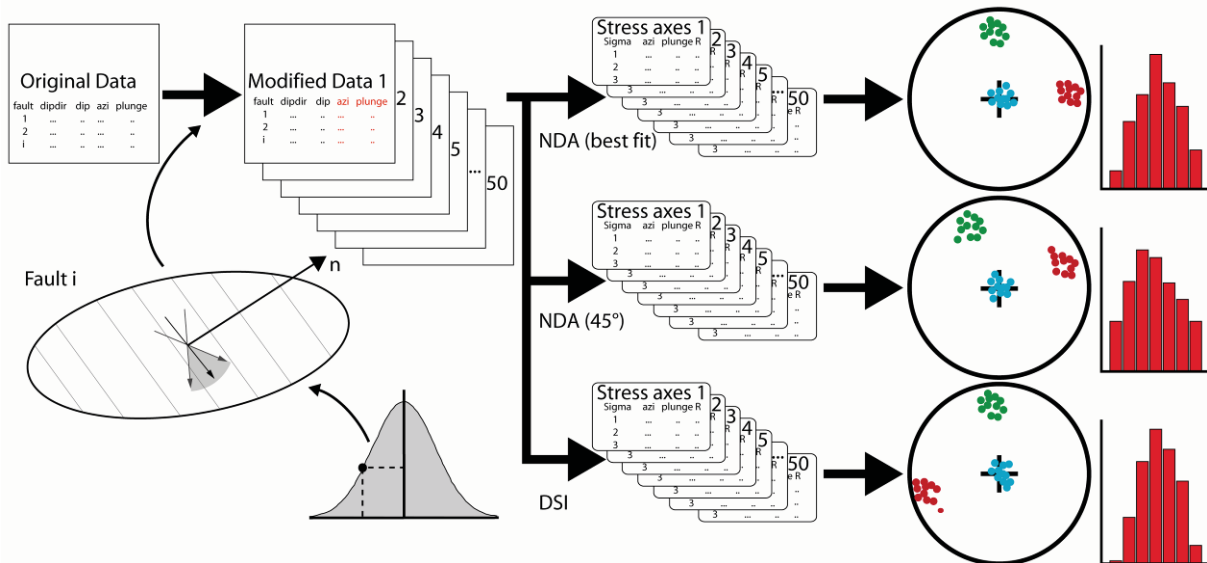


Figure 1 Workflow to obtain input data sensitivity. In step 1, 50 modified data sets are created by randomly modifying the azimuth and plunge of the striation orientation of all faults, following a Gaussian distribution. In step 2 this cluster of modified datasets is used to calculate 50 sets of stress axes and stress ratios, using three different paleostress calculation methods. These are then plotted in stereoplots and histograms. This workflow only describes the procedure for one set of input data and one standard deviation. The workflow is repeated for 2 additional standard deviations and then repeated for 2 two other input data sets.

this is one of the reasons why NDA was used instead of DSI, in addition to the “stability analysis” using synthetic data discussed in Appendix 4). However, the analysis of the Mammendorf dataset also shows a difference between the NDA and DSI results, both in the stress axis orientation as in the R-value. Although we will touch on this issue in the discussion, the aim of this section of this Appendix is not to compare the two paleostress calculation methods with each other, but to determine the effect of increasing artificial measurement errors on the outcome of individual paleostress methods.

The results presented below show that for all three methods, increasing the standard deviation of the artificial error, increases the spread of both the resultant stress axes and the R value. Furthermore, for the Groningen (9° and 20° standard deviations) as well as the Mammendorf (standard deviation equals 20° dataset), the DSI method produces second set of stress axes for 5-10% of the 50 random datasets. These sets clearly deviate from the main set of stress axes, both in the orientation of the

principle stresses, and in the stress ratio. The histograms of the Groningen data clearly show a bimodal distribution.

Discussion

The secondary paleostress results calculated for the Groningen and Mammendorf datasets have large implications. The calculation two very distinct stress tensors, based on what are essentially the same data, means that one can never be completely certain whether any calculated paleostress tensor is correct. A similar result is shown in Appendix 4, where single outliers are shown to strongly influence the result of the DSI stress tensor. The NDA method appears to be more stable. The calculation of discrepant stress axes with the DSI method in 5-10% of the cases of the higher standard deviations, might be the result of the least square regression used in the DSI method. Least square regression is a method to fit a trend line to a collection of measurements by minimizing the sum of the squared difference between the data and the trend line (see for example: Davis, 2002). The problem with the least square criterion in general is very sensitive to outliers¹ in the data (e.g.: Will and Powell, 1991; Davis, 2002). Will and Powell (1991) describe how the use of a “classical least squares estimator” for example in the DSI can result in “surprising” results when used on real data, that is not free of outliers, or when the data is not Gaussian distributed. One possibility is to visually inspect the data and (manually) remove these outliers, but since this a four-dimensional problem, this approach is impractical (Will and Powell, 1991). In addition, in “real” data measurement errors in the field data can not be avoided (Shan et al., 2006), and the removal of measurement errors is more complex than the removal of outliers. In seismic based fault displacement studies on the other hand, particularly the reconstruction step is known to introduce a lot of errors (Gartrell and Lisk, 2005).

Regarding the different orientation of principle stresses and the R-value using different paleostress calculation methods, Sippel (2008) discusses the difficulty of the NDA to calculate the correct stress ratio, as it is based on the eigenvectors and eigenvalues and not on the fault-slip pattern. Also the orientation of the stress axes might not correctly fit with the fault-slip data. It however must be noted that neither the DSI nor NDA is able to calculate the reported stress ratio 0.333 used to construct the artificial Shan dataset (Shan et al., 2003).

For the Mammendorf dataset, the orientation of the stress axes of the NDA and DSI results are the same, but the sign is different, as σ_2 and σ_3 are inverted. This is however not at all surprising considering that Sippel et al. (2009) shows this data set has an R-value of 0. In a stress tensor with $R=0$, σ_2 and σ_3 are the same size. This is not reflected in the R-value of the NDA-calculated stress tensors, but the DSI stress tensor has an average R-value of around 0.11

¹ Will and Powell (1991) define an outlier as “a measurement that is discrepant with respect to the trend of the majority of the data, for example, as a consequence of belonging to a different stress field or of erroneous measurement, especially the wrong sense-of-shear; incorrect geological interpretation, recording or keypunch errors, etc”.

Conclusions

There appear to be problems associated with both the NDA and DSI paleostress calculation. The NDA might have difficulties calculating the correct stress ratio, or the correct stress axes orientation (Sippel, 2008). This section, as well as the other appendices, shows that the DSI is not stable and can calculate very different stress axes based on what essentially is the same data. This throws a shadow of doubt on any paleostress tensor, calculated with a least squared regression algorithm, as one is never certain if the resultant tensor is correct. As a result, we stand by our decision to use the NDA methods, although we concede that this method might not correctly represent the stress ratio.

References:

- ◇ Angelier, J., 1984. Tectonic analysis of fault slip data sets. *Journal of Geophysical Research* 89, 5838-5848.
- ◇ Angelier, J., 1990. Inversion of field data in fault tectonics to obtain the regional stress-III. A new rapid direct inversion method by analytical means. *Geophysics Journal International* 103, 363-376.
- ◇ Angelier, J., 1994. Fault Slip Analysis and Paleostress Reconstruction. In: Hancock, P. L. (Ed.), *Continental Deformation*. Pergamon Press, Oxford, 53-100.
- ◇ Bergerat, F., 1987. Stress Fields in the European platform at the time of Africa-Eurasia collision. *Tectonics* 6(2), 99-132.
- ◇ Bott, M. H. P., 1959. The mechanics of oblique slip faulting. *Geological Magazine* 96(2), 109-117.
- ◇ Caiazza, C., Ascione, A., Cinque, A., 2006. Late Tertiary–Quaternary tectonics of the Southern Apennines (Italy): New evidences from the Tyrrhenian slope. *Tectonophysics* 421, 23-51.
- ◇ Davis, J. C., 2002. *Statistics and Data Analysis in Geology*. John Wiley, USA, pp. 637.
- ◇ Fellin, M. G., Martin, S., Massironi, M., 2002. Polyphase Tertiary fault kinematics and Quaternary reactivation in the central-eastern Alps (western Trentino). *Journal of Geodynamics* 34, 31-46.
- ◇ Gapais, D., Cobbold, P. R., Bourgeois, O., Rouby, D., de Urreiztieta, M., 2000. Tectonic significance of fault slip data. *Journal of Structural Geology* 22, 881-888.
- ◇ Gartrell, A. P., Lisk, M., 2005. Potential New Method for Paleostress estimation by Combining Three-dimensional Fault Restoration and Fault Slip Inversion Techniques: First Test on the Skua Field, Timor Sea. In: Boulton, P. & Kaldi, J. (Eds.), *Evaluating fault and cap rock seals*. AAPG Hedberg Series 2, 23-26.
- ◇ Hecht, C. A., Lempp, C., Scheck, M., 2003. Geomechanical model for the post-Variscan evolution of the Permian–Mesozoic basins in Northeast Germany. *Tectonophysics* 373, 125-139.
- ◇ Hibscher, C., Jarrige, J.-J., Cushing, E. M., Mercier, J., 1995. Paleostress analysis, a contribution to the understanding of basin tectonics and geodynamic evolution. Example of the Permian/Cenozoic tectonics of Great Britain and geodynamic implications in western Europe. *Tectonophysics* 252, 103-136.
- ◇ Hippolyte, J.-C., Angelier, J., Bergerat, F., Nury, D., Guieu, G., 1993. Tectonic-Stratigraphic record of paleostress time changes in the Oligocene basins of the Provence, southern France. *Tectonophysics* 226, 15-35.

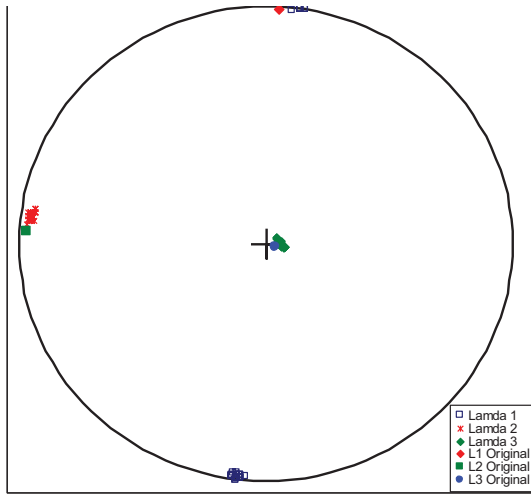
- ◇ Kleinspehn, K. L., Pershing, J., Teyssier, C., 1989. Paleostress stratigraphy: A new technique for analyzing tectonic control on sedimentary-basin subsidence. *Geology* 17, 253-256.
- ◇ McBride, J. H., 1989. Remarks on the derivation of the paleostress system from inferred faults on deep seismic reflection records. *Tectonophysics* 168, 275-282.
- ◇ Metropolis, N., Ulam, S., 1949. The Monte Carlo Method. *Journal of the American Statistical Association* 44(247), 335.
- ◇ Michon, L., van Balen, R. T., Merle, O., Pangnier, H., 2003. The Cenozoic evolution of the Roer Valley Rift System integrated at a European scale. *Tectonophysics* 367, 101-126.
- ◇ Ortner, H., Reiter, F., Acs, P., 2002. Easy handling of tectonic data: the programs TectonicVB for Mac and Tectonics FP for Windows(tm). *Computers & Geosciences* 28, 1193-1200, see also <http://www.tectonicsfp.com/>.
- ◇ Reicherter, K. R., Peters, G., 2005. Neotectonic evolution of Central Betic Cordilleras (Southern Spain). *Tectonophysics* 405, 191-212.
- ◇ Rocher, M., Cushing, M., Lemeille, F., Lozac'h, Y., Angelier, J., 2004. Intraplate paleostresses reconstructed with calcite twinning and faulting: improved method and application to the eastern Paris Basin (Lorraine, France). *Tectonophysics* 387, 1-21.
- ◇ Saintot, A., Angelier, J., 2002. Tectonic paleostress fields and structural evolution of the NW-Caucasus fold-and-thrust belt from Late Cretaceous to Quaternary. *Tectonophysics* 357, 1–31.
- ◇ Shan, Y., Lin, G., Zhan, L., Zhao, C., 2006. Influence of measurement errors on stress estimated from single-phase fault/slip data. *Journal of Structural Geology* 28, 943-951.
- ◇ Shan, Y., Suen, H., Lin, G., 2003. Separation of polyphase fault/slip data: an objective-function algorithm based on hard division. *Journal of Structural Geology* 25(6), 829-840.
- ◇ Sippel, J., 2008. The Paleostress History of the Central European Basin System. Dr. rer. nat. thesis, Freien Universität.
- ◇ Sippel, J., Scheck-Wenderoth, M., Reicherter, K., Mazur, S., 2009. Paleostress states at the south-western margin of the Central European Basin System - Application of fault-slip analysis to unravel a polyphase deformation pattern. *Tectonophysics - Progress in understanding sedimentary basins* 470(1-2), 129-146.
- ◇ Turner, F. J., 1953. Nature and dynamic interpretation of deformation lamellae in Calcite of three marbles. *American Journal of Science* 251, 276-298.
- ◇ Vandycke, S., 2002. Paleostress records in Cretaceous formations in NW Europe: extensional and strike-slip events in relationships with Cretaceous-Tertiary inversion tectonics. *Tectonophysics* 357, 119-136.
- ◇ Wallace, R. E., 1951. Geometry of shearing stress and relation to faulting. *Journal of Geology* 59, 111-130.
- ◇ Will, T. M., Powell, R., 1991. A robust approach to the calculation of paleostress fields from fault plane. *Journal of Structural Geology* 13(7), 813-821.
- ◇ Wojtal, S., Pershing, J., 1991. Paleostresses associated with faults of large offset. *Journal of Structural Geology* 13(1), 49-62.
- ◇ Yamaji, A., 2000. The multiple inverse method: a new technique to separate stresses from heterogeneous fault-slip data. *Journal of Structural Geology* 22, 441-452.

- ◇ Zolohar, J., Vrabec, M., 2007. Paleostress analysis of heterogenous fault-slip data: the Gauss method. *Journal of Structural Geology* 29(11), 1798-1810.

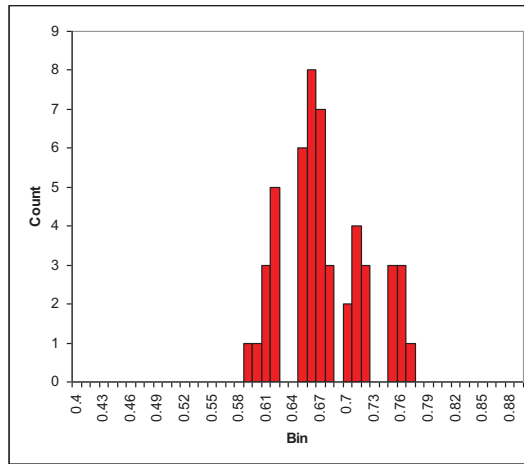
The results

Shan (2003) Data

NDA (best Fit)

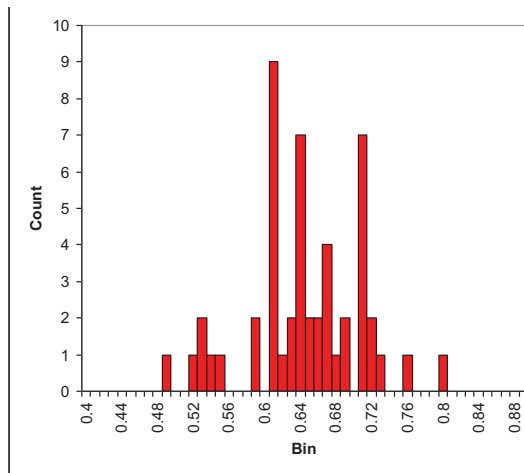
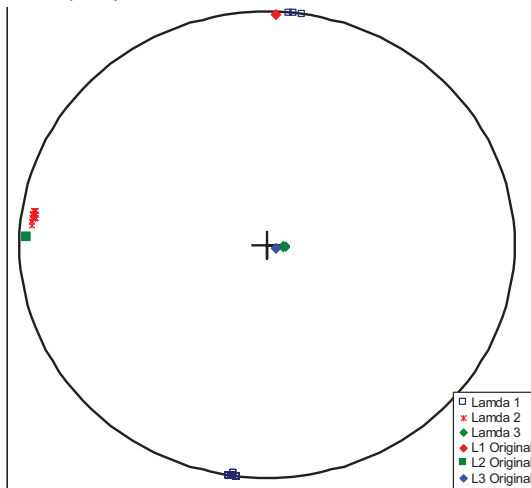


Standard Deviation = 2



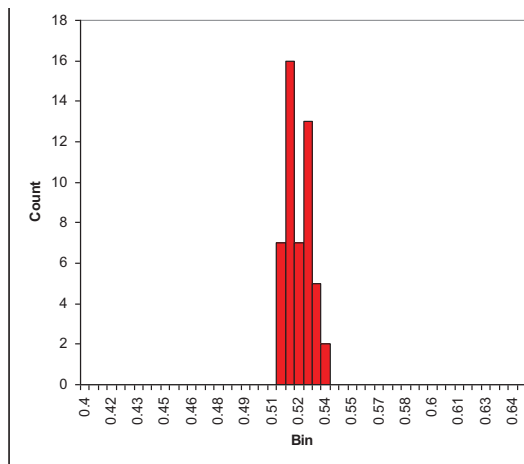
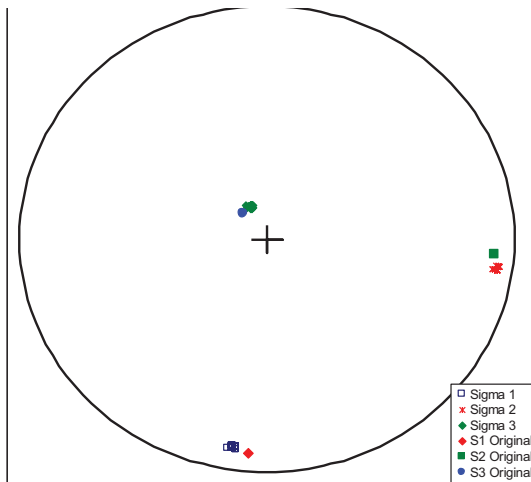
Bin size: 0.01

NDA (45°)



Bin size: 0.01

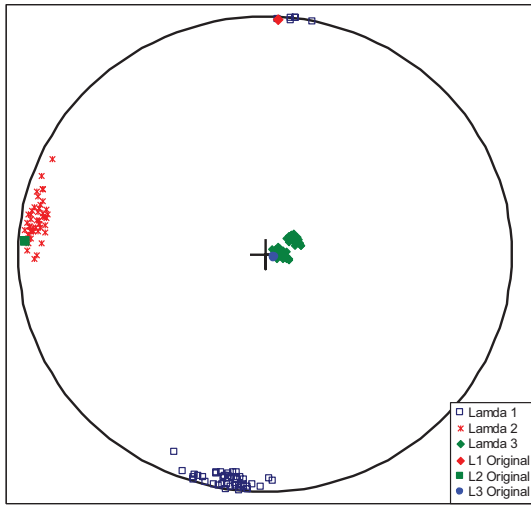
DSI



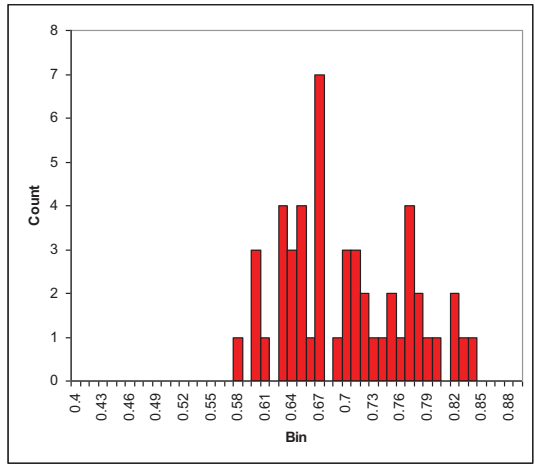
Bin size: 0.005

Shan (2003) Data

NDA (best Fit)

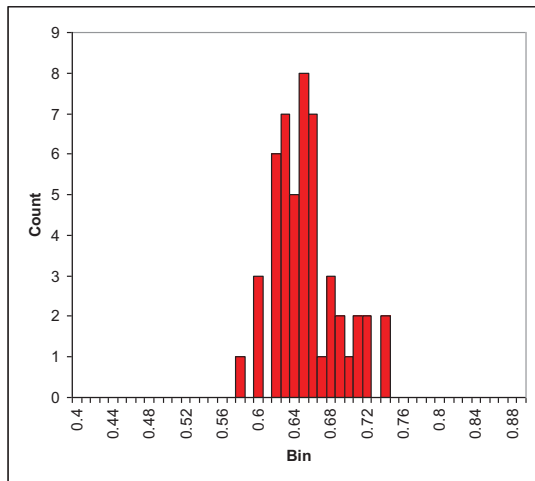
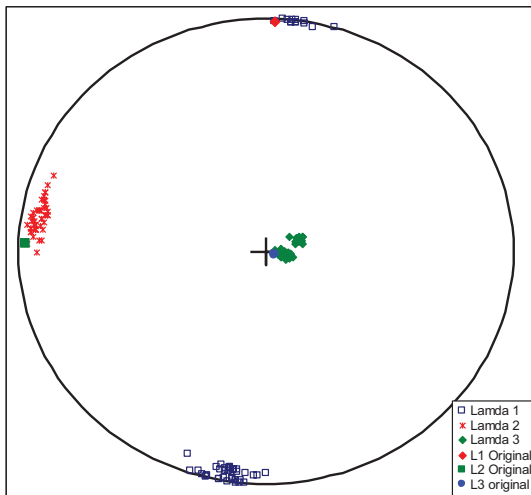


Standard Deviation = 9



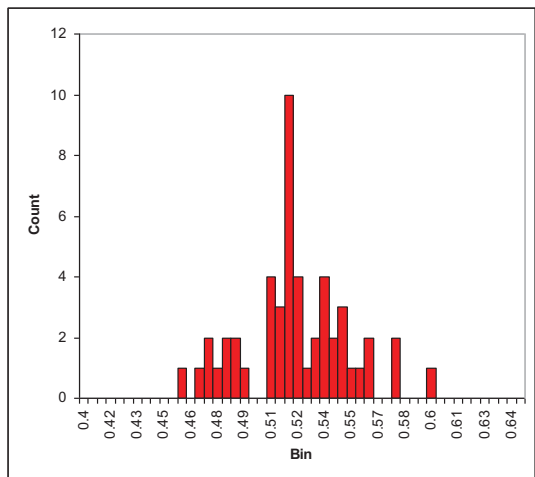
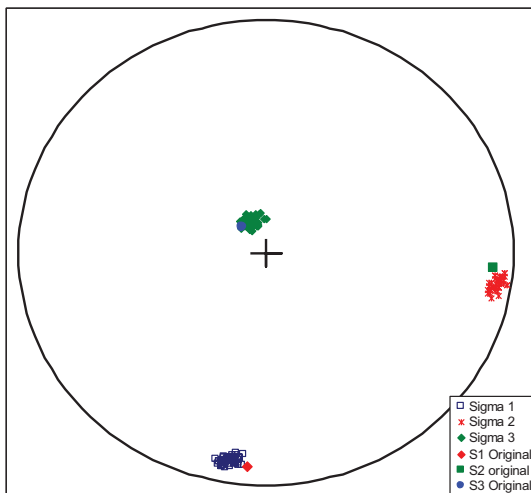
Bin size: 0.01

NDA (45°)



Bin size: 0.01

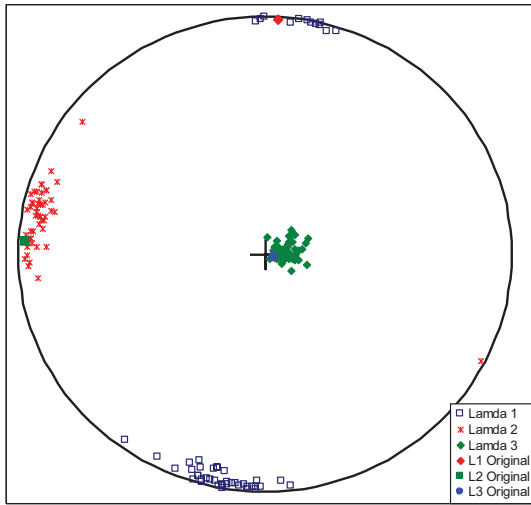
DSI



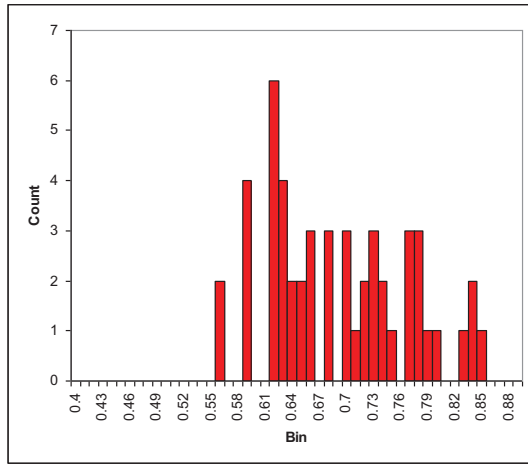
Bin size: 0.01

Shan (2003) Data

NDA (best Fit)

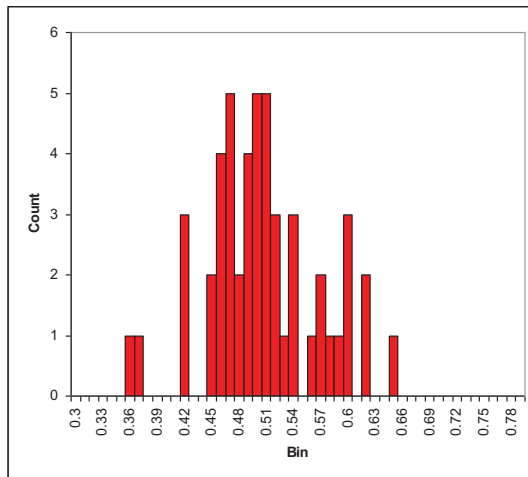
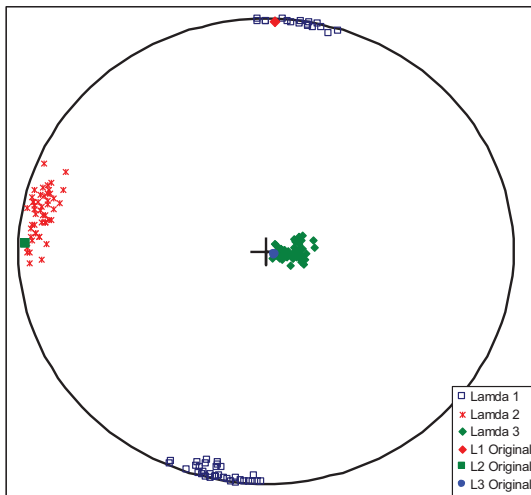


Standard Deviation = 20



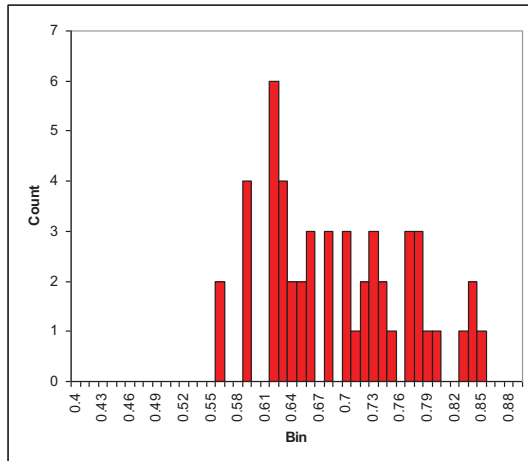
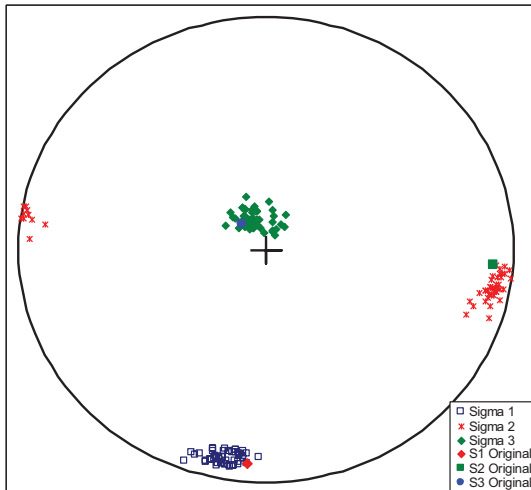
Bin size: 0.01

NDA (45°)



Bin size: 0.01

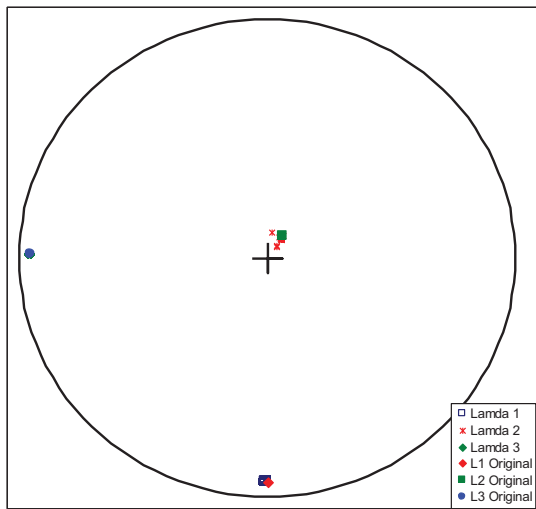
DSI



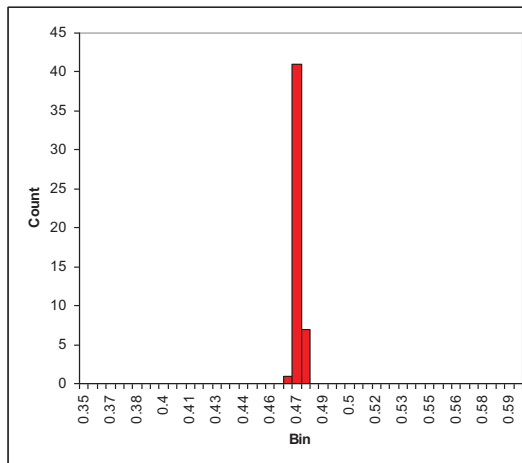
Bin size: 0.01

Mamendorf Data set

NDA (best Fit)

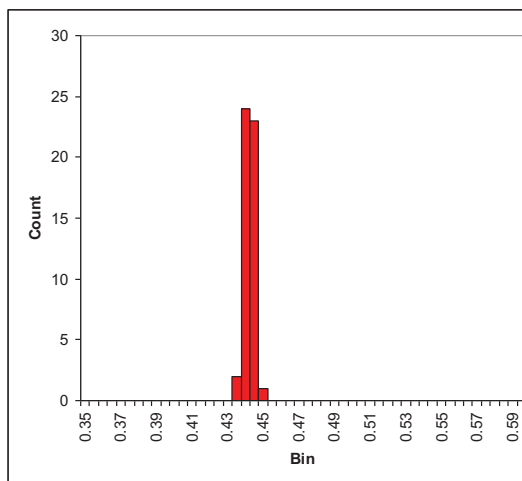
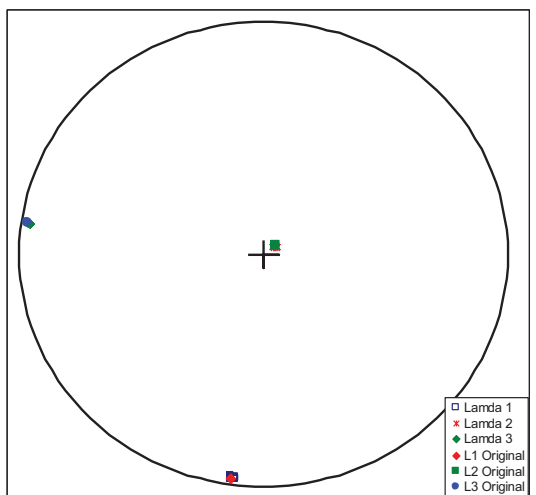


Standard Deviation = 2



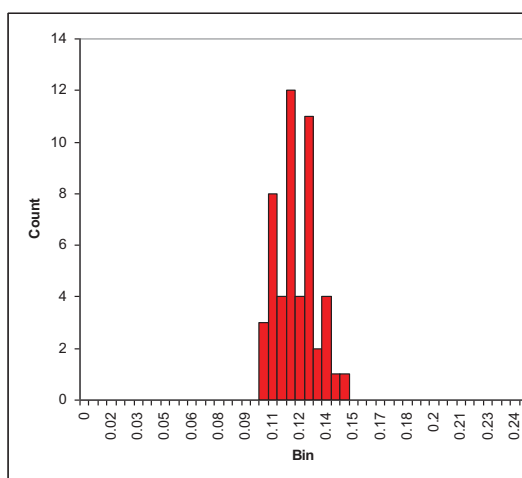
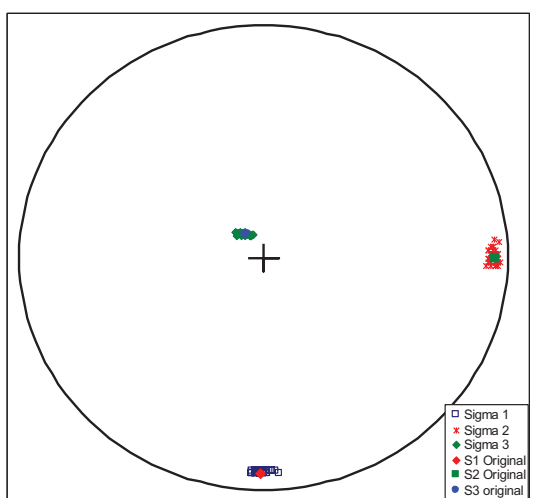
Bin size: 0.005

NDA (45°)



Bin size: 0.005

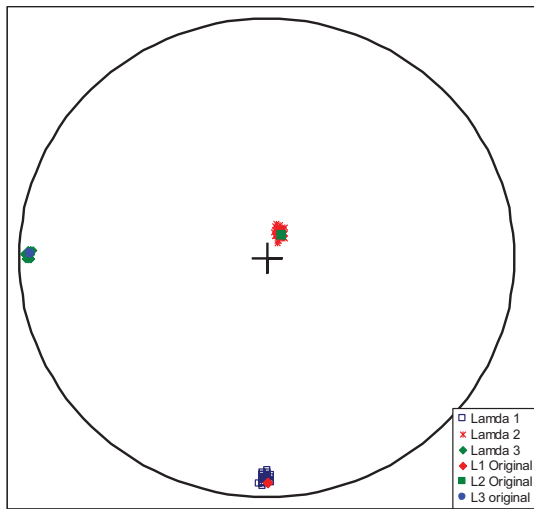
DSI



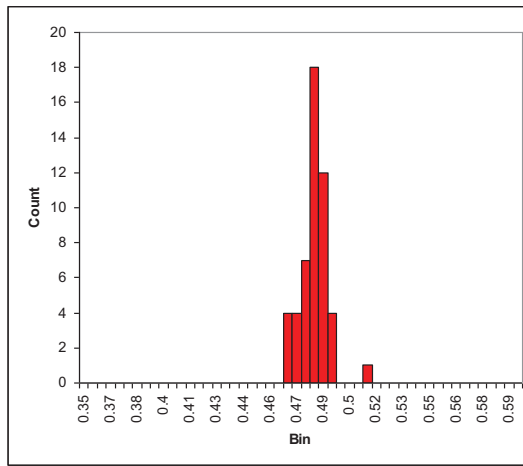
Bin size: 0.005

Mamendorf Data set

NDA (best Fit)

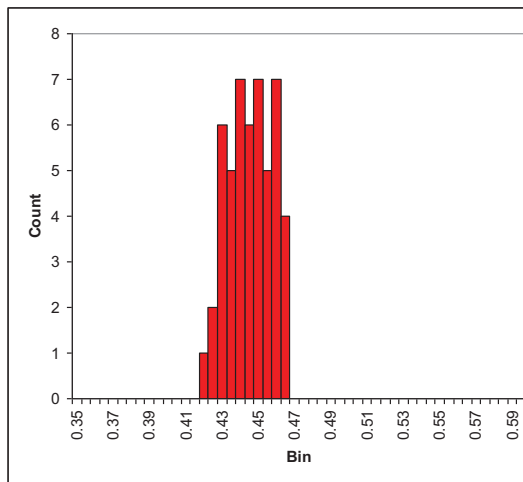
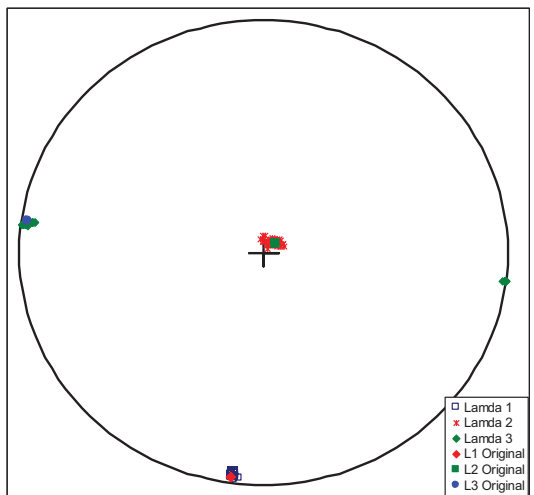


Standard Deviation = 9



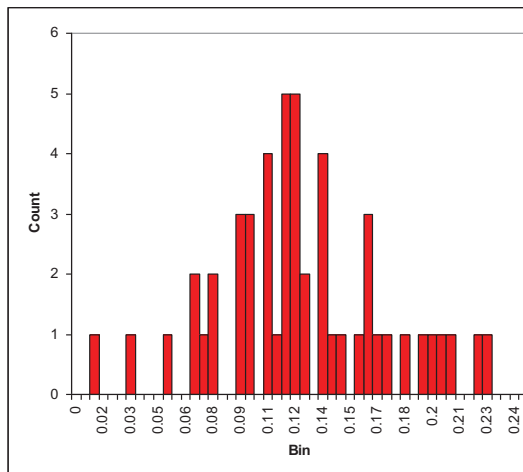
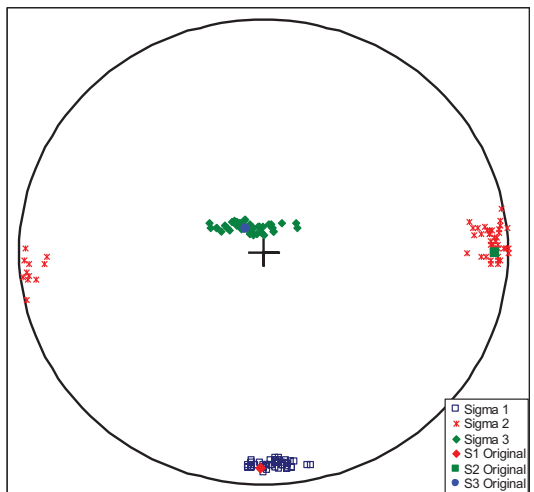
Bin size: 0.005

NDA (45°)



Bin size: 0.005

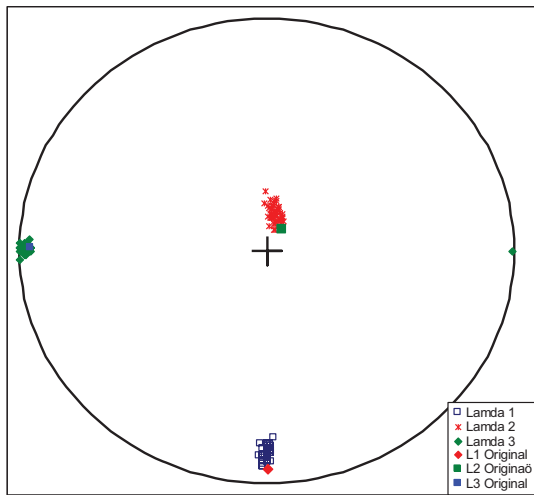
DSI



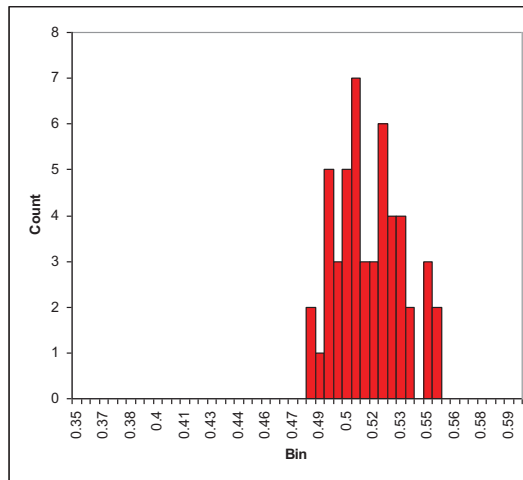
Bin size: 0.005

Mamendorf Data set

NDA (best Fit)

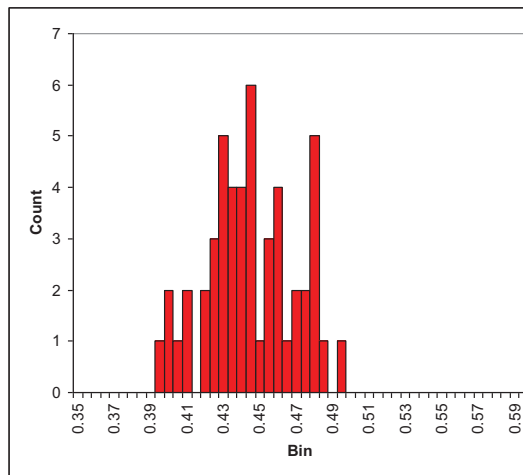
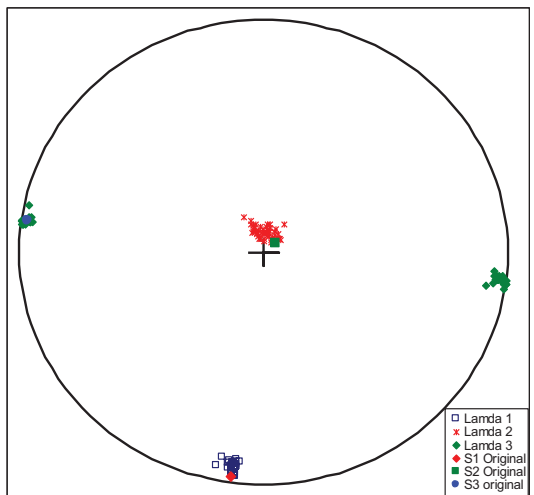


Standard Deviation = 20



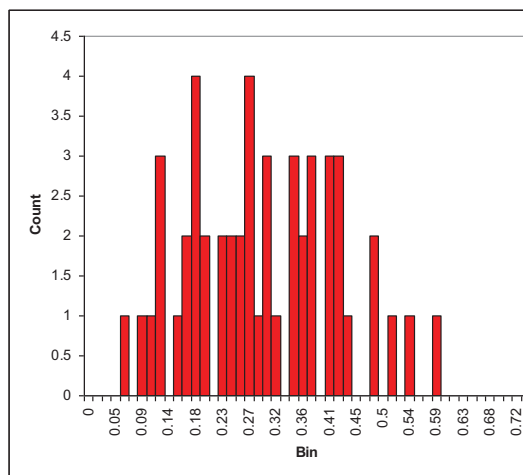
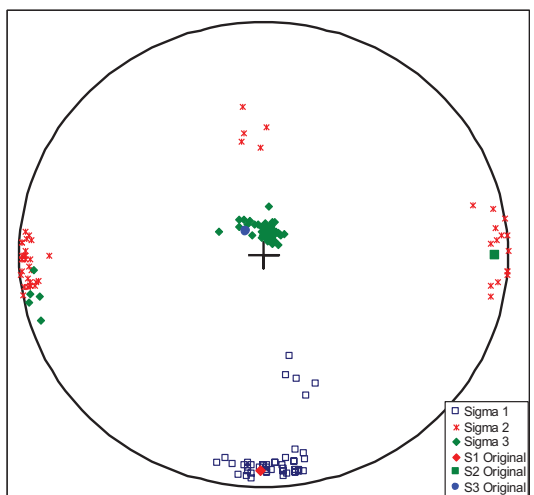
Bin size: 0.005

NDA (45°)



Bin size: 0.005

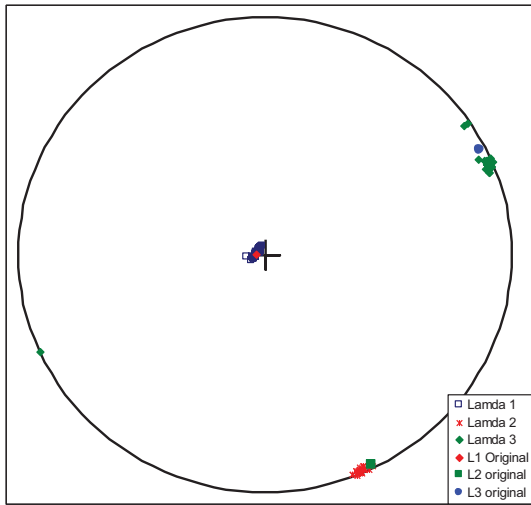
DSI



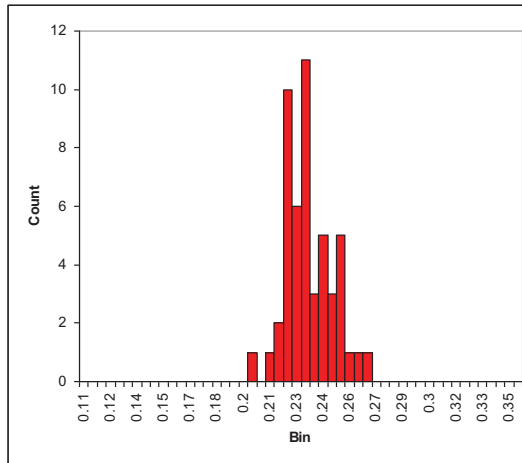
Bin size: 0.015

Groningen North Sea Group Data

NDA (best Fit)

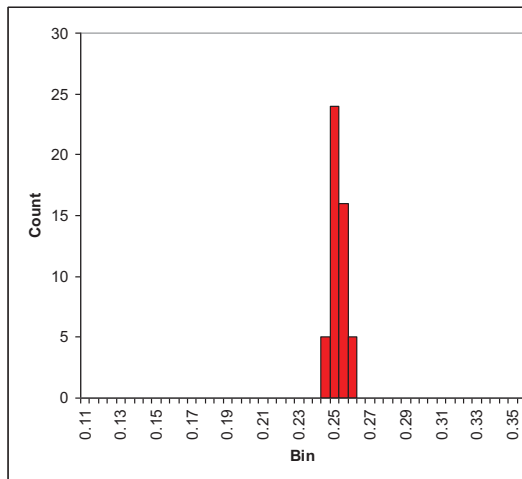
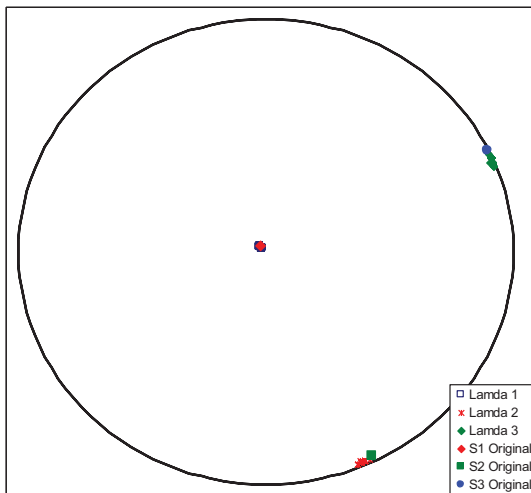


Standard Deviation = 2



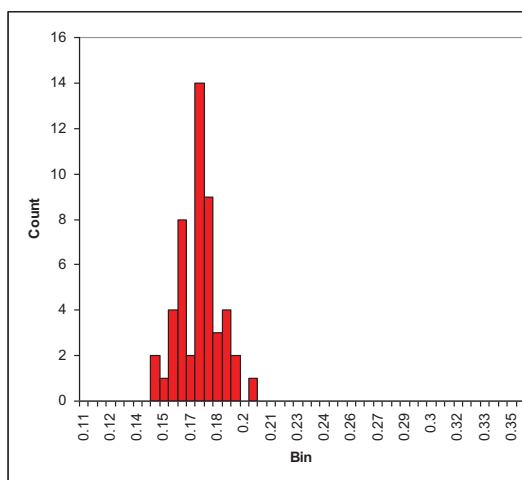
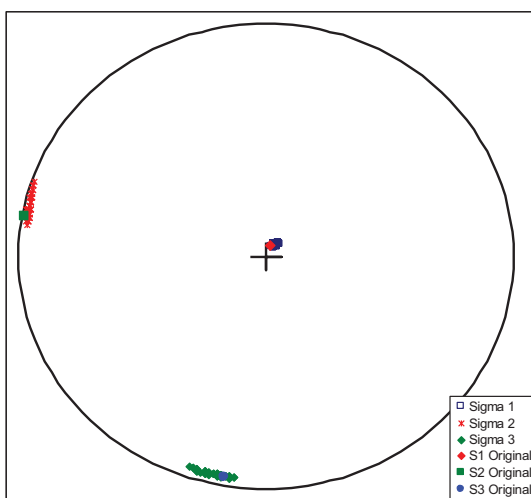
Bin size: 0.005

NDA (45°)



Bin size: 0.005

DSI

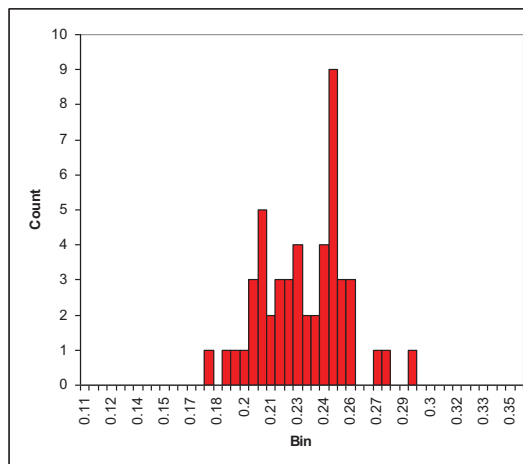
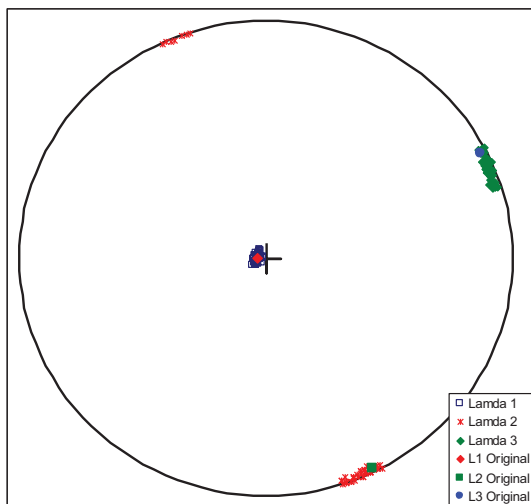


Bin size: 0.005

Groningen North Sea Group Data

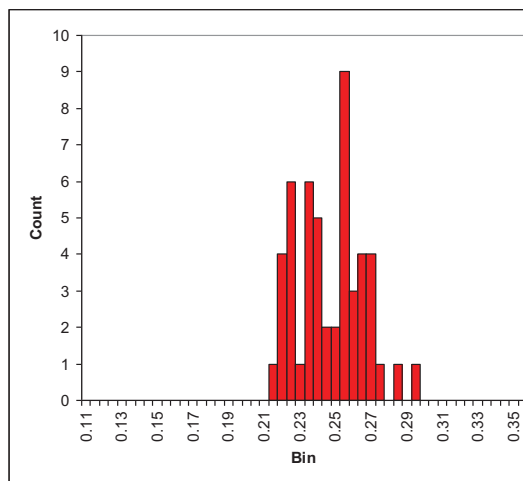
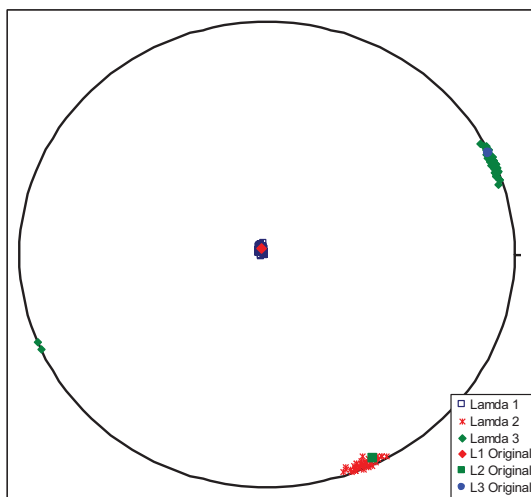
Standard Deviation = 9

NDA (best Fit)



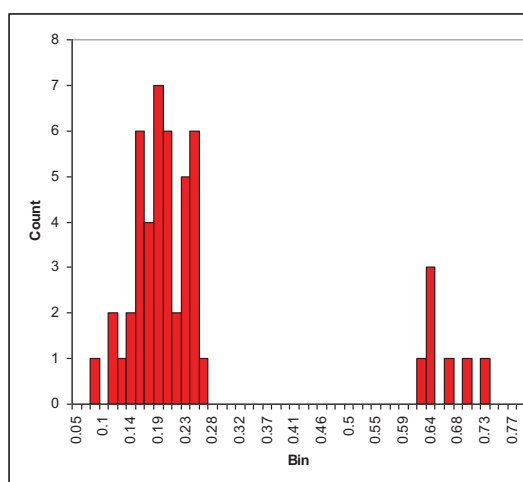
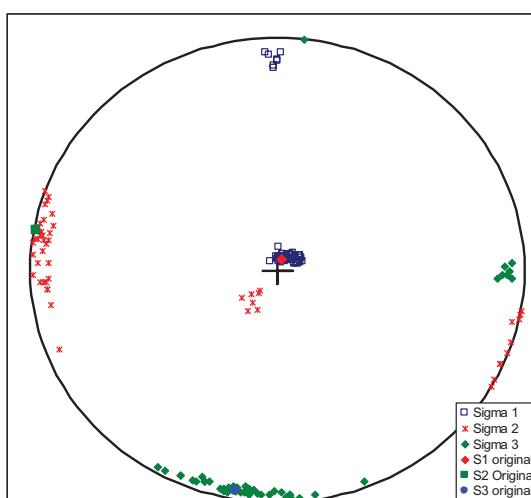
Bin size: 0.005

NDA (45°)



Bin size: 0.005

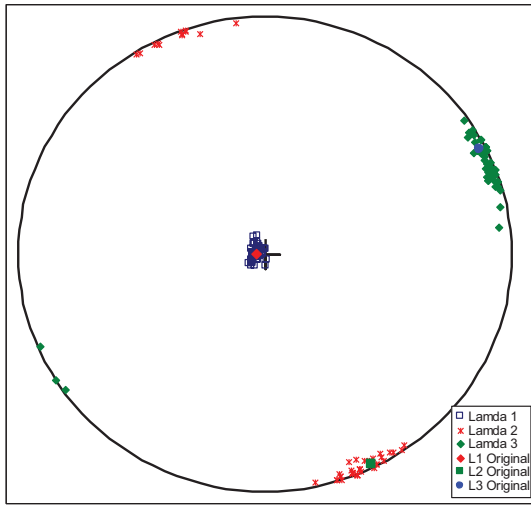
DSI



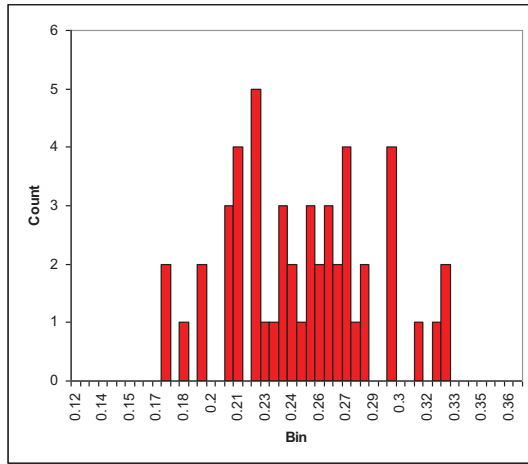
Bin size: 0.015

Groningen North Sea Group Data

NDA (best Fit)

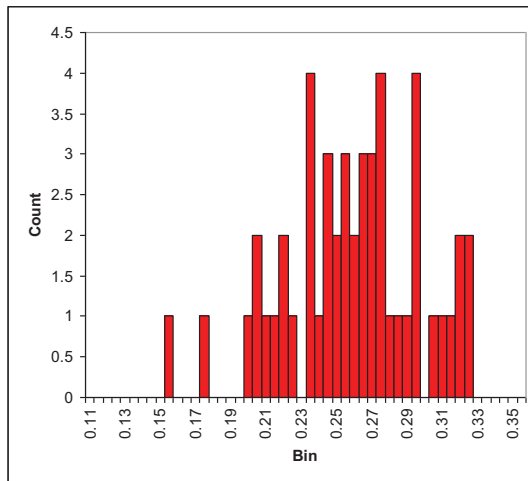
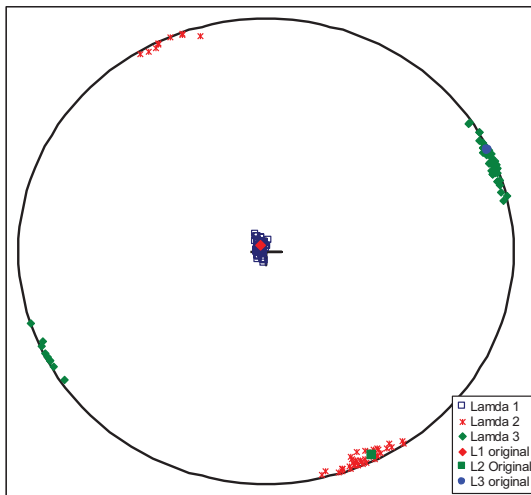


Standard Deviation = 20



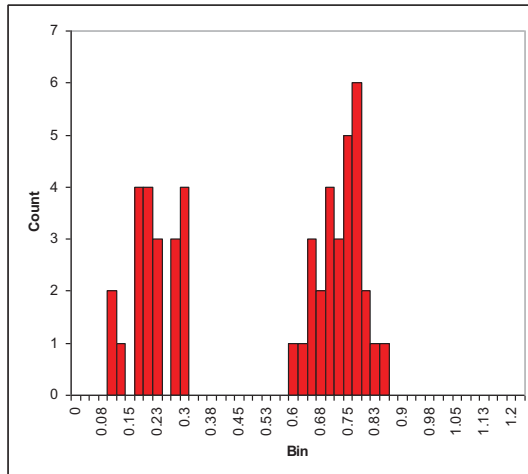
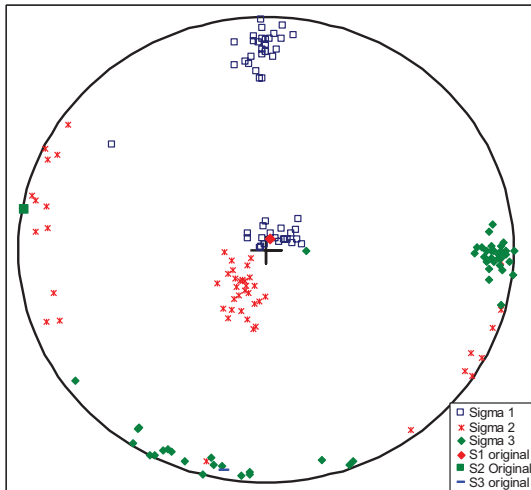
Bin size: 0.005

NDA (45°)



Bin size: 0.005

DSI

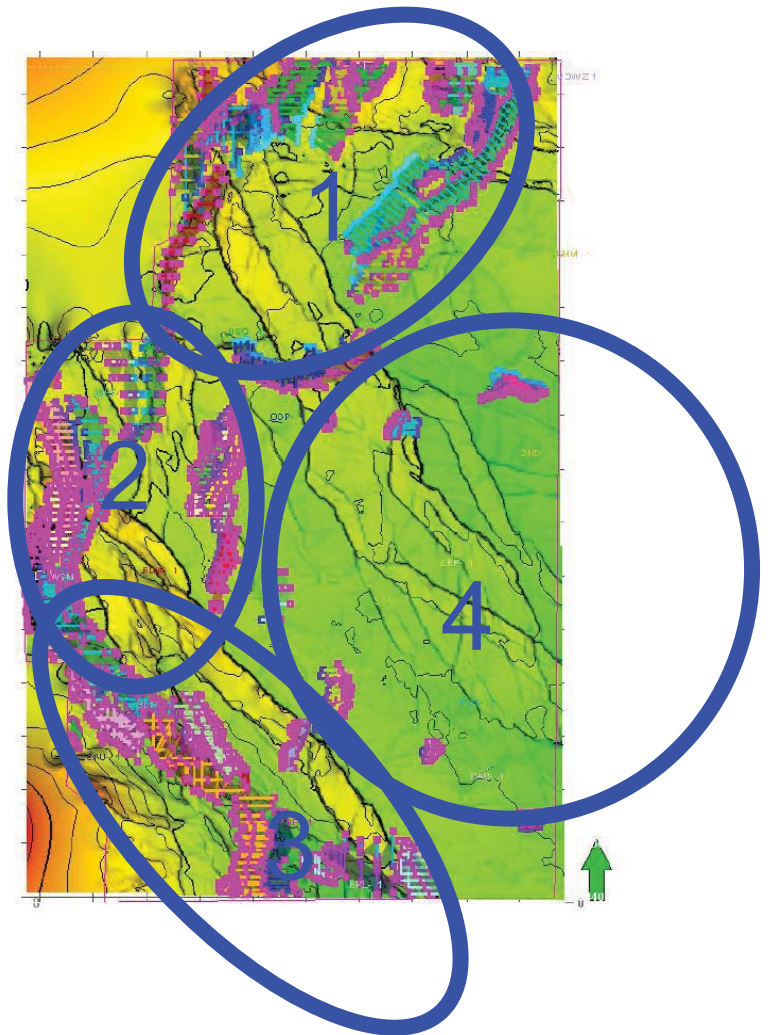


Bin size: 0.025

Appendix 3: Bootstrapping the data

To evaluate the statistical robustness of the dataset, the dataset was subjected to a modified “sampling without replacement bootstrapping”-test. The term “modified” is used as the resampling was not done at random, but was coupled to the fault trends observed in the survey. The aim of this analysis is to see whether the fault orientation influences the calculated paleostress result. There are four main areas in the fault orientation and these will act as a separator for the data in this analysis.

The fault and slip orientation in the data set was split into four groups (see figure), where trend 1 corresponds to the NE-SW fault trend in the NW of the survey, trend 2 corresponds to the N-S trend along the western border, and trend 3 corresponds to the NW-SE trend in the SW of the survey. The faults in trend 4 are all faults in the centre and east of the survey, not included in any of the other trends. This set only contains faults in the Cretaceous deposits (this is the area of the faults described in



Chapter 2). The datasets for the Tertiary and Cretaceous faults were resampled using these trends, and the paleostresses were recalculated with the NDA-method, using a 30° Θ angle.

A second analysis was used to evaluate the effect of fault orientation, as well as the effect of the applied slip vectors. Here the paleostress tensor was recalculated in the case of pure dip-slip. This was done for the entire Tertiary and Cretaceous faults sets, as well as the four Tertiary and four Cretaceous fault trend sub-sets. Pure dip-slip was assumed by making the orientation of the slip vector parallel to the dip direction of the fault.

The results of the bootstrapping are shown in table C-1 for the Tertiary and in table C-2 for the Cretaceous. For the case of pure dip slip, table C-3 shows the results of the Tertiary and C-4 for the Cretaceous. In these tables, the first line shows the results for the entire dataset, and in table C-3 and C-4 the second line shows the results for the entire data set, recalculated with pure dip slip.

The results in table C-1 and C-2 show that the orientation of the bootstrapped principle stresses only differ significantly from the results of the entire dataset in the N_all-trend1-subset. For this subset, the

orientation of σ_2 and σ_3 stress axis is rotated. It must be noted here that for the entire dataset, the R-value is quite low (around 0.3).

For all other data sets in tables C-1 and C-2, the orientation of the sub-set principle stresses is similar to the orientation of the principle stresses in the entire data set. The variation in the principle stresses is generally within 17° (in the case of the N_all-trend1-subset within 35°). This variation is not necessarily the result of the monotone fault orientation, but can also be caused by the reduced amount of fault orientations in the analysis. Angelier (1994) already discussed that the quality of the paleostress analysis depends on the amount of used faults, as well as their spatial distribution.

It is surprising to see that for the case of pure dip slip, the stress orientations of the bootstrapped trend subsets do not differ significantly from the entire data set. Again N-All trend1- sub sets, shows a switch in σ_2 and σ_3 axes, but all other data sets show paleostress orientations similar to the original dataset. Also note that the fluctuation diagrams are of a better quality (i.e. closer to the Gaussian bell shape).

Slip vectors in this study nearly are very close to pure dip slip normal faulting. The sum of all the small errors in the inferred slip vectors might lead to poorer quality than the results using pure dip-slip (see also Appendix 2).

References:

- ◇ Angelier, J., 1994. Fault Slip Analysis and Paleostress Reconstruction. In: Hancock, P. L. (Ed.), Continental Deformation. Pergamon Press, Oxford, 53-100.

The Results

Table C-1

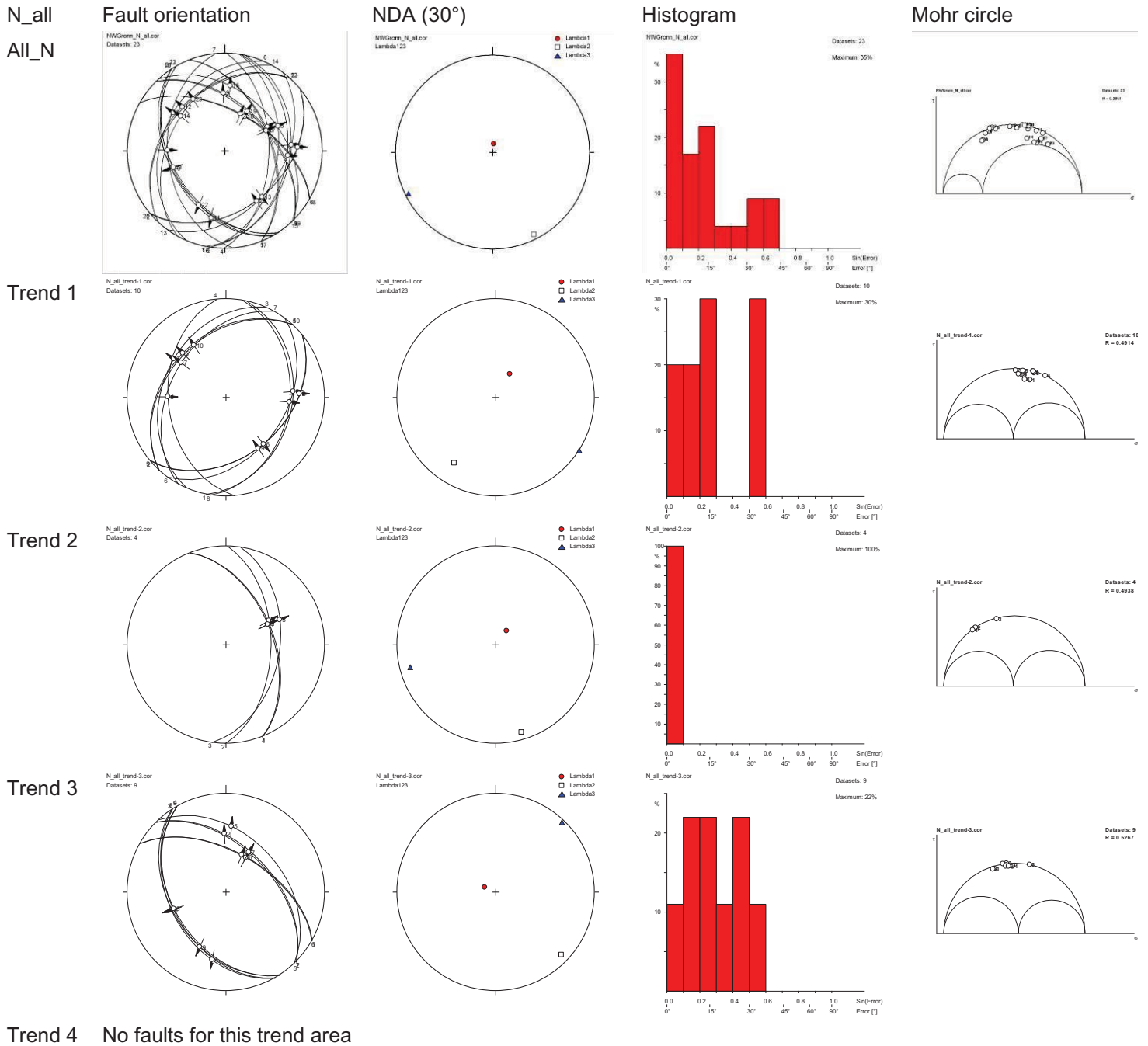
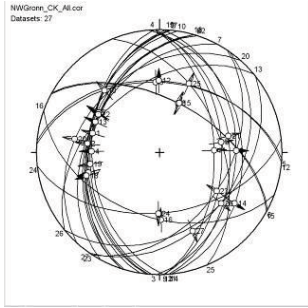


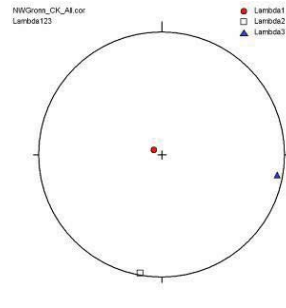
Table C-2

CK_all
All-CK

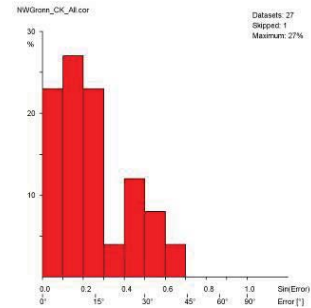
Fault orientation



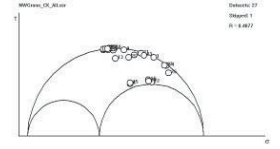
NDA (30°)



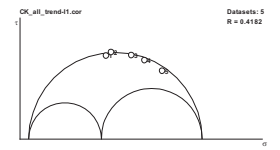
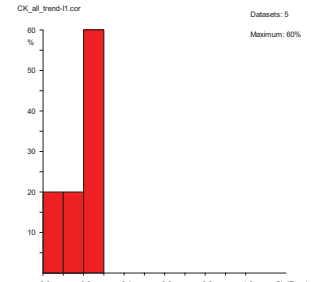
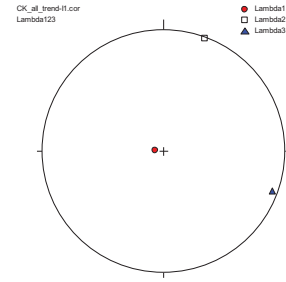
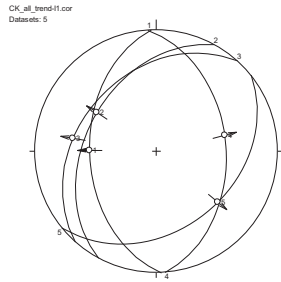
Histogram



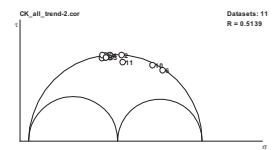
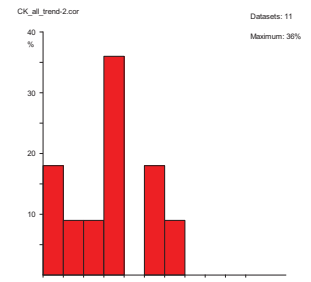
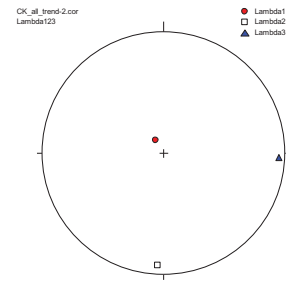
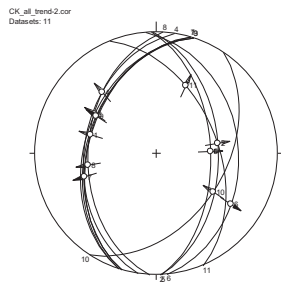
Mohr circle



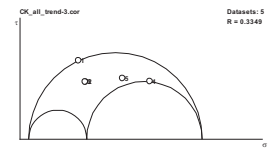
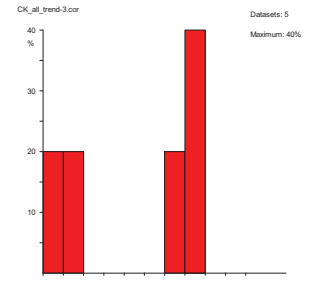
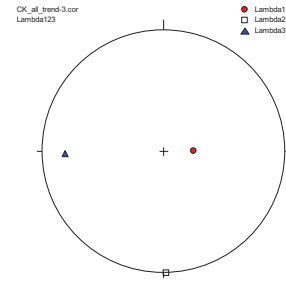
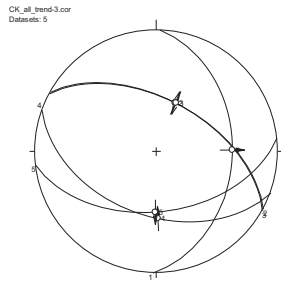
Trend 1



Trend 2



Trend 3



Trend 4

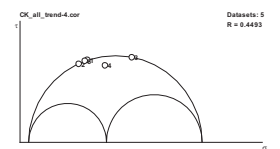
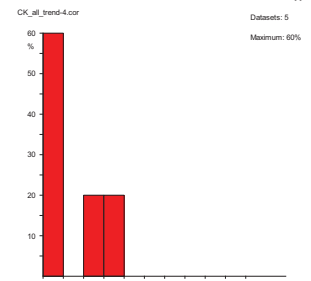
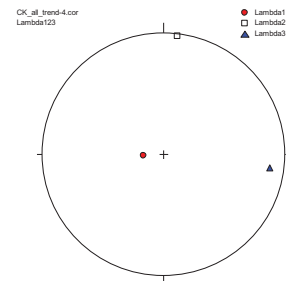
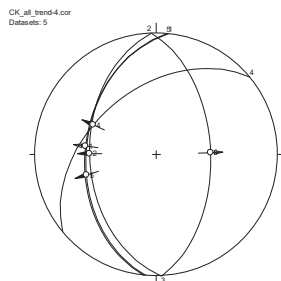


Table C-3

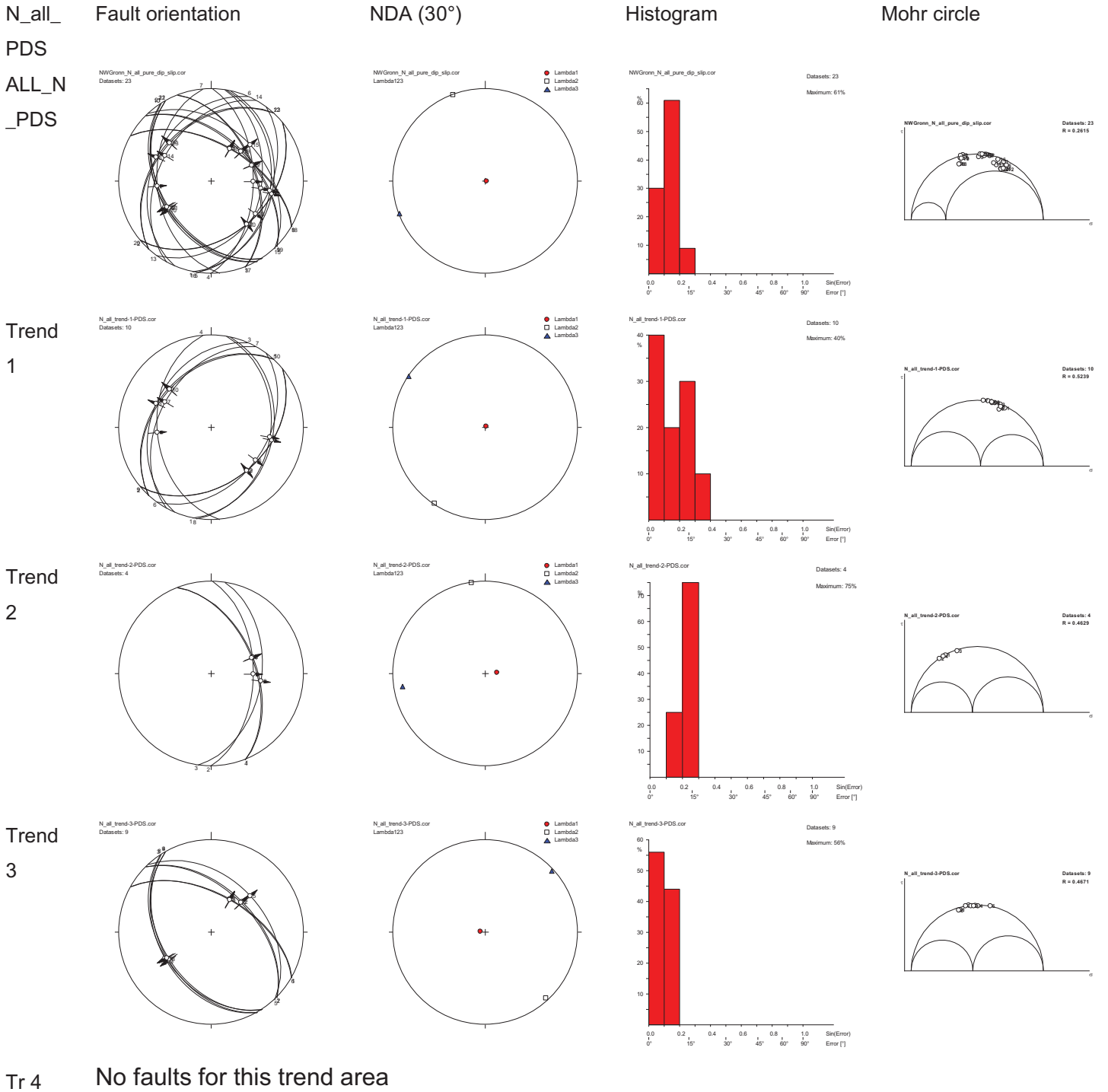


Table C-4

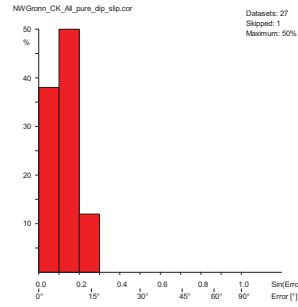
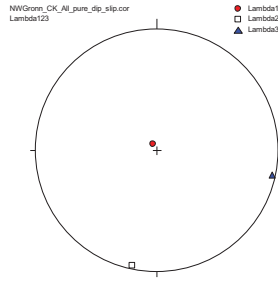
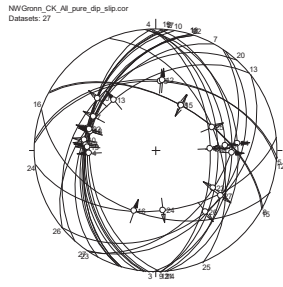
CK_all_P
DS
ALL_CK_
PDS

Fault orientation

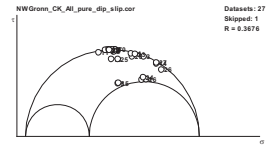
NDA (30°)

Histogram

Mohr circle

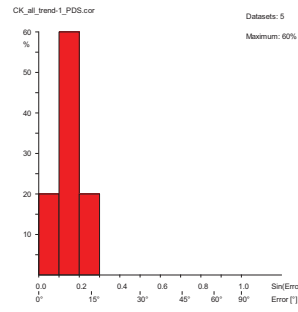
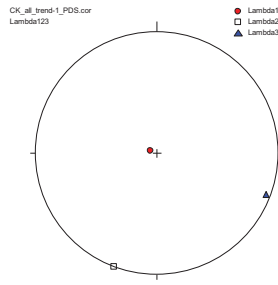
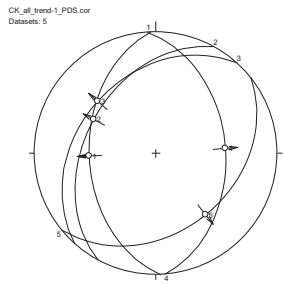


Datasets: 27
Skipped: 1
Maximum: 50%

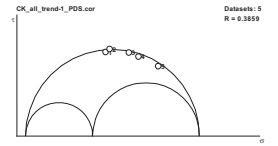


Datasets: 27
Skipped: 1
R = 0.2576

Trend 1

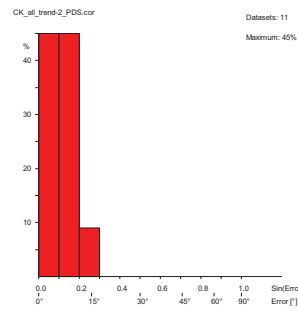
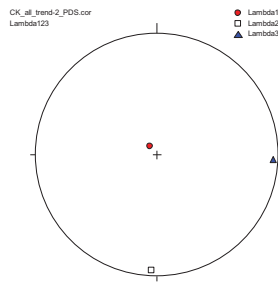
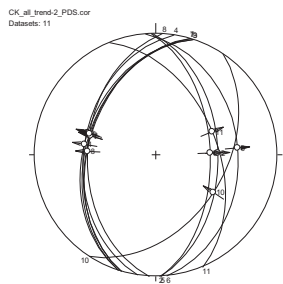


Datasets: 5
Maximum: 60%

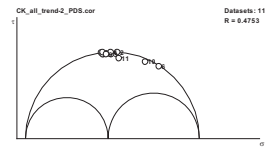


Datasets: 5
R = 0.3859

Trend 2

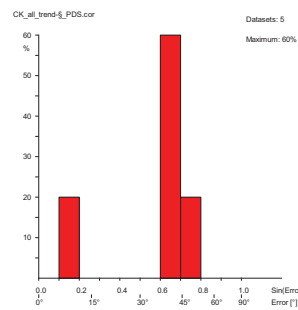
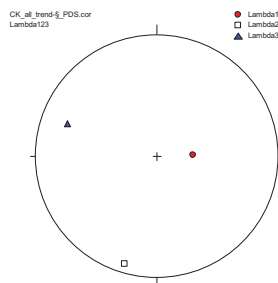
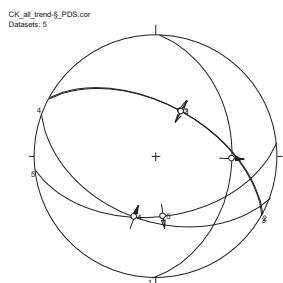


Datasets: 11
Maximum: 45%

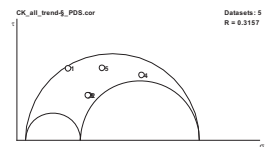


Datasets: 11
R = 0.4753

Trend 3

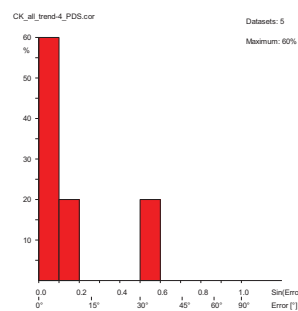
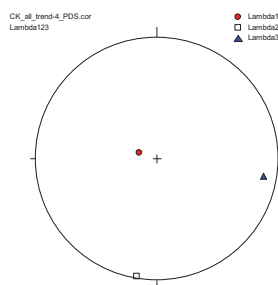
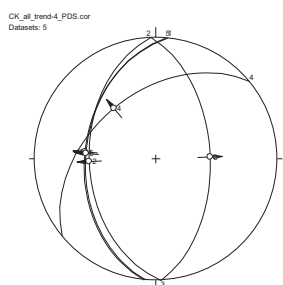


Datasets: 5
Maximum: 60%

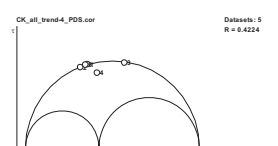


Datasets: 5
R = 0.2197

Trend 4



Datasets: 5
Maximum: 60%



Datasets: 5
R = 0.4224

Appendix 4: Synthetic data Paleostress sensitivity test

Synthetic data was used to investigate the sensitivities of the Direct Stress Inversion (DSI) method and Numerical Dynamic Analysis (NDA) to outliers. Here, 44 faults, together defining an N-S graben with pure dip slip deformation, form the backbone of this analysis. This fault set consist of two subsets with a random dip direction between 85° and 95° or 265° and 275° (each 22 faults), and a random dip between 55° and 65°. This setup was chosen as it represents a N-S orientated extension by a perfect set of conjugate fractures, but allowing for the inherent variability in orientation and expected measurement error of 5°. Based on the Andersonian theory of faulting (Anderson, 1942), one would expect the paleostress tensor of this fault-set to have a vertical σ_1 and E-W oriented σ_3 .

The paleostress analysis of this backbone does not yield results for the DSI metho. This probably stems from the symmetry in the data set, as Angelier (1994) already noted that the Direct Inversion Method can not handle conjugate faults. The NDA method does not experience this problem and shows a vertical σ_1 and E-W oriented σ_3 . The R-value is 0.5, but we note the comments of Sippel (2008) that the NDA does not always produce the correct stress ratio.

In the following nine datasets we have added an increasing number of outlier faults. Here again we observe that DSI is unable to produce a result for most of these, and when it does, the stress axes are very much influenced by the outliers and stress ratio is low (approaching 0). It is clear that heterogeneous data and outliers have a very strong influence on the calculation of the DSI. Of course it would be possible to manually remove these outliers or separate the data. However, as noted by Will and Powell (1991), in some situations it can be quite difficult to determine which data points correspond to the stress tensor under review, and which are outliers. The NDA results seem to be uninfluenced by the inclusion of outliers.

References:

- ◇ Anderson, E. M., 1942. The Dynamics of Faulting. Oliver&Boyd, Edinburgh, First edition, pp. 206.
- ◇ Angelier, J., 1990. Inversion of field data in fault tectonics to obtain the regional stress-III. A new rapid direct inversion method by analytical means. *Geophysics Journal International* 103, 363-376.
- ◇ Angelier, J., 1994. Fault Slip Analysis and Paleostress Reconstruction. In: Hancock, P. L. (Ed.), *Continental Deformation*. Pergamon Press, Oxford, 53-100.
- ◇ Sippel, J., 2008. The Paleostress History of the Central European Basin System. Dr. rer. nat. thesis, Freien Universität.
- ◇ Will, T. M., Powell, R., 1991. A robust approach to the calculation of paleostress fields from fault plane. *Journal of Structural Geology* 13(7), 813-821

DSI = Direct stress inversion (Angelier, 1990). NDA = Numerical Dynamic Analysis (Turner&Spang)

Method	Code/ faults	Stereogram/ P/T-axes	Stress	Histogram	MohrCircle
DSI	Syn1	<p>Syntheticdata1:130 Datasets: 44</p>	<p>Syntheticdata1:130 Datasets: 44</p>	<p>Syntheticdata1:130 Datasets: 44 Maximum: 100</p>	<p>Syntheticdata1:130 Datasets: 44 R = 0.4980</p>
NDA	44	<p>Syntheticdata1:130 Datasets: 44</p>	<p>Syntheticdata1:130 Datasets: 44</p>	<p>Syntheticdata1:130 Datasets: 44 Maximum: 100</p>	<p>Syntheticdata1:130 Datasets: 44 R = 0.4980</p>

Mean vect: R
P: 090 / 90 106
B: 180 / 90 106
T: 090 / 00 99?

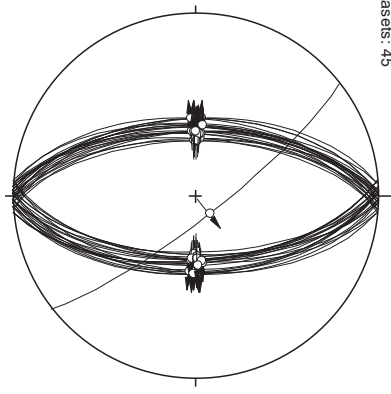
Lambda 1
Lambda 2
Lambda 3

Syntheticdata1:cor
Lambda123

Datasets: 44
Maximum: 100

Datasets: 44
R = 0.4980

SyntheticData2.fpl
Datasets: 45



Error

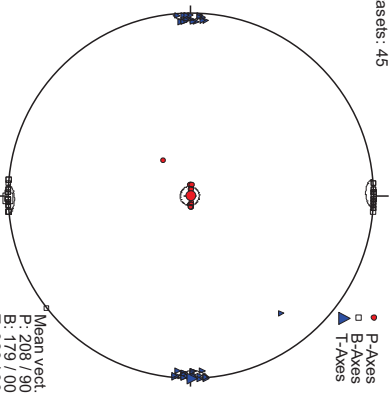
Error

Error

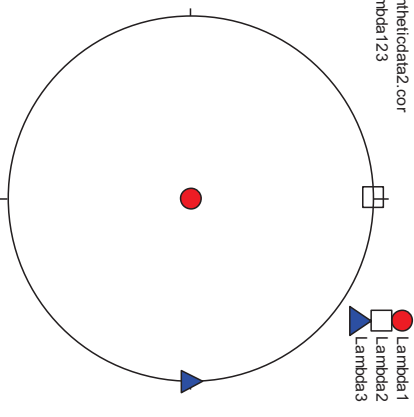
DSI

Syn2

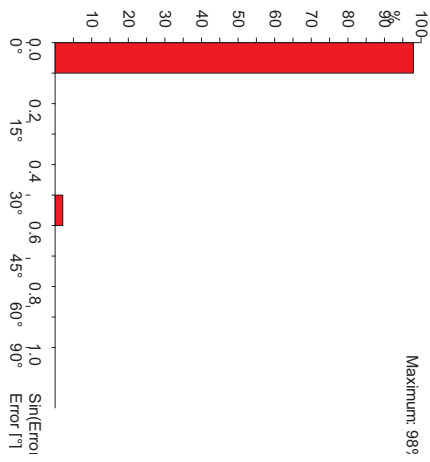
SyntheticData2.i30
Datasets: 45



SyntheticData2.cor
Lambda123

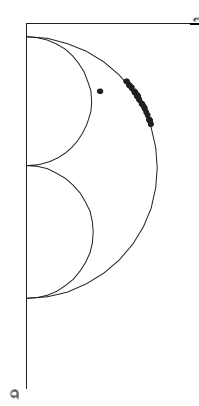


SyntheticData2.cor



Datasets: 45
Maximum: 98%

SyntheticData2.cor

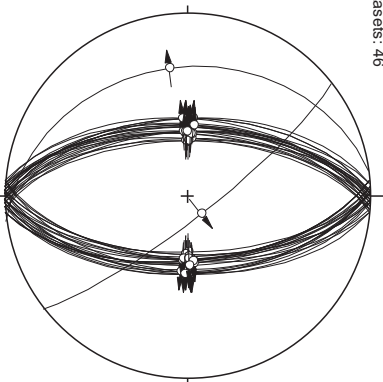


NDA

45

Mean Vect: R
P: 120 / 90
B: 178 / 90 98°
T: 089 / 00 98°

SyntheticData3.cor
 Datasets: 46



Error

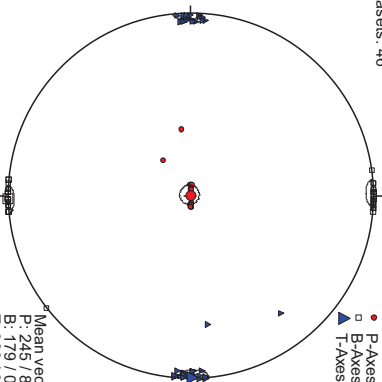
Error

Error

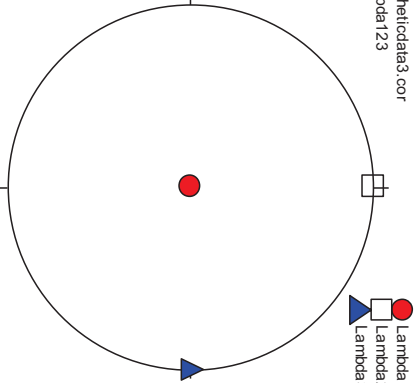
DSI

Syn3

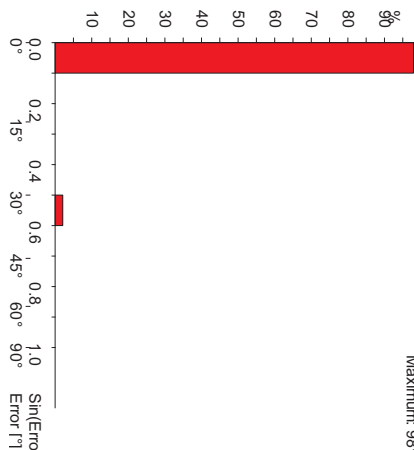
SyntheticData3.130
 Datasets: 46



SyntheticData3.cor
 Lambda123

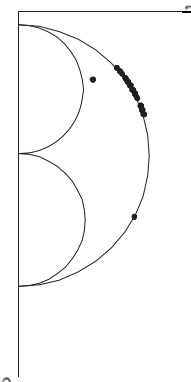


SyntheticData3.cor



Datasets: 46
 Maximum: 98%

SyntheticData3.cor



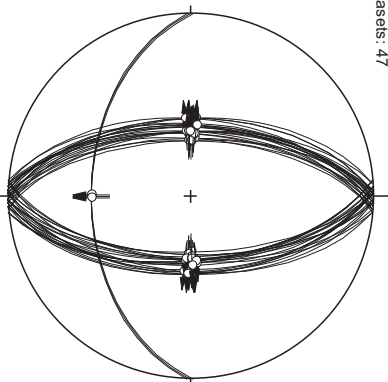
Datasets: 46
 R = 0.4931

NDA

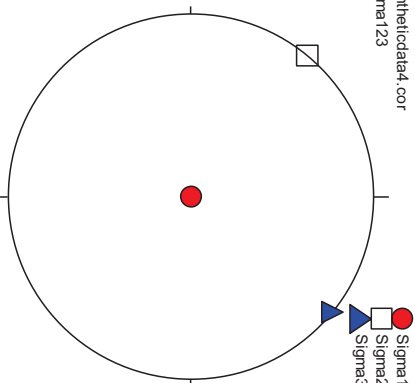
46

Mean Vect: R
 P: 44 / 80 90°
 B: 78 / 00 99°
 T: 089 / 01 98°

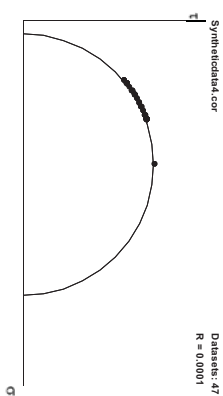
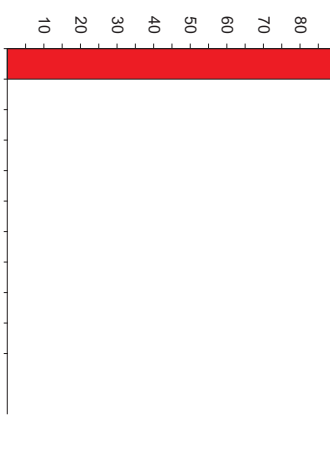
SyntheticData4.ipi
Datasets: 47



SyntheticData4.cor
Sigma123

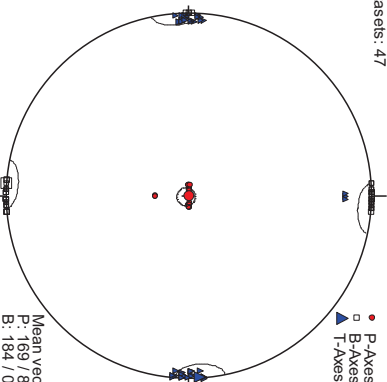


SyntheticData4.cor
Datasets: 47
Maximum: 100

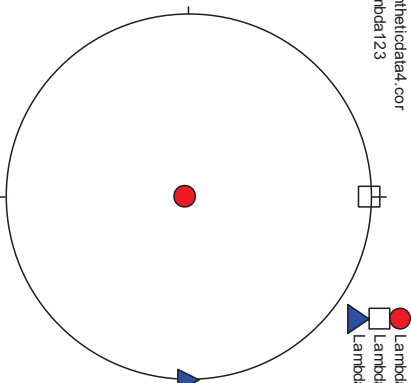


Datasets: 47
R = 0.0001

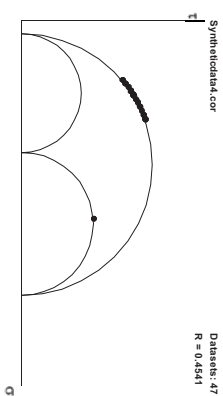
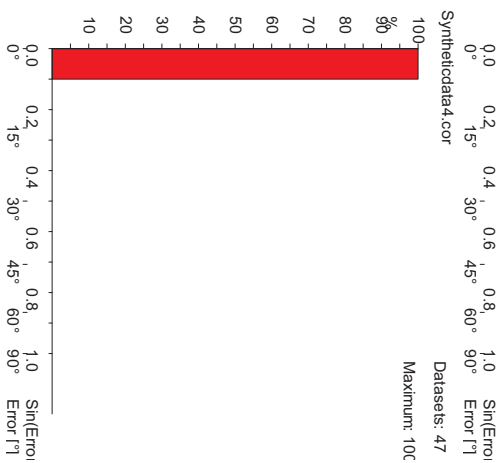
SyntheticData4.i30
Datasets: 47



SyntheticData4.cor
Lambda123

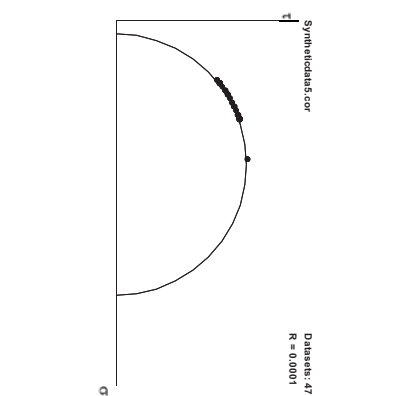
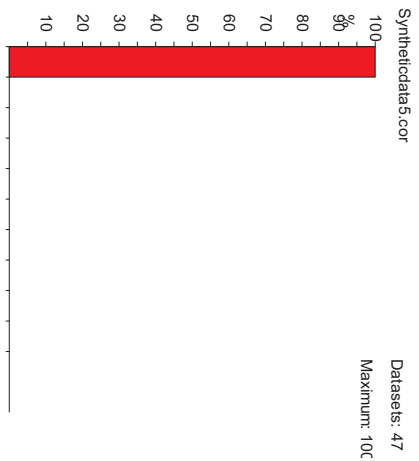
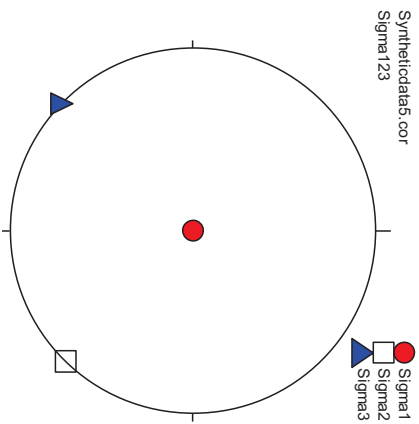
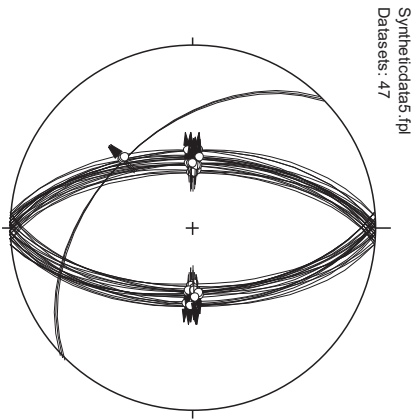


SyntheticData4.cor
Datasets: 47
Maximum: 100



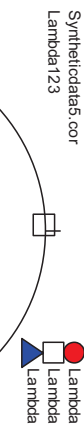
Datasets: 47
R = 0.4541

Mean vect. R
P: 184 / 00 90°
B: 184 / 00 87°
T: 086 / 01 87°



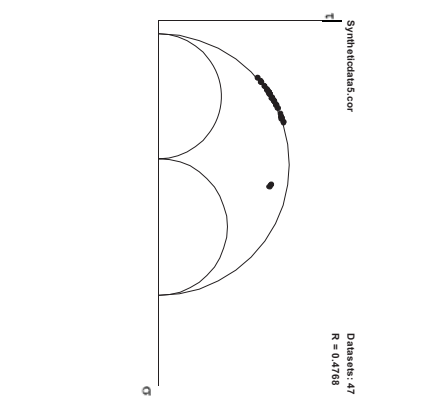
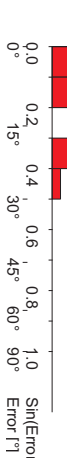
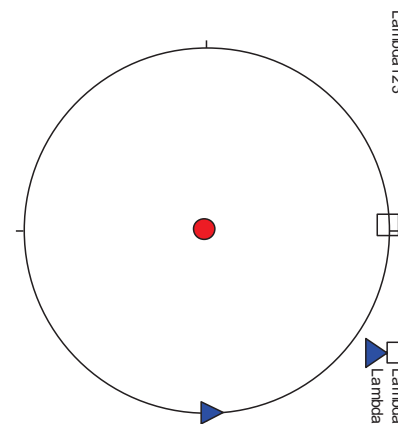
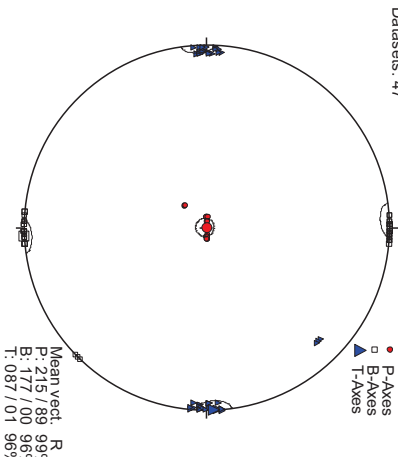
DSI

Syn5

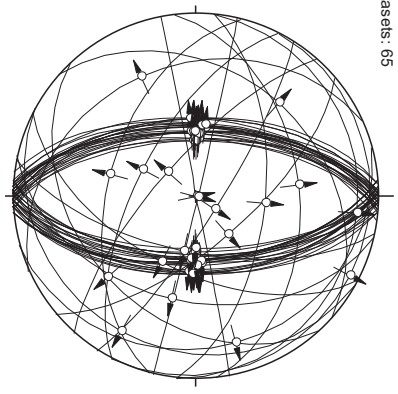


NDA

47



SyntheticData6: fpl
 Datasets: 65



Error

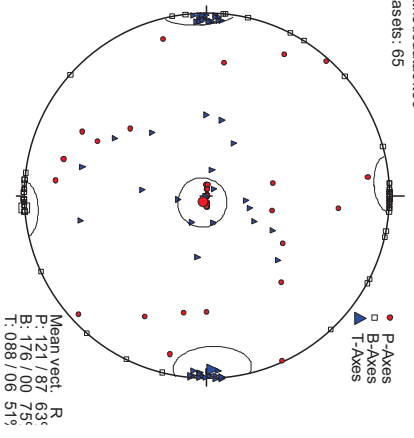
Error

Error

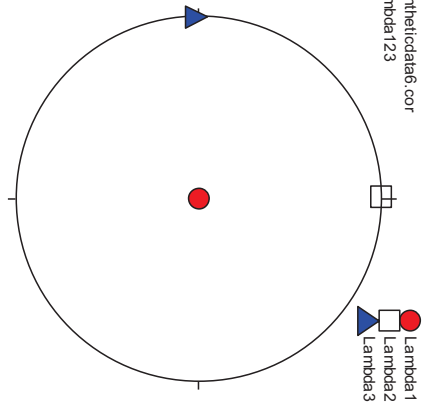
DSI

Syn6

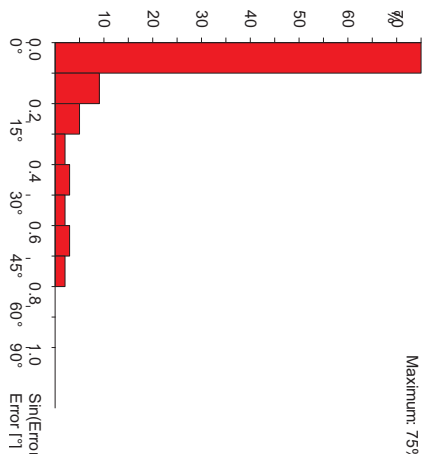
SyntheticData6: l30
 Datasets: 65



SyntheticData6: cor
 Lambda123

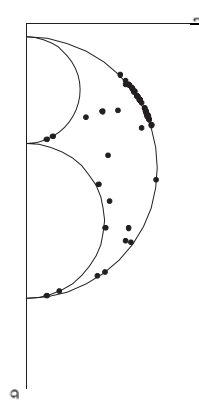


SyntheticData6: cor



Datasets: 65
 Maximum: 75%

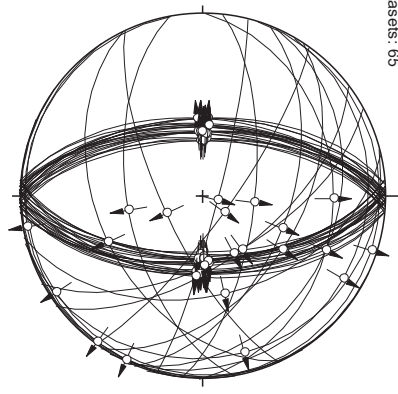
SyntheticData6: cor



NDA

65

Synthetic data 7: ipi
 Datasets: 65



Error

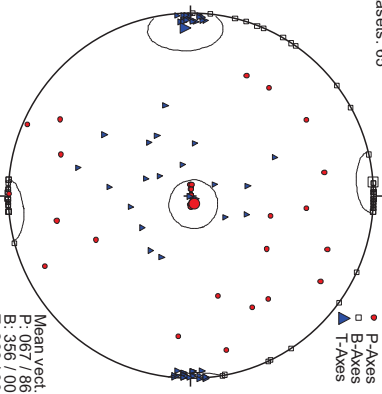
Error

Error

DSI

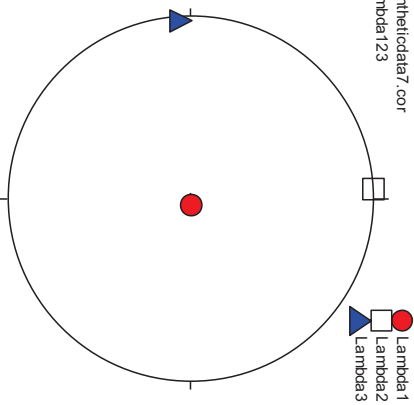
Syn7

Synthetic data 7: 130
 Datasets: 65

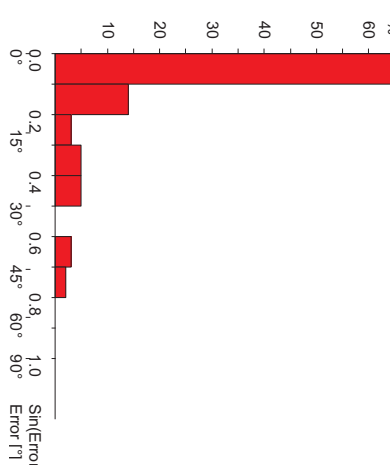


Mean Vec: R
 P: 190 / 64°
 B: 356 / 00° 70°
 T: 288 / 09° 52°

Synthetic data 7: cor
 Lambda 123

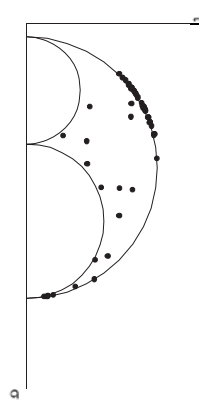


Synthetic data 7: cor
 %



Datasets: 65
 Maximum: 69%

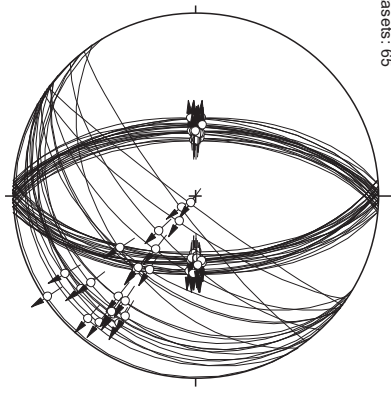
Synthetic data 7: cor



NDA

65

SyntheticData8 :ipi
 Datasets: 65



Error

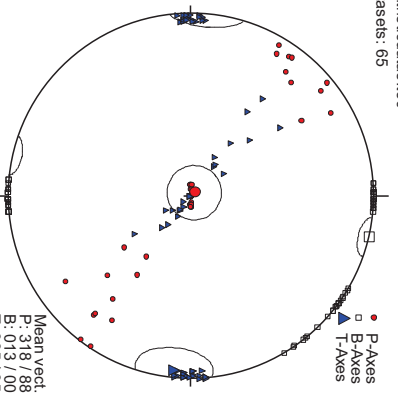
Error

Error

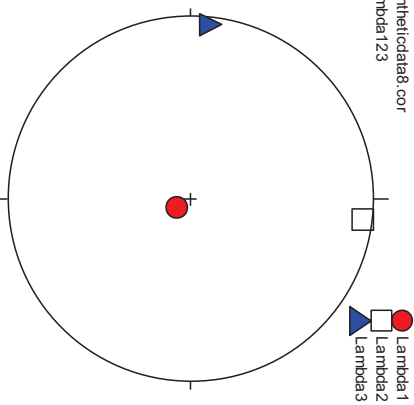
DSI

Syn8

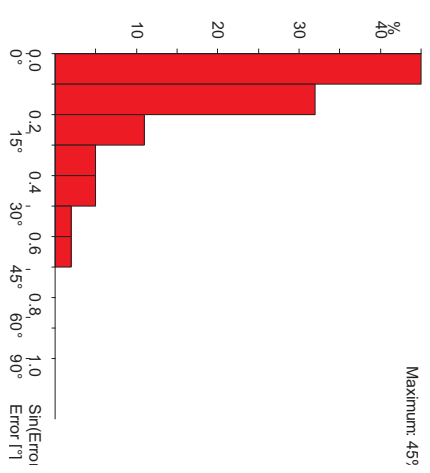
SyntheticData8 :i30
 Datasets: 65



SyntheticData8 :cor
 Lambda123

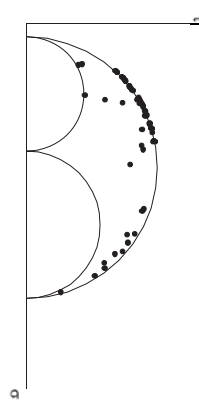


SyntheticData8 :cor



Datasets: 65
 Maximum: 45°

SyntheticData8 :cor

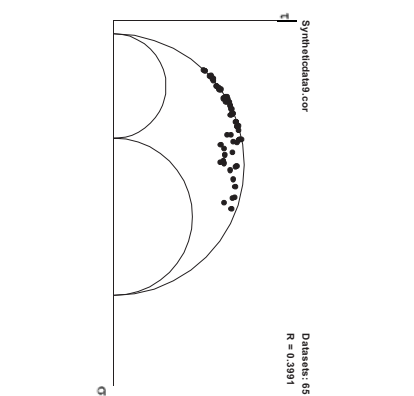
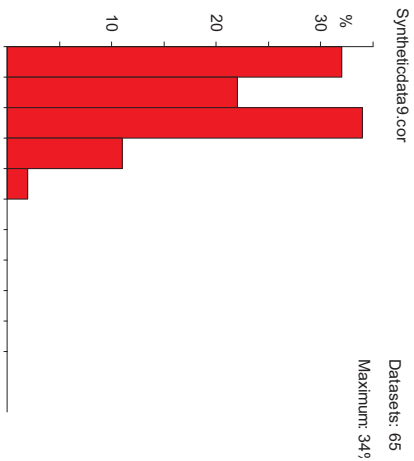
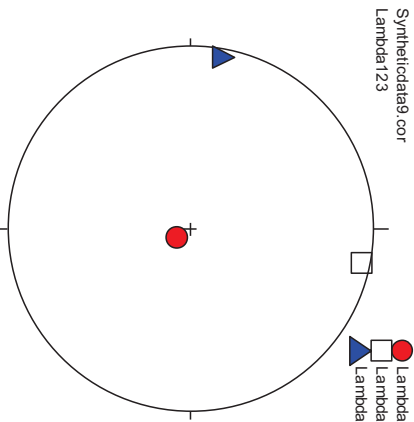
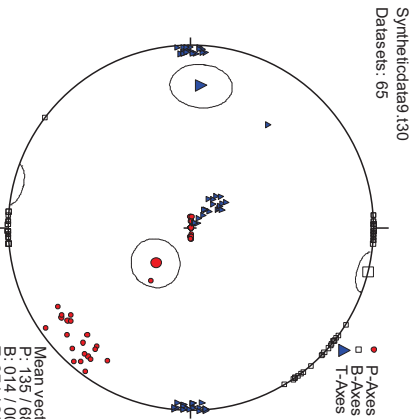
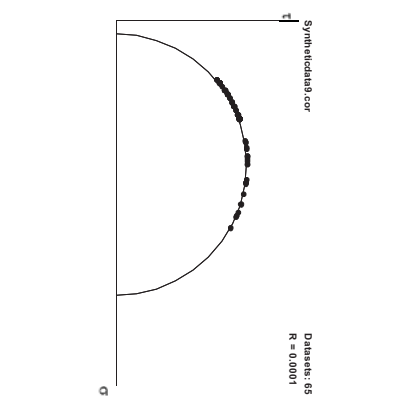
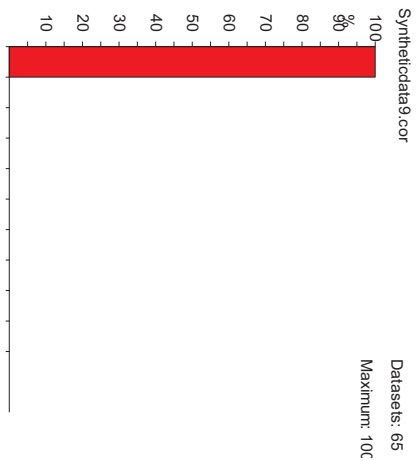
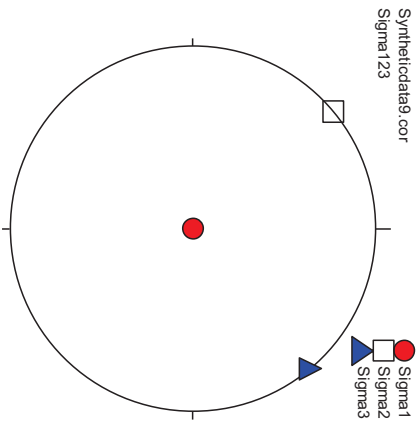
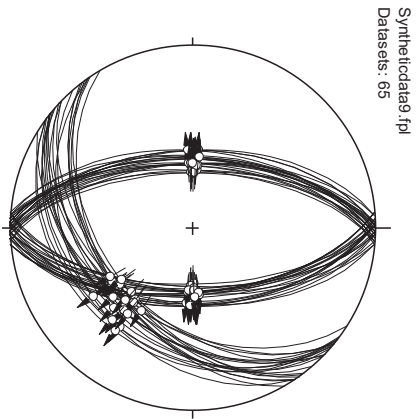


Datasets: 65
 R = 0.4374

NDA

65

Mean Vec: R
 : 118 / 56
 B: 013 / 00 88
 T: 095 / 05 519



DSI

Syn9

NDA

65

Mean vect: R
: 195 / 63°
B: 012 / 00 86°
T: 274 / 23 59°

Appendix 5: Differences between NDA with different Θ angles

In the NDA method, the theta angle (Θ , angle of internal friction) needs to be defined prior to calculation. A value of 30° is generally used for neoformed faults, as this value is empirically shown to give the best results (Sperner et al., 1993; Meschede, 1994; Sperner, 1996). For reactivated faults, the value of 45° is recommended (Klaus Reicherter, personal communication, 2006). Tectonics FP allows the calculation of the so-called “best-fit theta angle”. This angle is the result of a stepwise calculation of the PT-axes using different theta angles between 10° and 85° until an optimum clustering of the PT-axes is found (Tectonics FP Help). In this appendix a comparison is made between the use of theta angles of different values. These values are 30° , 45° and the best fit theta angle, calculated by Tectonics FP. The different fault sets described in Chapter 1 were used for this analysis.

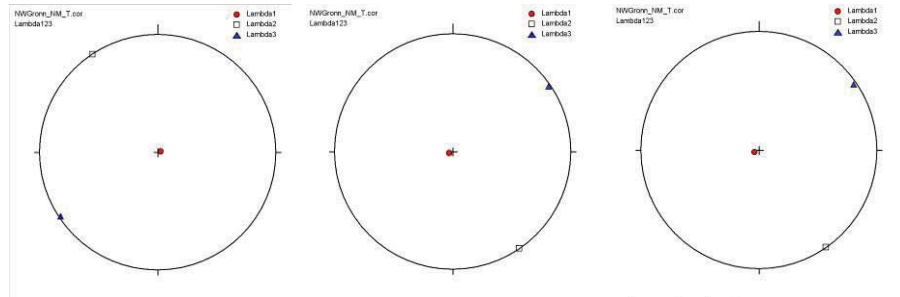
The comparison of output using these theta angles shows that the differences between the output paleostress axes are within 20° and often smaller than 10° . This places them well within the general uncertainty of the analysis as well as the uncertainty usually associated with field measurements. The R-value does not show a significant difference when different theta values are used either. The use of different theta angles (between 30° and 60°) is shown not to have a large impact on the output of the NDA method in this dataset.

References:

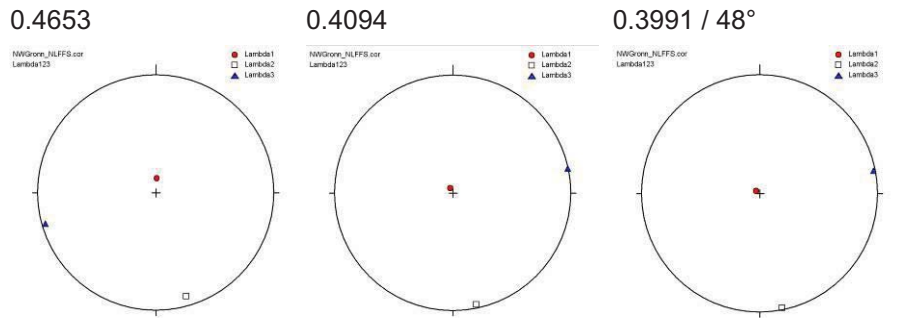
- ◇ Meschede, M., Ratschbacher, L., Frisch, W., Herrman, U. R., 1994. The relation between plate convergence and paleostress fields: fault-slip analyses in southern Mexico and along the Motagua-Polochic fault system in Guatemala. TSK 5, Göttingen, 6.4.1994, Göttinger Arbeiten Geologie und Paläontologie, 252-255.
- ◇ Sperner, B., 1996. Computer programs for the kinematic analysis of brittle deformation structures. In: Frisch, W. (Ed.), Tübinger Geowissenschaftliche Arbeiten Reihe A, 27, Tübingen.
- ◇ Sperner, B., Ratschbacher, L., Ott, R. 1993. Fault-striae analysis: a Turbo pascal program for graphical presentation and reduced stress tensor calculation. Computers & Geosciences 19(9), 1361-1388.

Code: Paleostress axis (NDA 30°): Paleostress axis (NDA 45°): Paleostress axis (best fit):

NM



R / Theta
NLFFS

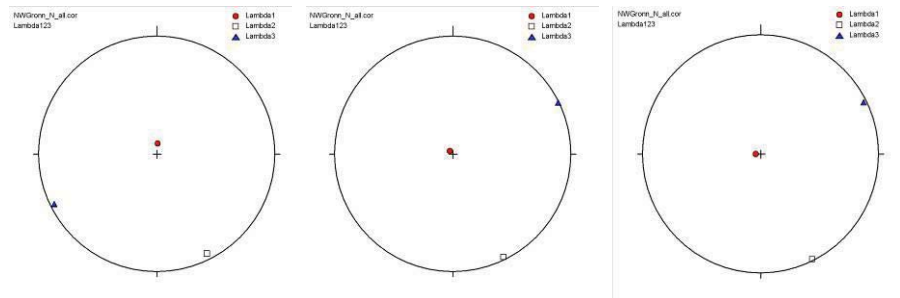


R / Theta
NL_undef
N_B

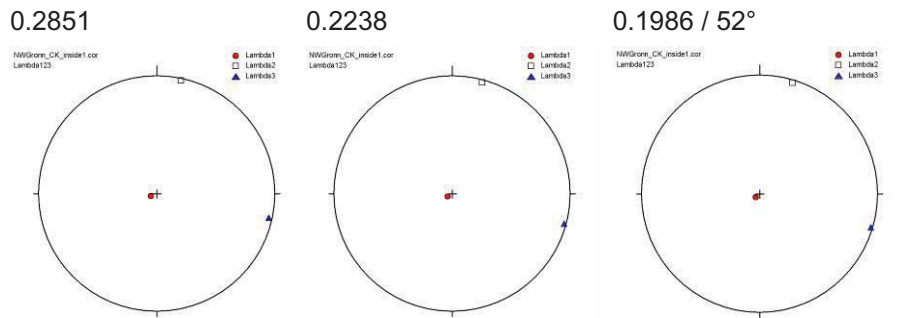
0.1863 0.1401 0.1249 / 50°

No fault movement
No fault movement

All North Sea data



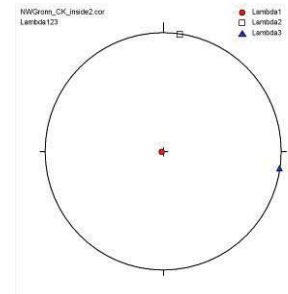
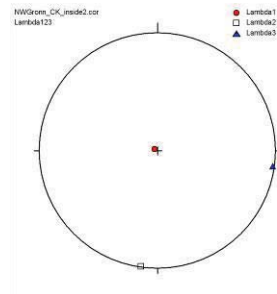
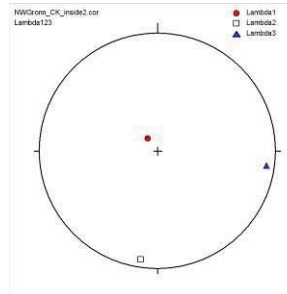
R / Theta
CK_Chalk_
inside1



R / Theta



CK_Chalk_inside
2



R / Theta

0.3563

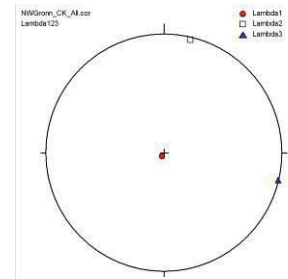
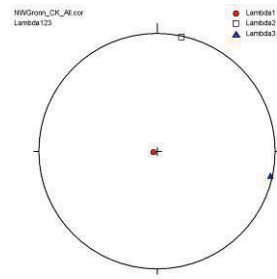
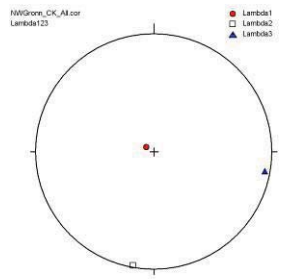
0.3767

0.3784 / 48 °

CK_B

No fault movement

All Chalk Data



R /theta

0.4077

0.3878

0.3795 / 52°

KN_B

Deposits to thin

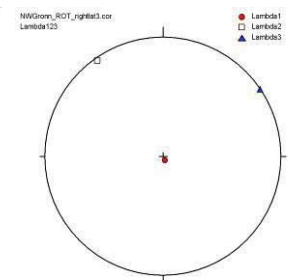
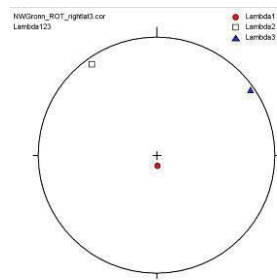
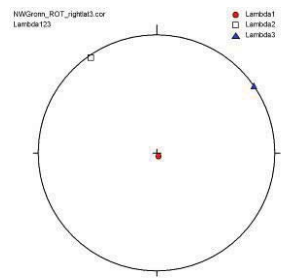
RNRO1_T

Deposits to thin

PZ_T

Deformation not brittle

ROTL_T



R / Theta

0.3980

0.3889

0.3973 / 32°

Appendix 6: The stratigraphy of the Dutch Zechstein⁶

In the Dutch subsurface, the Zechstein can be subdivided in a marine lower part (Z1-Z3) and a playa type upper part (Z4 and Z5), with a more clastic type of deposits (Geluk, 1997, 2000). In the northern Netherlands the oldest five of the total seven Zechstein cycles are preserved, but the record gets incomplete towards the south (see Fig. 1, see also Chapter 3, Taylor, 1998; TNO-NITG, 2004; Geluk, 2007).

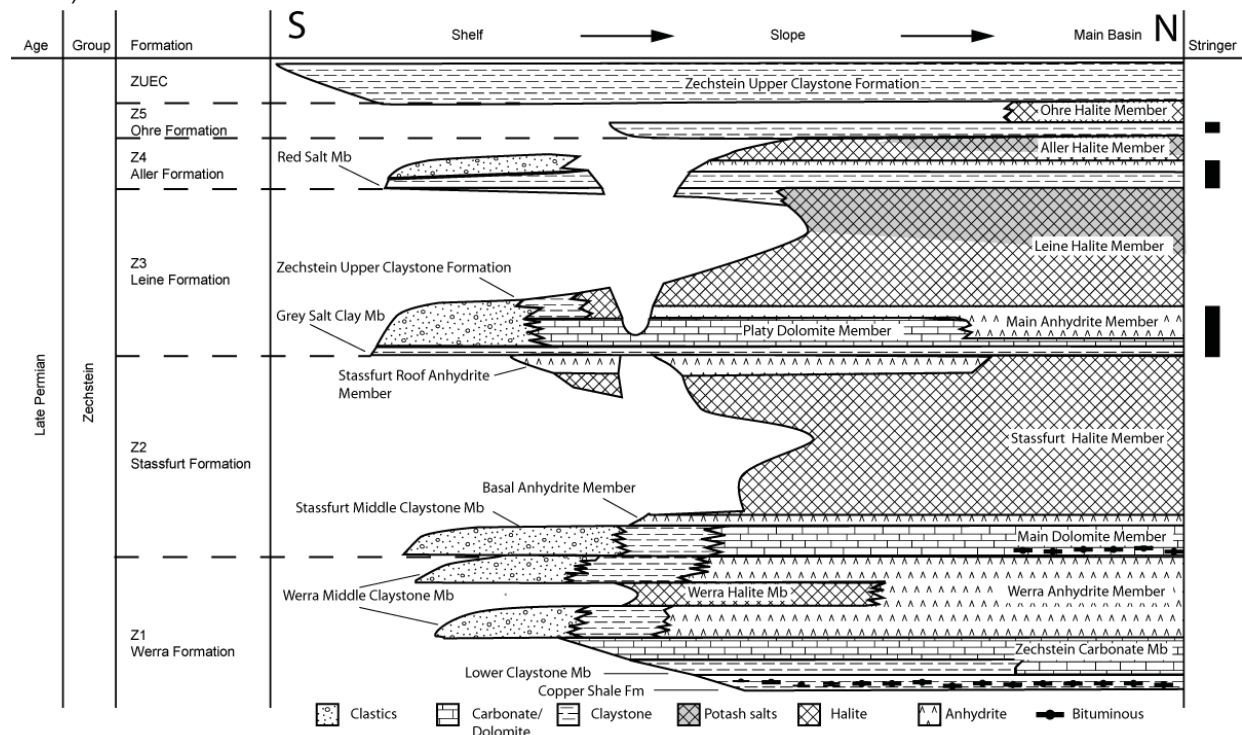


Figure 1: Simplified stratigraphic column for the Dutch subsurface. South is to the left, north to the right. Note the subdivision between shelf, slope and basin. Based on Van Adrichem-Boogaert and Kouwe, 1993-1997, Geluk, 2000 and TNO-NITG, 2004

The Zechstein carbonates facies

Time equivalent Zechstein carbonate deposits in the Netherlands are subdivided in shelf, slope and basin facies (Taylor, 1998; Geluk, 2000; Geluk, 2007, see also Fig. 1). This subdivision is based on the Zechstein carbonate members that show a pronounced sigmoidal shape in N-S sections. This results from the members being draped on the underlying aggradational infill of the basin. The maximum thickness of the carbonate members is observed on the slope. The platform carbonates consist of shallow water deposits such as lagoonal, bioclastic or oolitic carbonates, reefs and carbonatic sandstones which experienced occasional subaerial exposure. The slope facies consists of a transition of platform to basin facies: In the carbonate deposits of the Zechstein individual reefs and off-platform highs are observed in the slope facies (Geluk, 2000). Slumps, grain and mass flows are

⁶ This is an extended stratigraphic description of the Zechstein formation in the Netherlands, based on the stratigraphic section of Chapter 3

also observed. The basin facies were deposited in water depths of several tens of meters with a basin depth up to 200 m during Z2 deposition. Basin carbonates can contain high Total Organic Content (TOC) (Geluk, 2000). Redeposition of platform facies is observed in the basin.

Zechstein stratigraphy

The Z1 Werra deposits, including the bitumous Coppershale deposits, are less than 50 m thick in the Netherlands (Geluk, 2007). Both the Groningen area and the off-shore study area contain no Z1 halite, as deposition was restricted to the Central Netherlands Basin (see Fig. 1). The Main Zechstein Basin was formed by a starved basin, with mixed carbonate, clay and evaporitic anhydrite deposition.

The 30-90 m thick Z2 Main Dolomite member is deposited directly on top of the Z1 deposits in both study areas. The Z2 halites (Stassfurt Formation) are deposited after the Basal Anhydrite Member. They reach thicknesses between 500 and 600 m of primary thickness in both study areas, but this thickness was later modified by salt tectonics (Geluk, 2007). On the slope and platform anhydrite is deposited as a last Stassfurt deposit before the deposition of the Z3 Leine Formation. This starts with a roughly 1 m thick grey shale (Grey Salt Clay), which is characterized by a sharp Gamma-ray peak in wireline logs, though not as strong as the equivalent Z1 Copper Shale formation (Taylor, 1998). The Z3 Platy Dolomite is equivalent to the Seaham Formation in Durham and the Brotherton formation, found in Yorkshire (Taylor, 1998). The dolomite reaches thicknesses of 30 m (in Seaham, Smith, 1995) to 75-90 m on the shelf, which is considerably more than in the basin where it reduces to several meters (Taylor, 1998). The Platy Dolomite consists of grey microcrystalline dolomite, with thin shaly layers (Taylor, 1998). Depositional settings were mainly shallow, quiet water, with water depths up to several tens of meters (Taylor, 1998; Geluk, 2000). On top of the Z3 Carbonate, a series of sabkha cycles is identified, which consists of algal mats and nodular anhydrite before grading into the overlying Hauptanhydrit (Main Anhydrite, Taylor, 1998). In the Gorleben salt structure (east of Hamburg, Germany), this member consist of grey to blue anhydrite with brownish shaly marls and thin layers of magnesite, which represents algae structures (Siemann and Ellendorff, 2001). In the Dutch part of the basin the thickness of the Main Anhydrite increases from 3 m on the shelf to 45 m in the basin, with local excursions to 100 m and complex changes in thickness (Taylor, 1998; Geluk, 2000).

The Z3 halite deposits of the Leine Formation, contain a halite basal part, but the upper part consists of two thick potassium-magnesium salt layers, which includes beds of bischofite, kieserite, carnallite and sylvite (Coelewij et al., 1978). Thicknesses of the Z3 halite are 200-300 m in the Groningen area, while in the offshore study area primary thickness of roughly 100 m are observed (Geluk, 2007).

During the deposition of the Z4 Aller Formation permanent hypersaline conditions were reached. The Aller formation consists of the Red Salt Clay and a thin layer of the Pegmatit Anhydrit member, both being only several meters thick (Geluk, 2007), followed by Z4 Salt. The Z4 deposits reaches no more than 50 m thickness (Geluk, 2007). The middle of the Z4 Salt consists of potassium-magnesium salts, and the top contains alterations of halite and claystone. Combined with the deposition of sabkha anhydritic claystones along the basin edge, these deposits were interpreted as playa deposits (Geluk, 1997, 2000). The Z5 Ohre Formation is only deposited in the northeast of the Dutch onshore and the northwest of the offshore. It consists of a several meter thick basal claystone and a halite layer with a

thickness up to 15 m (Geluk, 2007). The Z5 was not deposited in the present study areas. The Z6 and Z7, described by Best (1989) are not found in the Netherlands. The youngest Zechstein deposit is the Upper Claystone Formation. It occurs throughout the Netherlands and is comprised of red and grey anhydritic claystones, and is between 10 and 50 m thick (Geluk, 2007).

References

- ◇ Best, G., 1989. Die Grenze Zechstein/Buntsandstein in Nordwest-Deutschland nach Bohrlochmessungen. *Zeitschrift der Deutschen Gesellschaft für Geowissenschaften* 140, 73-85.
- ◇ Coelewijn, P. A. J., Haug, G. M. W., Kuijk, H. v., 1978. Magnesium-salt exploration in the Northeastern Netherlands. *Geologie en Mijnbouw* 57(4), 487-502.
- ◇ Geluk, M. C., 1997. Peleogeographic maps of Moscovian and Artinskian; contributions from the Netherlands. In: DSoleau, S. & De Wever, P. (Eds.), *Peri-Thetys stratigraphic correlations*. *Geodiversitas* 19, 229-234.
- ◇ Geluk, M. C., 2000. Late Permian (Zechstein) carbonate-facies maps, the Netherlands. *Geologie en Mijnbouw/ Netherlands Journal of Geosciences* 79(1), 17-27.
- ◇ Geluk, M. C., 2007. Permian. In: Wong, T. E., Batjes, D. A. J. & De Jager, J. (Eds.), *Geology of the Netherlands*. Royal Netherlands Academy of Arts and Sciences, Amsterdam, 63 - 84.
- ◇ Siemann, M. G., Ellendorff, B., 2001. The composition of gases in fluid inclusions of late Permian (Zechstein) marine evaporites in Northern Germany. *Chemical Geology* 173, 31-44.
- ◇ Smith, D. B., 1995. Chapter 3: North-east England (Durham Province), *Marine Permian of England*. *Geological Conservation Review* 8, 205.
- ◇ Taylor, J. C. M., 1998. Upper Permian - Zechstein. In: Glennie, K. W. (Ed.), *Petroleum Geology of the North Sea. Basic Concepts and Recent Advances* (fourth edition). Blackwell Science, Oxford, 174-211.
- ◇ TNO-NITG. 2004. *Geological Atlas of the Subsurface of the Netherlands - onshore*. TNO-NITG, Utrecht, pp. 103.
- ◇ Van Adrichem-Boogaert, H. A., Kouwe, W. F. P., 1993-1997. *Stratigraphic Nomenclature of the Netherlands; revision and update by RGD and NOGEP*. TNO-NITG, *Mededelingen Rijks Geologische Dienst*, Haarlem, 50, pp. 50.

Summary

The pre-drilling prediction of (paleo)-stress helps defining fracture and fault patterns which can either help or hinder hydrocarbon production, and helps to decipher the tectonic history of the crust. At the moment, paleostress studies are mostly based on the detailed mapping of faults and movement directions in the field. This limits the applicability of this approach to areas where the rocks of interest are outcropping and excludes sedimentary basins. In this work, a method is developed and tested to determine the paleostress stratigraphy solely based on 3D reflection data, and the initial work for a similar approach for ductile evaporites is presented.

For the determination of paleostress, knowledge of the orientation and slip direction of the individual faults in the set is required. Both in field and seismic surveys it is relatively easy to determine the fault orientation. Determining the slip direction however remains a challenge in seismic data. In field studies, measurement of the slickenside orientation provides a quick and easy slip direction determination, but these structures are too small to be resolved in seismic data. Due to the converging pattern of slip lines, the measured slickenline does not need to represent the tectonic movement direction. Furthermore, since faults generally rupture in a number of seismic events distributed over the fault plane, contradicting slip directions formed during the same tectonic phase can overprint each other, complicating the interpretation of field based slip determination.

The easiest way to determine the slip direction on faults is by connecting two points that were on direct opposite sides of the fault, prior to deformation. Unfortunately, no faulted channels or lineaments were present in the data set. By careful mapping of the Allan lines however, the slip directions of a number of faults, over a number of time periods were constrained. This data allowed for the determination of the paleostress stratigraphy of the NW corner of the Groningen High in the Netherlands, spanning from the Triassic to present-day. The paleostress states correspond well with published paleostress data.

The roughness of fault planes is however not limited to the scale of slickensides. Also larger undulations are present on the fault surfaces. Recent publications, based on LiDAR measurements of outcropping faults suggest that these undulations are in the direction of fault slip. Detailed interpretation of several faults in the relatively brittle Upper Cretaceous Chalk from the same area showed that in reflection seismic, undulations are present in interpretations in different directions. It is also shown that these undulations are unlikely to be the result of aliasing, or interpolation effects. The determination of the orientation and slip direction of over 200 faults allowed the determination of the Upper Cretaceous paleostress. This result corresponds well to the paleostress results with the geometrically determined slip direction, and published results.

The Late Permian Zechstein deposits of Europe consist for a large part of (ductile) evaporites. This interval decouples sub- and supra-salt deformation. The ductile deformation of these deposits does not allow the determination of the paleostress evolution using the above discussed method. However, an enclosed brittle layer, fully encased in the ductile salts, allows the visualization of the extremely complex deformation patterns, and can serve as a strain marker in these deposits. Structures observed, include various types of disharmonic folds, superimposed on the harmonic folding, which follows the top of the salt, ductile rupture (boudins) and zones of early diagenetic/sedimentary thickness

increase. The latter seem to affect younger deformation. These zones seem to influence the location of salt structures, showing that early structures can affect the salt tectonics and deformation of supra-salt deposits.

Zusammenfassung

Vorhersagen über den (Paläo-)spannungen im Vorfeld von Bohrungen erlauben Aussagen über Bruch- und Störungsmuster, welche im Zuge der Kohlenwasserstoffproduktion sowohl hilfreich, als auch hinderlich sein können. Desweiteren helfen sie bei der Entschlüsselung der tektonischen Geschichte der Erdkruste.

Paläospannungsstudien basieren z. Z. weitestgehend auf der detaillierten Kartierung von Störungen und Bewegungsrichtungen im Aufschluss. Die Anwendbarkeit dieses Ansatzes ist auf Bereiche begrenzt, in denen die entsprechenden Gesteine im Aufschluss zugänglich sind, was Sedimentbecken ausschließt.

In der vorliegenden Arbeit wurde eine Methode entwickelt und getestet die Paläospannungsstratigraphie einzig auf der Basis von 3D reflexionsseismischen Bildern zu ermitteln. Desweiteren wird ein entsprechender Ansatz zur Anwendbarkeit der Ergebnisse auf duktile Evaporite vorgestellt.

Zur Ermittlung der Paläospannungen sind Informationen über Orientierung und Bewegungsrichtung individueller Störungen eines Datensatzes notwendig. Die Orientierung einer Störung lässt sich sowohl im Gelände, als auch aus der Seismik relativ einfach bestimmen. Ihre Bewegungsrichtung aus seismischen Daten zu gewinnen ist hingegen eine Herausforderung. Harnische, welche im Aufschluss schnell und einfach auf den Bewegungsvektor schließen lassen, sind zu kleinmaßstäblich um in seismischen Daten aufgelöst zu werden. Desweiteren konvergieren Harnische in der Regel entlang der Störungsfläche, weshalb ein gemessener Bewegungsindikator nicht unbedingt die wahre tektonische Bewegungsrichtung anzeigt. Darüber hinaus verteilt sich der Gesamtversatz einer Störung auf eine Vielzahl von untergeordneten seismischen Ereignissen entlang der Störungsfläche. Die Folge sind eine Vielzahl sich überlagernder Bewegungsrichtungen innerhalb eines tektonischen Regimes, was die Deutung der absoluten Bewegungsrichtung aus Aufschlussdaten zusätzlich erschwert.

Der einfachste Weg den Bewegungsvektor einer Störung zu bestimmen ist es zwei auf gegenüberliegenden Seiten der Störung befindliche Punkte miteinander zu verbinden, welche vor der Deformation unmittelbar nebeneinander lagen. Leider waren keine gestörten Kanäle oder Lineare im Datensatz enthalten. Durch sorgfältiges Kartieren der „Allan lines“ konnte jedoch der Versatz an einer bestimmten Anzahl Störungen über bestimmte Zeiträume eingegrenzt werden. Diese Daten erlaubten eine Rekonstruktion der Paläospannungsstratigraphie des Nordwestlichen Teils des Groningen Hochs in den Niederlanden über den Zeitraum von der Trias bis heute. Die Paläospannungszustände sind in guter Übereinstimmung mit bereits publizierten Paläospannungsdaten.

Die Rauigkeit von Störungsflächen ist nicht auf Harnische beschränkt. Es finden sich auch Uregelmäßigkeiten größeren Maßstabs. Aktuelle Veröffentlichungen zeigen anhand von LIDAR Messungen an offenliegenden Störungsflächen, dass diese Unregelmäßigkeiten die Bewegungsrichtungen der Störungen anzeigen. Detaillierte Interpretation einiger Störungen in relativ spröden Gesteinen der Oberkreide aus der entsprechenden Gegend zeigen in der Reflexionsseismik Unregelmäßigkeiten, auch wenn diese Flächen in verschiedenste Richtungen interpretiert wurden. Es

wird gezeigt, dass diese Unregelmäßigkeiten mit großer Wahrscheinlichkeit nicht auf Aliasing oder Interpolationseffekte zurückzuführen sind.

Die Analyse der Raumlage und Bewegungsrichtung von über 200 Störungen erlaubte die Bestimmung der Paläospannung in der Oberkreide. Das so gewonnene Ergebnis ist in Übereinstimmung mit den Paläospannungsergebnissen aus geometrisch bestimmten Bewegungsrichtungen, sowie mit Literaturdaten.

Die Oberpermischen Zechstein Ablagerungen in Europa bestehen in erster Linie aus (duktilen) Evaporiten. Dieses Intervall entkoppelt Sub- und Suprasalzdeformation voneinander. Das duktile Deformationsverhalten dieser Ablagerungen erlaubt es nicht die Paläospannung mit Hilfe der vorgestellten Methoden zu bestimmen. Allerdings ermöglicht ein vollständig in das duktile Salz eingeschlossenes, sprödes Schichtpaket die Visualisierung des extrem komplexen Deformationsmusters und dient als Verformungsindikator in diesen Ablagerungen. Sichtbare Strukturen umfassen neben verschiedenen Typen disharmonischer Faltung, welche die der Oberseite der Salzschieht folgenden harmonische Faltung überlagern, auch duktile Brüche (Boudins) und Zonen frühsedimentärer/diagenetischer Mächtigkeitzunahme, welche die spätere Deformation zu beeinflussen scheint. Diese Zonen scheinen die Lokalisierung von Salzstrukturen zu beeinflussen, was zeigt das junge Strukturen Einfluss auf die spätere Salztektonik und Deformation von den, das Salz überlagerenden, Ablagerungen haben können.

Curriculum Vitae

Heijn W. van Gent

Heijnderik Willem van Gent

Nationality: Dutch

Date of Birth: February 28, 1982

Education and Employment

December 2009 – present

Post-Doc at the Institute for Geologie – Endogene Dynamik, RWTH Aachen, Germany.

February 2006 – December 2009

PhD student at the Institute for Geologie – Endogene Dynamik, RWTH Aachen, Germany.

Quantitative reconstruction of the temporal evolution of stress in the Dutch Basins – Stress and strain from reflection seismic data.

September 2001 - January 2006

Master of Geology, Faculty of Geosciences, University of Utrecht.

Scaled Analogue Models of the Evolution of Normal Fault Systems in Carbonates. Supervisor: Professor J.L. Urai, Institute for Geologie – Endogene Dynamik, Rheinisch-Westfälische Technische Hochschule (RWTH), Aachen, Germany.

September 2000 - July 2001

Propeduse Earth Sciences, Faculty of Geosciences, University of Utrecht.

Diploma: September 2001. Grade: With distinction.

Research interests

The shape of faults, Paleostress, Stress and Geomechanics, Geology of the Netherlands, Seismic interpretation, Palinspastic and structural reconstruction, Dilatant faults, Scaled analogue modeling with materials other than sand, Quantifying sand box deformation, Salt tectonics, Boudins and brittle rupture, Structural geology, the coupling of sedimentation and tectonics, Fieldwork with coupled sedimentological and tectonic questions, Astronomical forcing of sedimentation.

Acknowledgements

"Waar kan ik heen? Ik kan niet naar Duitsland, 'k wil niet naar Duitsland, daar zijn ze zo streng"

"Where can I go? I can't go to Germany, won't go to Germany, they are so strict there"

- *Het Goede Doel - Belgie (is er leven op Pluto?)*

The idea of a promotion as I have come to understand it is to prove that the candidate is able to conduct fundamental and original academic research on his own. "On his own" in this context however does not mean the same thing as "alone", and there are many people without whose help this dissertation would not have been possible.

The first person I would like to thank is Janos Urai. His original ideas, guidance and counseling helped me to produce the work currently before you. Janos has the power to believe in the capabilities of his students, even when they themselves do not (anymore). We have talked many times on how to proceed after I got stuck. Although I know he was not all too enthusiastic about the topic in the beginning of my doctoral studies, he more than compensated by being extremely enthusiastic when the results started to come in.

I want to thank you for taking me aboard of your team, even after I completely flunked during my job interview on the question: "What is a Mohr-circle?"...

This work was co-supervised by Prof. Peter Kukla, and I am also greatly helped by Prof. Reicherter. I want to thank them both very much for their support and help, and the time they spent answering my questions.

Much help I also received from Stefan Back and I want to thank him for his constant support and liters of coffee that helped me to interpret seismic data more efficiently.

The initial two years of this thesis were part of the Special Focal Program 1135 "Dynamics of Sedimentary Systems under varying stress regimes: The example of the Central European Basin" of the German Science Foundation (DFG). Through this program I came in contact with Judith Sippel, Mauro Cacace and Tina Lohr. Discussions with them have where always fruitful and I want to thank them for their help. Judith is also thanked for the dataset from the Mammendorf quarry, which is discussed in Appendix 2.

Many doctoral and PhD students in geology use their acknowledgements to reflect on all the exciting places they have been. I have been to Assen, the Netherlands... and it was one of the best experiences in the last three years. Whether it was barbequing in a park in Groningen with Rik Sneep, sitting on the couch and watching episodes of House, MD, Life and the occasional Grey's Anatomy with Corinne Faassen, or trying to sleep in a not too stable mobile home in the middle of November-storms sweeping over a deserted holiday park, for some reason, my stays in Assen where the best part of my doctoral studies. I want to thank everyone who helped to make that possible. I particularly want to thank Rik and Corinne for allowing me to stay with them.

The data used in this study was supplied by the Nederlandse Aardolie Maatschappij, a Shell operated, 50-50 joint venture with ExxonMobil. I want to thank Rien Herber, Jürgen Grötsch, Frank Pardoel, Jos

Terken, Martin de Keijzer, Kees van Ojik, Joris Steenbrink, Daan den Hartog-Jager, Rene Villafuerte, Rik Sneep, and many others for the use of the data, their help, support and discussion during my various stays in the Assen offices. Particularly I want to thank Jos Terken and Martin de Keijzer, who were my most important contacts and helped me very much with clearing the various papers, abstracts and this thesis for publication.

I have had a lot conceptual insights by discussions and e-mail contact with many different people. I can not name them all, but here I would like particular thank M.C. Geluk for his insight on the internal structure of salt, I. Papanikolaou for his discussions on how faults slip, and T. Candela and T. Wiatr for discussions on the fractal dimensions of exhumed fault surfaces.

I would also like to thank the other doctoral students Joyce Schmatz, Johannes Schoenherr, Zsolt Schleder, Marc Holland, Maartje Houben and Shiyuan Li for their discussions and the good times we had. The Hiwis I would like to thank for their support and their help with all the often quite tedious jobs I had for them. Also the other staff of the Neotectonics and Georisks; Maggie, Christoph, Thomas, Nadine are thanked for both discussion and good times.

Joyce, as well as Bettina Leesmeister, and later Evelyn Bützler helped me very much with my German. German institutions of any kind are notorious in their use of the so-called "Beamtendeutsch", a sub-language of German, complex even for German nationals. I want to thank everybody that helped correct my errors, and also those who were patient when receiving them. This specifically applies for Simon Virgo and Joyce who help correct the German summary of this thesis.

After working on my Bachelor thesis in Utrecht, my supervisor, Hans de Bresser suggested I could do my M.Sc. research at the institute of Janos Urai in Aachen. This choice shaped the rest of my life as this promotion is a direct result of that work, and I am indebted to Hans for his suggestion.

Of course my family and friends are thanked for their support. I never really talked about the project with either of my parents, their partners, my sisters, or my friends, but their listening ear, or just sitting drinking a beer and playing Halo 3 on a TV-screen the size of my first apartment until 3 o'clock in the morning helped very much to wind down and charge up after weeks of non-stop ground breaking research.

The most important person I would like to thank, and who I saved for last, is my girlfriend Janneke. Lieve Janneke, als jij niet altijd rustig achter me had gestaan, als een rots in de woelige branding van mijn gedachten, me rustig had gemaakt als ik woedend, vertwijfeld, bang, zenuwachtig of alles tegelijk was, naar me had geluisterd en raad gegeven, voor me gekookt had, ook als ik weer eens VEULS te laat thuis kwam, me wakker had gemaakt als ik me weer eens verslapen had, dan weet ik niet of ik mijn promotie af had gemaakt. Ik hoop dat ik het zelfde voor jou kan doen de komende tijd. Ik weet wel dat als ik niet naar je geluisterd had op die ochtend in April 2006, dat ik dan hier niet meer gezeten. Bedanken op deze pagina doe ik echter niet, dat doe ik wel persoonlijk.